Multimetallic Emitters for Bioimaging and Display Applications

Ruth Daniels

Ph.D. 2017

Multimetallic Emitters for Bioimaging and Display Applications

Ruth Daniels

MChem. (Hons), AMRSC

A thesis in part-fulfilment of the requirements of the University of Northumbria at Newcastle for the degree of Doctor of Philosophy. Research undertaken in the Faculty of Health and Life Sciences

November 2017

Abstract

Multimetallic Emitters for Bioimaging and Display Applications

Ruth Daniels

The luminescent properties of transition metal complexes of heavy metals such as platinum(II) and irdium(III) are often highly luminescent and therefore are interesting for use as phosphorescent dopants in organic light-emitting diodes (OLEDs) and as luminescent probes in bioimaging. The majority of complexes investigated to date contain only one metal centre with multimetallic complexes becoming more widely studied in recent decades.

This work explores the synthesis of novel dinuclear emitters based on cyclometallated Pt(II) and Ir(III) centres. In particular, complexes in which the metal centres are rigidly-linked via cyclometallating bridging ligands. The complexes described in this work are highly luminescent with high quantum yields in degassed solution and relatively short luminescence lifetimes.

Dinuclear platinum(II) complexes linked via pyrimidine-based bis-bidentate ligands incorporating mono- and bis-thiophene cyclometallating units have been prepared and their photophysical properties investigated. These complexes were observed to emit in the orange (610 nm) and near-infrared (730 nm) regions of the spectrum for the mono- and bis-thiophene respectively, with relatively high quantum yields (ϕ = 0.15–0.85).

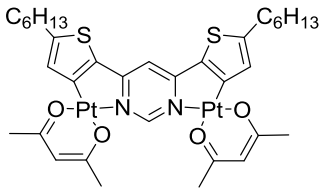

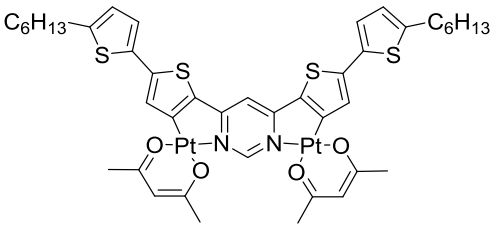

A further dinuclear platinum(II) complex, rigidly-linked via a bis-tetradentate bridging ligand offering O^N^C^N coordination, was successfully prepared. To the best of our knowledge, this is the first example of di-platinum(II) complex in which the two metal centres are linked via this type of bridging ligand.

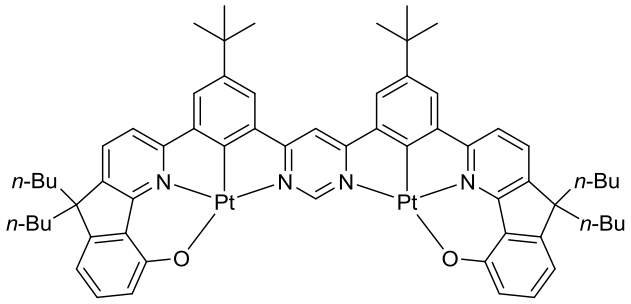

Dinuclear iridium(III) complexes linked via bis-bidentate bridging ligands based on the central heterocycle pyrimidine have been prepared. These pyrimidine-linked complexes exhibited high quantum yields in degassed dichloromethane solution at room temperature, in the range 0.88-1.0. A representative structure is shown below. Variation of the monodentate chloride ligands to alternative ligands such as cyanide and acetonitrile was also investigated. Incorporation of a cyanide ligand was observed to blue-shift the emission relative to the analogous chloro complex.

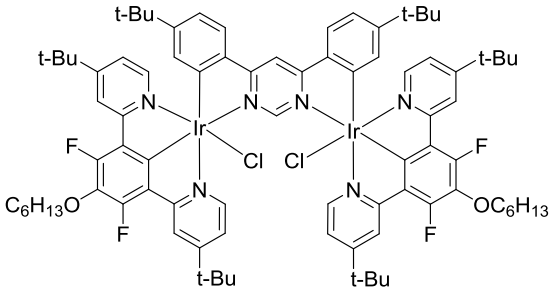

The effect of varying the central heterocycle of the bis-bidentate bridging ligand was investigated. The identity of the central heterocycle of the bridging ligand has been shown to have significant effects on the properties of the resulting dinuclear Ir(III) complexes, as is discussed below.

Di-iridium(III) complexes linked via 2,5-pyrazine based bridging ligands have been successfully prepared. However, photodegradation of the complexes was observed in chlorinated solvents. To resolve this problem, a bis-bidentate bridging ligand incorporating a thiazolo[5,4]thiazole core was employed and the resulting di-iridium complex showed improved photostability.

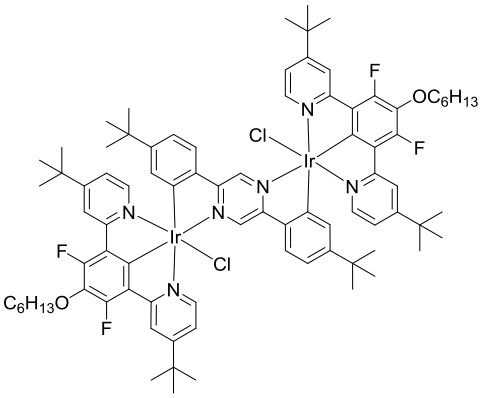

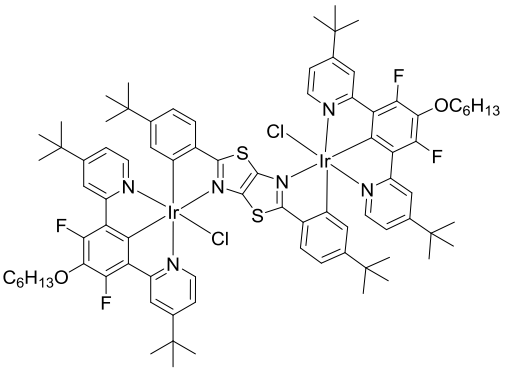

A 2,3-pyrazine-linked dinuclear iridium complex was synthesised and was observed to have a twisted geometry at room temperature and therefore, is chiral. Through a high-temperature NMR experiment, it was shown that this complex racemises at 80 °C.

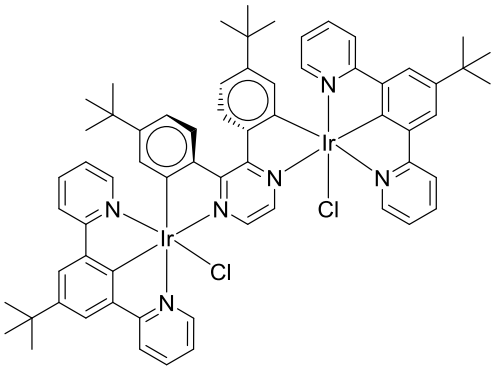

Finally, incorporating pyridazine as the central heterocycle leads to the sharing of a monodentate chloride ligand between the two iridium centres. This leads to the formation of a cationic dinuclear iridium(III) complex. This complex was investigated as a luminescent probe in bioimaging.

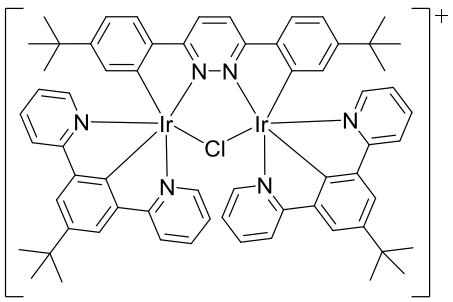

Declaration

I declare that the work contained in this thesis has not been submitted for any other award and that it is all my own work.

Name: Ruth Daniels

Signature:

Date: 01.11.2017

Acknowledgements

Firstly, I would like to thank my supervisor Associate Professor Valery Kozhevnikov for giving me the opportunity to carry out this research project within his group and also for his guidance, enthusiasm, encouragement and support throughout my PhD.

I would like to thank Northumbria University for providing the financial support for this work.

I would also like to thank Professor J. A. Gareth Williams, Dr Marcus C. Durrant, Marsel Shafikov, Dr. Helen Bryant, Professor Julia Weinstein, Luke McKenzie, Jonathan Shewring and Dr. Fernando Dias for their help in gathering photophysical and computational data for this work, in addition to their assistance with the bioimaging and OLED devices.

I am grateful to all the members of staff at Northumbria University with special thanks to Gordon Forrest, Dr. Karen Haggerty and Samantha Bowerbank for their technical support. Thank you to Dr. Graeme Turnbull for imparting a wealth of knowledge and wisdom. I would also like to thank the members of the Kozhevnikov groups, past and present, including Alfiya Suleymanova and Ross Martinscroft.

Huge thanks go to all my friends and colleagues in EBA606 and EBA510a, for all the support and the fun times throughout my PhD. Extra special thanks go to Hannah Sykes and Rachel Bulmer for their friendship and support, making my time at Northumbria extremely special.

Finally, I would like to thank all of my family and friends for their love, support and encouragement throughout the duration of my PhD. Thank you to my Mum, Dad, Matthew, Jo and to my friends Steph, Alexis, Helen, Mike, Kenny, Emma, Annelise, Lucy, Gilly and Emilie.

A very special thank you to my partner Stephen who has showed unconditional love, support, encouragement and patience throughout my PhD. I couldn't have done this without you.

Contents

Abbreviations

AcOH	Acetic acid
MeCN	Acetonitrile
acac	Acetylacetonate
BCP	Bathocuproine
bzq	Benzoquinoline
bpy	2,2′-Bipyridine
CBP	4,4′-Bis(*N*-carbazolyl)-1,1′-biphenyl
Mebib	Bis(*N*-methylbenzimidazolyl)benzene
Phbib	Bis(*N*-phenylbenzimidazolyl)benzene
Mebip	Bis(*N*-methyl-2-benzimidazolyl)pyridine
BPB	1,4-Bis(pyridin-2-yl)benzene
$CHCl_3$	Chloroform
DFT	Density functional theory
NPB	*N*,*N*′-Di(1-naphthyl)-*N*,*N*′-diphenyl-(1,1′-biphenyl)-4,4′-diamine
DAPI	4′,6-Diamidino-2-phenylindole dihydrochloride
DCM	Dichloromethane
DMF	Dimethylformamide
DMSO	Dimethyl sulfoxide
MTT	3-(4,5-Dimethylthizol-2-yl)-2,5-diphenyltetrazolium bromide
dpyb	1,3-Dipyridylbenzene
DSSCs	Dye-sensitised solar cells
EtOAc	Ethyl acetate
EQE	External Quantum Efficiency
FRET	Förster resonance energy transfer
GFP	Green fluorescent protein
HCl	Hydrochloric acid

HOMO	Highest occupied molecular orbital
IC	Internal conversion
ISC	Intersystem crossing
iTMCs	Ionic transition metal complexes
LC	Ligand-centred
LMCT	Ligand-to-metal charge transfer
LECs	Light-emitting electrochemical cells
LCD	Liquid crystal display
LUMO	Lowest unoccupied molecular orbital
τ	Luminescence lifetime
ϕ	Luminescence quantum yield
MC	Metal-centred
MLCT	Metal-to-ligand charge transfer
MMLCT	Metal-metal-to-ligand charge transfer
MeOH	Methanol
NHCs	N-heterocyclic carbenes
NIR	Near-infrared
k_{nr}	Non-radiative rate constant
NMR	Nuclear magnetic resonance
Δ_o	Octahedral crystal field splitting parameter
OLED	Organic light-emitting diodes
phen	1,10-Phenanthroline
ppy	2-Phenylpyridine
PhOLEDs	Phosphorescent organic light-emitting diodes
PDT	Photodynamic therapy
PET	Photoinduced electron transfer
PLQY	Photoluminescence quantum yield
PLEDs	Polymer light-emitting devices

PPA	Polyphosphoric acid
KPF_6	Potassium hexafluorophosphate
k_r	Radiative rate constant
AgOTf	Silver trifluoromethanesulfonate
SOC	Spin-orbit coupling
tpy	2,2′:6′,2″-Terpyridine
TBACN	Tetrabutyl ammonium cyanide
dpm	2,2,6,6-Tetramethyl-3,5-heptanedionate
thpy	2-(2-Thienyl)pyridine
TLC	Thin layer chromatography
TD-DFT	Time-dependent density functional theory
TEM	Transmission electron microscopy
TREM	Time-resolved emission imaging microscopy
WOCs	Water oxidation catalysts
WOLEDs	White organic light-emitting diodes

Chapter 1

Introduction

1.0 Introduction

Interest in luminescent complexes of second and third row transition metals has increased greatly in recent decades.[1] A large number of research groups have reported on the synthesis, characterisation and photophysical properties of a wide range of complexes, particularly of ruthenium(II), platinum(II) and iridium(III).

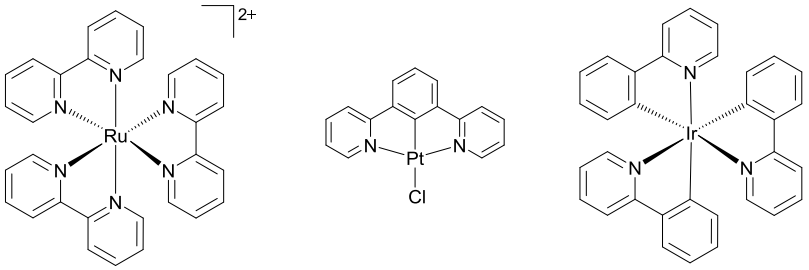

1.0.1 $[Ru(bpy)_3]^{2+}$ **1.0.2** Pt(dpyb)Cl **1.0.3** *fac*-$Ir(ppy)_3$

Figure 1: A figure to show the structure of $[Ru(bpy)_3]^{2+}$ and *fac*-$Ir(ppy)_3$. These luminescent metal complexes and their derivatives have been extensively studied and have been utilised in a number of applications.

The increase in studies of such complexes can be attributed to their potential to be utilised for a wide range of applications such as organic electronic devices, chemical sensors, bio-imaging and photocatalysis.[2] The most popular contemporary application is in organic light-emitting diode (OLED) devices. These devices have become widely studied for use in display and lighting technology and have most recently been used in products such as mobile phones and flat-screen televisions.[3]

The suitability of these types of luminescent metal complexes for such applications originates from their favourable photophysical properties in addition to good chemical and photochemical stability and, in some cases, colour tunability of emission across the entire visible spectrum.[2]

This research is concerned with the synthesis and characterisation of multimetallic triplet emitters for use in applications such as bio-imaging and OLEDs. Relative to the study of monometallic

luminescent transition metal complexes, there have been fewer investigations of multimetallic complexes, in particular those in which the metal centres are rigidly linked.

In this chapter, a review of the literature will discuss the development of luminescent transition metal complexes; briefly discussing the synthesis and photophysical properties of monometallic compounds before explaining in more detail the research carried out relating to multimetallic complexes. The advantages of multimetallic complexes over their monometallic counterparts will also be reviewed.

1.1 Luminescence Principles

Luminescence is the emission of light by a substance where the original energy source is not heat (incandescence). Luminescence can be caused by the energy generated by exothermic chemical reactions (chemiluminescence) or electrical energy (electroluminescence). The metal complexes discussed here are photoluminescent in that the source of energy is the absorption of photons, although electroluminescence is also possible in some cases.

In the case of a transition metal complex, features of luminescence are dependent on the metal and ligand components of the complex. The molecular orbitals formed on the combination of specific metal and ligand orbitals often have either dominant metal or ligand character. The mixing of ligand and metal character coupled with the order of the molecular orbitals influences the nature of the lowest energy transition (Figure 2) and therefore, the properties of luminescence.

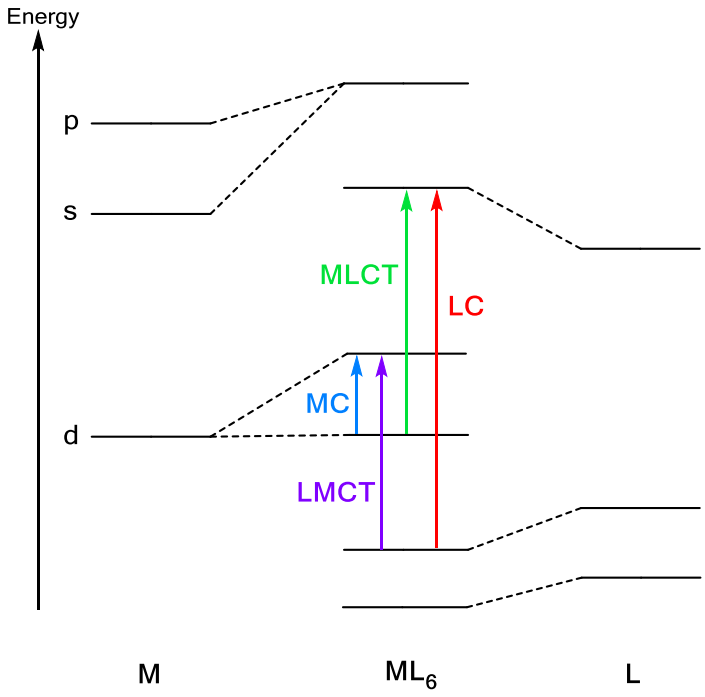

Figure 2: Molecular orbital diagram for an octahedral metal complex, depicting the transitions possible upon excitation.

1.1.1 Absorption

As a photon of a particular energy is absorbed, the molecule is promoted to an excited state through a transition corresponding to the energy of the photon absorbed. As shown in Figure 2, octahedral complexes like those formed by Ir(III) and Ru(II) can have four possible transitions to form excited states. These transitions are metal-to-ligand charge transfer (MLCT), ligand-to-metal charge transfer (LMCT), ligand-centred (LC) and metal-centred (MC). The identity of the lowest excited state is determined by the ordering of the molecular orbitals which in turn is directly related to the molecular structure of the metal complex. Methods of synthetically modifying the structure of a transition metal complex in order to adjust the energies of the molecular orbitals will be discussed in later sections of this review.

The energy stored in the excited state of the molecule following absorption can be lost radiatively through luminescence or non-radiatively through processes such as vibrations and rotations. These processes have rate constants k_r and k_{nr} respectively.

1.1.2 Emission

There are two types of photoluminescence; fluorescence (singlet-singlet) and phosphorescence (triplet-singlet).

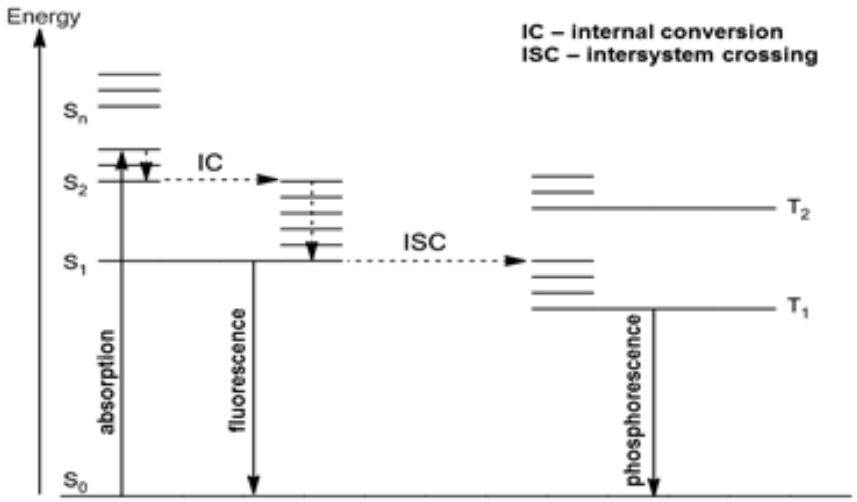

Figure 3: A Jablonski diagram to illustrate the electronic and vibrational transitions that occur in emission of both fluorescence and phosphorescence, following absorption of a photon. Solid downward arrows represent radiative processes, whereas dashed arrows correspond to non-radiative processes.

Considering the Jablonski diagram shown in Figure 3, in the case of fluorescence, a photon is absorbed and the metal complex is promoted to a singlet excited state (S_2). Non-radiative relaxation of this excited state, through thermal vibrations and rotations, to a lower vibrational state of the same electronic state or internal conversion (IC) to a lower electronic level (S_1) can then occur. This is followed by emission of light due to radiative relaxation from the lowest excited state. Fluorescence is a spin-allowed process.

For phosphorescence, the molecule is similarly promoted to a singlet state (S_2) on absorption of a photon before relaxing to a lower electronic excited state (S_1). Unlike in fluorescence, intersystem crossing (ISC) then occurs. This is a transition to a state with a different spin multiplicity (T_1) and is of more importance in molecules that exhibit large spin-orbit coupling (SOC) constants. The large SOC constant resulting from the presence of a heavy metal ion leads to more efficient intersystem crossing and relaxation of the spin selection rule. Therefore, the

radiative rate constant (k_r) for the formally spin-forbidden process phosphorescence, relaxation from the T_1 state to the ground state S_0, is increased and phosphorescence becomes observable at room temperature.

Emission via phosphorescence is advantageous for applications. In the case of OLEDs, the ability to harvest triplet excited states increases the theoretical efficiency of devices to 100% (statistically shown to be limited at 25% in fluorescence-based devices).[4] In addition, the longer lifetime of triplet excited states results in the ability to distinguish triplet emission from short-lived autofluorescence in bio-imaging applications.[5]

1.1.3 Non-Radiative Processes

A high rate of non-radiative decay of excited state energy via processes such as vibrations and rotations is promoted by a large difference in geometry of the metal complex between the ground state and the excited state. One of the main ways in which distortion can occur is through population of antibonding metal-centred (MC) e_g orbitals. In an octahedral metal complex, a small value of Δ_o results in d-d excited states (e_g) that are close in energy to lower-lying excited states such as metal-to-ligand charge transfer (MLCT) states (π^*).

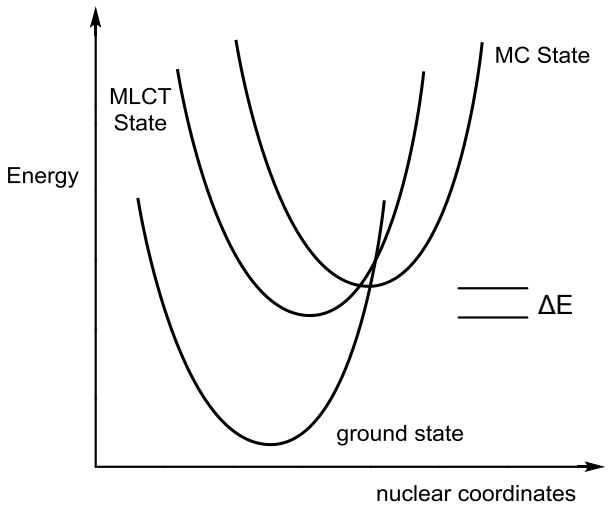

Figure 4: An energy diagram to illustrate how a MC d-d state close in energy can lead to deactivation of a lower-lying MLCT state.

Upon excitation to a MLCT state, these close MC states can be thermally populated at room temperature, leading to a large degree of distortion of the metal complex and deactivation of the lower-lying state through vibrations. This results in a loss of luminescence.

1.1.4 Measurable Luminescence Quantities

Experimentally measurable parameters, lifetime of emission (τ) and quantum yield (ϕ), are related to the radiative and non-radiative rate constants and are therefore used to quantify observed luminescence. The equations relating τ and ϕ to the rate constants are shown below.

$$\tau_{obs} = \frac{1}{k_r + k_{nr}} \quad \text{and} \quad \phi = k_r \times \tau_{obs}$$

1.2 Monometallic Transition Metal Complexes

Luminescent metal complexes containing a single metal centre in which the metal centre is chelated by ligands such as those shown in Figure 5 have been studied by a large number of research groups.

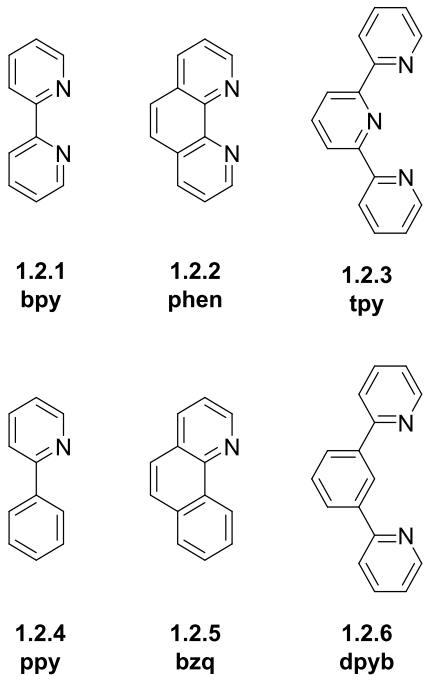

Figure 5: A figure to show the most common chelating ligands used in the synthesis of transition metal complexes. Many derivatives of these ligands have now been synthesised and utilised in the preparation of such complexes.

Initially the majority of work was focussed on complexes of ruthenium(II) and osmium(II) with polypyridyl ligands.[6-9] In recent decades, many research groups have begun working on complexes of Pt(II) and Ir(III). The interest in complexes of heavy transition metals was initially sparked by the study of $[Ru(bpy)_3]^{2+}$ and today is sustained by their potential application in many areas of applied chemistry.[9, 10]

The growing number of applications for which complexes of heavy transition metals can be utilised has resulted in complexes of platinum(II) and iridium(III) being intensively studied. Initially, the focus was on the synthesis of complexes incorporating polypyridyl ligands such as 2,2′-bipyridine (bpy), 1,10-phenanthroline (phen) and 2,2′:6′,2″-terpyridine (tpy). More recently the focus has shifted to Pt(II) and Ir(III) complexes of cyclometallating ligands such as 2-phenylpyridine (ppy) and 1,3-dipyridylbenzene (dpyb).[5, 11-30]

Cyclometallating ligands have significant advantages over their polypyridyl analogues. During the cyclometallation reaction, proligands such as 2-phenylpyridine form five-membered metallacycles through the activation of the C-H bond of the phenyl ring *ortho* to the 2-pyridyl fragment. This reaction involves abstraction of a proton and consequently, cyclometallating ligands are anionic and form very strong, covalent metal-carbon bonds. In 2-phenylpyridine, for example, the C^- atom is a very strong σ-donor whilst the pyridyl moiety is a good π-acceptor, meaning that such ligands offer a very strong ligand-field. Incorporation of cyclometallating ligands means that the higher-lying metal-centred d-d excited states of a complex, which act as a major pathway for the non-radiative deactivation, are raised in energy and much less likely to be thermally populated at room temperature. As result, excited state energy is more likely to be lost radiatively, leading to the high quantum yields observed for metal complexes of cyclometallating ligands.[19, 31, 32]

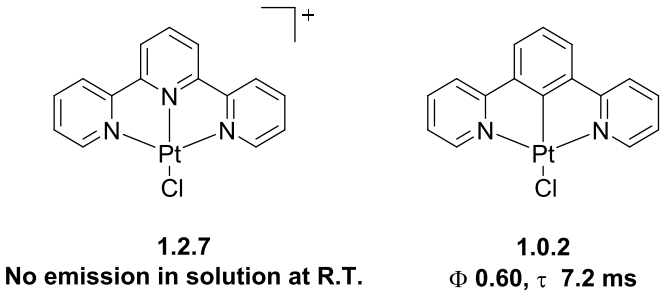

Figure 6: A figure to illustrate the effect of cyclometallating ligands on the photophysical properties of a square planar Pt(II) complex. The luminescence from the terpyridyl platinum(II) complex is lost via population of low-energy deactivating MC d-d states. The cyclometallating ligand in the cyclometallated analogue raises the energy of the d-d states as discussed above. Therefore, emission is observed in solution at room temperature.[17, 20, 33]

Additionally, the ability to tune the emission energy and hence the colour of emission is greatly improved with the incorporation of cyclometallating ligands. The shift of the ^{3}MC excited states to higher energy increases the scope for variation in the size of the energy gap between the highest occupied molecular orbital (HOMO) and the lowest unoccupied molecular orbital (LUMO) of a complex. As a result the colour tunability of the metal complex is increased.[11, 32, 34] Generally, the ease of tuning the emission energy of a metal complex containing cyclometallating ligands is also facilitated by the distinct localisation of the HOMO and LUMO on separate moieties of the molecule as shown in Figure 7. This means that the selective functionalisation of the aryl or pyridyl rings will exclusively alter the energies of either the HOMO or LUMO and therefore, the energy of the emission of the transition metal complex.[31, 35]

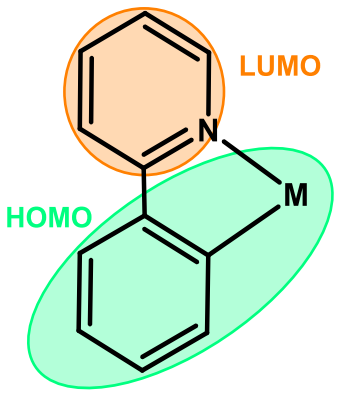

Figure 7: An illustration of the localisation of the HOMO and LUMO on the general structure of a cyclometallated metal complex in which 2-phenylpyridine is the ligand. The same localisation of the HOMO and LUMO occurs with complexes of other cyclometallating ligands. Generally, the HOMO is localised on the metal centre and the cyclometallated aryl ring of the ligand. The LUMO is localised on the heterocycle, the pyridyl moiety in this case.

As previously stated, transition metal complexes of cyclometallating ligands such as 2-phenylpyridine and 1,3-dipyridylbenzene are now widely investigated with studies of both their structural and phototphysical properties carried out. In the following sections, the synthetic methods and photophysical properties of monometallic Pt(II) and Ir(III) complexes incorporating bidentate and terdentate ligands, including the strategies employed in refining them for use as emitters in an array of applications, will be discussed.

1.2.1 Platinum(II) and Iridium(III) Complexes of Cyclometallating Bidentate Ligands

Homoleptic and heteroleptic cyclometallated complexes of both Pt(II) and Ir(III) bearing bidentate ligands such as 2-phenylpyridine and its derivatives have been observed to be highly luminescent in fluid solution and tunable across the visible spectrum.[31]

In the 1980s, it was first observed that mononuclear square planar d^8 complexes, such as those of platinum(II), could be obtained as luminescent species, even in solution at room temperature. Key to this is ensuring that there is a large enough energy gap between the lowest excited state and the deactivating MC d-d states, as discussed previously. Cyclometallated Pt(II) complexes are characterised by high quantum yields and long-lived excited states with emission thought to originate from excited states that are predominantly of ^{3}LC character mixed with ^{1}MLCT character through the strong spin-orbit coupling of the heavy transition metal.[13, 36]

Homoleptic bis-cyclometallated platinum(II) complexes, for example *cis*-[Pt(ppy)$_2$], were first prepared in low yield by the treatment of *trans*-[PtCl$_2$(SEt$_2$)$_2$] with the lithiated ligand, for example 2-(*o*-phenyl-pyridine)lithium. The range of bis-cyclometallated platinum(II) complexes reported by Von Zelewsky *et. al.* are shown in Figure 8.[37-39]

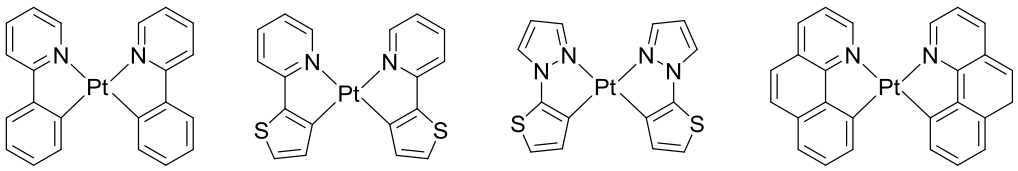

1.2.8 **[Pt(ppy)$_2$]** **1.2.9** **[Pt(thpy)$_2$]** **1.2.10** **[Pt(thpz)$_2$]** **1.2.11** **[Pt(bzq)$_2$]**

Figure 8: Bis-cyclometallated platinum(II) complexes prepared by Von Zelewsky and co-workers.[37-40]

Attempts to prepare homoleptic platinum(II) complexes of the type shown above by the treatment of the 2-arylpyridines with K_2PtCl_4 did not lead to formation of the homoleptic complexes, but the isolation of cyclometallated complexes with the general formula [Pt(C^N)(HC^N)Cl] in high yield. The molecular structure of these complexes include one cyclometallated C^N ligand, a monodentate chloride ligand and one HC^N ligand acting as a N-donor with a pendant, non-coordinating aryl ring as is illustrated in Figure 9, using 2-phenylpyridine as an example.[41, 42]

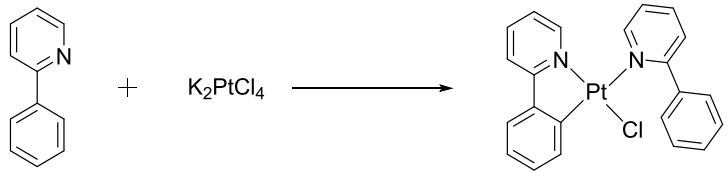

1.2.4 **ppy** **1.2.12** **[Pt(ppy)(ppyH)Cl]**

Figure 9: Reaction scheme to show the platinum(II) complex isolated on the reaction of 2-phenylpyridine with potassium tetrachloroplatinate.

Luminescence of the bis-cyclometallated Pt(II) complexes of the type shown in Figure 8 is only observed at 77 K in a rigid acetonitrile matrix, with lifetimes in the μs range. The exception to this is [Pt(thpy)$_2$] for which a quantum yield of 0.30 was recorded in acetonitrile solution at room temperature.

Given that homoleptic, bis-cyclometallated platinum(II) complexes exhibit poor luminescence efficiency, the focus shifted to heteroleptic complexes of Pt(II) in order to acquire more emissive platinum(II) complexes. Heteroleptic complexes with the general formula [Pt(C^N)(LX)] have several advantages over their homoleptic counterparts. Physical properties of the complexes such

as the charge and solubility can be varied through appropriate selection of the ancillary ligand. Additionally, the ancillary ligand gives further control over the identity of the lowest energy excited state. Through substitution of electron-donating or -withdrawing groups on the LX ligand, the amount of electron density on the metal centre can be altered. This leads to variation in the amount of MLCT character mixed into the lowest energy transition and therefore, modification of both the emission colour and luminescence lifetime.[43]

In 1995, Pt(II) complexes of cyclometallating ligands 2-phenylpyridine and 2-thienylpyridine were reported where the ancillary LX ligands incorporated were based on the N^N ligands 2,2-bipyridine and ethylene diamine. It was found that the identity of the ancillary ligand altered the nature of the emitting state of the final complex.[44]

β-Diketonate ligands such as acetyl acetonate (acac) and dipivolylmethane (dpm) are also widely utilised as ancillary ligands in heteroleptic platinum(II) complexes. The synthetic procedure used in the preparation of such complexes is shown in Figure 10.

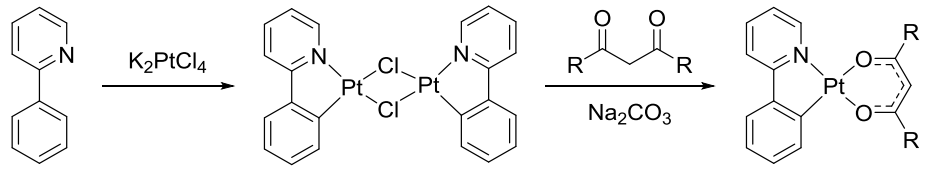

Figure 10: A reaction scheme to show the synthetic route used in the preparation of heteroleptic [Pt(C^N)(LX)] complexes in which the LX ligand is a β-diketonate ligand. In this example, 2-phenylpyridine is shown as the cyclometallating ligand.[43]

In 2002, Thompson *et.al.* reported the synthesis of a series of complexes with the general structure [Pt(C^N)(O^O)], as shown in Figure 11. All of the complexes were highly luminescent in frozen glass solution at 77 K with several also being emissive in degassed solutions at room temperature (ϕ = 0.02–0.25). The highly structured emission spectra observed and luminescence lifetimes measured, in the microsecond range, are consistent with emission originating from an excited state with mixed ^{3}LC-MLCT character.[13, 43]

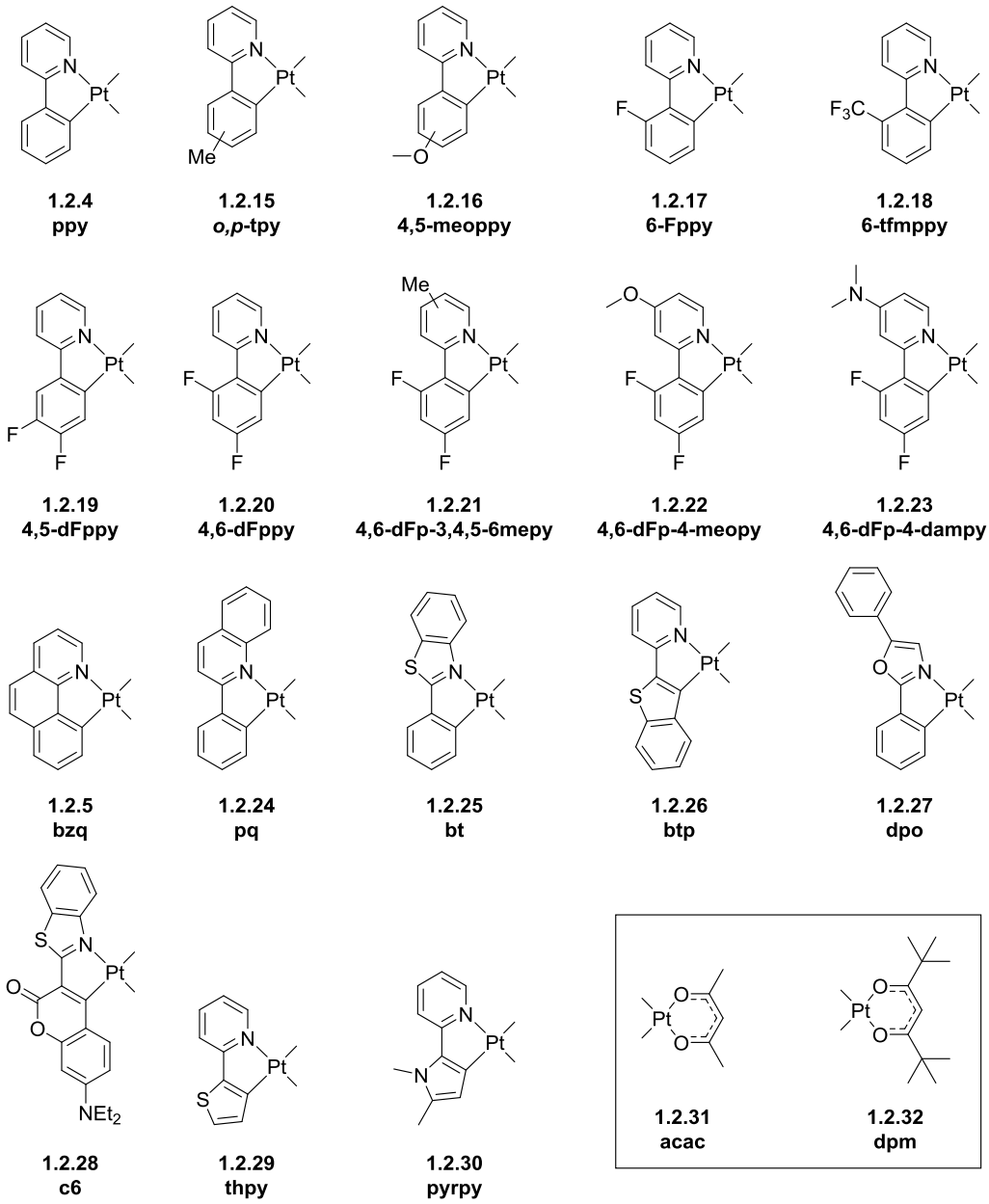

Figure 11: A figure to show the cyclometallating and β-diketonate ligands used to prepare [Pt(C^N)(O^O)] complexes.[43]

It was reported by Thompson and co-workers that the photophysical properties of the heteroleptic platinum(II) complexes, bearing combinations of the C^N and β-diketonate ligands shown above, are strongly governed by the nature of the cyclometallating ligand and the substituents present on the C^N system. It was observed that variation of the β-diketonate ligands, acac and dpm, had no significant effect on the emission characteristics of the final complexes.[43]

In 2011, Huang and co-workers reported the study of heteroleptic platinum(II) complexes of four different β-diketonate ligands; NDBM, NPTPD, DBM, and CPNPD, as shown in Figure 12. These

particular O^O-coordinating ligands were chosen as they have triplet-state energy levels lower in energy than those of acac and dpm. In order to investigate the effect of this on the excited state properties of the final heteroleptic Pt(II) complexes, the photophysical properties of the four Pt(II) complexes were investigated and compared with those of [Pt(ppy)(acac)]. The four heteroleptic Pt(II) complexes exhibited intense luminescence in solution at room temperature with quantum yields in the range ϕ = 0.02–0.11. The photophysical properties showed that the excited state from which these complexes emit can be attributed to mixtures of ^{3}MLCT, ^{3}LLCT and ^{3}LC/ILCT. It was observed that the excited state properties of the Pt(II) complexes could be significantly tuned through variation of the β-diketonate ligand with emission wavelengths ranging from blue-green (485 nm) to yellow (550 nm).[45]

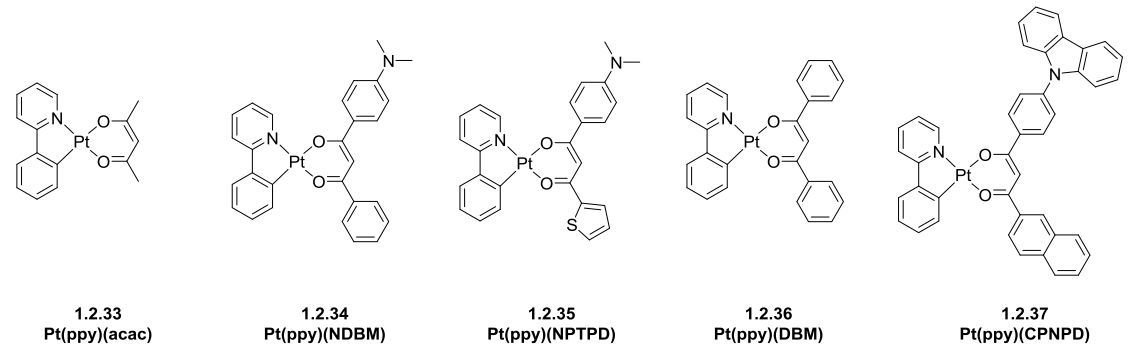

Figure 12: Series of heteroleptic Pt(II) complexes reported by Gao and co-workers bearing 2-phenylpyridine as the cyclometallating ligand and incorporating four different β-diketonate ligands.

The homoleptic and heteroleptic platinum(II) complexes described in this section are facile to synthesise, charge neutral and air stable. Additionally, the ability to tune the absorption and emission wavelength through independent variation of the cyclometallating and ancillary ligands offers further benefits. Consequently, these cyclometallated complexes are good candidates for utilisation in applications, for example, optoelectronic devices.

Similarly to the Pt(II) complexes already discussed in this section, homoleptic and heteroleptic complexes of iridium(III) incorporating bidentate cyclometallating ligands have also been intensively studied.

The earliest and now most widely studied example of a homoleptic Ir(III) complex was reported in 1985 by Watts *et. al*. The tris-cyclometallated complex, *fac*-[Ir(ppy)$_3$], is a bright green emitter with phosphorescence originating from an excited state with predominantly ^{3}MLCT character. The quantum yield for *fac*-[Ir(ppy)$_3$] was originally reported as $\phi = 0.40$ in degassed toluene solution at room temperature, however, this value has now been revised upwards to $\phi = 0.97$. This homoleptic Ir(III) complex was first synthesised via the reaction of Ir(acac)$_3$ with an excess of ppyH in glycerol at reflux. A further two synthetic methods that have been reported for the preparation of homoleptic iridium(III) complexes as shown in Figure 13. Methods B and C offer advantages over method A. For example, the (C^N)$_2$Ir(O^O) and dichloro-bridged dimers can be prepared in high yield from IrCl$_3$.H$_2$O, a relatively cheaper starting material than Ir(acac)$_3$. Secondly, methods B and C give higher yields of the desired Ir(C^N)$_3$ product (80-85% vs. 45-60%).[23, 24, 31, 34, 46]

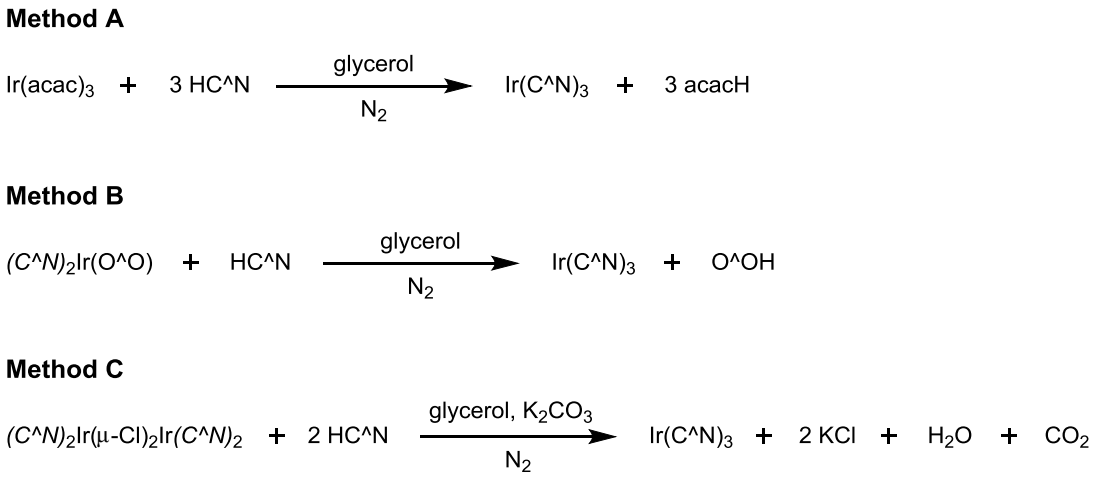

Figure 13: Reaction schemes to show the three synthetic routes that can be used in the preparation of homoleptic tris-cyclometallated iridium(III) complexes such as *fac*-Ir(ppy)$_3$.[24]

The synthetic routes shown above have been extended to homoleptic iridium(III) complexes of a wide range of cyclometallating ligands. A selection of the bidentate C^N-coordinating ligands reported in the literature are shown in Figure 14, incorporating different aryl and heterocyclic rings in conjunction with a variety of electron-donating and -withdrawing substituents.

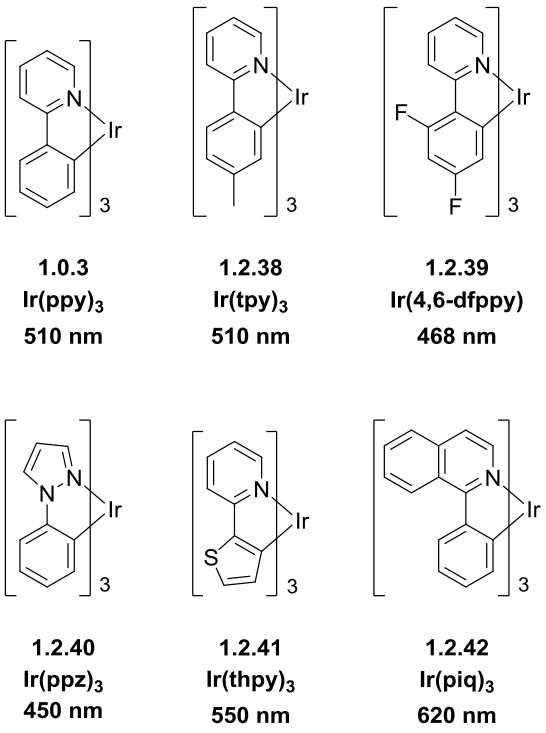

Figure 14: A figure to show a selection of homoleptic Ir(C^N)$_3$ complexes reported in the literature and their emission maxima recorded at 298 K.[24, 47, 48]

The structural and electronic properties of the cyclometallating ligands have a significant effect on the photophysical properties of the Ir(C^N)$_3$ complex. The introduction of electron-withdrawing fluoro- groups as with 4,6-dfppy results in a blue-shift of the emission of Ir(4,6-dfppy)$_3$ (468 nm) relative to the emission of the unsubstituted Ir(ppy)$_3$ (510 nm). Conversely, incorporating electron-donating substituents results in a red-shift of the emission. For example, variation of the phenyl ring of ppy to an electron-rich thiophene ring in thpy results in a red-shift of 40 nm. Increasing the size of the conjugated aromatic system of a cyclometallating ligand also results in a red-shift of the emission. As shown in Figure 14, the homoleptic complex Ir(piq)$_3$ bearing an isoquinoline group rather than a pyridyl ring displays emission of 620 nm, a red-shift of 110 nm compared with Ir(ppy)$_3$.[24, 47]

Homoleptic Ir(III) complexes are formed as a mixture of facial (*fac*) and meridional (*mer*) isomers in which the configuration of the C^N ligands around the iridium centre is as shown below.

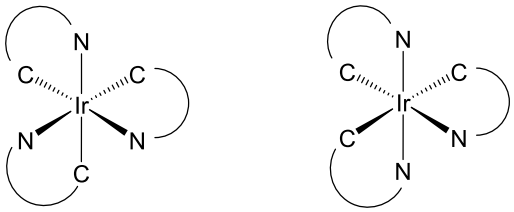

1.2.43 *fac*-Ir(C^N)$_3$ **1.2.44** *mer*-Ir(C^N)$_3$

Figure 15: A figure to show the general structures of the facial and meridional isomers formed in the preparation of homoleptic iridium(III) complexes.

Thompson *et. al.* reported the selective synthesis of facial or meridional isomers of Ir(C^N)$_3$ complexes bearing cyclometallating ligands derivatised from 2-phenylpyridine and 2-phenylpyrazole. Their corresponding photophysical properties were also investigated. It was found that the reaction conditions imparted significant control over the configuration of the homoleptic iridium(III) complex. In general, at higher temperatures (> 200 °C) it is predominantly the facial isomer that is formed with the meridional isomer being the main product formed at lower temperatures (< 150 °C). This, coupled with the fact that the meridional isomer can be efficiently converted to the facial isomer at higher temperatures, suggests that the meridional isomer is the kinetic product with the facial isomer being the thermodynamic product. The two different isomers were also observed to have significantly different photophysical properties. The meridional isomers display emission spectra that are broader and red-shifted compared with those of the facial isomers. In addition, for the meridional isomers, the phosphorescence quantum yields are lower and much shorter luminescent lifetimes are observed.[24]

Homoleptic iridium(III) complexes, as discussed above, are easily synthesised with control over the configuration of the product possible through careful selection of the reaction conditions. They exhibit good photophysical properties and the ability to tune the emission of such complexes over much of the visible spectrum means that this class of iridium(III) complexes are good candidates for applications such as OLEDs. For example, Thompson *et. al.* reported OLEDs based on Ir(ppy)$_3$ to have internal quantum efficiencies of greater that 80%.[49]

A second class of highly phosphorescent, tris-chelated iridium(III) complexes reported in the literature are heteroleptic complexes in which the Ir(III) centre is bound to two cyclometallating ligands and one ancillary ligand, anionic or neutral. The selection of an anionic LX ancillary ligand such as a β-diketonate leads to formation of a neutral complex, whereas incorporation of a neutral ancillary ligand such as a diimine ligand gives a cationic Ir(III) complex.[31]

In the synthesis of homoleptic iridium(III) complexes, it was found that many of the cyclometallating ligands that could be incorporated into Ir(III) phosphors do not lead to the formation of tris-cyclometallated complexes such as those discussed previously. It is thought that this is due to both steric and electronic effects. Heteroleptic complexes of the general formulae $[Ir(C\hat{}N)_2(L\hat{}X)]$ and $[Ir(C\hat{}N)_2(N\hat{}N)]^+$ are easily prepared, with many examples showing efficient room temperature phosphorescence from mixed LC-MLCT excited states, similar to their tris-cyclometallated analogues.[31, 50-52]

In 2001, Thompson *et. al.* reported the synthesis and characterisation of a series of neutral $[Ir(C\hat{}N)_2(L\hat{}X)]$ complexes (Figure 16) incorporating a range of C^N and monoanionic L^X ancillary ligands. These heteroleptic complexes are prepared using a two-step synthetic procedure as shown in Figure 17. Firstly, iridium chloride reacts with the cyclometallating ligand in refluxing 2-ethoxyethanol, resulting in the formation of the corresponding dichloro-bridged dimer in good yields, greater than 75%. It has been shown, through crystallographic studies, that each of the Ir(III) centres within the dimer are octahedrally coordinated by two bridging chlorides and two C^N-coordinating ligands. The two cyclometallating aryl rings are positioned *cis* to each other around the iridium centre as a result of the strong *trans* influence of the formally C^- atoms. In the second step, the dichloro-bridged dimers are easily converted to monometallic complexes through treatment of the dimer with a bidentate, anionic ancillary L^X ligand, for example, a β-diketonate, 2-picolinic acid or an N-alkylsalicylimine. The final heteroleptic iridium(III) complexes are air stable, can be sublimed and formed in high yields, often greater than 80%.[50]

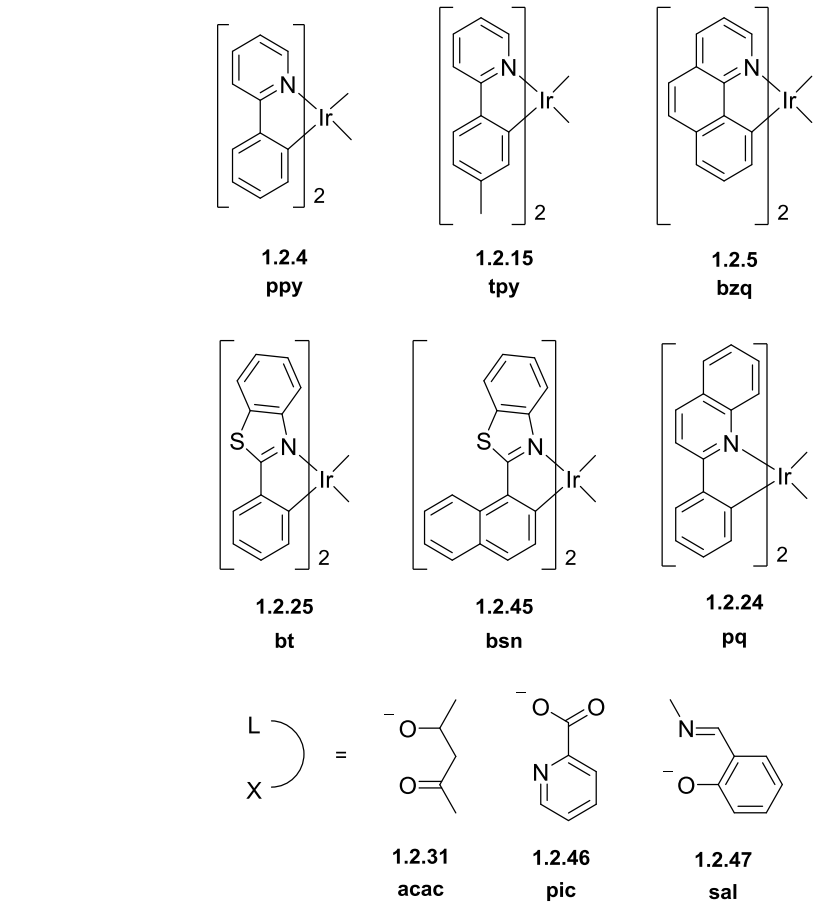

Figure 16: A figure to show the [Ir(C^N)$_2$(LX)] complexes prepared by Thompson and co-workers.[50]

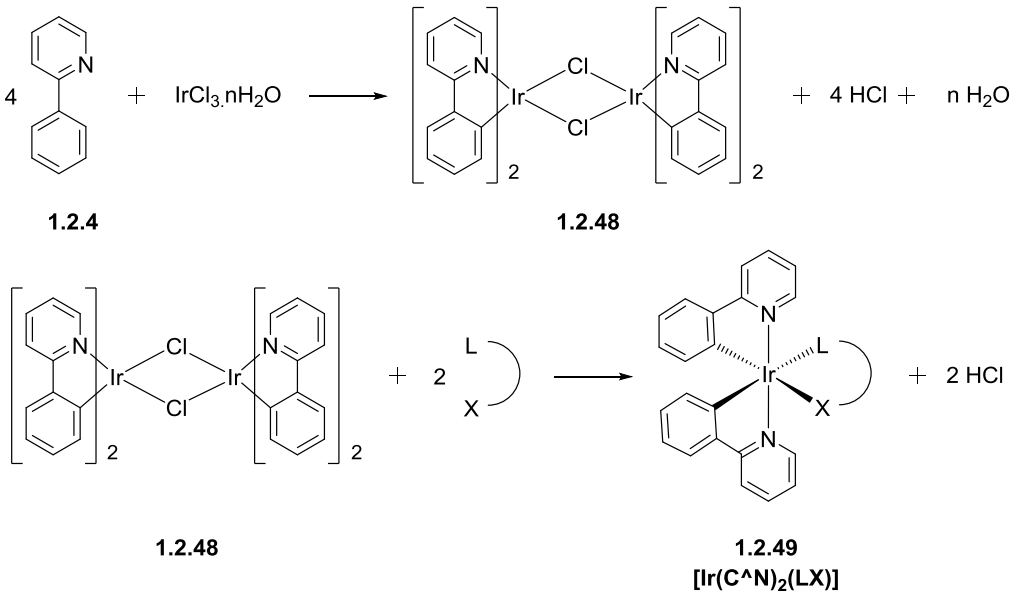

Figure 17: Reaction scheme to show the two-step synthetic procedure utilised in the preparation of neutral, heteroleptic complexes of the general formula [Ir(C^N)$_2$(LX)]. In this reaction scheme, the cyclometallating ligand 2-ppy is shown as an example.[50]

The photophysical properties of the [Ir(C^N)$_2$(L^X)] complexes were also investigated by Thompson and co-workers and the data obtained is shown in Table 1.[50]

Table 1: Photophysical data reported by Thompson and co-workers for [Ir(C^N)$_2$(L^X)] complexes.[50]

C^N	LX	Absorbance λ (log ε)	Emission λ_{max} (nm)	Lifetime (μs)[a]		Quantum Efficiency*
				298 K	77 K	
ppy	acac	260 (4.5), 345 (3.8), 412 (3.4), 460 (3.3), 497 (3.0)	516	1.6	3.2	0.34
tpy	acac	270 (4.5), 370 (3.7), 410 (3.5), 460 (3.4), 495 (3.0)	512	3.1	4.5	0.31
bzq	acac	260 (4.6), 360 (3.9), 470 (3.3), 500 (3.2)	548	4.5	23.3	0.27
bt	acac	269 (4.6), 313 (4.4), 327 (4.5), 408 (3.8), 447 (3.8), 493 (3.4), 540 (3.0)	557	1.8	4.4	0.26
bt	pic	206 (4.6), 326 (4.6), 355 (4.1), 388 (3.9), 437 (3.8), 475 (3.7)	541	2.3	3.6	0.37
bt	sal	276 (4.6), 325 (4.3), 450 (3.7), 540 (2.9)	562	1.4	3.1	0.22
bsn	acac	274 (4.7), 300 (4.6), 345 (4.5), 427 (4.0), 476 (4.0), 506 (3.9)	606	1.8	2.5	0.22
pq	acac	268 (5.0), 349 (4.4), 433 (3.9), 467 (3.9), 553 (3.6)	597	2.0		0.1

(a) Lifetime and quantum efficiency measurements were made in 2-MeTHF, except for the 77 K lifetime of [Ir(ppy)2(acac)], which was carried out in a CH_2Cl_2 frozen glass. The lifetimes have error bars of ± 10%, and the quantum efficiencies are ± 20%.

The absorption spectra observed for the heteroleptic Ir(III) complexes were similar to those of the dichloro-bridged dimers and the [Ir(C^N)$_2$(bpy)]$^+$ complexes of the same cyclometallating ligands. This indicates that the dominant transitions in these [Ir(C^N)$_2$(L^X)] complexes are due to the 'Ir(C^N)$_2$' fragment. All of the reported heteroleptic complexes are emissive at room temperature with luminescence lifetimes in the range of 1-5 μs and quantum yields between 0.1 and 0.4 for degassed 2-MeTHF solutions. Thompson *et. al.* reported that, like the Ir(C^N)$_3$ complexes, these [Ir(C^N)$_2$(L^X)] complexes emit from an MLCT excited state. The emission wavelengths observed range from 512 nm (green) for [Ir(tpy)$_2$(acac)] to 606 nm (red) for [Ir(bsn)$_2$(acac)], as can be seen in Table 1. The emission spectra recorded show that variation of the cyclometallating ligand has a noticeable effect on the emission wavelength. Across the series of complexes in which the cyclometallating ligand is varied, via the introduction of electron-

donating groups or an increase in the ligand conjugation length, a red-shift of 94 nm is observed. Conversely, altering the ancillary LX ligand seems to have a relatively small effect, with only a 21 nm red-shift observed on going from $[Ir(bt)_2(pic)]$ through $[Ir(bt)_2(acac)]$ to $[Ir(bt)_2(sal)]$. This observation suggests that there is a significant $^3(\pi\text{-}\pi^*)$ contribution from the C^N ligand to the emitting state. Despite this, the L^X ligands can assist in modulation of the photophysical properties through electronic effects on the iridium(III) centre. For example, for the $[Ir(bt)_2(LX)]$ series, the emission maxima obtained increased according to the donor strength of the LX ancillary ligands, pic < sal ≈ acac.[31, 50, 53] Following this study by Thompson *et. al.*, a large number of research groups have reported the synthesis of heteroleptic $[Ir(C^N)_2(L^X)]$ complexes with emission spanning the visible spectrum.[50, 54-57]

Heteroleptic bis-cyclometallated iridium(III) complexes incorporating neutral N^N ancillary ligands have also been investigated. Introduction of neutral N^N ancillary ligands gives cationic iridium(III) complexes. The preparation of such complexes is carried out using a synthetic procedure similar to that employed in the synthesis of $[Ir(C^N)_2(L^X)]$ complexes, as shown in Figure 18. Compared with the preparation of neutral heteroleptic iridium(III) complexes, cationic complexes can often be synthesised in good yields under milder conditions with the final complexes commonly isolated as PF_6 salts following a counter ion exchange reaction using saturated $KPF_{6(aq)}$ solution.[29, 58]

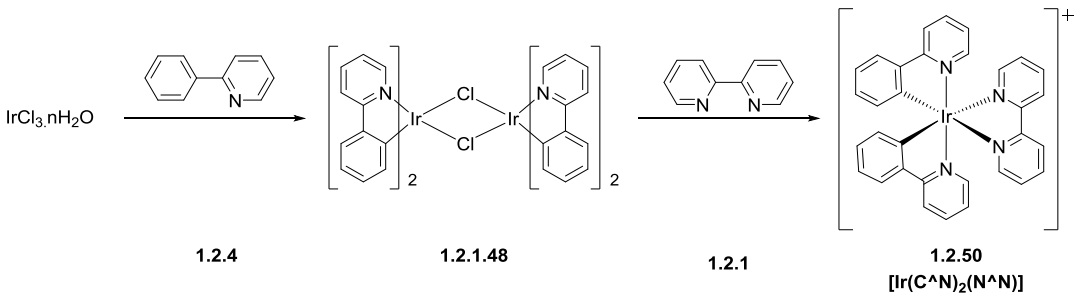

Figure 18: A reaction scheme to show the synthesis of heteroleptic $[Ir(C^N)_2(N^N)]^+$ complexes. Firstly, synthesis of the iridium(III) dichloro-bridged dimer is carried out via the reaction of IrCl3 with the cyclometallating ligand, in this case 2-phenylpyridine. Secondly, this dimer is cleaved using a neutral diimine ancillary ligand to give the cationic $[Ir(C^N)_2(N^N)]^+$ complex.[29]

Bernhard and co-workers reported a series of six cationic Ir(III) complexes showing emission across the visible spectrum from blue to red (Figure 19). The observation of both high-energy, vibrationally-resolved ^{3}LC bands and low-energy, broad ^{3}MLCT bands in the emission spectra suggests that the luminescence of these complexes originated from a mixed excited state.[29]

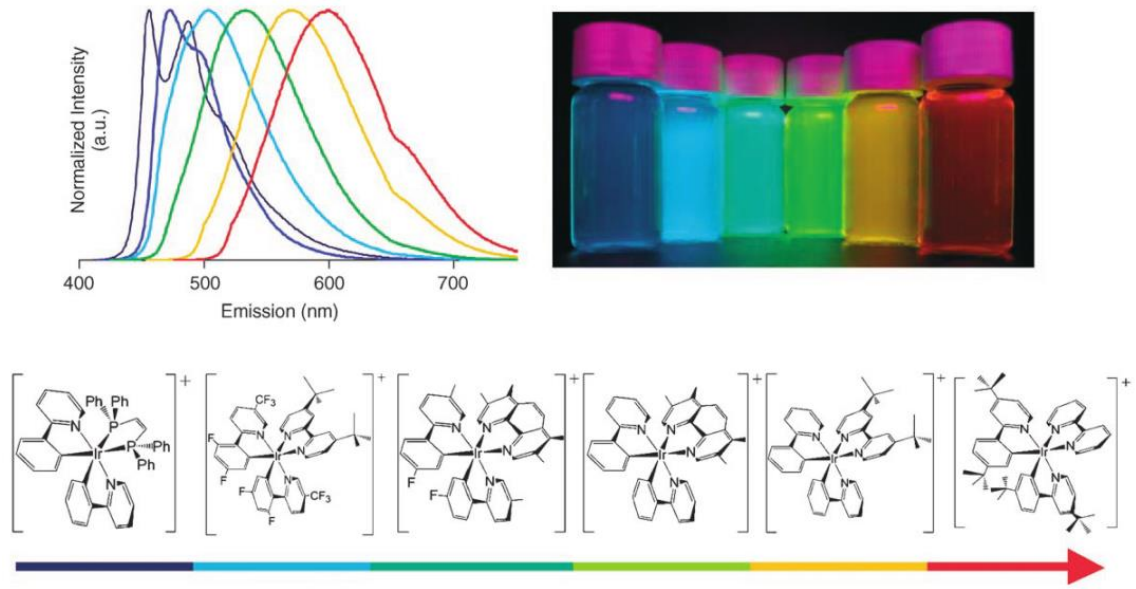

Figure 19: A figure to show a series of six cationic [Ir(C^N)$_2$(N^N)]+ complexes. The complexes exhibit emission across the visible spectrum from blue to red, as can be seen from the emission spectra shown.[29]

As shown above, the photophysical characteristics of these heteroleptic complexes can be tuned in order for their application in optoelectronic devices. In 2014, Iha and co-workers reported a series of four cationic iridium(III) complexes displaying emission ranging blue-green (522 nm) to orange (602 nm). The structure of these cationic complexes are shown in Figure 20. These complexes have quantum yields ranging from ϕ = 0.23–0.96 and luminescence lifetimes in the microsecond range. It was reported that the excited state from which these complexes emit was mainly ^{3}MLCT$_{Ir(ppy)\rightarrow N^N}$ in character.[59]

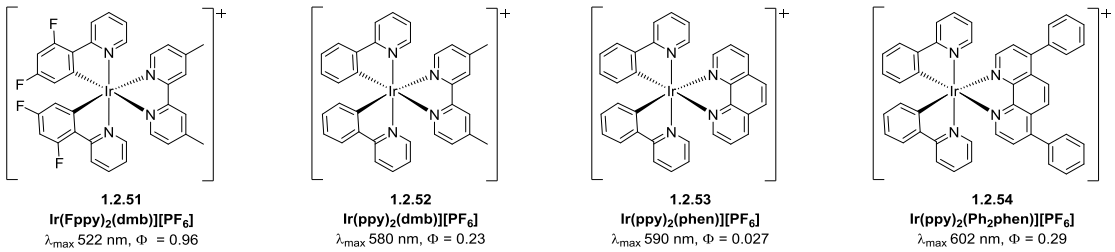

Figure 20: A figure to show the structures of cationic iridium(III) complexes prepared by Iha and co-workers. The structures of both the cyclometallating and diimine ancillary ligand are altered, resulting in complexes exhibiting emission varying from blue-green to orange.[59]

A further series of cationic iridium(III) complexes were prepared by Zysman-Colman *et. al.* as shown below in Figure 21. Through the substitution of one, two or three methoxy- groups on the cyclometallating ligand, the emission of these complexes was shifted significantly to the red. This series of complexes display red to near-infrared emission with wavelengths ranging from 595 nm to 730 nm. Unfortunately, the quantum yields obtained for this series of red emitters are relatively low, between ϕ = 0.15–0.001, and the luminescence lifetimes are very short (ns). The observation of low quantum yields, relative to the blue-green emitter discussed above, is consistent with the energy gap law.[60]

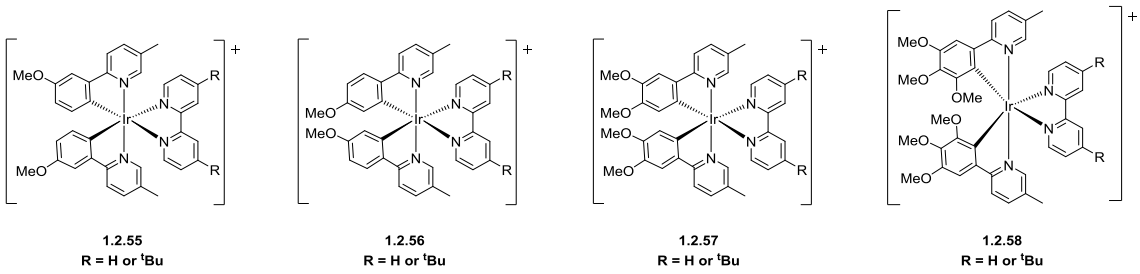

Figure 21: A figure to show the series of eight complexes prepared by Zysman-Colman and co-workers in 2015.[60]

The photophysical characteristics and colour tunability of the heteroleptic iridium(III) complexes discussed in this section have led to this class of cyclometallated iridium(III) complexes being widely investigated for use in an array of applications.

In this section, monometallic homo- and heteroleptic complexes of Pt(II) and Ir(III), incorporating a variety of cyclometallating and ancillary ligands, have been discussed. As has been previously

stated, many of these complexes are ideal candidates for utilisation as emitters in optoelectronic devices such as OLEDs, amongst many other applications. The strategies that can be used to tune the photophysical properties of such complexes will be discussed further in section 1.2.3.

1.2.2 Platinum(II) and Iridium(III) Complexes of Cyclometallating Terdentate Ligands

There are three classes of cyclometallating terdentate ligands that have been utilised in the preparation of cyclometallated transition metal complexes of Pt(II) and Ir(III); N^N^C, C^N^C and N^C^N. In this section, the focus will be on N^C^N-coordinating ligands.

Terdentate ligands have a number of advantages over their bidentate counterparts. It is known that non-radiative decay is favoured if there is large distortion of a complex on going from the ground state to the excited state. The amount of distortion can be decreased by increasing the rigidity of a system. Therefore, to reduce non-radiative decay and improve the photophysical properties of a transition metal complex, it is beneficial to increase the rigidity. Terdentate ligands are inherently more rigid than bidentate ligands and consequently, can give complexes with higher luminescence efficiencies. Cyclometallating ligands with tridentate coordination also give complexes with higher chemical and thermal stability and for metals such as iridium(III), such ligands also offer a route achiral complexes.[61]

Many research groups have focused on the synthesis of platinum(II) complexes of cyclometallating terdentate ligands in recent decades.

Che *et. al.* investigated Pt(II) complexes of the general formula, [Pt(N^N^C)Cl] and reported a series of complexes in which the N^N^C-coordinating ligand was derived from 6-phenyl-2,2′-bipyridine bearing different substituents at the 5-position of the central pyridyl ring. This class of N^N^C ligands combines the cyclometallating ability of 2-ppy with the π-acceptor properties of 2-bpy. The series of complexes prepared by Che and co-workers is shown in Figure 22. Figure 22 also shows the absorption and emission spectra of complex **1.2.61**. These neutral Pt(II) complexes are air and moisture stable showing photoluminescence at room temperature, both in solution and solid state. Only a very small variation in emission maxima (562 -568 nm) was

observed on variation of the substituent on the central pyridyl ring. The lack of a trend in emission maxima suggests that there may be very limited electronic communication between the substituent and the Pt-N^N^C core. The emission spectra recorded show broad, structureless peaks, indicative of emission from an MLCT state. The luminescence lifetimes are in the microsecond range (0.52-1.47 μs) and the quantum yields were measured in the range ϕ = 0.025-0.068. Despite the low quantum yields, these complexes show improved photophysical properties relative to Pt(II) complexes of 2,2′:6′,2″-terpyridine. A further study of this class of [Pt(N^N^C)X] complexes by Che *et. al.*, showed that replacement of the monodentate chloride ligand with a monoanionic isocyanide ligand results in higher quantum yields (ϕ = 0.060–0.11). This is likely due to the strong ligand field of the R-N≡C ligand.[62-64]

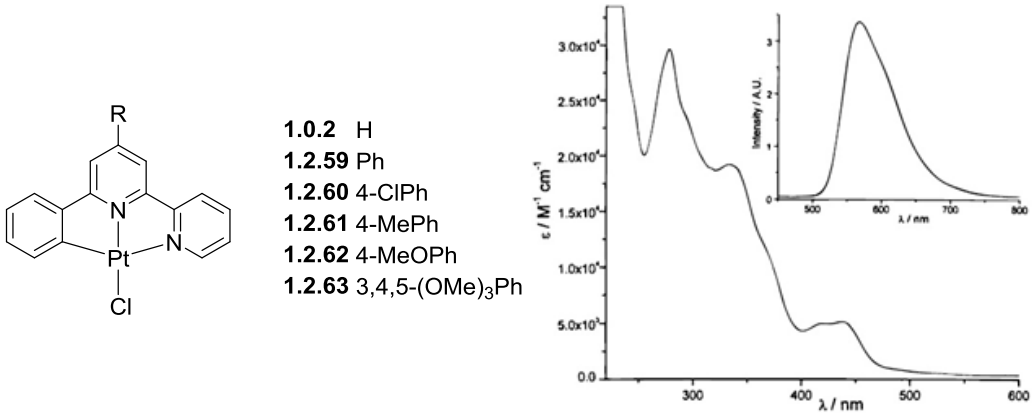

Figure 22: A figure to show the series of [Pt(N^N^C)Cl] complexes studied by Che and co-workers. The absorption and emission spectra of complex **1.2.61** recorded in CH_2Cl_2 at 298 K.[62]

Studies carried out by a large number of research groups have shown that Pt(II) complexes of N^N^C ligands exhibited emission from triplet charge transfer excited states whereas the luminescence displayed by complexes of C^N^C ligands was assigned as originating from a perturbed $^3\pi$-π^* (LC) state. Despite all the research into Pt(II) complexes of N^N^C and C^N^C-coordinating terdentate ligands, the luminescence of Pt(II) complexes of N^C^N terdentate ligands were not investigated prior to 2003.[18]

In 2003, Williams *et. al.* reported the photophysical properties of a platinum(II) complex of N^C^N-coordinating ligand 1,3-dipyridylbenzene (dpyb). Cárdenas first prepared this complex

in 1999.[65] The synthetic method used by Williams and co-workers for the preparation of [Pt(dpyb)Cl] and derivatives bearing substituents at the 5-position of the central phenyl ring is shown in Figure 23.[18]

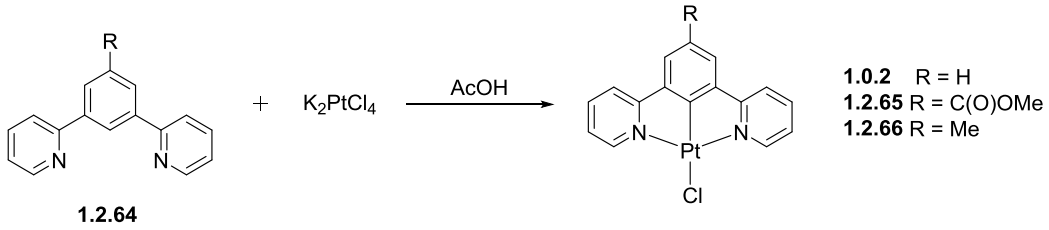

Figure 23: The synthetic route used in the preparation of luminescent platinum(II) complexes. The terdentate proligand was reacted with K_2PtCl_4 in acetic acid at reflux for 3 days. The desired complexes were isolated as yellow solids in yields ranging from 40-59%.[18]

This new class of luminescent platinum(II) complexes were found to be highly emissive in solution with quantum yields significantly higher than previously reported Pt(II) complexes of terdentate ligands (ϕ = 0.58–0.68 in degassed CH_2Cl_2). The complexes display highly-structured emission spectra with maxima increasingly red-shifted as the electron-donating character of the substituent increases (C(O)OMe < H < Me). This, along with the small Stokes shift observed and the relatively long luminescence lifetimes (7.0-8.0 μs), suggests that the emission originates from an excited state with primarily $^3\pi$-π^* (LC) character.

Platinum(II) complexes of N^C^N-coordinating terdentate ligands exhibit superior photophysical properties compared with complexes of N^N^C and C^N^C ligands. It was proposed by Williams *et. al.* that the N^C^N ligand has a stronger ligand field which helps to raise the MC d-d states, removing this pathway of non-radiative decay within the resulting Pt(II) complexes. Additionally, for the [Pt(N^C^N)Cl] complexes, there is an improved ability to tune the absorption and emission properties over a wide range (~ 5000 cm^{-1}) via the variation in the substituents on the terdentate ligand. These photophysical properties result in these complexes being ideal candidates for applications such as OLEDs and bioimaging. Continued research into Pt(II) complexes of terdentate N^C^N ligands has focused on the optimisation of their photophysical properties for such applications. This has been done by further variation of ligand substituents or through the replacement of the monodentate chloride ligand with alternative monodentate ligands, both

neutral and anionic (eg. pyridine and PhO^-), shifting the emission further to the blue or to the red.[18, 21, 61, 66-68]

The reports highlighting the favourable effects of terdentate N^C^N ligands on complexes of Pt(II) have led to the widespread study of iridium(III) complexes incorporating N^C^N-coordinating terdentate ligands. In 2004, Williams *et. al.* reported the first example of a charge-neutral, cyclometallated Ir(III) complex in which the metal centre is bound to a terdentate N^C^N ligand. The structure of the iridium(III) complex and the synthetic route utilised in its preparation is shown in Figure 24.[25]

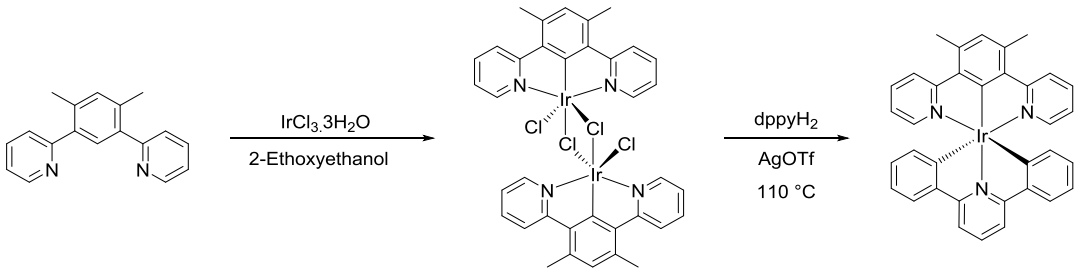

Figure 24: A reaction scheme to show the synthetic method used in the preparation of the first example of a cyclometallated Ir(III) complex incorporating a terdentate N^C^N-coordinating ligand. The first step is the synthesis of the dichloro-bridged iridium(III) dimer and is analogous with the preparation of dichloro-bridged dimers of cyclometallating, bidentate ligands. The second step involves the reaction of the dimer with molten 2,6-diphenylpyridine at 110 °C, in the presence of silver triflate.[25]

In the synthesis of this bis-terdentate Ir(III) complex, in order to ensure terdentate binding of the N^C^N ligand, it is necessary to incorporate substituents at the 4- and 6-positions of the central phenyl ring. The presence of substituents at these positions ensures that the competitive bidentate binding observed for terdentate N^C^N ligands with iridium(III) is blocked. Using this method, the desired complex shown in Figure 24 was isolated as an orange solid.[17, 25, 27]

Investigation of the photophysical properties of this complex showed that the complex is strongly luminescent in degassed acetonitrile solutions with a broad, structureless emission maximum observed at 585 nm at 295 K. The complex has a luminescence quantum yield of $\phi = 0.21$ with an emission lifetime of 3.9 μs in degassed solution. The properties obtained indicate that the

emission originates from a primarily CT state. This bis-terdentate Ir(III) complex, being both charge neutral and an intense orange emitter, has desirable characteristics for use in OLEDs.[25] Since this first report, iridium(III) complexes of terdentate N^C^N ligands have been investigated by a number of research groups. A selection of the complexes reported are shown below in Figure 25.

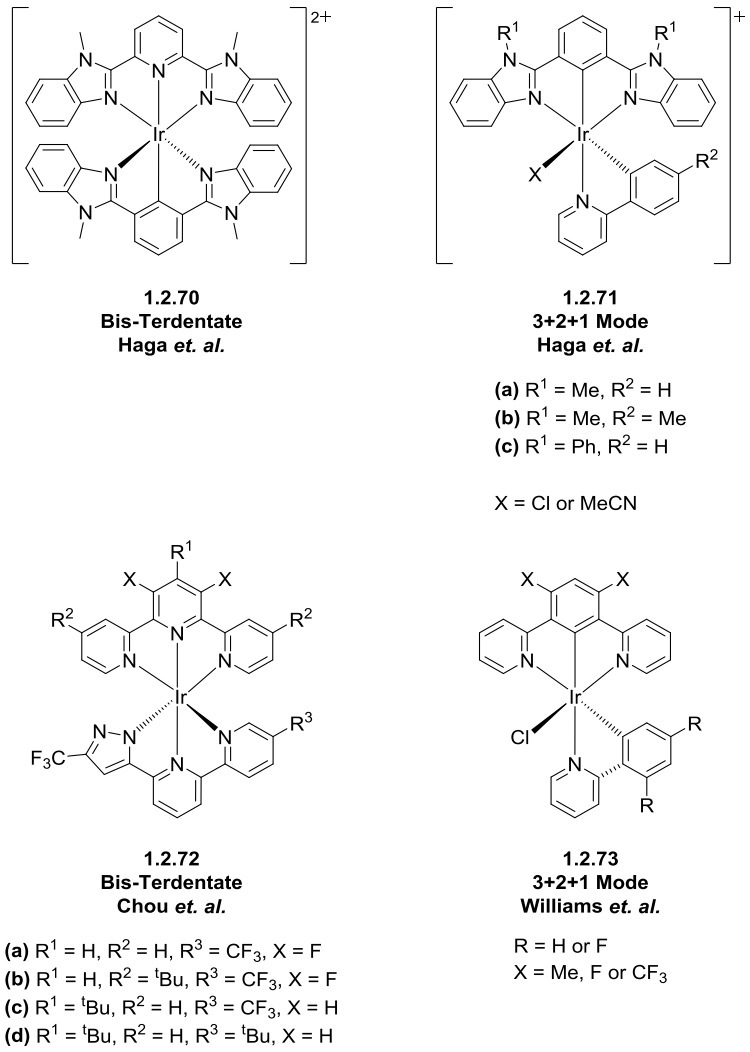

Figure 25: A figure to illustrate the structures of monometallic iridium(III) complexes, both cationic and neutral, incorporating terdentate ligands as reported by research groups in recent decades.[28, 30, 69, 70]

Following on from the work by Williams and co-workers, further bis-terdentate complexes have been reported. In 2005, Haga *et. al.* synthesised a highly luminescent bis-terdentate iridium(III) complex of the N^C^N-coordinating ligand 1,3-bis(1-methyl-benzimidazol-2-yl)benzene (Mebib). The second terdentate ligand incorporated into this complex was the N^N^N ligand 2,6-

bis(1-methyl-benzimidazol-2-yl)pyridine (Mebip). The coordination of both the monoanionic Mebib ligand and the charge-neutral Mebip to an iridium(III) centre leads to the formation of a cationic Ir(III) complex. This complex is an orange emitter with the emission maxima recorded at 593 and 623 nm. The quantum yield for this complex is comparable with the previously discussed bis-terdentate complex (ϕ = 0.10) and the luminescence lifetime was measured to be 1.6 μs. The photophysical data obtained indicates that emitting state has mixed ^{3}LC and ^{3}MLCT character.[69] Further research into bis-terdentate iridium(III) complexes was carried out by Chou and co-workers in 2015. A series of charge-neutral complexes was prepared in which the 3+ charge on the metal centre was balanced by coordination to one monoanionic N^C^N ligand, derived from 1,3-dipyridylbenzene, and a dianionic N^N^N ligand based on 2-pyrazol-3-yl-6-phenylpyridine. The series of complexes prepared by Chou *et. al.* exhibit intense phosphorescence across the visible spectrum, from green (490 nm) to red (600 nm). The emission maxima were tuned via substitution on the terdentate ligands N^C^N and N^N^N ligands. The luminescence quantum yields ranged from 0.22 to 0.72 and the emission lifetimes were measured in the range ϕ = 0.81–3.37 μs. This class of highly luminescent, chemically robust bis-terdentate iridium(III) complexes shows good potential for use in OLEDs. A device reported in this work, using **1.2.72 (a)** showed an EQE of 12.1%.[70]

A second class of highly luminescent iridium(III) complexes incorporating terdentate N^C^N ligands were also reported alongside the bis-terdentate complexes previously discussed. In 2005, whilst investigating the bis-terdentate Ir(III) complexes, Haga and co-workers reported the synthesis of complexes in which the iridium centre was coordinated to one terdentate terpyridine-based ligand, a bidentate ligand derived from 2,2′-bipyridine and a monodentate chloride ligand (3+2+1 mode). It was observed that these mixed ligand environments led to cationic complexes with higher quantum yields than the bis-terdentate systems also investigated in this study (ϕ = 0.19 vs ϕ = 0.10).[69] Further investigation of such systems by Haga *et. al.* and Williams and co-workers was carried out. The complexes synthesised, in which the polypyridyl ligands were replaced with cyclometallating N^C^N- and N^C-coordinating ligands, are shown in Figure 25.

Such complexes are generally readily accessible from the dichloro-bridged iridium dimers as shown in Figure 26.[28, 30]

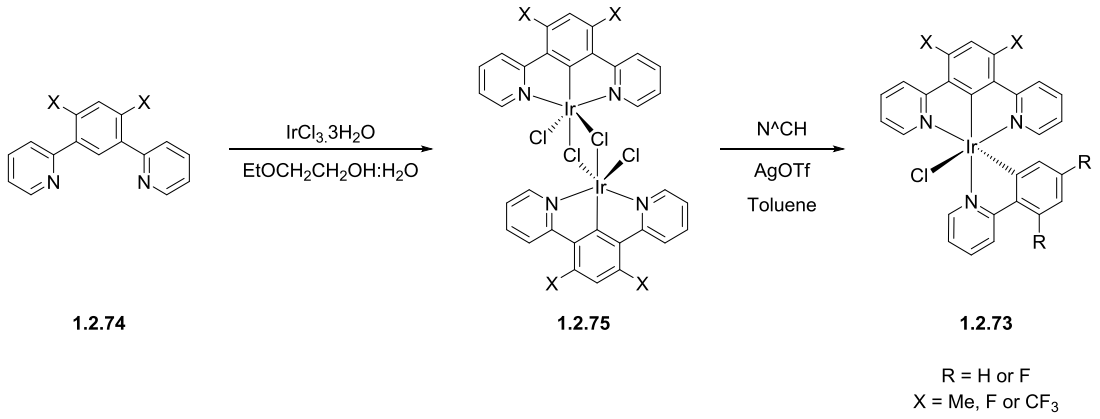

Figure 26: Synthetic route utilised in the preparation of the mixed ligand iridium(III) complexes reported by Williams and co-workers in 2012. The first step is formation of the dichloro-bridged iridium(III) dimer via the reaction of the terdentate N^C^N ligand with $IrCl_3.3H_2O$. Secondly, this dimer reacts with the selected bidentate ligand in the presence of AgOTf as a chloride scavenger. The desired 3+2+1 Ir(III) complexes were isolated in moderate to high yields (35-94%).[30]

The range of complexes prepared by Haga and co-workers (Figure 25) showed strong orange emission with quantum yields in the range $\phi = 0.77–0.95$ for the neutral complexes and $\phi = 0.16–0.24$ for the cationic complexes in which X = MeCN. [Ir(Phbib)(ppy)Cl] showed the highest quantum yield of $\phi = 0.95$. Replacement of the monodentate chloride ligand with neutral MeCN was observed to drastically decrease the luminescence quantum yield. The luminescence lifetimes for all complexes were in the microsecond range. The series of mixed-ligand 3+2+1 complexes prepared by Williams *et. al.*, with terdentate ligands derived from 1,3-dipyridylbenzene, also showed significantly higher emission quantum yields than previously studied bis-terdentate complexes ($\phi = 0.20–0.70$). These complexes were shown to be highly luminescent in degassed CH_2Cl_2 solution at room temperature with the emission maxima tunable from blue to red (476-593 nm) through modulation of the ligand substitution pattern. As a result of their excellent photophysical properties, the complexes reported by Williams and co-workers were successfully employed in the fabrication of highly efficient OLEDs showing EQEs between 1.3–10.9%. The performance of these OLED devices is comparable and, in some cases, is superior to that observed for tris-bidentate iridium(III) complexes such as *fac*-$Ir(ppy)_3$. The presence of both a terdentate

N^C^N ligand and a bidentate N^C-coordinating ligand in the mixed ligand systems discussed here offers additional opportunities for fine-tuning the emission energy, resulting in additional control over the photophysical properties.[28, 30]

The complexes of platinum(II) and iridium(III) discussed in this section, incorporating terdentate N^C^N ligands, have been shown to be highly luminescent with high quantum yields and relatively short emission lifetimes. The emission wavelengths can be successfully tuned across the entire visible spectrum through the systematic functionalisation of the cyclometallating ligands on the metal centre. Overall, in this section it has been shown that complexes of cyclometallating terdentate ligands are comparable or superior to the best emitters reported with bidentate ligands.

1.2.3 Colour Tuning Strategies for Cyclometallated Complexes

As mentioned previously, colour tuning of the absorption and emission of cyclometallated transition metal complexes is possible as the HOMO and LUMO of the cyclometallating ligands are localised on separate moieties; with the HOMO being primarily associated with the metal centre and the metallated aryl ring and the LUMO localised on the heterocyclic ring. Therefore, substituents introduced onto the aryl ring predominantly influence the energy of the HOMO whereas substituents introduced onto the heterocyclic ring primarily affect the LUMO. The addition of electron-withdrawing substituents (eg. -F, -CF_3, -CN) generally stabilise molecular orbitals while electron-donating groups (eg. -alkyl, -NH_2, -NR_2) normally destabilise molecular orbitals. Consequently, this simplified concept of colour tuning, within cyclometallated complexes of transition metals such as platinum(II) or iridium(III), leads to strategies that can be applied to tune the emission from blue to red.

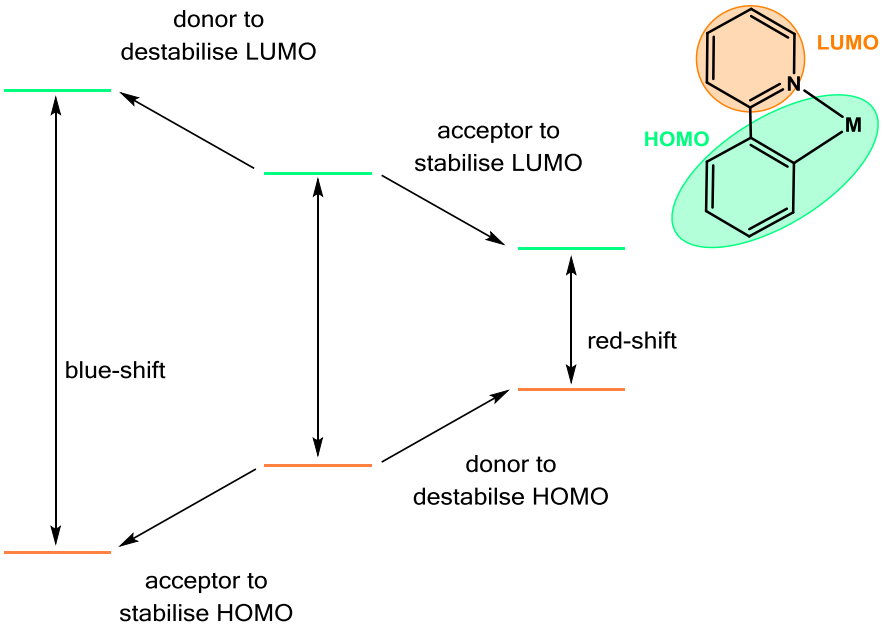

Figure 27: A figure to illustrate the colour tuning strategies that can be utilised through independent modulation of the HOMO and LUMO energies.

As is shown in Figure 27, a blue-shift in the emission can be achieved either by the addition of electron-withdrawing groups to the aryl ring to stabilise the HOMO or electron-donating groups to the heterocyclic ring to destabilise the LUMO. This results in an increase in the HOMO-LUMO gap and a blue-shift. In addition, a blue-shift can also be achieved by replacing the heterocyclic ring (eg. pyridine) with more electron-rich azeheterocycles such as pyrazole. Figure 28 shows that substitution of fluoro- groups on the phenyl ring of the cyclometallating ring results in a blue-shift of 42 nm. A larger blue-shift of 60 nm is observed on the substitution of the pyridine ring for pyrazole. The effects of these colour tuning methods are additive and therefore, when both the aryl ring and the heterocyclic ring are altered, the blue-shift observed is larger still (102 nm, comparing the emission of $Ir(dfppz)_3$ (390 nm) and $Ir(ppy)_3$ (492 nm) at 77 K).[24, 48]

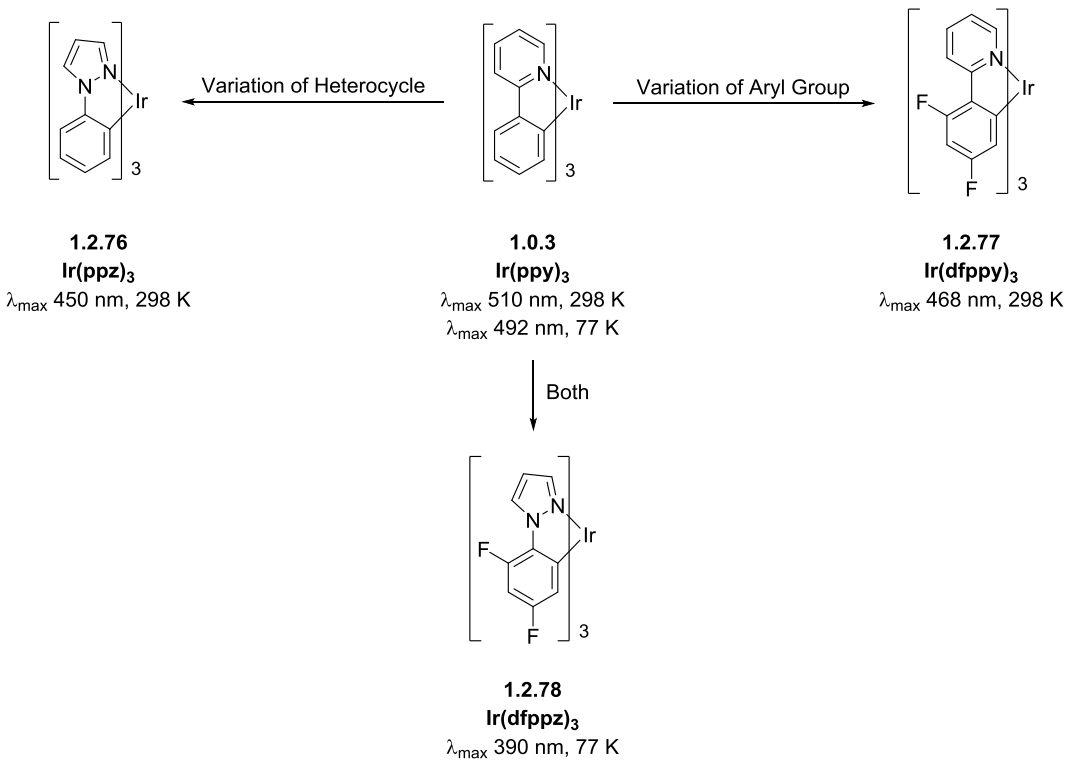

Figure 28: Strategies for blue-shifting the emission of cyclometallated metal complexes by raising the LUMO and lowering the HOMO.[24, 48]

As discussed in previous sections of this review, factors such as ligand field strength and the rigidity of the final complex can have a significant effect on the photophysical properties observed. The preparation of efficient blue emitters has proved to be a challenge. This is likely due to the fact that the increased HOMO-LUMO gap required for high-energy blue emission leads to the emitting state being closer to the deactivating MC d-d states. This often leads to a reduction in quantum yields as the emission is shifted to the blue. Therefore, in order to obtain efficient blue emitters, it is particularly important to incorporate cyclometallating ligands with high ligand field strengths capable of providing rigidity to the final complex. The bidentate Pt(II) complex shown in Figure 29 has the required combination of electron-withdrawing and electron-donating groups, on the aryl and pyridyl rings respectively, to lead to emission in the deep blue region of the spectrum. The blue-shift observed, relative to Pt(ppy)(acac), is accompanied by a substantial decrease in quantum yield. The Pt(II) complex incorporating the related terdentate N^C^N ligand shows efficient blue emission at room temperature with a quantum yield of $\phi = 0.60$. This is as a

result of the stronger ligand field provided by the cyclometallating N^C^N ligand and the inherent rigidity of such terdentate ligands.

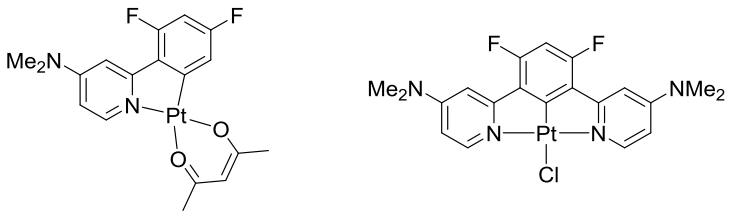

1.2.79
λ_{max} 440 nm at 77 K
$\Phi < 10^{-3}$

1.2.80
λ_{max} 453 nm at 298 K
$\Phi = 0.60$

Figure 29: A figure to illustrate the importance of high ligand field strength and rigidity in the preparation of efficient blue emitters.[68]

In order to achieve a red shift in the emission, it is necessary to incorporate electron-donating groups onto the aryl ring, destabilising the HOMO, or to add electron-withdrawing groups to the heterocyclic ring to stabilise the LUMO. This gives a decrease in the HOMO-LUMO gap and a red-shift. In addition a red-shift can be achieved by incorporating cyclometallating ligands with increasingly extended conjugation. As the conjugation length of a molecule increases, the HOMO-LUMO gap decreases resulting in a shift of the absorption and emission to the red.

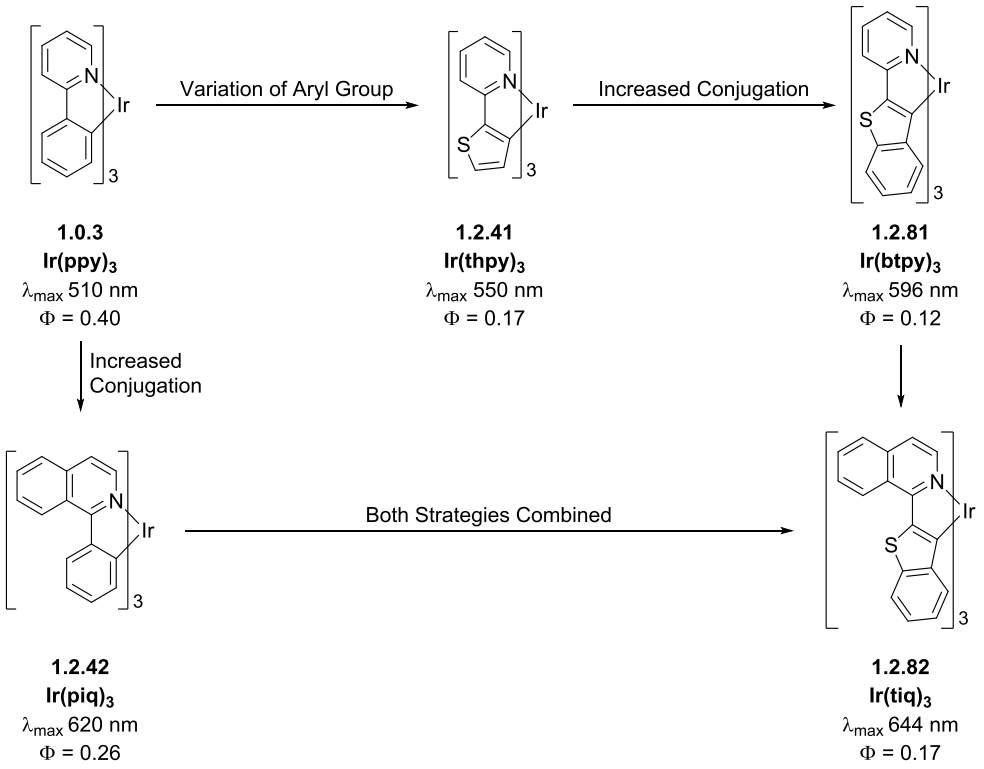

Figure 30: Examples to illustrate some of the strategies that can be used to red-shift the emission of cyclometallated complexes.[47]

As is shown in Figure 30, the replacement of the phenyl ring in $Ir(ppy)_3$ for a more electron-rich thiophenyl ring in $Ir(thpy)_3$ results in a red-shift of 40 nm. Increasing the conjugation of $Ir(thpy)_3$ to give $Ir(btpy)_3$ gives a further red shift of 46 nm, giving orange emission at λ_{max} = 596 nm. A larger red-shift of 110 nm, relative to $Ir(ppy)_3$, can be achieved by replacing the pyridyl moiety with an isoquinoline unit leading to emission in the red region of the spectrum (λ_{max} = 620 nm). Again, the effects of strategies to red-shift the emission are additive and therefore, through combining increased conjugation on both the heterocyclic and aryl moieties with a more electron-rich aryl ring, a substantial bathochromic shift is observed resulting in emission in the red region (λ_{max} = 644 nm).[47]

As the emission wavelength of a complex shifts to the red, the luminescence quantum yield tends to decrease in agreement with the energy gap law. As the HOMO-LUMO energy gap becomes smaller, non-radiative decay of the excited state energy via vibrations is more allowed. The complexes shown in Figure 30 show a decrease in quantum yield as the conjugation length of the molecule is extended. Increasing the conjugation raises the energy of the HOMO and this can lead

to a decrease in the orbital contribution to the lowest excited state from the metal centre. As a result, the triplet state becomes increasingly like an organic triplet. Therefore, it can be concluded that adding an increasing number of conjugating groups will not lead to efficient red emitters.

These colour-tuning strategies are widely used in the preparation of complexes of transition metals, such as platinum(II) and iridium(III), that exhibit absorption and emission wavelengths across the entire visible spectrum.

1.3 Multimetallic Transition Metal Complexes

The design of luminescent multinuclear complexes of transition metals, particularly of ditopic polypyridyl bridging ligands, is widely studied in coordination chemistry. Such complexes are important in areas of catalysis, supramolecular chemistry, as functional materials, in molecular recognition and in optoelectronic devices.[71-78] Multimetallic complexes have a number of advantages over their mononuclear counterparts. Improved light-harvesting can be achieved as multinuclear complexes have increased molar extinction coefficients relative to monometallic complexes and frequently have lower energy absorption maxima. This property is especially important in applications such as solar energy conversion and photocatalysis.[79-82] Additionally, the presence of a second metal facilitates spin-orbit coupling and increases the radiative rate constant leading to more efficient phosphorescence from triplet states for multimetallic complexes.[83]

There is a wide variety of bridging ligands utilised in the preparation of polymetallic emitters. The specific bridging ligand selected can have significant effects on the chemical and photophysical properties of the final complex. In systems with bridging ligands that incorporate large, flexible spacer groups, holding the metal centres far apart, the metal-containing units retain their individual properties. Complexes of this type are used to investigate electron- or energy-transfer between the metal-containing units. In contrast to this, in multinuclear systems in which the two metal ions are held in close proximity and both bound to a common heterocyclic ring, the

properties of the final complex are substantially different from the analogous mononuclear complexes.[72, 83-85]

Many of the multimetallic complexes reported in the literature were initially based on Ru(II) polypyridyl units with metals such as Os(II) and Re(I) often also incorporated. Increasingly, due to the excellent excited-state properties of cyclometallated complexes of Pt(II) and Ir(III), metal-containing units of Pt(II) and Ir(III) have been increasingly utilised in the preparation of multinuclear complexes.

There are a variety of bridging ligands available, varying from those offering bis-monodentate bridges between metal centres to those acting as bis-tetradentate bridging ligands. In this section, multimetallic complexes incorporating cyclometallated platinum(II) and iridium(III) units linked by such bridging ligands will be discussed.

1.3.1 Monodentate Bridged

Multinuclear complexes in which the metal centres are bridged by ligands offering bis-monodentate coordination have been studied by a number of research groups. The bridging ligands of this kind reported in the literature vary from cyanide to poly-N-heterocyclic carbenes and are utilised to link two or more metal centres in the preparation of both homo- and heterometallic complexes.[62, 72, 86-89]

Dinuclear complexes of platinum(II) have been studied in order to investigate the intramolecular excimer/aggregate formation possible via metal-metal and/or ligand-ligand (π-π) interactions. The formation of excimers or aggregates, possible with square planar Pt(II) d^8 complexes, has been widely studied for white-light generation in optoelectronic devices.[72, 90] In 1999, Che and co-workers reported the preparation of diplatinum complexes in which the cyclometallated Pt(N^N^C) units were linked by a diphosphine or pyrazole, as shown in Figure 31. These complexes all display photoluminescence with photophysical properties differing as a function of bridging ligand. For the complex $[(Pt(N^N^C))_2(dppm)]^{2+}$, it was concluded that Pt-Pt interactions were occurring between the two Pt(II) centres. In the absorption spectra, a moderately intense band above 400 nm was observed and assigned to $^1[d\sigma^* \rightarrow \pi^*]$. Broad, structureless

emission was observed with a peak maximum at 652 nm, attributed to a ^{3}[dσ*, π*] excited state. In addition, the emission was red-shifted at 77 K, thought to be due to the shortening of Pt-Pt contacts with lattice contraction. For the diplatinum(II) complex, $[(Pt(N^N^C))_2(dppC_n)]^{2+}$, there is a larger separation between the two platinum(II) centres as a result of the longer carbon chain of the diphosphine bridging ligand. In contrast to the previous complex, the absorption spectrum for $[(Pt(N^N^C))_2(dppC_n)]^{2+}$ showed no moderately intense band above 400 nm and on cooling to 77 K, the emission observed was blue-shifted, showing different behaviour than was observed for the ^{3}[dσ*, π*] excited state in $[(Pt(N^N^C))_2(dppm)]^{2+}$. Therefore, it was concluded that there were no Pt-Pt interactions in this bimetallic Pt(II) complex and the emission for this complex was assigned to a ^{3}MLCT excited state. In the case of the pyrazole-linked complex, there are negligible Pt-Pt interactions observed at room temperature. At 77 K it is thought that the intramolecular separation between [Pt(N^N^C)] units may decrease sufficiently to give weak π-π interactions. This is confirmed by the observation of low-energy shoulders in the solution and solid-state emission spectra at 77 K. This work by Che *et. al.* shows that the bridging ligand incorporated into a multinuclear complex can have a significant effect on photophysical properties of the resulting complex.[62]

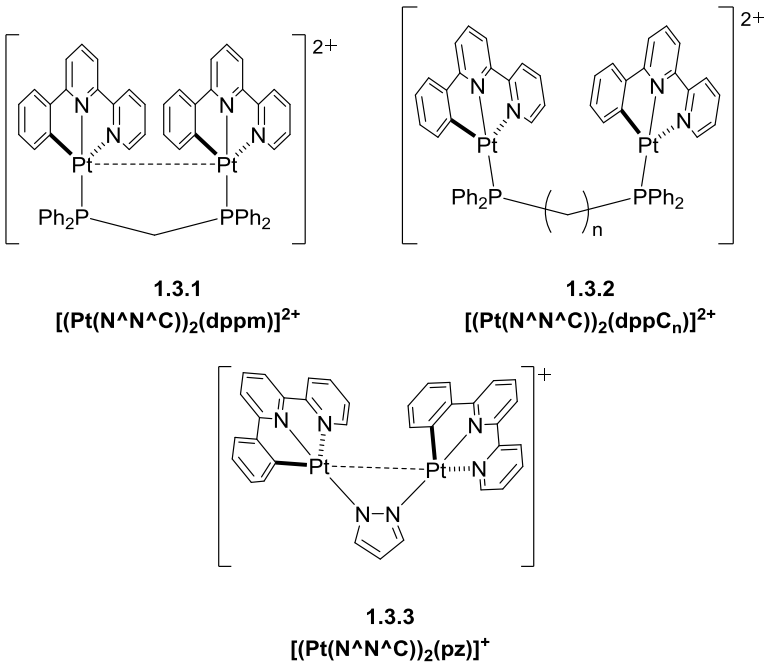

1.3.1
$[(Pt(N^N^C))_2(dppm)]^{2+}$

1.3.2
$[(Pt(N^N^C))_2(dppC_n)]^{2+}$

1.3.3
$[(Pt(N^N^C))_2(pz)]^{+}$

Figure 31: A figure to illustrate the structures of binuclear platinum(II) complexes reported by Che *et. al.* in 1999. The complexes were isolated in high yields (53-79%) by reaction of the monometallic precursor with the appropriate diphosphine or pyrazole bridging ligand.[62]

Similar results were obtained by Thompson and co-workers in the study of pyrazole-linked di-platinum(II) complexes as shown in Figure 32. It was observed that simple synthetic control of the extent of Pt-Pt interactions could be achieved through variation of the substituents present on the bridging ligands.[86]

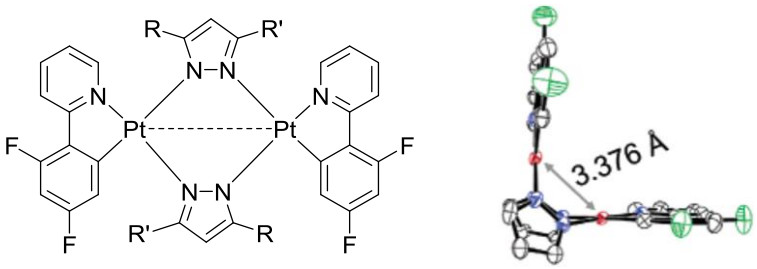

1.3.4

(a) R = H, R' = H
(b) R = Me, R' = Me
(c) R = ^{t}Bu, R' = Me
(d) R = ^{t}Bu, R' = ^{t}Bu

Figure 32: The structures of pyrazole-linked dinuclear platinum(II) complexes reported by Thompson and co-workers with a side view of **1.3.1.4 (a)** to illustrate the potential for Pt-Pt interactions, dependent on the R groups present on the bridging ligands.[86]

The incorporation of more sterically demanding R groups at the 3- and 5-positions of the pyrazolate bridges was found to force the two Pt(C^N) units closer together, therefore enhancing the Pt-Pt interactions. For example, the Pt-Pt distance in complex **1.3.4 (a)** where R/R′ = H is 3.376 Å whereas for complexes **1.3.4 (c)** and **1.3.4 (d)**, the Pt-Pt distances are decreased to 3.046 Å and 2.834 Å respectively. This decrease in Pt-Pt manifests itself in the observation of an additional lower energy band between 400 and 500 nm in the absorption spectra for **1.3.4 (c)** and **1.3.4 (d)**, assigned to singlet metal-metal-to-ligand charge transfer (MMLCT) transitions. These broad absorption bands are red-shifted as the Pt-Pt distance is decreased, demonstrating that the energy of the ^{1}MMLCT state is highly dependent on the intramolecular separation between the two platinum(II) centres. The control over the photophysical properties that these bis-monodentate pyrazolate ligands afford to the final complexes make this type of dinuclear complexes ideal candidates for a range of applications.[86]

Homometallic dinuclear iridium(III) complexes incorporating bis-monodentate bridging ligands have also been reported. The linear, ambidentate ligand cyanide was used as a ditopic bridging ligand to link bis-cyclometallated iridium(III) units in the preparation of a tetranuclear Ir(III) complex, reported by Nazeeruddin *et. al.* in 2011. The two-dimensional tetranuclear complex was isolated in high yield (74%) using the synthetic procedure shown in Figure 33. The complex is highly luminescent (λ_{em} = 496, 521 nm, ϕ = 0.66) with the photophysical characteristics observed being largely similar to the analogous monometallic complex.[87]

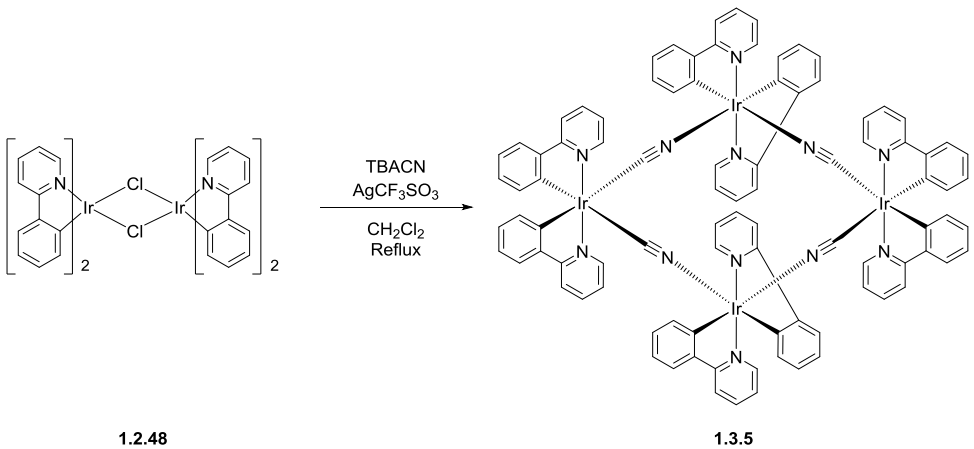

1.2.48 **1.3.5**

Figure 33: The synthetic route used in the preparation of the two-dimensional tetranuclear iridium(III) reported by Nazeeruddin and co-workers. The complex was isolated as a yellow solid in high yield (74%).[87]

Alkynyl ligands form strong σ M-C and η---(M) bonds and therefore, have a relatively strong ligand field. Consequently, such ligands have been successfully employed as auxiliary ligands in the synthesis of luminescent metal complexes of transition metals such as Pt(II) and Au(III).[91-98] Combining the benefits of alkynyl ancillary ligands and cyclometallated Ir(III) complexes, Lalinde and co-workers reported the first examples of dinuclear Ir(III) complexes in which the two metal centres are linked by η^2 alkynyl bridging ligands, as shown in Figure 34. All of the bimetallic complexes are emissive in fluid solution at room temperature and at 77 K. The emission spectra are broad and featureless with maxima ranging between 505 and 515 nm at 298 K. Theoretical calculations carried out by Lalinde *et. al.* suggest that the emission originates from an excited state with mixed ^{3}MLCT/^{3}LLCT character. The quantum yields for these complexes are in the range ϕ = 0.007–0.024. These values are relatively low and it has been suggested that the flexibility of these systems in solution leads to efficient non-radiative decay.[88]

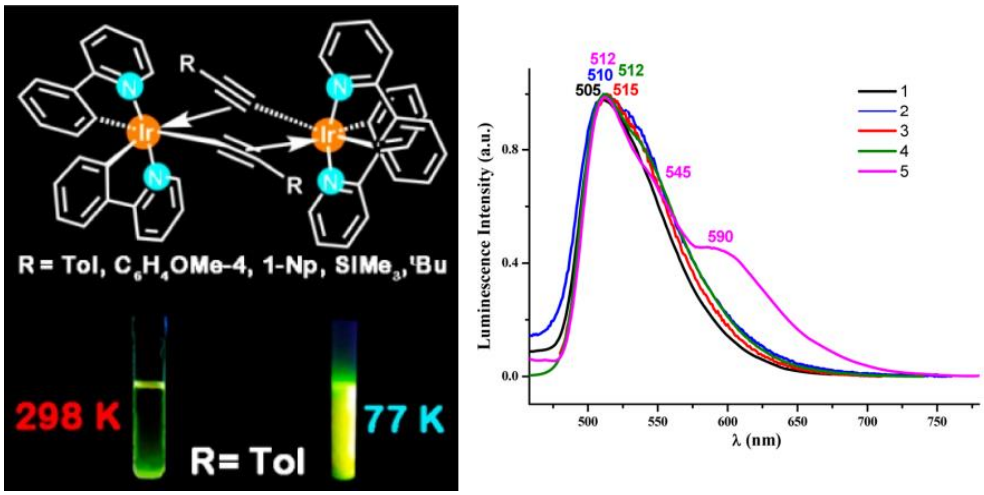

Figure 34: The alkynyl-bridged dinuclear iridium(III) complexes (left), in which the R-group on the ancillary alkynyl ligand are varied, all show emission in solution at room temperature and at 77 K. The emission spectra of these complexes measured at 298 K in CH_2Cl_2 for R = Tol, C_6H_4OMe-4 and 1-Np and in THF for R = $SIMe_3$ and ^{t}Bu are shown (right).[88]

It was shown by Lalinde and co-workers that the alkynyl ligands utilised to bridge Ir(III) centres in the dinuclear complexes shown above did facilitate electronic communication between the two metal centres. Alkynyl groups were also incorporated into the bridging ligand used by Williams

et. al. in the preparation of a heterotrimetallic complex of Ir(III), Pt(II) and Au(III) in 2015. This complex was studied in relation to white-light generation from a single multinuclear complex with the electronic communication between the three metal centres investigated. As shown in Figure 35, the three cyclometallated metal centres in this trinuclear complex were linked via a 1,3,5-triethynylbenzene core. Electronic communication was also facilitated by this bridging ligand, as can be concluded from the emission spectra obtained, although the trimetallic complex still retains the properties of the monometallic units it is comprised from. Dual emission was observed, containing bands assigned to the iridium and platinum components. These bands appear as a broad peak at 577 nm, originating from the Pt(II) moiety, with a shoulder at higher energy, assigned to emission from the Ir(III) unit. There was no higher energy emission detectable from the Au(III) component at room temperature. These observations are indicative of energy transfer from the Au moiety to the Ir and Pt units. Williams and co-workers suggested that this occurs via Förster resonance energy transfer (FRET) with a significant contribution from through-bond Dexter energy transfer.[72]

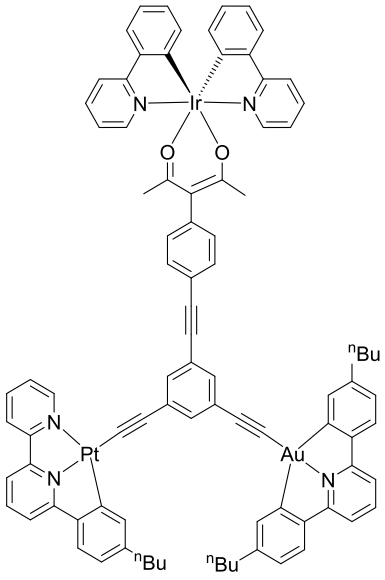

1.3.6

Figure 35: The structure of the heterotrimetallic reported by Williams *et. al.* in 2015 in which the metal centres are linked through a 1,3,5-triethynylbenzene core. [72]

The bridging ligand linking the three metal-containing units in this complex showed minimal conjugation and as a result, the metal complexes retained much of their individual character. In order for efficient white light generation to be obtained, with emission observed from all three moieties, further improvements must be made.[72]

A further class of strong-field ligands popular in the synthesis of transition metal complexes are N-heterocyclic carbenes (NHCs). Such ligands have previously been used in the preparation of bimetallic complexes of Pt(II) and Au(III). In 2016, Peris and co-workers reported the synthesis of a dinuclear Pt(II) complex in which the cyclometalled platinum(II) fragments are linked via pyrene-bis-N-heterocyclic carbene bridging ligands, as shown in Figure 36. This complex displayed strong luminescence with vibronically-resolved emission bands observed between 372 and 437 nm. The quantum yield of this complex (ϕ = 0.031) is relatively low in comparison to other cyclometallated Pt(II) complexes, but higher than those complexes with similar pyrene-based bis-NHC ligands. The photophysical properties observed, including a luminescence lifetime in the nanosecond range, suggest that the luminescence exhibited has fluorescent character with the excited state localised on the pyrene-based bridging ligand. It was found that there was very little participation from the cyclometallated platinum(II) fragments. Consequently, Peris *et. al.* were unsuccessful in preparing efficient phosphorescent emitters utilising NHC-based bridging ligands.[89]

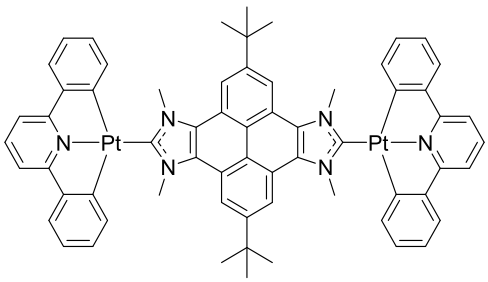

1.3.7

Figure 36: The structure of the dinuclear platinum(II) complex prepared by Peris *et. al.*, in which the two metal centres are linked via the bis-monodentate pyrene-bis-N-heterocyclic carbene ligand.[89]

From the multinuclear complexes discussed in this section, with metal centres linked via bis-monodentate bridging ligands, it is possible to conclude that the class of bridging ligand incorporated has a substantial effect on the properties of the final complex and whether efficient phosphorescence is observed.

1.3.2 Bidentate Bridged

A more widely studied class of bridging ligands utilised in the preparation of multimetallic complexes is those offering bidentate coordination to multiple metal centres. There are a variety of common bidentate binding modes that have been previously employed within such bridging ligands, including N^N, N^C, N^O and O^O.

By far the most intensively investigated of these binding modes is the N^N mode, for which a wide range of polypyridyl ligands have been utilised. A selection of the bridging ligands utilised in the preparation of multinuclear complexes are shown in Figure 37.

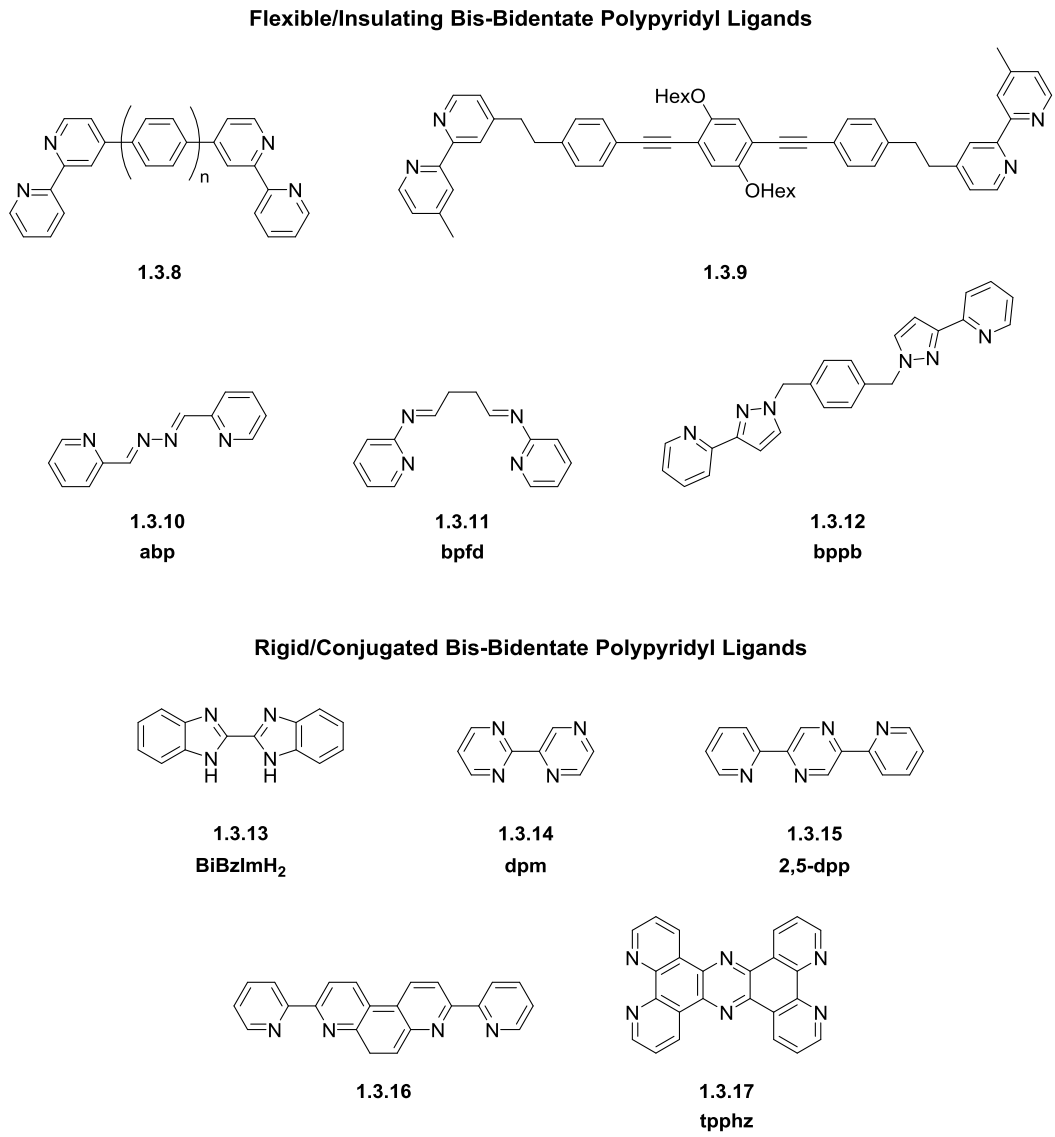

Figure 37: A figure to show a selection of the bis-bidentate polypyridyl ligands used in the preparation of multinuclear complexes. The range of ditopic ligands includes both flexible and rigid ligands that are both non-conjugated and conjugated.[78, 99-109]

Bis-bidentate ligands bearing 2,2′-bipyridine binding sites separated by phenylene or phenyleneethynylene spacer units have been used to prepare both homo- and hetero- multimetallic complexes of Ru(II) and Ir(III), in which the length of the insulating spacer groups was varied. These types of complexes were synthesised by De Cola and co-workers and Williams *et. al.* using a 'complex as ligand' approach and in situ Suzuki cross-coupling reactions of complexes respectively. The separation between the metal-containing units in these multinuclear assemblies, imposed by such polypyridyl bridging ligands, leads to the observation of fast and efficient electronic energy transfer within the heterometallic complexes, from the cyclometallated Ir(III)

centres to the Ru(II) moiety. The rapid energy transfer to the Ru(II) centre was found to be unaffected by the length of the spacer unit of the bridging ligand. This energy transfer process can be rationalised by considering the energies of the excited states for the corresponding mononuclear complexes for each metal-containing unit within an assembly. Although the bridging ligands bearing phenylene-based spacer groups provide sufficient electronic communication for efficient energy transfer, they also provide insulation meaning that each component within the heterometallic assemblies retains the photophysical properties of the corresponding monometallic complex.[78, 99-101, 110]

Utilising more flexible and, in some cases non-conjugated, bridging ligands, such as the abp, bpfd and bppb linkers shown in Figure 37, enabled further investigation of the effect of increased spacer length and extent of conjugation on the properties of dinuclear iridium(III) complexes. Comparing complexes of **1.3.10** and **1.3.11**, the shorter and more conjugated bridging ligand (**1.3.10**) gives an Ir-Ir separation of 5.124 Å relative to 6.996 Å with **1.3.11**. The closer proximity of the metal centres and conjugation in the abp-linked di-iridium complex allows electronic communication between the cyclometallated Ir(III) centres, resulting in red-shifted charge-transfer absorption bands and the appearance of an additional band above 450 nm.[102] The dinuclear Ir(III) complex prepared using the non-conjugated bppb bridging ligand shows photophysical properties consistent with the findings discussed above. The lack of electronic communication between the metal centres in such multinuclear complexes leads to absorption and emission properties similar to that observed for the related mononuclear complexes.[103]

When the metal centres of multinuclear complexes are linked via more rigid, conjugated polypyridyl bridging ligands it is observed that the chemical and photophysical properties of the resulting complexes are significantly different from the corresponding monometallic complexes. For example, the bimetallic complex in which Ir(tfmpyb) [tfmpyb = 1,3-di(2-pyridyl-4,6-bis(trifluoromethyl))benzene] units were linked by bridging ligand BiBzIm (Figure 37) was found to have substantial electronic coupling between the iridium centres, accounting for the difference in absorption and emission observed for the mono- and dinuclear complexes. A cationic dinuclear iridium(III) complex prepared by Zysman-Colman *et. al.*, incorporating 2,5-dpp [2,5-dpp = 2,5-

dipyridylpyrazine] as the bridging ligand, also showed significantly different photophysical properties with respect to the analogous mononuclear complex. A large red-shift in the emission (~ 125 nm) was observed at 77 K on going from the mono- to the dinuclear complex, with the emission maxima for the bimetallic complex observed at 715 nm. No emission was detected at room temperature for the dinuclear Ir(III) complex. It is thought that emission from excited state of the di-iridium complex at room temperature is quenched as a result of non-radiative decay, consistent with the large red-shift observed and the energy gap law.[104-106] Further multinuclear complexes of cyclometallated Ir(III) subunits have been synthesised using rigid, conjugated polypyridyl bridging ligands with the final complexes displaying properties beneficial for use in both molecular devices and bioimaging.[107, 108, 111]

In comparison to polypyridyl linked multimetallic complexes, there are relatively few examples of multimetallic complexes in which the metal centres are linked via a cyclometallating bridging ligand. In 2004, Tsuboyama *et. al.* reported the synthesis of dinuclear iridium(III) complexes in which $Ir(ppy)_2$ fragments were linked via the cyclometallating bridging ligand, 1,4-bis(pyridin-2-yl)benzene (BPB) as shown in Figure 38. This complex could only be isolated in very small yield following separation of the mixture of diastereoisomers formed. Comparing the photophysical properties of the dinuclear complex to the related mononuclear complex, $Ir(ppy)_3$, it was observed that the emission of the di-iridium complex is significantly red-shifted (~ 150 nm) and shows a much smaller quantum yield ($\phi_p = 0.040$ compared with $\phi_p = 0.97$ for $Ir(ppy)_3$). From the emission spectra and the short luminescence lifetime recorded for this complex, emission is assigned to a ^{3}MLCT excited state.

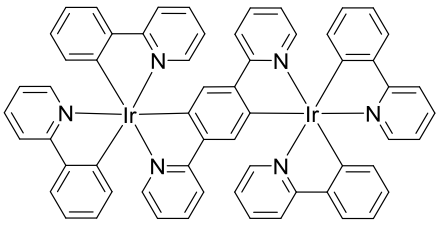

1.3.18
$(ppy)_2Ir(BPB)Ir(ppy)_2$

Figure 38: The structure of the dinuclear iridium(III) complex reported by Tsuboyama and co-workers in 2004, utilising the cyclometallating bis-bidentate bridging ligand BPB to link the two cyclometallated Ir(III) centres.[112]

Following on from this, Kozhevnikov and co-workers reported di-platinum(II) complexes and mixed-metal Pt(II)/Ir(III) complexes wherein the metals are rigidly-linked through pyrimidine- and pyrazine-based cyclometallating bridging ligands, as shown in Figure 39. Using these bridging ligands, two metal centres are coordinated to a common heterocyclic ring, facilitating electronic communication and allowing conjugation of the LUMO across the entire aromatic system of the C^N^N^C bridging ligand. Consequently, this leads to luminophores that have intrinsically different properties from the related mononuclear complexes in which the separate metallic units do not retain their individual identities. It was observed in the study of these complexes that the introduction of additional metal centres allows further control over the photophysical properties of the resulting multinuclear complexes. With respect to their monometallic analogues, red-shifted absorption and emission maxima were observed for all of the bi- and trimetallic complexes. This is due to the delocalisation of the LUMO which results in its stabilisation and a decrease in the HOMO-LUMO gap. Additionally, the incorporation of additional metal centres was seen to increase the radiative rate constants despite the red-shift. Ordinarily, a decrease in the value of k_r would be expected with decreasing energy of emission in agreement with the energy gap law. It is thought that this effect could be due to the increase in spin-orbit coupling resulting from the presence of a second heavy metal ion. In conjunction with this, non-radiative decay is kept to a minimum by the rigidity of the systems and therefore, the quantum yields of these multinuclear complexes are high, even in the red region of the spectrum (ϕ = 0.36–0.41). The excellent photophysical properties obtained for this class of cyclometallated complexes mean that they are ideal candidates for use in an array of applications.[84, 85]

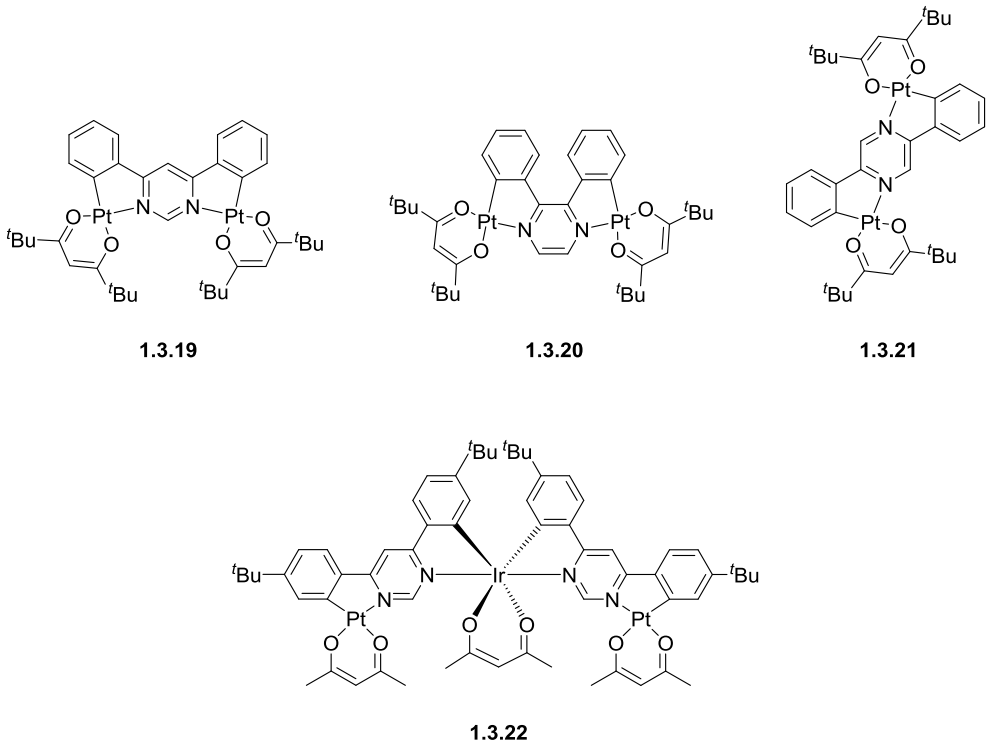

Figure 39: A figure to illustrate the structures of the multimetallic complexes prepared by Kozhevnikov *et. al.* in which the metal centres are linked via cyclometallating bis-bidentate bridging ligands, through a common heterocyclic ring.[84, 85]

The pyrimidine ring has been further employed in the preparation of cyclometallated multinuclear complexes as shown by Zhou and co-workers in 2016. Zhou *et. al.* reported the synthesis of a dinuclear complexes in which the metal centres are linked via the cyclometallating bridging ligand 2-(4-(*tert*-butyl)-phenyl)pyrimidine (Figure 40). The complexes showed highly efficient orange (580 nm) and red (603 nm) luminescence for R = H and R = F respectively, with quantum yields ranging from ϕ = 0.43–0.68 in solution. Again, the emission for the dinuclear complexes is significantly red-shifted relative to the corresponding mononuclear complexes (~ 80 nm). The bimetallic complexes reported by Zhou and co-workers were applied to OLEDs resulting in devices exhibiting the highest EQEs recorded for di-iridium(III) complexes (17.9% for **1.3.24**).[113, 114]

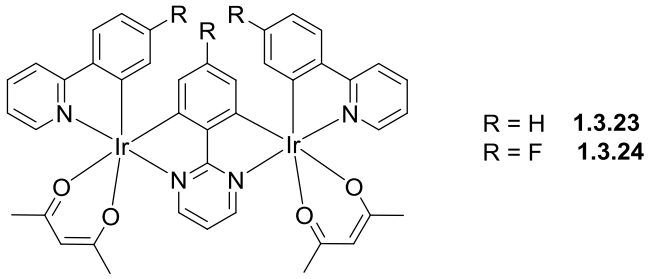

Figure 40: The structure of the dinuclear iridium(III) complexes reported by Zhou and co-workers, using the cyclometallating bridging ligand 2-(4-(*tert*-butyl)-phenyl)pyrimidine to rigidly link the two metal centres.[113]

In 2017, Kozhevnikov and co-workers further demonstrated the potential of pyrimidine-based ligands in the preparation of highly luminescent multinuclear complexes and reported the synthesis of a tetrametallic mixed Pt(II)/Ir(III) complex exhibiting emission in the red region of the spectrum (λ_{em} = 611 nm) with a high quantum yield of ϕ = 0.76.[115]

In addition to polypyridyl and cyclometallating bridging ligands offering bis-bidentate binding sites, ditopic ligands with N^O and O^O binding sites (Figure 41) have also been used in the preparation of multinuclear complexes.

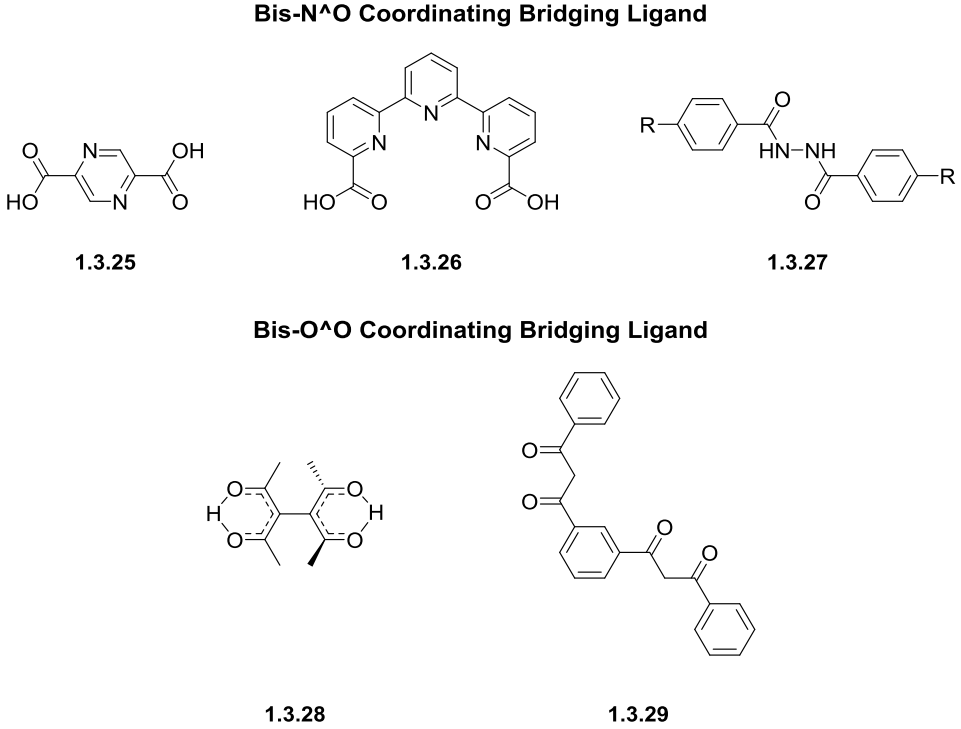

Figure 41: A selection of the bis-bidentate bridging ligands bearing N^O and O^O binding sites utilised in the preparation of homometallic di-Ir(III) and heterometallic Ir(III)/Pt(II) complexes.[116-121]

Dinuclear iridium(III) complexes in which cyclometallated Ir(III) units are linked via rigid bis-N^O bridging ligand have been prepared by a number of research groups. Mazzanti and co-workers reported a di-iridium(III) complex bridged by a ligand based on terpyridine-carboxylate whilst Bryce *et. al.* prepared a bimetallic complex of iridium(III) linked through a non-innocent diarylhydrazide bridging ligand. The resulting multinuclear complexes synthesised using these rigid bis-N^O ligands were isolated in moderate to high yields (30-86%) with facile separation of diastereoisomers for the diarylhydrazide-linked complex achieved. The photophysical properties observed for these bis-N^O-bridged complexes are distinct from the analogous monometallic complexes, displaying red-shifted, tunable emission with high quantum yields. This shows that such complexes have potential for application in optical devices. Bryce and co-workers employed the diarylhydrazide-linked dinuclear complex $(ppy)_2Ir(\mu\text{-}L)Ir(ppy)_2$ in an OLED device, from which high efficiency green emission was obtained (EQE = 11%).[117, 118]

Ditopic bridging ligands incorporating O^O bidentate coordination sites have also been utilised in the preparation of multinuclear complexes, including those of cyclometallated Pt(II) and Ir(III) subunits (Figure 41). Bridging ligands incorporating diketonate binding sites have been particularly important. In 2008, Thompson and co-workers reported the synthesis of platinum dyads, linking cyclometallated Pt(II) centres via a bridging ligand composed of two 2,4-pentadione (acac) units covalently linked at the 3-position. The homodyads displayed photophysical properties that closely resembled those of the equivalent mononuclear complexes, although presence of the bridging ligand does increase the radiative rate constant of the dyads relative to the monometallic analogues. Contrastingly, the heterodyads undergo efficient energy transfer, governed by the electronic coupling allowed between the two metal-containing units via the bridging ligand. The bridging ligand was also found to play a key role in the photophysical properties observed for multinuclear complexes reported by Do *et. al* in 2010. The cyclometallated Pt(II) and Ir(III) centres were linked via a 1,3-bis(3-phenyl-3-oxopropanoyl)benzene bridging ligand offering two diketonate binding sites separated by a phenylene spacer. The resulting bimetallic complexes showed weak red emission in solution (λ_{em} = 615 nm) with quantum yields in the range ϕ = 0.0023–0.0030. In solution, the lowest excited

state has a major contribution from the ^{3}LX state localised on the bridging ligand. The emission observed in the solid state was much more intense (λ_{em} = 570 nm), likely as a result of ^{3}MLLCT transitions resulting from the interaction of pyridine rings in the peripheral cyclometallated Ir(III) units present.[120, 121]

1.3.3 Terdentate Bridged

Terdentate ligands, as discussed previously, have structural advantages over ligands offering coordination with lower denticities. The use of bridging ligands offering terdentate binding sites have been investigated by several research groups for the preparation of multinuclear complexes. Bis-terdentate bridging ligands offering two terdentate coordination sites are commonly employed, with those based on N^N^N, N^N^C and N^C^N coordination being the most widely investigated.

Ditopic bridging ligands based on the polypyridyl ligand terpyridine have been utilised in the preparation of dinuclear iridium(III) and platinum(II) complexes as shown in Figure 42.

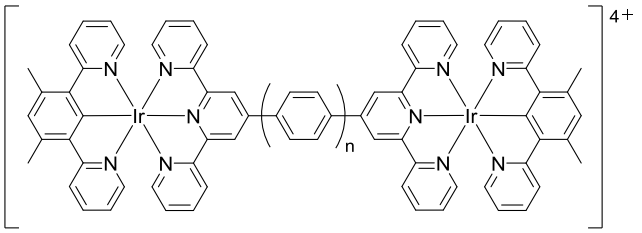

1.3.30
(dpyx)Ir(tpy-ph$_n$-tpy)Ir(dpyx)
n = 0, 1, 2

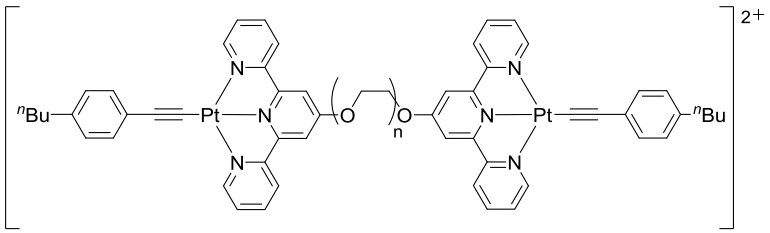

1.3.31
LPt(tpy-(OCH$_2$CH$_2$)$_n$O-tpy)PtL
n = 1, 2, 3, 4

Figure 42: A figure to show the structures of dinuclear complexes of Ir(III) and Pt(II) in which the cyclometallated metal-containing units are linked via terpyridine-based bridging ligands.[12, 122]

For the Pt(II) complex shown in Figure 42, the optical properties were not investigated although self-assembly through intramolecular interactions of the metal-containing subunits was observed, dependent on bridge length and temperature. On the other hand, for the dinuclear Ir(III) complex, the photophysical properties were studied with emission observed from charge transfer states between 600-620 nm. Only the complex of the short tpy-tpy bridging ligand showed appreciable phosphorescence at room temperature. This emission is observed to be slightly red-shifted relative to the mononuclear analogue, likely due to the strong electronic delocalisation across the bridging ligand. This effect is reduced in the bimetallic complexes of longer bridging ligands and therefore, only very weak luminescence is observed that is similar to that observed for the corresponding monometallic complexes.[12, 122]

Although a large number of structures have been reported incorporating terpyridine-based terdentate ligands, these complexes are rarely luminescent at room temperature. Therefore, as previously discussed, the use of terdentate cyclometallating ligands is advantageous. Cyclometallating bis-terdentate bridging ligands bearing two N^N^C- or N^C^N-coordinating binding sites have also been utilised in the synthesis of multimetallic complexes of Ir(III) and Pt(II) as shown in Figure 43.[83]

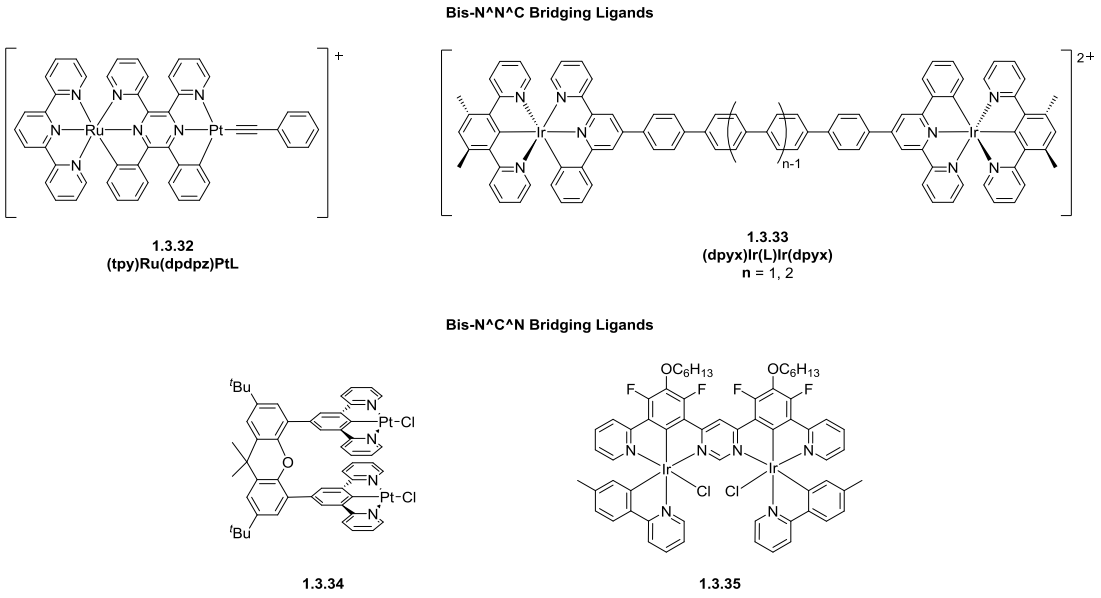

Figure 43: Structures of multimetallic complexes in which the cyclometallated Pt(II) and Ir(III) centres are linked via cyclometallating bis-terdentate bridging ligands bearing N^N^C or N^C^N binding sites.[83, 123-125]

In 2011, Abruña and co-workers reported the synthesis of the heterobimetallic Pt(II)/Ru(II) complex bridged by the cyclometallating bis-N^N^C ligand 2,3-di(2-pyridyl)-5,6-diphenylpyrazine (dpdpz). This complex was observed to emit in the near-infrared (NIR) region of the spectrum (780 nm) with a quantum yield higher than that of the related mononuclear ruthenium(II) complex (ϕ = 0.0015 vs. 0.00057). It was suggested that this may be due to efficient energy transfer from the Ru(II) centre to the Pt(II) unit.[124] Earlier, in 2008, Williams *et. al.* reported the synthesis of dinuclear iridium(III) complexes linked via a bridging ligand bearing two-N^N^C separated by a tri- or tetraphenylene spacer group. The emission spectra recorded for these di-iridium(III) complexes showed emission in the red region of the spectrum (λ_{em} = 632-633 nm, ϕ = 0.027), thought to originate from a $^3\pi$-π^* state at 298 K. As observed for the similar bis-bidentate bridged complexes discussed in section 1.3.2, the large phenylene spacer groups of the bridging ligands result in these dinuclear complexes displaying photophysical properties similar to those of the mononuclear complexes.[123] Williams and co-workers also reported the synthesis of a di-platinum(II) complex in which the metal centres were each cyclometallated by an N^C^N-coordinating binding site and rigidly-linked via a xanthene core (Figure 43). Within this complex, the two platinum centres are held in a face-to-face arrangement enabling intramolecular Pt-Pt interaction to occur. The di-platinum(II) complex displayed deep red emission in solution at room temperature (λ_{em} = 690 nm, ϕ = 0.20, τ = 1.7 μs) resulting from the formation of an intramolecular excimer between the two metal-containing subunits. The relatively high luminescence efficiency, despite the low energy of the emission, demonstrated that exploiting intramolecular excimer formation may be a useful strategy by which to obtain efficient red emitters.[126] Ditopic terdentate N^C^N bridging ligands were also used in the preparation of dinuclear iridium(III) complexes reported by Kozhevnikov *et. al.*, with an example shown in Figure 43. These rigidly-linked complexes in which the Ir(III) centres are linked via a common heterocyclic ring showed red luminescence equal to some of the best red emitters in the literature (λ_{em} = 625 nm, ϕ = 0.65, τ < 1 μs). Based on the photophysical properties observed, these di-iridium(III) complexes are extremely strong candidates for use as dopants in OLEDs or as sensitisers in applications such as dye-sensitised solar cells (DSSCs) or photocatalysis.[83]

1.3.4 Tetradentate Bridged

Compared to all classes of bridging ligand previously discussed in this literature review, there are very few examples of bis-tetradentate bridging ligands. There are currently no reports of cyclometallating bis-tetradentate bridging ligands in the literature.

Figure 44 shows the structure of a dinuclear platinum(II) complex reported by Houjou and co-workers in 2017. The di-Pt(II) complex is an example of a fused salen complex in which a bis-salen ligand, offering bis-tetradentate coordination, is utilised to rigidly-link two platinum centres leading to a highly stable bimetallic complex. Houjou *et. al.* investigated both the optical properties and the potential for Pt-Pt interactions within this complex to result in excimer formation and emission from MMLCT states.[127]

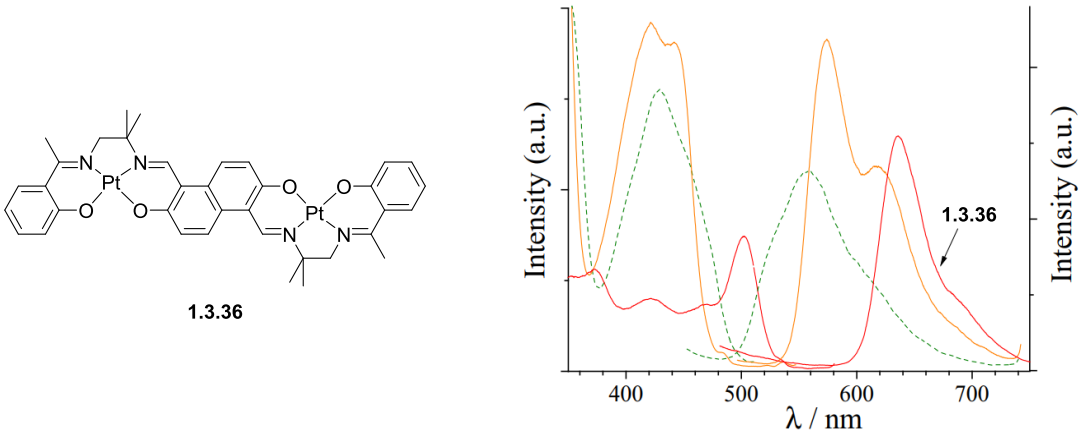

Figure 44: The structure of the dinuclear Pt(II) complex in which the two metal centres are linked via a salen-type bridging ligand offering bis-tetradentate coordination via two equivalent O^N^N^O binding sites (left). The emission spectra recorded for the di-platinum(II) complex, in *o*-dichlorobenzene solution, is shown as the solid red line, labelled **1.3.36**, in the spectra shown (right).[127]

The photophysical properties of the complex shown above were recorded in *o*-dichlorobenzene solution at room temperature. The bis-salen linked di-platinum(II) exhibited red phosphorescence centred at 636 nm with the low-energy tail extending to the NIR region of the spectrum. As can be seen in the emission spectra shown in Figure 44, the emission observed from this bimetallic Pt(II) complex is red-shifted by 62 nm relative to the corresponding monometallic complex PtL^{b}. The emission was assigned to a mixed ^{3}LC-^{3}MLCT excited state and with no emission bands attributable to ^{3}MMLCT transitions despite the close proximity of the Pt(II) centres (3.43 Å).

The rigid, conjugated bis-salen ligand utilised in the formation of this dinuclear platinum(II) complex results in a complex with advantageous structural and photophysical properties. This suggests further potential for investigation of bis-tetradentate ligands in the preparation of highly luminescent transition metal complexes.[127]

1.4 Applications of Luminescent Metal Complexes

Luminescent metal complexes of transition metals such as Pt(II) and Ir(III) have attractive chemical and photophysical properties that are extremely desirable for use in an array of applications, ranging from electroluminescent devices such as OLEDs to bioimaging and catalysis.

As mentioned in section 1.1.2, the heavy metal atoms within these systems have large SOC constants and therefore, are able to facilitate efficient intersystem crossing. Consequently, the spin selection rule becomes relaxed and the formally spin-forbidden $T_1 \rightarrow S_0$ transition can occur, leading to phosphorescence. The ability of a molecule to exhibit phosphorescence, harvesting both singlet and triplet excitons, means that 100% theoretical internal quantum efficiency is achievable.[96, 128]

In particular, complexes of cyclometallating ligands have been widely investigated for utilisation in the aforementioned applications. One of the attractions of such complexes is the ease with which the excited state properties can be tuned via simple ligand modifications. In addition to facile colour tunability, high quantum yields and luminescence lifetimes in the microsecond range are also advantages of cyclometallated transition metal complexes.

The utilisation of luminescent complexes of cyclometallating ligands in electroluminescent devices, such as OLEDs and LECs, as well as in bioimaging and as chemical sensors will be discussed in the following sections.

1.4.1 Organic Light-Emitting Diodes (OLEDs) and Light-Emitting Electrochemical Cells (LECs)

Electroluminescent devices such as organic light-emitting diodes (OLEDs), and light-emitting electrochemical cells (LECs), based on phosphorescent metal complexes, have attracted much attention due to their potential for application in large area displays and solid-state lighting. Electroluminescence in such devices arises from the radiative decay of excited states that are formed via the recombination of charge carriers, holes and electrons, injected from the anode and cathode respectively. As stated previously, the presence of a heavy metal atom enables both singlet and triplet excitons to be radiatively active. This phenomenon was first observed in the 1950s by Bernanose and co-workers.[3, 129, 130]

The first commercialised OLED was fabricated in 1987 by Tang and VanSlyke at Eastman, showing efficient low-voltage electroluminescence from a thin-film device.[3, 11] Since this first report, there has been a large number of successes in the fabrication of phosphorescent OLEDs (PhOLEDs), making use of heavy-metal triplet emitters. Baldo *et. al.* investigated the utilisation of the platinum(II) porphyrin complex, octaethyl-porphine Pt(II) (PtOEP), whereas, Thompson and Forrest fabricated highly-efficient devices incorporating cyclometallated iridium(III) complexes such as *fac*-Ir(ppy)$_3$ and Ir(ppy)$_2$(acac).[3, 49, 130-132]

OLEDs have a number of advantages over more traditional technologies, such as liquid crystal diplays (LCDs). For example, OLED devices can be produced from low-cost materials using fabrication methods suitable for scaling to large areas. This class of display does not require backlighting and light is only emitted from required pixels, therefore resulting in devices that are more efficient and capable of being much thinner and lighter. Additionally, due to the robustness of OLEDs, they may be deposited on a wide range of substrates, both rigid and flexible. These benefits have led to rapid development of this technology with OLEDs already widely utilised in displays for mobile phones and televisions.[11]

The general structure of a multilayer OLED is shown in Figure 45. The anode in these devices is generally indium tin oxide (ITO), whereas the cathode is usually a metal such as aluminium. The thin organic layers between the two electrodes promote more efficient injection of electrons and

holes towards the emissive layer. The structures of the organic compounds utilised in the conducting layers of the device are shown in Figure 46. The most important layer is the emissive layer, containing the organometallic transition metal complex as the emitter. The emitter can either be deposited directly between the charge transport layers or, as is more common, the emitter can be doped into a host material such as CBP, as is shown in Figure 46.[3, 11]

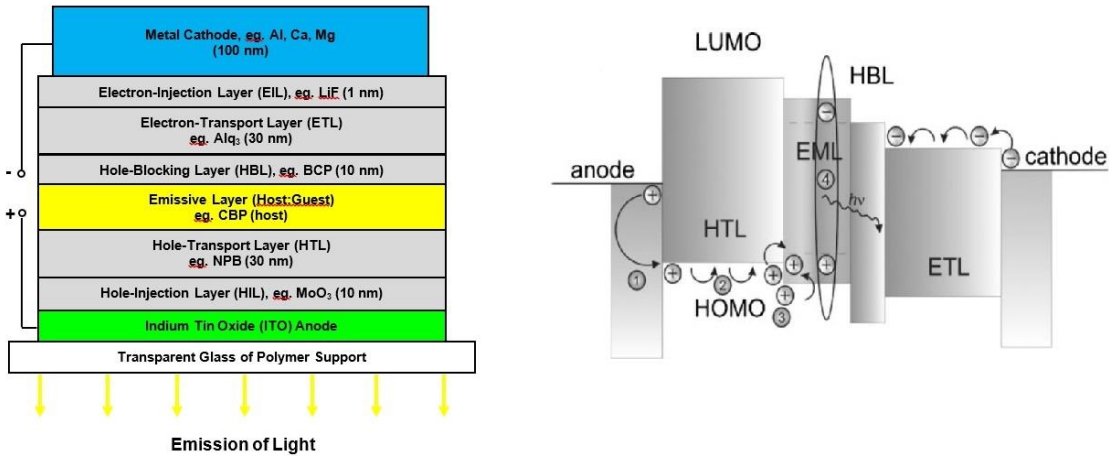

Figure 45: A schematic to show the structure of a typical multilayer OLED (left) and the idealised working principle of a multilayer device (right). Following the injection of charge carriers under the influence of an external electrical field from the cathode and anode (1) electron and hole transport occurs via a hopping mechanism along the LUMO and HOMO levels of the molecule, respectively. (2) Accumulation of the electrons and holes takes place in the emissive layer (3) Formation of excitons occurs (4) Excitons collapse resulting in the emission of light.[3, 11, 133]

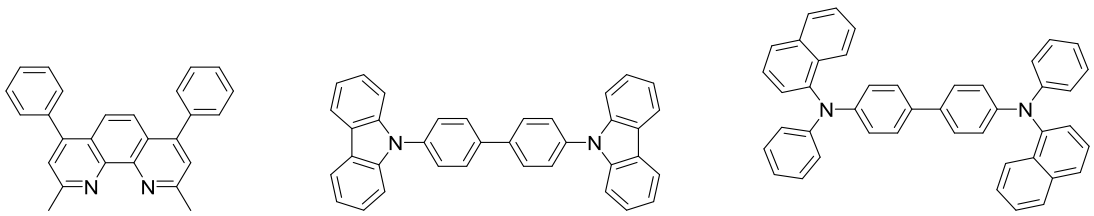

1.4.1 **BCP** **1.4.2** **CBP** **1.4.3** **NPB**

Figure 46: A figure to show the structures of the conjugated organic compounds utilised in the conducting layers of the OLED device as described above. Organic molecules other than those shown above can be utilised as hosts in the emissive layer and in the conducting layers of multilayer OLED devices.[3]

Using this type of device structure, various OLED devices have been fabricated including both those for full-colour displays and those emitting white light for use in solid-state lighting applications.

For multi-coloured displays, it is a requirement to incorporate OLEDs based on emitters displaying efficient blue (~450-470 nm), green (~500-550 nm) and red (~650-700 nm) emission.[11] Examples of cyclometallated iridium(III) complexes utilised as emitters in the fabrication of highly-efficient monochromatic OLEDs are shown in Figure 47. Adachi *et. al.* reported a green-emitting device incorporating $Ir(ppy)_2(acac)$ as the dopant and showing a maximum external quantum efficiency (η_{ext}) of 19.0% and a power efficiency (η_p) of 60 ± 5 lm W^{-1}. The highest efficiencies were obtained by doping the $Ir(ppy)_2(acac)$ in concentrations between 5-12%.[131] Green emitters generally have higher efficiencies relative to red and blue triplet emitters and as a result the fabrication of highly efficient red and, in particular, blue OLEDs has presented more of a challenge. The comparatively poor performance of red emitters can be explained using the energy gap law. A deep red PhOLED was obtained through the use of the tris-cyclometallated complex $Ir(piq)_3$ using a hybrid of triphenylamine/oxadiazole as the host material within the emitting layer. This device displayed an η_{ext} of up to 21.6% with a η_p of 16.1 lm W^{-1}.[134] The development of a true blue emitter with a high quantum yield is challenging as a result of the large energy gap required. This leads to the energy of the lowest excited state being in closer proximity to the deactivating ^{3}MC states giving a potentially thermally accessible pathway for non-radiative decay. A typical iridium(III) complex employed in blue OLEDs is FIrpic as shown below. This complex displays sky-blue emission. Utilising the complex $Ir(dfppy)(fppz)_2$, the fabrication of an device displayed deep blue phosphorescence was possible. This OLED showed a high external quantum efficiency of 8.5% and a power efficiency of 8.5 lm W^{-1}.[133, 135]

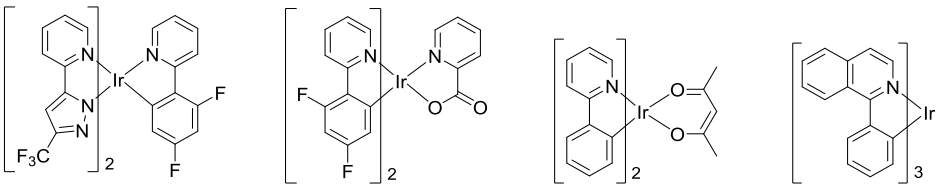

Figure 47: Examples of cyclometallated iridium(III) complexes that have been utilised in the fabrication of highly-efficient monochromatic OLED devices, exhibiting phosphorescence across the visible spectrum from blue (450 nm) to red (620 nm).[50, 54-57, 135, 136]

In addition to monochromatic OLEDs, there has been increased interest in white-emitting OLEDs (WOLEDs) due to their potential in applications such as solid-state lighting and backlighting. White light has three characteristics defined by (i) CIE coordinates (Commission Internationale d'Eclairage) of (0.33, 0.33) (ii) the colour temperature (CT), shown by the black body curve on the CIE chart in Figure 48 (iii) the colour rendering index (CRI), for which a black body radiator has a value of 100. Considering all these characteristics it has been shown that, for lighting applications, that white light with a warmer colour temperature (< ~5000 K) is preferred over the theoretical ideal white light with the CIE coordinates (0.33, 0.33).[133, 137]

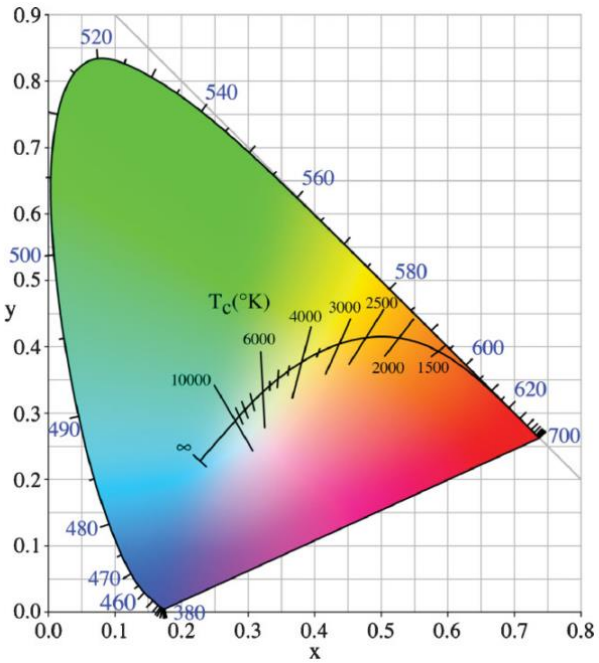

Figure 48: CIE (x,y) chromaticity chart. Within the boundary of this diagram, all of the colours of the visible spectrum are described by specific CIE coordinates. The curve shown within the diagram shows the colour temperatures relating to a black body radiator.[137]

In the fabrication of WOLEDs, it is important to select both the right combination of emitters and the appropriate thickness for the layers of each emitter. Two main strategies have been utilised in the construction of WOLEDs offering balanced white light; the (R-G-B) strategy using individual layers of red, green and blue emitters and the (O-B) strategy incorporating only orange and blue emitters. The (R-G-B) type devices are popular as a more balanced white light can be achieved using this strategy. Thompson and co-workers reported a device comprised of Ir(III) bis-(2-

phenylquinolyl-N,$C^{2'}$) acetylacetonate (PQIr), tris-(phenylpyridine)iridium ($Ir(ppy)_3$) and bis-(4′, 6′-difluorophenylpyridinato)tetrakis(1-pyrazolyl)borate (FIr6), showing red, green and blue emission respectively. Following the investigation of a range of host materials, the optimised device showed a high EQE of 26% with a power efficiency of 64 lm W^{-1}.[138] Utilising the (O-B) strategy for the construction of a WOLED is advantageous when compared with the (R-G-B) method as, due to the requirement for less dopant materials, this class of device has both lower production costs and a simpler fabrication process. Using phosphorescent dopants FIrpic and the tris-cyclometallated iridium(III) complex of the ligand (9,9-diethyl-7-pyridinylfluoren-2-yl)diphenylamine), Kwok and co-workers prepared an (O-B) white-light-emitting device with CIE coordinates (0.31, 0.41) and a power efficiency of 7.6 lm W^{-1}.[139] Blue phosphors such as FIrpic tend to have short operational lifetimes due to low stability and therefore can impact the colour-stability and the device lifetime of a WOLED. Thompson *et. al.* reported an improvement in operational characteristics of WOLEDs through the replacement of the blue phosphor with a blue fluorophore. In these improved devices, the blue fluorophore harnesses all the singlet excitons while the remaining triplet excitons are harvested by the phosphorescent green and red emitters. Unwanted direct energy transfer between the fluorophore and the phosphors is minimised by the presence of a layer of undoped host material acting as a spacer.[137, 140]

In addition to the multi-dopant devices described above, it is possible to achieve white-light emission using a single dopant. Williams and co-workers found that through variation of the dopant concentration of the planar platinum(II) N^C^N complex shown in Figure 49, the colour of emission observed from the fabricated OLED devices could be varied from sky-blue to white light. The electroluminescence spectra recorded for each of the OLED devices fabricated are shown in Figure 49, with the dopant concentrations varied from 3-100%. At low concentrations, only the sky-blue phosphorescence of the monomer **1.2.80** is observable. As the dopant concentration is increased, there is the appearance of a broad band in the red region of the spectrum. This is due to the formation of triplet excimers or aggregates formed by Pt-Pt interactions. At 100%, in the neat film, there is almost no observation of the blue monomer emission.[68]

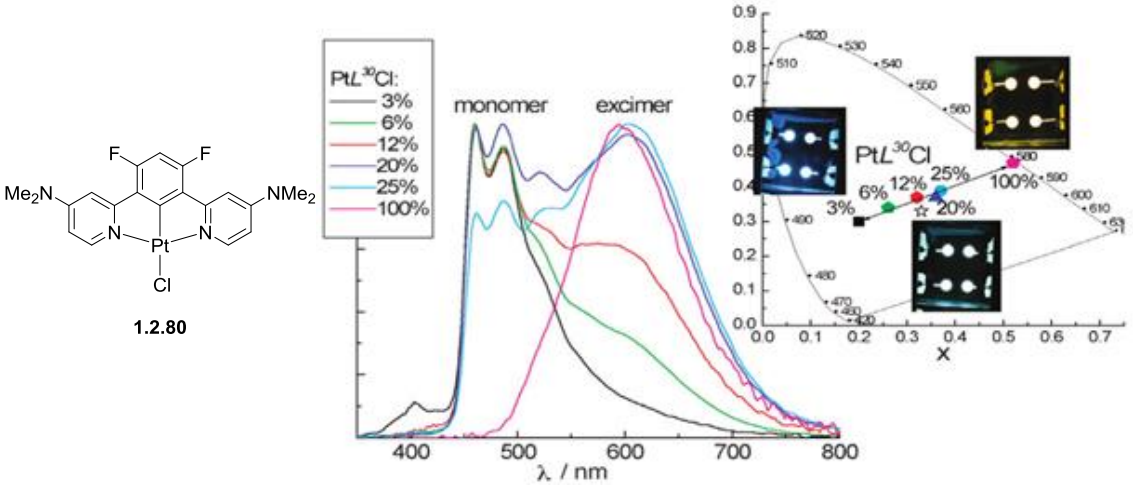

Figure 49: A figure to show the electroluminescence spectra and CIE chart for **1.2.80** at different doping concentrations.[68]

The CIE coordinates obtained for the WOLED devices fabricated become more red-shifted with increasing dopant concentration. For dopant concentrations 20 and 25%, the CIE coordinates observed were very close to white light; (0.36, 0.37) and (0.37, 0.39) respectively. In addition, for these devices, high CRI values of 87 and 88 were obtained. For the WOLED device with doping of **1.2.80** at 20%, the EQE was measured at 3.7% with a luminous efficiency of 7.4 cd A^{-1}. The CRI values observed for the WOLED devices fabricated in this work are among the highest values reported for devices based on triplet excimers.

An alternative class of electroluminescent devices that can be utilised in applications such as displays and lighting is light-emitting electrochemical cells (LECs). For incorporation into OLED devices, organometallic complexes must be charge-neutral, however, cationic transition metal complexes can be utilised as emitters in LECs.[133] Ionic transition metal complexes (iTMCs) of metals such as iridium(III) are particularly suitable for incorporation in such devices as a result of their excellent photophysical properties, high stability, reversible redox properties and colour tunability.[141, 142]

LECs offer several advantages over multi-layered OLEDs. Generally, LECs have simpler device architectures, consisting of a single layer of an ionic luminescent material sandwiched directly

between two air-stable electrodes, resulting in lower fabrication costs. Additionally, LECs generally have low turn-on voltages and are amenable to large-area solution processing.[141, 143]

In these single-layer devices, incorporating iTMCs, electrons and holes are directly injected into the emitting layer from the cathode and anode respectively. On the recombination of these electrons and holes there is emission of light. The ionic organometallic complexes incorporated into the emitting layer are capable of supporting the processes of charge injection, charge transport and emissive recombination. Charge transport occurs via a charge hopping mechanism.[29, 143]

Cationic iridium(III) complexes have been employed by a number of research groups in the fabrication of LECs.[60, 142, 144] Bernhard and co-workers reported the preparation of a single-layer LEC device in which the emitting layer was composed of the cationic, bis-cyclometallated iridium(III) complex $[Ir(df(CF_3)ppy)_2(dtbbpy)][PF_6]$, as shown in Figure 50. This device showed an EQE of 0.16% with a luminance of 33 cd m^{-2}.[142]

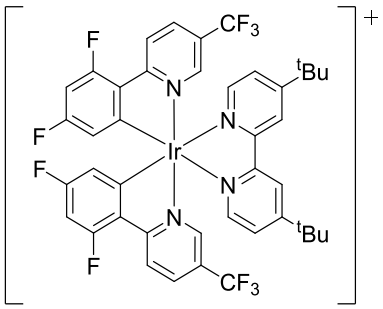

1.4.7

Figure 50: Structure of the cationic, bis-cyclometallated iridium(III) complex, $[Ir(df(CF_3)ppy)_2(dtbbpy)][PF_6]$, incorporated into a single-layer LEC by Bernhard and co-workers.[142]

Thompson *et. al.*, also using cationic, bis-cyclometallated Ir(III) complexes, fabricated electroluminescent LECs showing emission across the visible spectrum, from blue to red. The structures of the iridium(III) complexes utilised are shown in Figure 51. The structure of the green-emitting complex $[Ir(ppz)_2(dtbbpy)][PF_6]$ was varied through ligand modification in order to give the blue and red-emitting complexes. Substitution of fluoro groups at the 4- and 6-positions of the phenyl ring on the ppz ligand gave the blue emitter $[Ir(dfppz)_2(dtbbpy)][PF_6]$. Whereas, substitution of a *tert*-butyl group at the 5-position of the phenyl ring of the ppz ligand

in conjunction with replacement of the bpy ligand with the more conjugated biq ligand gave the red emitting complex [Ir(5-^{t}Buppz)$_2$(biq)][PF$_6$].

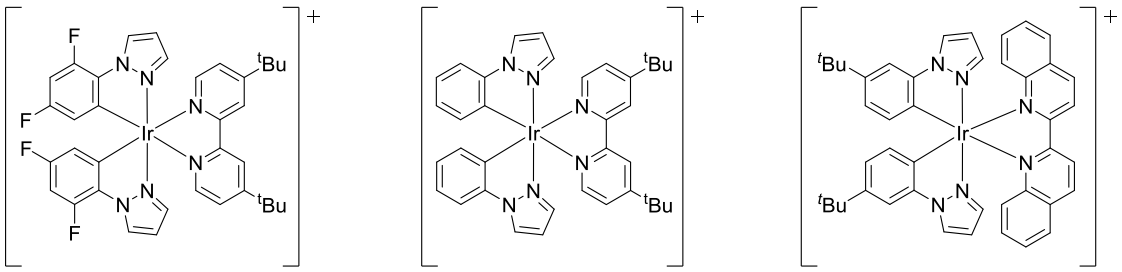

1.4.8
[Ir(dfppz)$_2$(dtbbpy)][PF$_6$]

1.4.9
[Ir(ppz)$_2$(dtbbpy)][PF$_6$]

1.4.10
[Ir(5-^{t}Buppz)$_2$(biq)][PF$_6$]

Figure 51: A figure to show the series of complexes reported by Thompson *et. al.* and incorporated into LECs showing electroluminescence across the visible spectrum, from blue to red.[29]

The devices fabricated using these complexes showed electroluminescence across a wide colour range with blue (492 nm), green (542 nm) and red (635 nm) emission observed. The EQEs were in the range 4.6-7.4% with the luminance values between 1700-11500 cd m^{-2}.[144]

The complexes discussed in this section illustrate that the chemical and photophysical properties of cyclometallated complexes of Ir(III) and Pt(II) are ideal candidates for use in electroluminescent devices such as OLEDs and LECs. Extensive investigation in this area continues in order to isolate complexes with improved properties and to maximise the performance of such luminescent complexes in devices. This includes achieving higher external quantum efficiencies, improved device stability and lifetime and finally better colour purity.[60]

1.4.2 Bioimaging

The utilisation of transition metal complexes as luminescent probes in the imaging of cells and biological tissues is a rapidly emerging area of research. In bioimaging, the design of luminescent molecules capable of both entering cells and targeting specific structures, whilst having low cytotoxicity, is essential for the understanding of processes occurring within biological systems.[67, 145]

Fluorescence microscopy is a tool widely used in the cell biology and biomedical science for the visualisation of biological tissues and the study of biological systems, from the interactions between single molecules to the investigation of the function of whole organisms. Fluorescence microscopy is a highly sensitive tool as a result of the efficiency with which light can now be detected. Excellent spatial resolution can be achieved using confocal microscopy with exceptional temporal resolution also attainable. Use of this technique for the imaging of biological samples relies on luminescence from fluorophores intrinsic to the cells or from external fluorescent probes. A wide range of fluorescent dyes are available commercially with many being based on fluorone cores and derivatives, for example, the rhodamine dyes and fluorescein. Alternatively, fluorescent proteins such as green fluorescent protein (GFP) have also been previously employed as fluorescent probes.[67, 145, 146]

Dyes based on luminescent complexes of metals such as Ir(III) and Pt(II) are interesting alternatives to organic fluorophores and have many superior chemical and photophysical properties that prove beneficial for bioimaging. Firstly, through the synthetic methods utilised in the preparation of these complexes a large variety of functionality can be integrated into the final structures. This is useful for the modulation of properties such as charge, lipophilicity, cytotoxicity and compartmentalisation within the cells. Additionally, metal-based dyes have high quantum yields, absorption and emission wavelengths tunable across the visible spectrum, large Stokes shifts, long luminescence lifetimes and enhanced photostabilities.[146, 147] Due to the long luminescence lifetimes of luminescent metal complexes, the short-lived autofluorescence of biological molecules can be eliminated using time-gated emission experiments such as time-resolved emission imaging microscopy (TREM). Figure 52 illustrates the concept utilised in TREM experiments.[67, 145]

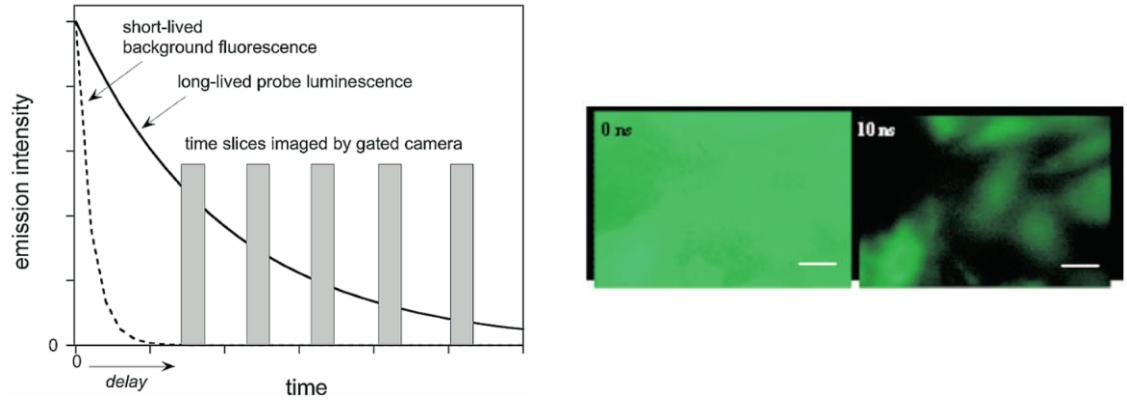

Figure 52: A figure to illustrate the concept of time-resolved emission imaging microscopy (TREM). (Left) A diagram to explain time-gating for the elimination of short-lived autofluorescence. Using a time-gated CCD camera, a series of images can be recorded at different time delays following the excitation pulse. (Right) Images of live CHO cells incubated with a [Pt(N^C^N)Cl] complex and imaged in the presence of a fluorescein solution in 1M NaOH, taken at 0 ns and 10 ns after the 355 nm excitation pulse.[67]

Ideally, in order for a luminescent probe to be useful as a bioimaging agent, it should satisfy a range of criteria. It is necessary for a luminescent probe to have a high extinction coefficient in the visible region of the spectrum. For work involving cells, excitation in the blue/green region of the spectrum is acceptable. However, for tissue samples, the optimal excitation wavelength lies in the deep red or NIR region (650-950 nm) resulting from good tissue penetration and low autofluorescence. A high emission quantum yield is desirable due to the fact that with increased brightness of the emission from the luminophore, a lower excitation intensity is required. Solubility in water is also essential, in conjunction with high cell permeability and low cytotoxicity. The cell permeability and cytotoxicity of a luminescent probe are strongly linked to its structure. A careful balance of these two factors, through synthetic design, is essential for an imaging agent to be successful. With respect to luminescent metal complexes as probes, a higher lipophilicity is generally linked to an increased cytotoxicity although sufficient lipophilicity is required for cell permeability. Additionally, cellular uptake and compartmentalisation are controlled by the charge, size and the substituents incorporated. A positively charged complex is likely to have higher cellular uptake due to facile interaction with the negative surface charge on cells. Finally, a high chemical and photostability are also required in order to avoid degradation and photobleaching of the luminescent probe. Using the criteria discussed, luminescent

cyclometallated complexes have been prepared that are capable of staining a range of cellular structures, from the cytoplasm and nucleus to the mitochondria and lysosomes (Figure 53).[145, 148]

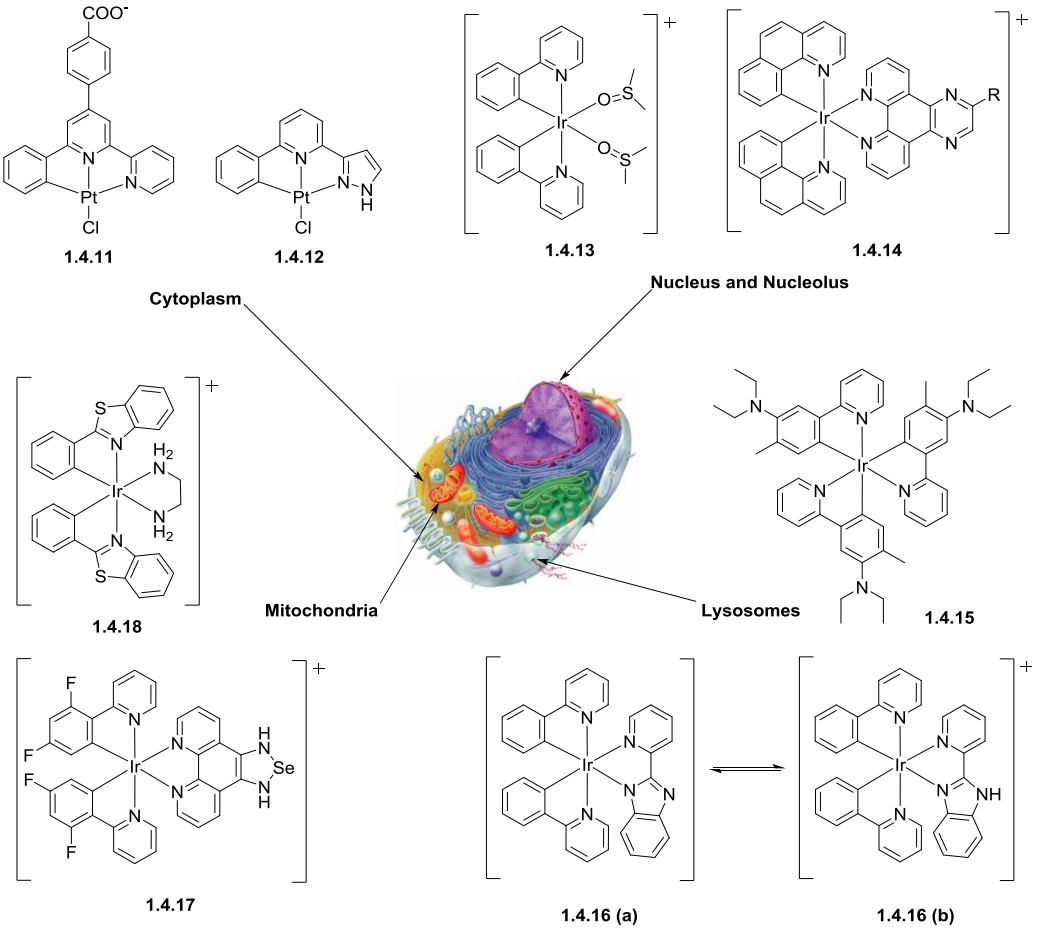

Figure 53: Phosphorescent cell stains based on cyclometallated complexes of Pt(II) and Ir(III). These luminescent probes localise in specific areas of cells; the cytoplasm, nucleus and nucleoli, mitochondria and lysosomes.[146-155]

Williams *et. al.* reported a series of highly emissive platinum(II) complexes for utilisation as TREM agents in bioimaging. The Pt(N^C^N)Cl complexes were shown to have low cytotoxicity, to be photochemically robust and exhibited efficient phosphorescence, making them ideal candidates for live-cell imaging.

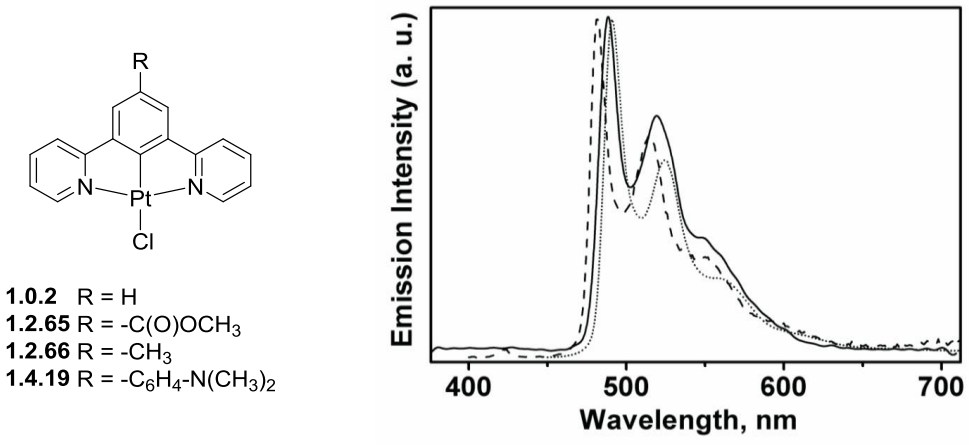

Figure 54: General structure of the cyclometallated platinum(II) complexes reported by Williams and co-workers for as bioimaging agents in TREM experiments (left). The emission spectrum of **1.0.2** is shown in water (dashed line), in aerated CH_2Cl_2 solution (dotted line) and HDF cell nuclei (solid line) (right).[67]

This research group have previously shown that such cyclometallated Pt(II) complexes absorb strongly in the UV ($\varepsilon \sim 10^4$ mol^{-1} dm^3 cm^{-1}) and visible ($\varepsilon \sim 200$ mol^{-1} dm^3 cm^{-1}) regions of the spectrum and also display intense phosphorescence in solution at room temperature, with quantum yields in the range $\phi = 0.60$-0.70 for degassed dichloromethane solutions.

Three cell lines were selected for incubation with **1.0.2**, (i) normal human dermal fibroplast (HDF) cells, (ii) neoplastic human cells taken from an invasive melanoma (C8161) and (iii) common animal-derived cells (CHO). The cytotoxicity of the platinum(II) complex was investigated using an MTT assay [MTT = 3-(4,5-dimethylthiazol-2-yl)-2,5-diphenyltetrazolium bromide]. The Pt(II) complex was found to have low cytotoxicity, only significantly reducing cell viability at high concentrations (100 μM) after incubation for 24 h (Figure 55).[67]

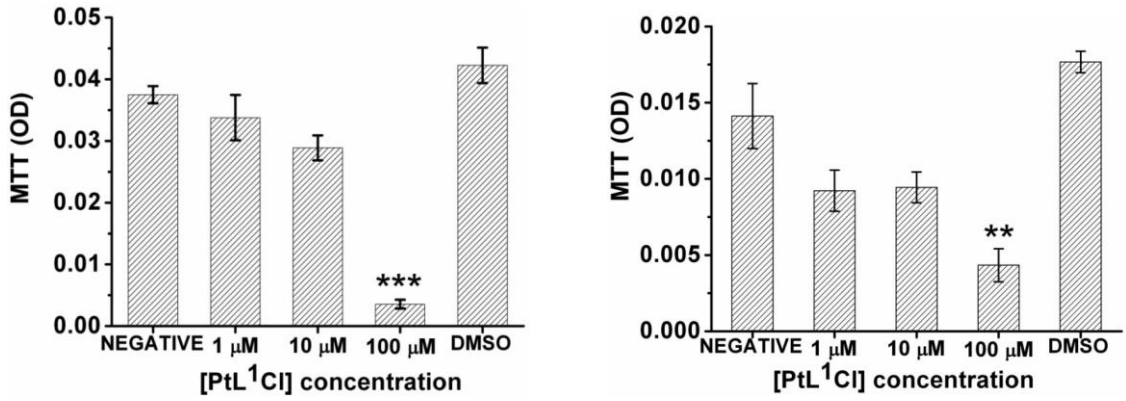

Figure 55: Cell viability of CHO (left) and HDF (right) cells as determined by MTT assay by Williams and co-workers. Cells were incubated for 5 min with the [Pt(N^C^N)Cl] at different concentrations, washed with PBS (three times) and incubated with fresh culture medium for 24 h (mean ± SEM, n = 3 for all experiments, **, P < 0.01).[67]

Cell imaging of all cell lines was carried out using **1.0.2** as a luminescent label. Maximum emission intensity was obtained after a short incubation of 5 min, suggesting high cell permeability. Upon excitation, the Pt(II) complex was observed to emit a green-yellow light with an emission profile almost identical to that recorded in aqueous solution (Figure 54).[67]

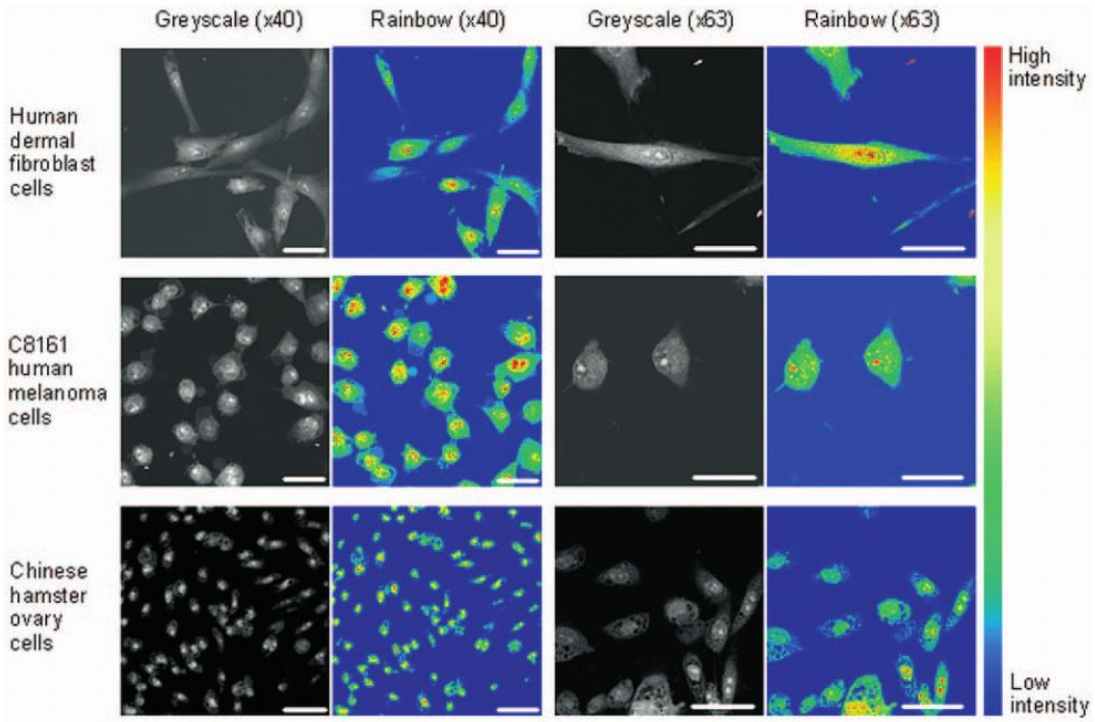

Figure 56: A figure to show the confocal micrographs of human dermal fibroplast, C8161 human melanoma and CHO cells. These cells were incubated for 5 min with 100 μM solution of **1.0.2** and then washed with phosphate buffer solution for 5 min. The images were captured following excitation at 488 nm. Areas in which **1.0.2** accumulates are shown as both grayscale and rainbow intensities. Scale bar: 10 μm.[67]

The compartmentalisation of the cyclometallated platinum(II) complex was first investigated using co-staining experiments with a common nuclear stain, DAPI. The preferred localisation of **1.0.2** in the nuclei of the cells was confirmed both by confocal microscopy (Figure 56) and high-resolution two photon images.

In this study, Williams and co-workers showed the huge potential for the utilisation of transition metal complexes in bioimaging as these charge-neutral, cyclometallated Pt(II) complexes have been effectively used as labels in a range of eukaryotic cells.[67]

Li and co-workers also demonstrated the successful application of transition metal complexes in bioimaging. Cationic, cyclometallated iridium(III) complexes displaying bright green and red emission were utilised as dyes in the imaging of living cells. The structures of the complexes used are shown in Figure 57. Both of the iridium(III) dyes showed exclusive staining of the cytoplasm, as can be observed in the confocal luminescence images shown below.[156]

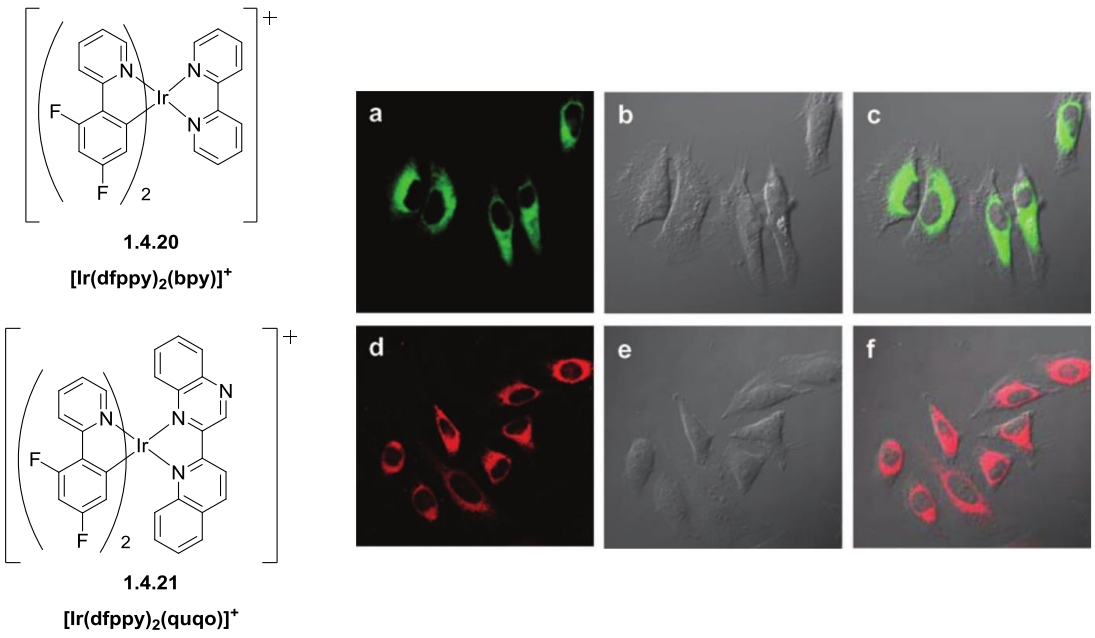

Figure 57: Chemical structures of the cationic iridium(III) complexes utilised for bioimaging of living HeLa cells (left). Confocal luminescence (a and d) and brightfield images (b and e) of HeLa cells incubated in 20 μM solutions of $[Ir(dfppy)_2(bpy)]^+$ (top) and $[Ir(dfppy)_2(quqo)]^+$ (bottom) in DMSO/PBS for 10 min are shown (right). Overlays of these two images (c and f) are also shown. (λ_{ex} = 405 nm)[156]

These promising results, in addition to the high cell permeability, low cytotoxicity, low photobleaching observed, show that such complexes are excellent candidates for specific phosphorescence bioimaging agents.[156]

The use of phosphorescent transition metal complexes in bioimaging has offered many advantages and opened up new opportunities, including new microscopy techniques. Further investigation in this field of research continues as the demand for imaging dyes with the advantageous properties of these complexes increases. Their synthetic versatility, facile modulation of photophysical properties and relatively long luminescence lifetimes mean that such compounds are extremely attractive for use as luminescent probes in biological systems.

1.4.3 Chemical Sensors

In addition to the application of luminescent transition metal complexes as bioimaging agents, similarly they have also been utilised as chemical sensors. A chemical sensor is a compound capable of detecting an analyte through enacting a change in the properties of the system, such as variation in the absorption, emission or redox potentials. Chemical sensors are particularly important as a result of their application in the detection of species of biological and environmental importance.[157, 158]

The use of photoluminescence techniques is an extremely effective tool in the detection of analytes due to their high sensitivity and selectivity, facile visualisation, excellent temporal and spatial resolution and short detection response time. Commonly, luminescent chemosensors are based on organic dyes with examples of lanthanide complexes also reported. More recently, phosphorescent transition metal complexes have been attracting increasing interest as chemosensors due to their advantageous photophysical properties and the sensitivity of those properties to changes in the local environment.[157, 158]

In general, a chemical sensor is comprised of two components; a receptor unit and a signalling unit. The receptor unit is involved in the selective binding of analytes whilst the signalling unit reports on the interaction between the receptor and the analytes. Incorporating a phosphorescent

transition metal complex as the signalling unit means that the chemical information obtained through analyte binding is converted into an optical signal.[157]

In the design of chemosensors, several approaches have been devised for linking a receptor unit to the phosphorescent signalling unit as is shown in Figure 58. These approaches include the "receptor-σ-signalling unit approach", the "receptor-conjugated-signalling unit approach" and the chemodosimeter approach" as described schematically in Figure 58.[157, 158]

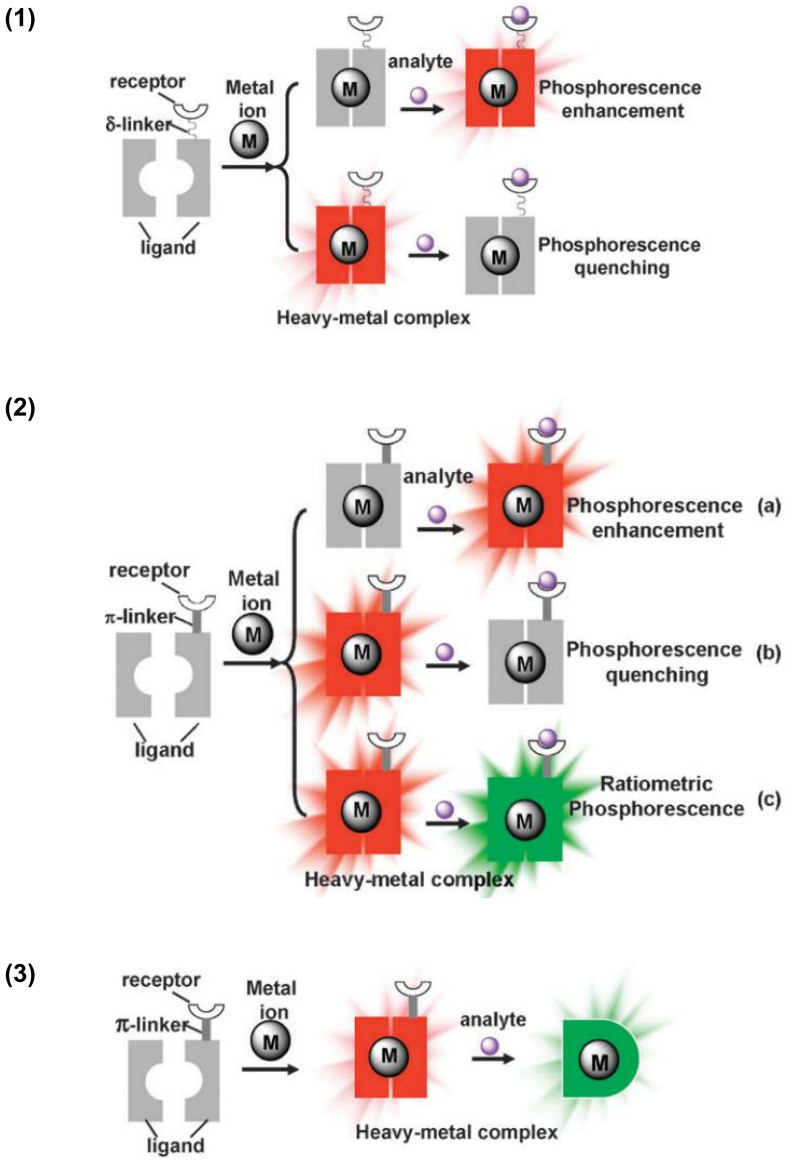

Figure 58: Schematic to show three approaches used in the design of chemosensors, linking the receptor unit to the phosphorescent signalling unit. (1) The "receptor-σ-signalling unit approach" in which the receptor unit is linked to the ligand of a phosphorescent complex via a spacer (2) The "receptor-conjugated-signalling unit approach" in which the receptor unit is conjugated to the ligand of metal complex without a spacer (3) The "chemodosimeter approach" in which the receptor unit is conjugated to the signalling unit but on binding of an analyte there is an irreversible chemical reaction between the phosphorescent metal complex and the analyte.[157, 158]

Each design approach described above endows the resulting chemical sensor with a different functionality leading to a variety of possible mechanisms of action. The first potential mechanism is the photoinduced electron transfer (PET) mechanism and is most common for chemosensors prepared using the "receptor-σ-signalling unit approach". Generally, this results in turn-on/turn-off phosphorescent chemosensors. In many cases, PET quenches the emission from heavy metal complexes and therefore, on binding to an analyte, the PET process can be inhibited and emission is observed (turn-on). In the second possible mechanism, binding of the receptor unit to an analyte perturbs the energy levels of the adjoined metal complex resulting in a change in the lowest excited state and in the emission properties observed. This mechanism is most often observed for "receptor-conjugated-signalling unit" type chemical sensors. The third mechanism is based on fluorescence resonance energy transfer (FRET) in which binding of the analyte results in a variation of the amount of energy transfer that occurs between an energy donor and acceptor. A further three mechanisms of action have been suggested for chemical sensors. Firstly, the detection of the variation in photophysical properties based on the extent of metal-metal interactions on binding of a d^8 metal complexes to analytes. Secondly, detection of variations in the emission intensity resulting from ligand distortion following binding of an analyte. Finally, the phosphorescence signal from a heavy metal complex can vary based on changes in the local environment resulting from interaction with an analyte.[157]

Chemical sensors acting by the different mechanisms of action described, possible due to the prudent design of such systems, are utilised in the detection of a range of analytes from metal cations to molecular oxygen (O_2). A selection of examples capable of sensing a variety of analytes is shown in this section.

There are many examples of chemical sensors for metal cations based on luminescent complexes of Pt(II) and Ir(III). The detection of metal cations such as Na^+, K^+, Mg^{2+} and Ca^{2+} is of significant interest in biological and environmental sciences. The use of macrocyclic moieties such as crown-ethers and aza-crown-ethers is common for binding metal cations and the incorporation of pendant macrocyclic receptor units on phosphorescent metal complexes have been widely reported. The

binding of the metal cation to the macrocyclic receptor perturbs the energy levels of the excited states on the Pt(II) or Ir(III) centre, leading to a change in the optical properties observed. For the platinum(II) complex shown in Figure 59, on binding of the aza-crown-ether to Mg^{2+}, there is conversion of the lowest excited state from the non-emissive ^{3}LLCT state to emissive ^{3}MLCT state resulting in a turn-on in the emission. Similarly, for the iridium(III) complex shown, the addition of Ca^{2+} resulted in a change of the lowest excited state from ILCT to LLCT in accordance with the second mechanism of action described above.[157, 159]

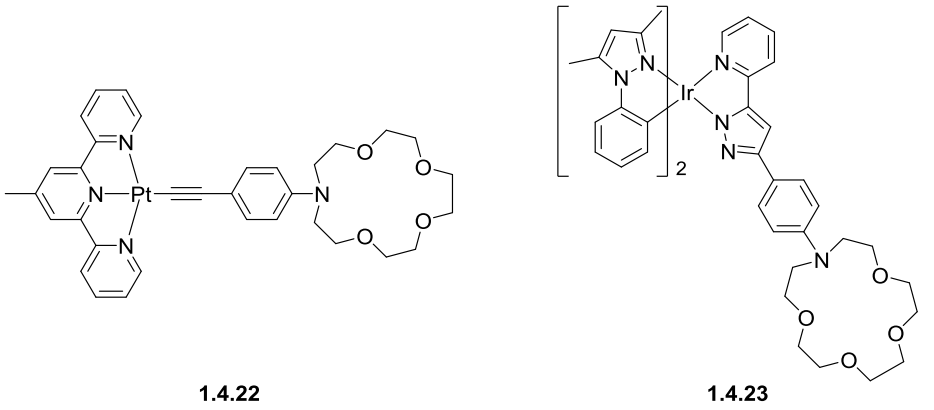

1.4.22 **1.4.23**

Figure 59: Structures of examples of platinum(II) and iridium(III) complexes bearing aza-crown-ether receptor units utilised in the detection of Mg^{2+} and Ca^{2+} cations respectively.[157]

In addition to metal cations of alkali and alkaline earth metals, phosphorescent metal complexes have been used in the detection of alternative metal cations such as Hg^{2+}. Mercury is highly toxic and therefore, its detection is of interest. It is well known that as a soft acid, Hg^{2+} cations interact preferentially with sulfur, a soft base. Consequently, incorporation of S atoms into the ligands of luminescent metal complexes has proved successful in the sensing of Hg^{2+} cations.

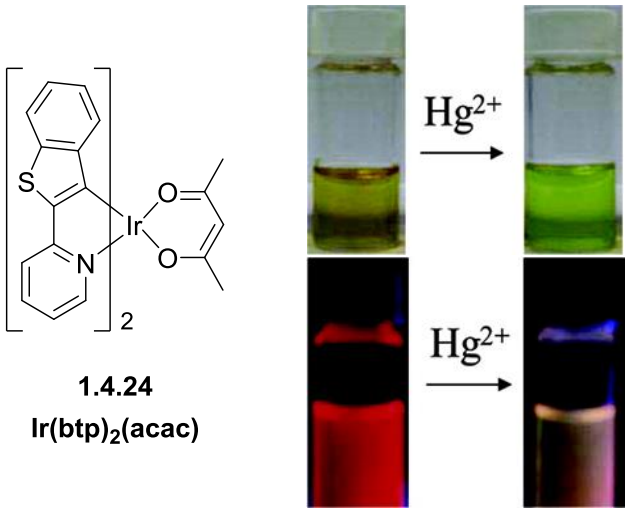

Figure 60: Huang *et. al.* reported the use of $Ir(btp)_2(acac)$ (**1.4.24**) as a sensor for Hg^{2+} ions in CH_3CN solutions.[160]

Huang and co-workers reported that the complex $Ir(btp)_2(acac)$ (**1.4.24**) was successful in the selective detection of Hg^{2+} ions in CH_3CN solutions using a multisignalling optical-electrochemical response. Addition of Hg^{2+} ions to **1.4.24** results in a blue-shift in both the absorption and emission bands. As shown in Figure 60, these changes can be observed by eye. The solution changes colour from orange to yellow-green and the colour of emission becomes orange from deep-red. Additionally, the electrochemical properties of the complex are altered.[157, 160]

A second class of analytes detectable using luminescent metal complexes as chemosensors are anions, for example F^-, Cl^-, PO_4^{3-} and CH_3COO^-. Two main approaches are used for sensing anions; the incorporation of acidic hydrogen-containing groups within the ligands or the exploitation of specific Lewis acid-base interactions such as that between boron and F^-. Functional groups bearing acidic hydrogen atoms capable of acting as receptor units include hydroxyl and pyrrole. Huang *et. al.* reported the utilisation of an iridium(III) complex bearing an imidazolyl moiety (Figure 61) in the detection of F^-, H_2PO4^- and CH_3COO^- anions. Upon addition of these anions to the complexes shown below, there is significant changes in both the absorption and emission properties. The solution colour changes from yellow-green to brown and the emission is quenched. It was suggested that following deprotonation, the PET process from the imidazolyl N lone pair quenches the emission from the complex as in the first mechanism of action.[157, 161]

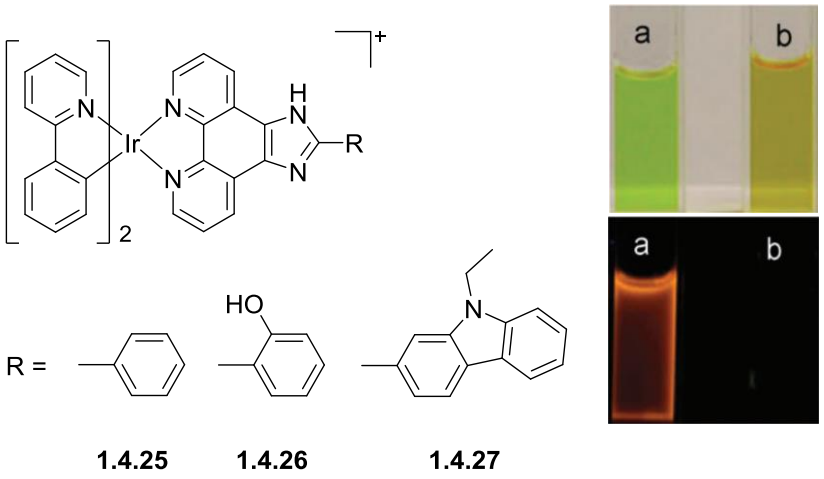

Figure 61: A figure to show the structure of the bis-cyclometallated Ir(III) complexes reported by Huang and co-workers (left). The changes in the solution colour and the emission upon binding to anions such as F^-, H_2PO4^- and CH_3COO^- are also shown (right).[157, 161]

In 2014, Gonzalez reported the cyclometallated Pt(II) complex (**1.4.28**) shown in Figure 62 as a highly selective chloride sensor. In buffered solutions containing the surfactant $CTA^+HSO_4^-$, upon addition of NaCl, the green luminescence of the complex was turned on. This change in the photophysical properties of the complex allowed for detection of chloride anions in the micromolar (μM) concentration range.[162]

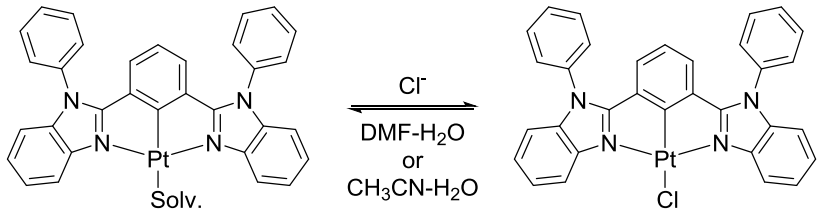

Figure 62: A scheme to illustrate the action of the cyclometallated Pt(II) complex, reported by Gonzalez, for the detection of chloride in aqueous media.[162]

Luminescent transition metal complexes, such as those discussed in this section, can also be used in the detection of alternative analytes including gases such as molecular oxygen (O_2) and variations in pH. Examples of such chemosensors will not be discussed in this literature review.[157]

In this section, chemical sensors based on complexes of Pt(II) and Ir(III) have been discussed. As a result of the excellent photophysical properties including long luminescence lifetimes, complexes such as these are excellent candidates for application as chemosensors for a range of analytes and local environment changes. Research in this area is ongoing to ensure that the development of chemical sensors boasting increased sensitivity and selectivity as well as improved water solubility is achieved.

1.5 Aims and Objectives

As has continually been shown throughout this literature review, the structure of a transition metal complex, including the identity of the metal centre and selection of ligands, has a significant effect on the chemical and photophysical properties of the final complex.

Cyclometallated mononuclear complexes of transition metals such as platinum(II) and iridium(III) have been widely studied and exhibit rich photophysical properties including colour tunability, high quantum yields and microsecond lifetimes. Consequently, these complexes have been successfully utilised in applications from OLEDs to bioimaging.

There are relatively few examples of luminescent multimetallic complexes although interest in this area has been growing in recent years. A large proportion of the multinuclear complexes investigated are linked via flexible bridging ligands. Examples of such complexes in which the metals are rigidly linked are still relatively rare and those incorporating rigid, cyclometallating bridging ligands are even less common.

The overall aim of this project is to synthesise and investigate novel bimetallic emitters in which the metal centres are rigidly-linked by cyclometallating bridging ligands and assess the suitability of such complexes for application in OLEDs and bioimaging. More specific aims of the project are listed below.

(1) Di-Platinum(II) Complexes

Based on previous research in the Kozhevnikov group, pyrimidine-based bis-bidentate bridging ligands incorporating bis-thiophene groups, such as those shown in Figure 63, are of interest for

the preparation of bimetallic platinum(II) complexes.[85, 163] These ligands offer both increased conjugation length and electron-rich moieties, both of which are strategies often used in shifting absorption and emission to the red.

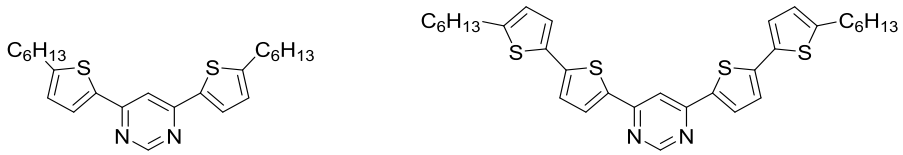

Figure 63: Structures of the pyrimidine-based bis-bidentate bridging ligands bearing mono- and bis-thiophene groups that are of interest use in the synthesis of dinuclear platinum(II) complexes.

Dinuclear platinum(II) complexes of the bis-bidentate ligands shown above, using acetylacetonate as an auxiliary ligand, will be prepared and their photophysical properties investigated. It is likely that such complexes will show emission in the near-infrared (NIR) region. Che *et. al.* have reported the synthesis of mononuclear platinum(II) complexes bearing rigid tetradentate N^C^N^O-coordinating ligands. These complexes proved to be excellent candidates for use in OLEDs. A multinuclear complex incorporating an equivalent ditopic bis-tetradentate ligand is an interesting target and to the best of our knowledge has never been reported before. Consequently, a di-platinum(II) complex in which the metal centres are linked via a rigid bis-tetradentate ligand (Figure 64) will be prepared and the photophysical properties of the final complex will be investigated.[164-167]

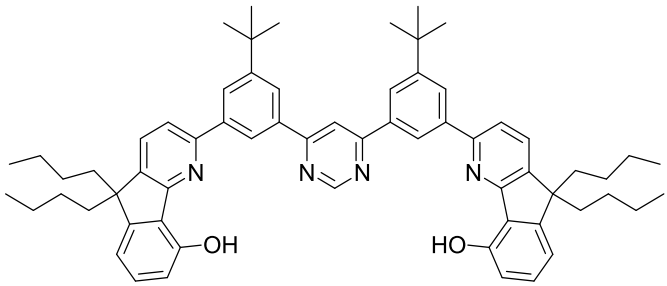

Figure 64: Proposed structure of the rigid bis-tetradentate ligand to be utilised in the synthesis of a dinuclear platinum(II) complex.

(2) Pyrimidine-Linked Dinuclear Iridium(III) Complexes

Bis-bidentate bridging ligands based around a central pyrimidine heterocycle were previously used in the Kozhevnikov group for the preparation of bimetallic platinum(II) and heterotrimetallic Pt(II)/Ir(III) complexes as shown in Figure 39.[84, 85] In this work, utilising similar pyrimidine-based bis-bidentate bridging ligands, a series of rigid dinuclear iridium(III) complexes of the general structure illustrated in Figure 65 will be prepared.

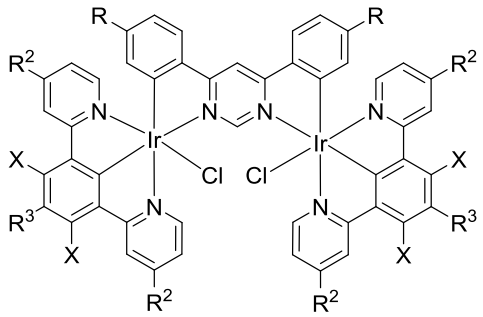

1.5.1

Figure 65: The general structure of the dinuclear iridium(III) complexes to be prepared in this work. The metal centres in these complexes are rigidly-linked via a pyrimidine-based bis-bidentate bridging ligand.

Terdentate N^C^N-coordinating auxiliary ligands will be incorporated in order to introduce additional rigidity to the multinuclear systems. Importantly, these terdentate ligands and the bis-bidentate bridging ligands will be symmetrical, ensuring that the final dinuclear complexes prepared are achiral. This is crucial if laborious separation of mixtures of diastereoisomers is to be avoided.

A range of different substituents, electron-withdrawing and –donating, will be incorporated into both the bridging and auxiliary ligands. The photophysical properties of the resulting series of dinuclear iridium(III) complexes will be measured and the effects of the structural variations on these properties will be investigated.

(3) Variation of the Central Heterocycle of the Bridging Ligands in Dinuclear Iridium(III) Complexes

In the general structure of the dinuclear iridium(III) complex shown in Figure 65, each component from the terdentate auxiliary ligand to the monodentate ligand can be modified in order to tune the photophysical characteristics of the final complex.

The central heterocycle of the bis-bidentate bridging ligand will be varied from pyrimidine to alternative heterocycles such as pyrazine and pyridazine as shown in Figure 66.

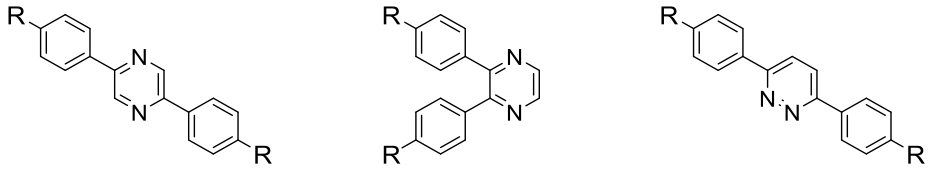

1.5.2 **1.5.3** **1.5.4**

Figure 66: A figure to illustrate the general structures of bis-bidentate bridging ligands in which the central heterocycles have been varied from pyrimidine to 2,5-substituted pyrazine (left), 2,3-substitued pyrazine (middle) and 3,6-substituted pyridazine (right).

Such modifications to the bis-bidentate bridging ligand are likely to have a large effect on the optical properties of the resulting dinuclear complexes, as has been previously shown in the Kozhevnikov group.[85] The chemical and photophysical properties of the di-iridium(III) complexes prepared using these bis-bidentate bridging ligands will be investigated.

(4) Variation of Monodentate Ligand in Dinuclear Iridium(III) Complexes

Similarly, the monodentate chloride ligand in the general structure illustrated in Figure 65 can also be modified. Chloride ligands in luminescent metal complexes are highly labile and therefore, complexes bearing monodentate chloride ligands can have detrimental effects on the operation of OLED devices in which they are utilised.

In this work, metathesis reactions will be carried out in order to introduce alternative monodentate ligands such as $^{-}$CN, MeCN and OH_2 to replace the labile chloride ligand. The resulting dinuclear iridium(III) complexes will be fully characterised and their optical properties measured.

Chapter 2

Dinuclear Platinum(II) Complexes

2.0 Dinuclear Platinum(II) Complexes

Platinum(II) complexes of cyclometallating ligands such as 2-phenylpyridine have been extensively investigated for use in an array of contemporary applications such as OLEDs, solar energy conversion and imaging.[84, 85] The structure and electronic properties of the ligands used in the synthesis of a luminescent metal complex are exceptionally important in modulating the chemical and photophysical properties of the final compound.

As discussed previously in section 1.2.3, systematic modification of the cyclometalling ligands used is a valuable tool in the facile tuning of the absorption and emission wavelengths of a luminescent complex. Strategies employed for tuning can involve the addition of electron-donating or -withdrawing substituents, exclusively altering the HOMO or LUMO energy levels, or variation of ligand conjugation. These strategies enable tuning of the absorption and emission across the visible spectrum. In particular, there is a need for the development of materials that exhibit improved absorption and emission in the red region of the spectrum. This is due to the requirement of such materials for use in applications such as dye-sensitised solar cells (DSSCs) and bio-imaging. Specifically, in order to shift to the red region of the spectrum, classical approaches used are (i) incorporation of a more electron-deficient heterocycle to lower the energy of the LUMO, (ii) use of more electron-rich aromatic units to raise the HOMO energy, and (iii) extension of the conjugated system of the ligand decreasing the HOMO-LUMO gap.[85]

Cyclometallated platinum(II) complexes incorporating auxiliary diketonate ligands, such as acetylacetonate, have been reported to be strongly luminescent at room temperature. [Pt(L)(acac)] complexes were reported by Kozhevnikov and co-workers in which the cyclometallating ligands (L) used were substituted with thienylpyridine cyclometallating ligands. The thiophene ring of a thienylpyridine ligand is more electron-rich than the corresponding aryl ring present in 2-phenylpyridine ligands. Consequently, the use of thienylpyridine ligands should result in a red-shift. A selection of the 2-(2-thienyl)pyridine ligands used, incorporating a range of substituents, are shown in Figure 67. These platinum(II) complexes **2.0.1**-**2.0.4** display red-shifted emission relative to the corresponding unsubstituted [Pt(thpy)(acac)] complex. This red-shift is attributed

to stabilisation of the LUMO as a result of increased delocalisation across the aromatic/heterocyclic substituents incorporated. The largest red-shift is exhibited by [Pt(L^4)(acac)] with emission observed at 622 nm compared with 558 nm for [Pt(thpy)(acac)].[85, 168]

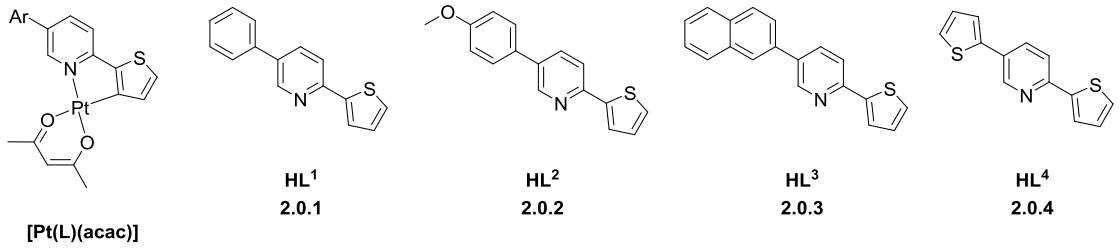

Figure 67: A figure to show the general structure of the [Pt(L)(acac)] complex prepared by Kozhevnikov *et. al.* and a selection of the substituted 2-(2-thienyl)pyridine proligands utilised in the synthesis of this series of platinum(II) complexes.[168]

Further research by Kozhevnikov *et. al.* into [Pt(L)(acac)] complexes of thienylpyridine ligands reported on the use of (oligo)thienylpyridines. In this work, two of the classical strategies used to red-shift emission were used; incorporation of electron-rich thiophene groups and increased conjugation length. The ligands and complexes reported are shown in Figure 68.[163]

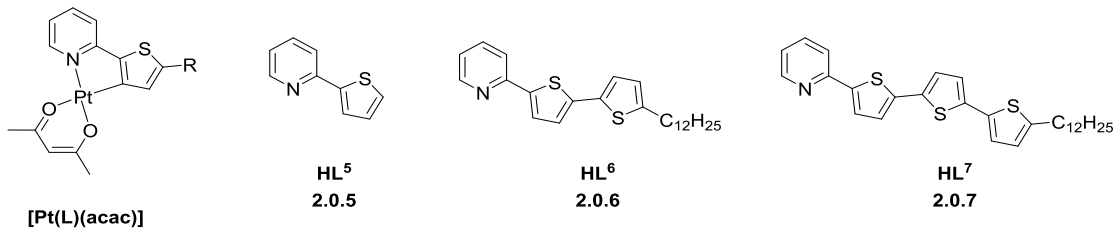

Figure 68: A figure to show the structures of the (oligo)thienylpyridine ligands used by Kozhevnikov and co-workers in the synthesis of a series of cyclometallated platinum(II) complexes. The conjugation length of HL^5 is increased through the incorporation of an additional one or two thiophene units to give HL^6 and HL^7 respectively. A dodecyl chain was added to HL^6 and HL^7 in order to increase solubility of the ligands and corresponding complexes.[163]

Measurement of the photophysical properties of the series of platinum(II) complexes **2.0.5**-**2.0.7** showed that extension from one to two and to three thiophenes results in a shift of the absorption bands to progressively longer wavelengths. This is the expected effect of increasing the conjugation length through elongation of the thiophene chain.[163] Investigation of the

luminescence properties of these complexes revealed some interesting results. [Pt(L^5)(acac)] displayed strong phosphorescence with the emission observed at 554 nm with a quantum yield of $\phi = 0.36$. The emission spectrum of [Pt(L^6)(acac)] was also recorded, exhibiting a very different spectrum from that of [Pt(L^5)(acac)]. Two sets of bands were observed, one at 495 nm and further bands at 706 and 775 nm, both with low intensities. The emission quantum yield of the complex was measured to be $\phi = 0.0058$. Through studying the excitation spectra of both the lower and higher energy bands in addition to determining the lifetime of the lower energy emission (< 0.5 ns), this band was assigned to spin-allowed fluorescence from the singlet excited state. Therefore, [Pt(L^6)(acac)] was found to display dual emission, exhibiting both fluorescence and phosphorescence. The relative ratios of the fluorescence and phosphorescence bands was found to be independent of concentration and therefore, it was concluded that the appearance of the additional emission band is not a result of aggregate or excimer formation. Further extension of the conjugation length in [Pt(L^7)(acac)] did give a red-shift in the emission, however, similar dual emission was observed with bands at 525 and 735 nm and the quantum yield measured to be $\phi = 0.002$, lower than [Pt(L^6)(acac)].

The observation of dual emission from [Pt(L^6)(acac)] and [Pt(L^7)(acac)] suggests that as the conjugation length of the ligand increases there is a lower degree of participation of the metal d orbitals in the HOMO states. As a result, the influence of the SOC from the heavy metal atom is reduced. This leads to a decrease in the rate of ISC and radiative decay from $T_1 \rightarrow S_0$. In addition, with increasing conjugation length, the S_1–T_1 energy gap increases, further decreasing the rate of intersystem crossing. This leads to a decrease in the yield of triplet formation, a decreased $T_1 \rightarrow S_0$ radiative decay rate and as the energy of the excited state decreases there is increased non-radiative decay. Consequently, fluorescence becomes observable whilst the intensity of phosphorescence decreases.[163]

Previous studies, such as those discussed, in which classical methods for red-shifting the absorption and emission of luminescent transition metal complexes have been employed, have shown that such strategies are not always successful in achieving highly luminescent red emitters.

An alternative strategy for achieving the desired red-shift, reported in the literature, is the addition of a second metal centre. As mentioned previously in section 1.3.2, Kozhevnikov *et. al.* synthesised a series of dinuclear platinum(II) complexes in which the two metal centres were rigidly-linked and both bound to a common nitrogen-containing heterocycle, as shown in Figure 69.[85]

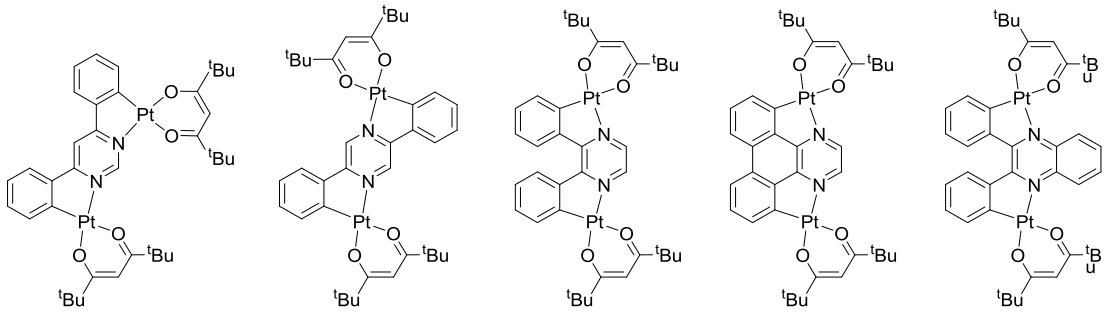

Figure 69: A figure to show the series of rigidly-linked dinuclear platinum(II) complexes reported by Kozhevnikov and co-workers. A range of heterocycles were used to link the two Pt(II) centres and their photophysical properties investigated.[85]

The dinuclear platinum(II) complexes shown above are all intensely luminescent in degassed solution at room temperature, exhibiting deep red emission and displaying very different properties compared with their mononuclear analogues. On introduction of a second Pt(II) centre, a significant red-shift in the absorption and emission of the complexes was observed. This red-shift in absorption was accompanied by an increase in the molar absorptivities by a factor of 2. In addition to the red-shift in the emission, an increase in the radiative decay constant (2-fold) is also observed. It is thought that the radiative $T_1 \rightarrow S_0$ transition becomes more allowed in the bimetallic complex as a result of a higher degree of SOC coupling resulting from the presence of a second heavy metal ion. The dinuclear platinum(II) complexes show relatively high quantum yields in the red region of the spectrum, but quantum yields for emitters in the NIR region were below 3%. Lifetimes in the microsecond region were also recorded.[85]

This same strategy, achieving a red-shift through incoporation of two or more metal centres into the same complex, has been successfully employed previously by Kozhevnikov *et. al.* in the preparation of a mixed metal Pt(II)/Ir(III) trinuclear complex and di-iridium(III) complexes.[83, 84]

2.1 Bis-Thiophene Di-Platinum(II) Complex

In this work, in order to achieve highly-luminescent red-shifted emitters, we have combined the classical strategy of increasing the conjugation of the ligand and the new alternative strategy of rigidly-linking two metal centres. We synthesised two dinuclear platinum(II) complexes of bis-bidentate cyclometallating ligands incorporating mono- and bis-thiophene groups as shown in Figure 70.

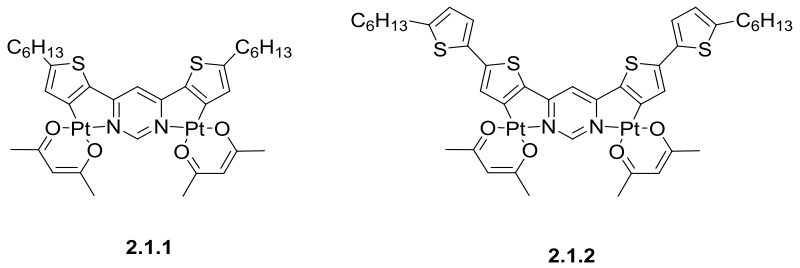

Figure 70: A figure to show the structures of the target di-platinum(II) complexes in which the two metal centres are rigidly-linked by 4,6-bis(5-hexylthiophen-2-yl)pyrimidine and 4,6-bis[5-(5-hexylthiophen-2-yl)thiophen-2-yl]pyrimidine bridging ligands and bear diketonate auxiliary ligands.

The first step in the synthesis of these two dinuclear platinum(II) complexes is the preparation of the bis-bidentate ligands. The C^N-N^C–coordinating bridging ligands, **2.1.5** and **2.1.8**, were prepared via Suzuki-Miyaura cross-coupling reactions using a synthetic procedure adapted from that reported by Kozhevnikov and co-workers for the preparation of similar pyrimidine-linked bridging ligands.[84] The bis-bidentate bridging ligands could be isolated, following recrystallisation from ethyl acetate, in yields of 84% and 90% respectively.

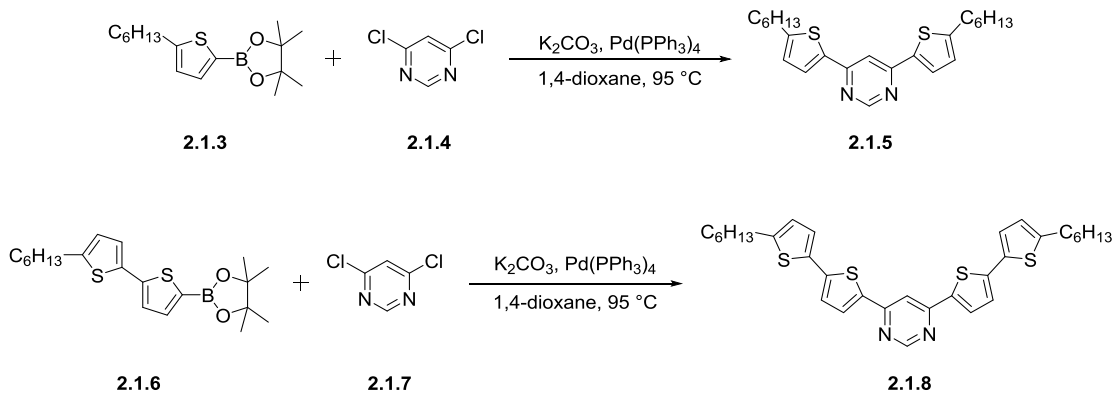

Figure 71: A reaction scheme to illustrate the synthetic route followed in the preparation of **2.1.5** and **2.1.8**.

The thiophene-containing bis-bidentate bridging ligands were then utilised in the synthesis of the corresponding dinuclear platinum(II) complexes as shown in Figure 72 and Figure 73 below.

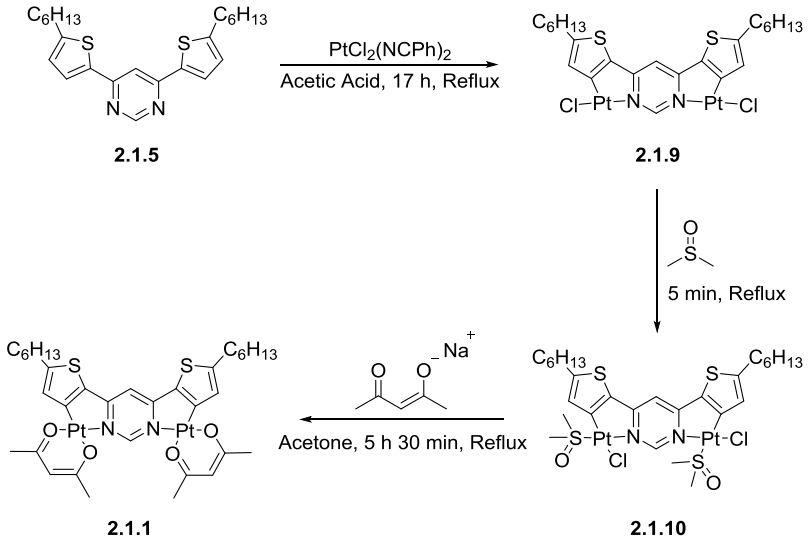

Figure 72: A reaction scheme to illustrate the synthesis of the dinuclear platinum(II) complex, **2.1.1**. The desired complex could be isolated in a yield of 43% following purification by column chromatograpy.

As is shown in Figure 72, the first step in the synthesis of **2.1.1** is reaction of the bridging ligand 4,6-bis(5-hexylthiophen-2-yl)pyrimidine with the platinum salt $PtCl_2(NCPh)_2$ to form a dichloro-bridged platinum dimer, **2.1.9**. This platinum dimer was then converted to the corresponding DMSO complex through refluxing the dichloro-bridged dimer in DMSO for 5 minutes. The DMSO complex, **2.1.10**, was the reacted with sodium acetylacetonate in acetone and the final

dinuclear platinum(II) complex, **2.1.1**, was isolated as a red solid in a yield of 43% following purification by column chromatography.

Using the same synthetic route, the equivalent bimetallic platinum(II) complex incorporating the bis-bidentate ligand **2.1.8** with extended, conjugated bis-thiophene moieties was prepared. This bis-N^C-coordinating ligand was reacted with K_2PtCl_4 to form the dichloro-bridged dimer **2.1.11**. In the same way as described for **2.1.1**, the platinum(II) dimer was first converted to the corresponding DMSO complex before reaction with sodium acetylacetonate to give the target dinuclear Pt(II) complex, **2.1.2**, as shown in Figure 73. This complex was also purified via column chromatography.

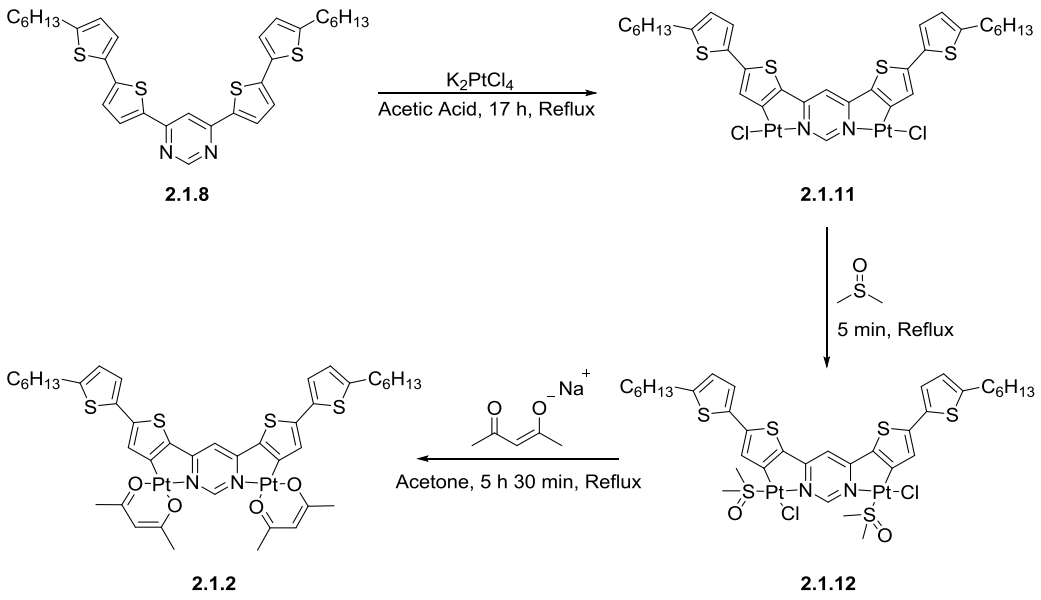

Figure 73: A reaction scheme to show the synthetic route used to isolate the dinuclear platinum(II) complex, **2.1.2**.

These complexes were characterised using ^{1}H and ^{13}C NMR spectroscopy and high-resolution mass spectrometry.

The ^{1}H NMR spectra of **2.1.1** and **2.1.2** show signals integrating to 44 and 60 protons respectively. The aromatic regions of these NMR spectra are shown below in Figure 74 and Figure 75. These figures illustrate the characteristic proton signals present in the NMR spectra that are used to identify the pure bimetallic platinum(II) complexes.

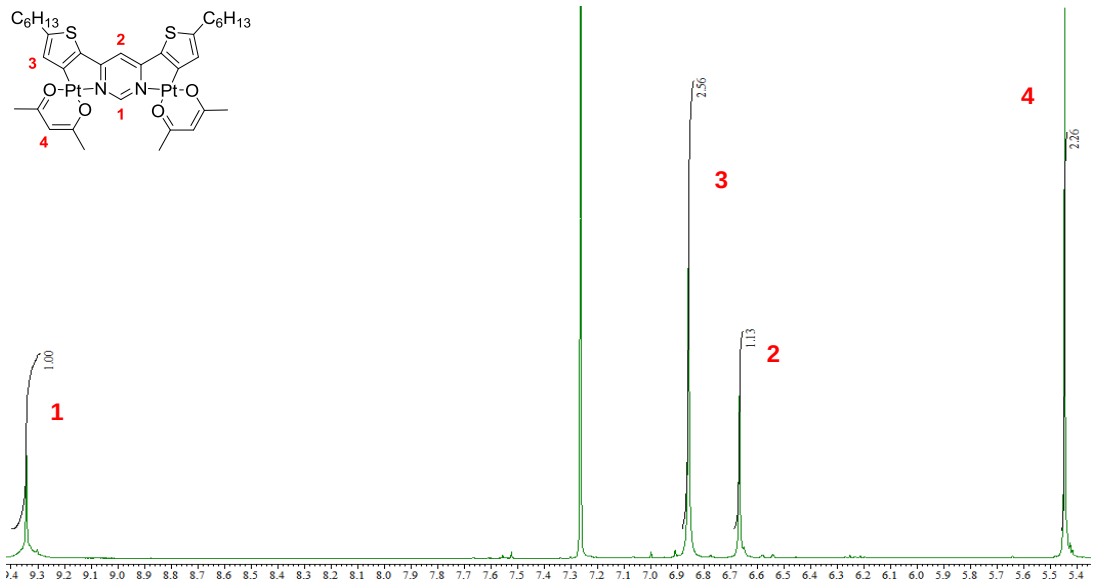

Figure 74: Aromatic region of the ^{1}H NMR spectra of dinuclear platinum(II) complex **2.1.1**.

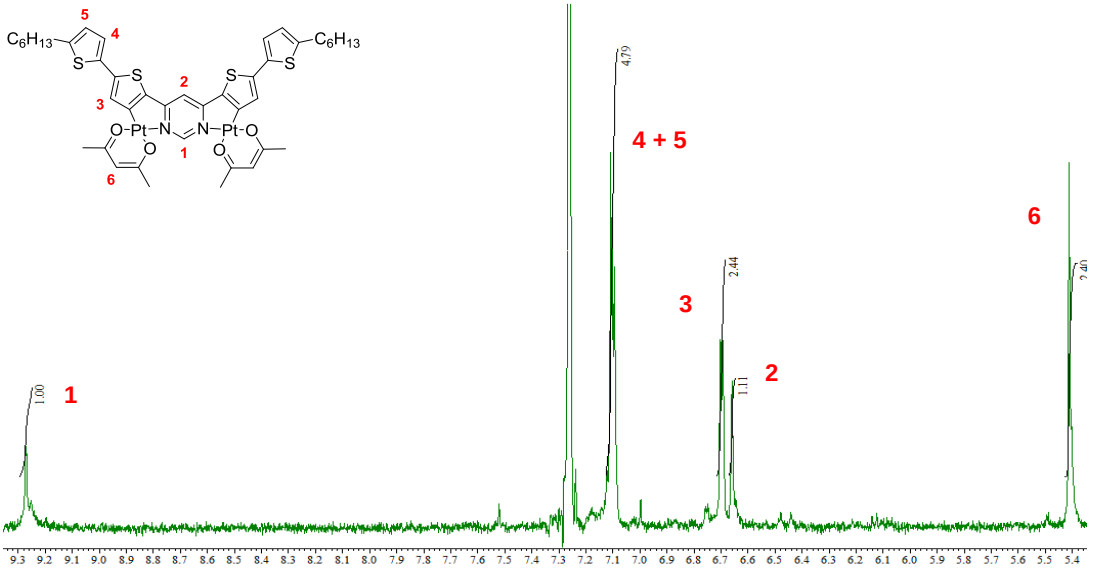

Figure 75: Aromatic region of the ^{1}H NMR spectra of dinuclear platinum(II) complex **2.1.2**.

The characteristic proton signals at high chemical shift (≈ δ 9.3 ppm) in both NMR spectra, correspond to the proton at the 2-position of the central pyrimidine ring. In addition, the peak at approximately δ 5.4 ppm in each of the spectra corresponds to the central proton of the acac auxiliary ligands. The 1:2 ratio between these proton signals, for both complexes **2.1.1** and **2.1.2**, confirms that we have isolated the dinuclear platinum(II) complexes.

The photophysical properties of these two dinuclear platinum(II) complexes were measured by Marsel Shafikov in the group of Professor Hartmut Yersin at Regensburg University. The

absorption and emission spectra for both the mono- and bis-thiophene bis-bidentate bridging ligands and their corresponding bimetallic platinum(II) complexes are shown in Figure 76. Numerical absorption and emission data are summarised in Table 2.

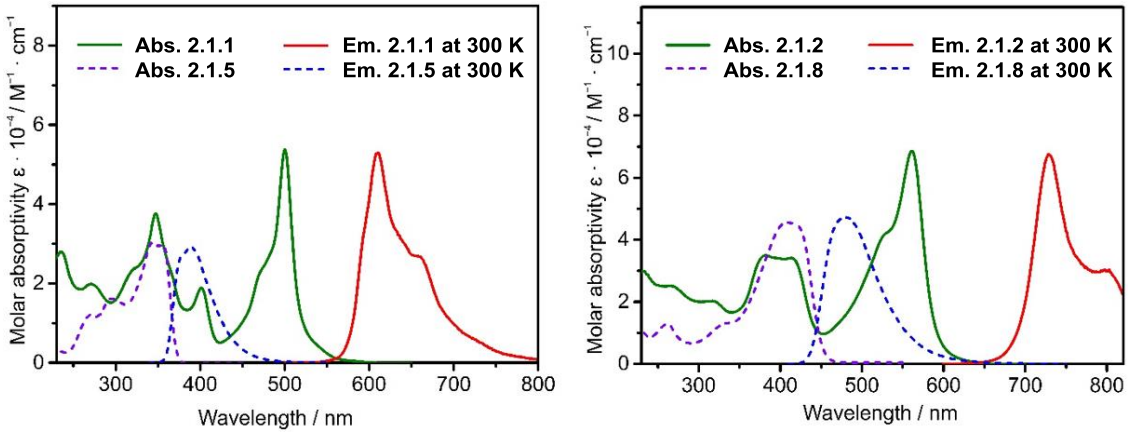

Figure 76: Absorption and emission spectra of the mono- and bis-thiophene bis-bidentate bridging ligands and their corresponding dinuclear platinum(II) complexes. The mono-thiophene analogues (**2.1.5** and **2.1.1**) are shown in the spectra on the left and the bis-thiophene compounds (**2.1.8** and **2.1.2**) are shown in the right.

Table 2: Ambient temperature absorption and emission data of the platinum(II) complexes **2.1.1** and **2.1.2**, and of proligands **2.1.5** and **2.1.8**.

	Absorption CH_2Cl_2 **solution** λ_{max}/ **nm** (ε / $M^{-1}\cdot cm^{-1}$)	**Emission** CH_2Cl_2 **solution** ($c \approx 10^{-5}$ **M)**		
		300 K (degassed solution)		
		λ_{max}/ **nm**	τ / **µs**	Φ_{PL}
2.1.1	235 (27873), 270 (19852), 347 (37593), 400 (18740), 470 (22443), 500 (53822)	610, 660	11.9	0.85
2.1.5	271 (12108), 296 (16236), 344 (30515), 355 (29884)	390	-	0.65
2.1.2	232 (28824), 270 (24862), 320 (20169), 380 (34900), 415 (34048), 527 (41546), 560 (68450)	730, 800	10.5	0.15
2.1.8	262 (12929), 332 (12987), 406 (45460), 420 (44841)	480	-	0.80

Firstly, from the absorption of the bis-bidentate proligands, it can be observed that increasing the conjugation length through the extension of the thiophene chain, going from **2.1.5** to **2.1.8**, leads to a red-shift in the energies of all absorption bands. This is the expected effect of increasing the conjugation length.

We also see the effect of this conjugation increase in the emission spectra of the two proligands, with the emission maxima of **2.1.8** red-shifted by 90 nm compared with **2.1.5**. Both of the bis-bidentate proligands are luminescent in degassed CH_2Cl_2 solution at room temperature with quantum yields measured at $\phi = 0.65$ and $\phi = 0.80$ for **2.1.5** and **2.1.8** respectively.

The absorption spectra of **2.1.1** shows higher energy bands between 235 and 347 nm that are comparable to peaks in the absorption spectra of the proligand **2.1.5**, suggesting that these bands arise from ligand-centred transitions. Lower energy bands above 400 nm are also observed and likely arise due to charge transfer transitions.[163] As we increase the length of the thiophene chain, in **2.1.2**, we again see a shift in the absorption bands to longer wavelengths ($\approx$ 60 nm) but still see bands corresponding to ligand-centred and charge transfer transitions.

The dinuclear platinum(II) complexes both exhibit strong phosphorescence at room temperature in degassed dichloromethane solution with a substantial red-shift of 120 nm observed on increasing the thiophene chain. Quantum yields for the **2.1.1** and **2.1.2** were measured to be $\phi = 0.85$ and $\phi = 0.15$ respectively. A large proportion of the emission of **2.1.2** is in the near-infrared region of the spectrum and therefore, could not be detected by the instrument used to perform luminescence measurements. As a result, the quantum yield measured is an underestimation of the true value. Luminescence lifetimes of 11.9 and 10.9 μs recorded for **2.1.1** and **2.1.2** respectively. These lifetimes are relatively long for a cyclometallated platinum(II) complex and may be suggestive of emission from an excited state with a high degree of ligand character. Importantly, no dual emission was observed in the spectra recorded for **2.1.2**, in which the bridging ligand features an extended thiophene chain. This contrasts with the report by Kozhevnikov *et. al.* previously mentioned. The absence of dual emission in this case suggests that introduction of a second metal centre leads to an increase in the contribution from the metal d orbitals in the emissive state, sufficiently promoting ISC and phosphorescence.

In this section of work, two dinuclear platinum(II) complexes, in which the metal centres are rigidly-linked by bis-bidentate ligands incorporating mono- and bis-thiophene cyclometallating units, have been prepared and their photophysical properties investigated.

The results of this work show that through combining both classical and new alternative strategies, the absorption and emission of cyclometallated platinum(II) complexes can be further shifted to the red. The bimetallic complexes prepared show emission in the orange-red (610-660 nm) and near-infrared (730-800 nm) regions of the spectrum.

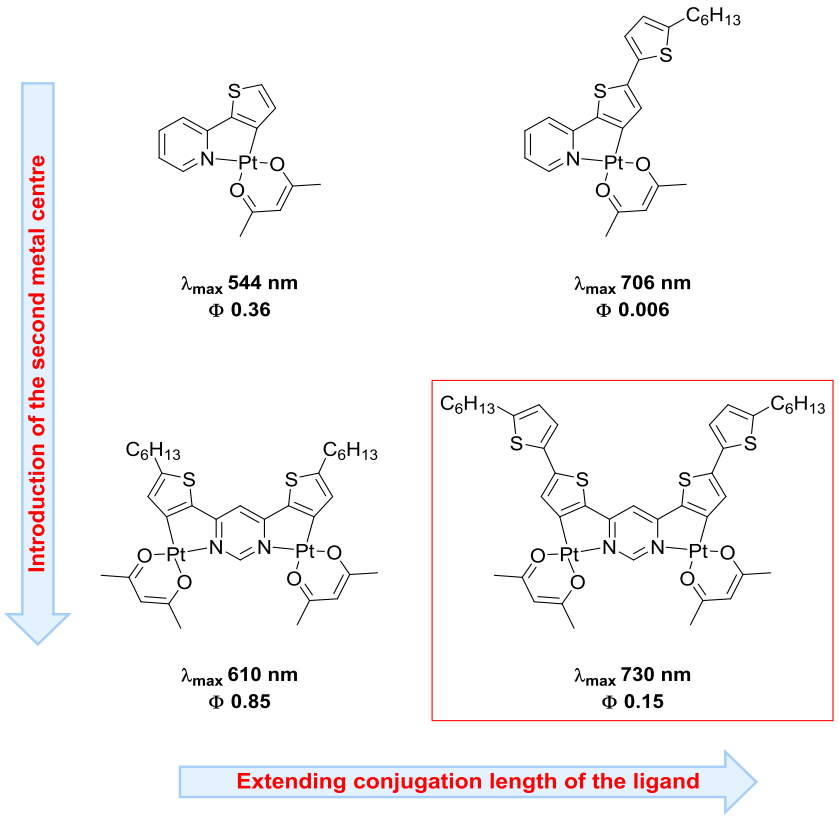

Figure 77: A scheme to illustrate the two strategies utilised in shifting emission of **2.1.2** to the NIR region of the spectrum; introduction of a second metal centre and extension of the conjugated system of the ligand.

In contrast to analogous monometallic platinum(II) complexes, no dual emission was observed on increasing the conjugation length of the cyclometallating ligand through the incorporation of additional thiophene groups. This suggests that there is sufficient metal-ligand orbital mixing for the high SOC of the Pt(II) centres to be effective in the promotion of ISC and phosphorescence from the T_1 excited state.[163]

The new emitters are now being evaluated as red and near-infrared emitters in applications such as OLEDs. The results will be published in due course.

2.2 Bis-Tetradentate Di-Platinum(II) Complex

As is shown throughout the work reported here, the bridging ligand selected to link two metal centres can have a large effect on the structural, chemical and photophysical properties of the resulting luminescent multimetallic complex. The preparation of dinuclear platinum(II) complexes with emission maxima in the red region of the visible spectrum has been previously discussed in sections 2.0 and 2.1. In complexes **2.1.1** and **2.1.2** previously discussed, the incorporation of two metal centres and an extended conjugated system lead to highly luminescent bimetallic Pt(II) complexes. The rigidity introduced by the bis-bidentate bridging ligand is also an important factor in the efficient luminescence exhibited by these complexes.

In this work, we have synthesised an unprecedented rigid, dinuclear platinum(II) complex through the use of a highly-conjugated bis-tetradentate bridging ligand.

Che *et. al*. suggested that the use of dianionic tetradentate ligands in the synthesis of neutral square planar platinum(II) complexes would give robust, rigid complexes with high thermal stability. Che and co-workers reported a wide range of dianionic tetradentate ligands with a variety of coordination modes as shown in Figure 78. These modes include (O^N^N^O), (N^N^N^N), (C^N^N^C), (O^C^C^O) and (O^N^C^N).

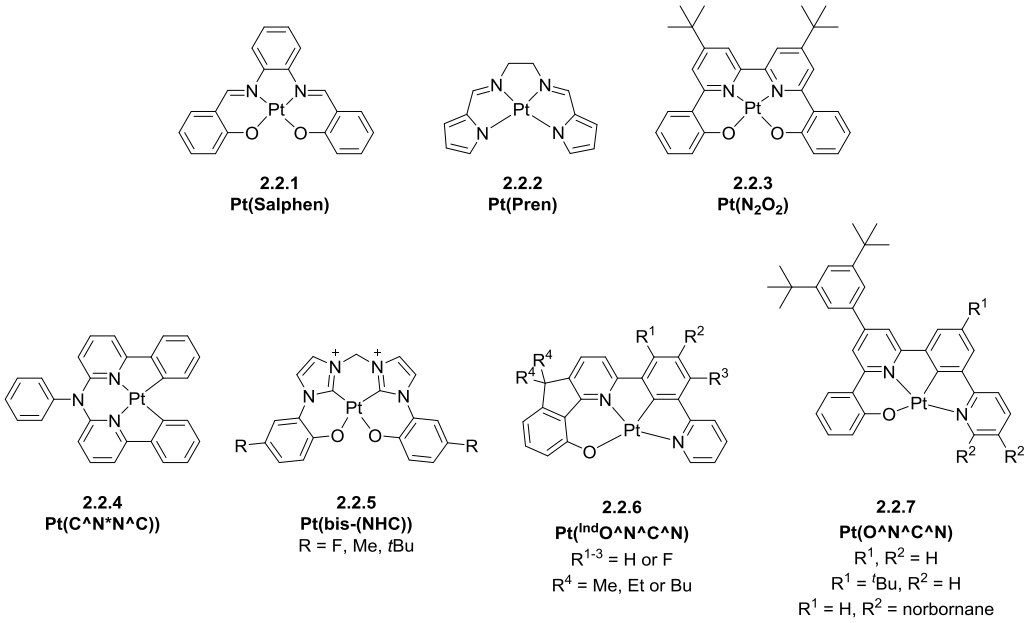

Figure 78: A figure to show a selection of the tetradentate ligands utilised in the preparation of charge-neutral, luminescent Pt(II) complexes as reported by Che and co-workers.[164, 167, 169-172]

Initially Che *et. al.* focussed on the synthesis of non-cyclometallating, dianionic, tetradentate ligand systems as shown in Figure 78 (top panel). These simple N-donor ligands are easily synthesised and structurally modified and from these ligands emissive Pt(II) complexes were prepared. The platinum(II) complex Pt(Pren), reported in 2005, exhibits yellow emission with the maxima at 566 nm and a lower energy shoulder at 613 nm in CH_3CN solution. This complex shows concentration-dependent emission both in solution and thin films, with an increase in concentration resulting in a red-shift. This lower energy emission was assigned to excimer or oligomer formation. Pt(Pren) was subsequently used in the fabrication of a highly efficient red electroluminescent device showing high brightness.[169, 170] Using these types of dianionic, tetradentate ligands in the preparation of Pt(II) complexes, emission in the red (630 nm) and yellow-green (550 nm) regions of the visible spectrum have been demonstrated.[169, 170]

Che and co-workers also reported a series of tetradentate Pt(II) complexes, based on bis(N-heterocyclic carbene) ligands, showing deep-blue emission (443-461 nm). The resulting complexes were used in the preparation of blue-emitting OLEDs with efficiencies in the range of 24-29%.[171, 172]

A third class of tetradentate ligand, with O^N^C^N coordination, was investigated by Che *et. al.* (Figure 78). These structurally rigid tetradentate ligands afford robust Pt(II) complexes exhibiting high luminescence quantum yields (ϕ = 0.60–0.99) and high thermal stability (>400 °C).[164-167]

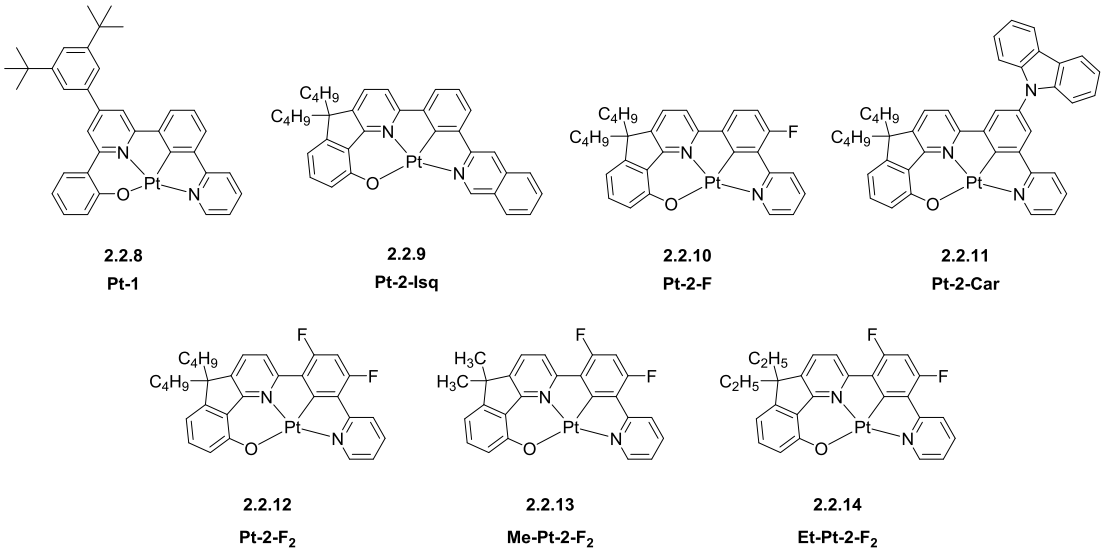

Figure 79: A figure to illustrate a selection of the tetradentate Pt(II) complexes reported by Che *et. al.*, displaying varied ligand substitution patterns. The changes in ligand substitution pattern have been observed to have a marked effect on the photophysical properties of the resulting Pt(II) complexes.[164, 165]

It has been observed that the substitution pattern of the tetradentate O^N^C^N ligand has a significant effect on the emission properties, for example, the ratio of monomer and excimer emission. Consequently, it is possible to exploit the ligand substitution pattern in order to utilise Pt(II) tetradentate complexes as emitters in monochromatic devices or as single emitters in white light-emitting devices. Figure 79 shows a selection of the tetradentate platinum(II) complexes reported.

The polymer light-emitting devices (PLEDs) of these complexes (top panel) were fabricated. **2.2.8** shows strong low-energy emission, in addition to monomer emission, assigned to the formation of excimers. Excimer emission is detrimental to the performance of monochromatic PLEDs as evidenced by the efficiency decrease of the **2.2.8** device from 9.53% to 7.25% and the lowering of colour purity. Excimer emission is not observed for **2.2.9**, **2.2.10** or **2.2.11**. This is due to the suppression of intermolecular interactions through the use of bulky substituents. As a result, complexes bearing tetradentate ligands with bulky substituents are ideal for utilisation in

monochromatic PLEDs. The device fabricated using **2.2.11** showed the best performance at 8wt% doping and an external quantum efficiency (EQE) of 15.55%.

2.2.12 was previously reported by Che and co-workers as a single emitter in both white light-emitting OLEDs and PLEDs showing EQEs of 16.5% and 9.7%. In order to investigate the effect of alkyl chain length on the extent of intermolecular reactions and attempt to control excimer emission, PLEDs of **2.2.13** and **2.2.14** were prepared. It was observed that the alkyl chains significantly affect the distance between two [Pt(O^N^C^N)] complexes and therefore, the intermolecular interactions. The EL spectra of **2.2.13** shows notable excimer emission at low concentrations of 4wt%. The intensity of this excimer emission increases quickly as the concentration is increased, equalling the intensity of monomer emission at 10wt%. Conversely, for **2.2.14** and **2.2.12**, excimer emission is unobservable at low concentrations and grows more slowly with desired balanced white emission observed at doping concentrations of 16wt% and 20wt% respectively. The longer ethyl chain of **2.2.14** leads to weaker interactions between [Pt(O^N^C^N)] molecules, resulting in the need for higher doping concentrations for balanced white emission. PLEDs of these complexes were fabricated with **2.2.14** giving the best performance. The optimised white light-emitting PLED, utilising **2.2.14** as a single emitter, was prepared using a doping concentration of 16wt% and showing an EQE of 12.73%.[165]

Building on the success of tetradentate O^N^C^N platinum(II) complexes reported by Che and co-workers; in this work we were interested in the preparation of a bis-tetradentate ligand for use in the synthesis of a luminescent, rigid, bimetallic Pt(II) complex.[164-167]

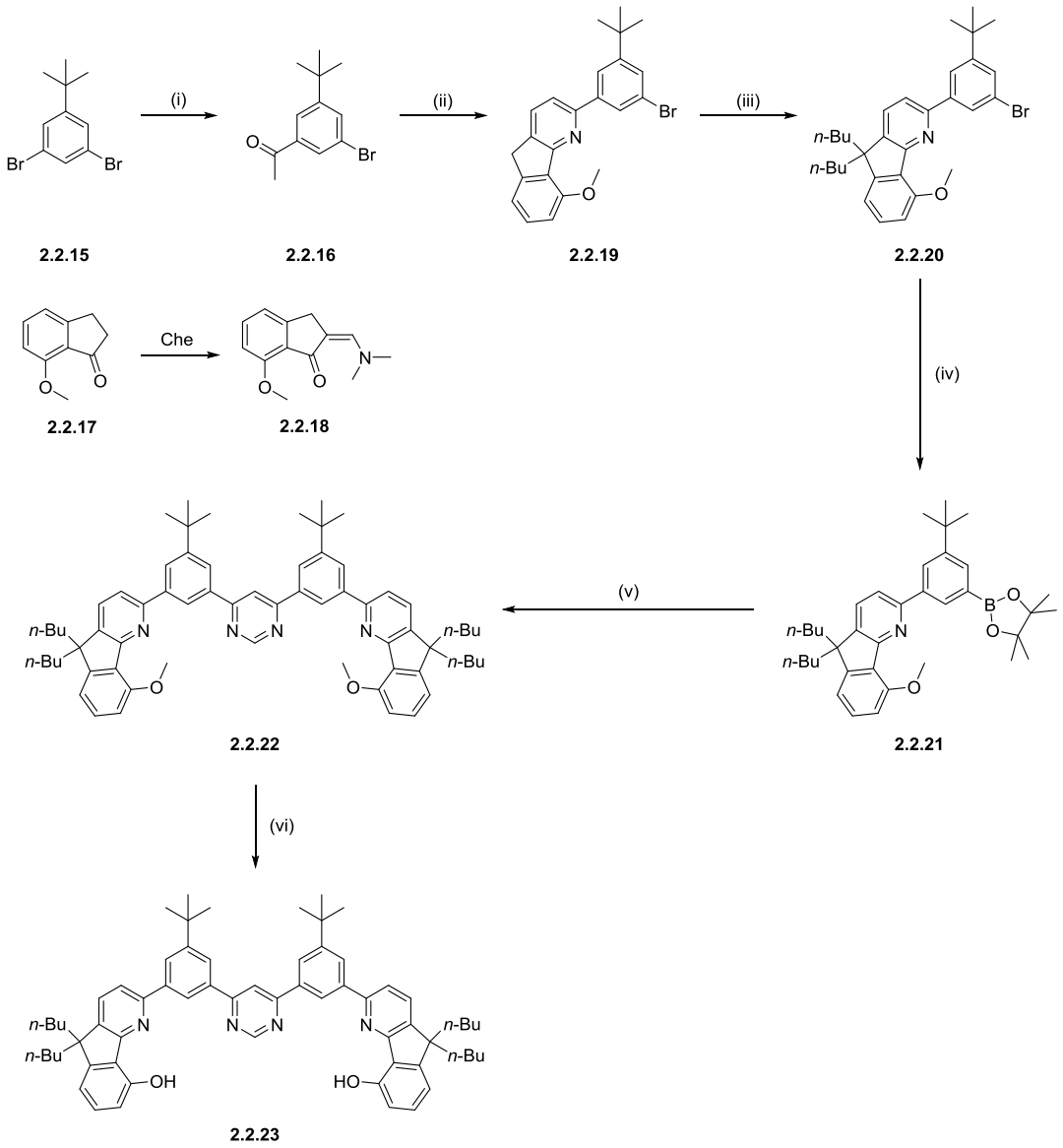

Figure 80: A reaction scheme to show the multi-step synthesis of the bis-tetradentate ligand **2.2.23**. (i) BuLi, N-methoxy-N-methylacetamide, Et_2O (anhydrous), 90%; (ii) **2.2.18**, KO^{t}Bu, THF (anyhydrous), NH_4OAc in AcOH, 83%; (iii) 1-Bromobutane, KO^{t}Bu, THF (anhydrous), 93%; (iv) Bis(pinacolato)diboron, KOAc, $Pd(dppf)Cl_2$, 1,4-dioxane (anhydrous), 87%; (v) 4,6-dichloropyrimidine, aq. K_2CO_3 (2M), $Pd(PPh_3)_4$, 1,4-dioxane (anhydrous), 14%; (vi) Pyridine hydrochloride, 70%.

The bis-tetradentate O^N^C^N-N^C^N^O ligand, **2.2.23**, was prepared as shown in Figure 80 and was isolated in good yield.[83, 84, 173] Compound **2.2.20** was prepared as described by Che *et. al.* using the synthetic route shown above. The desired compound was isolated in high yield (93%).[174] Compound **2.2.20** was then converted into the boronate derivative (**2.2.21**) via a Miyaura Borylation reaction through coupling with bis(pinacolato)diboron. The boronate derivative was also isolated in high yield (87%) and was further reacted with 4,6-dichloropyrimidine via a Suzuki-Miyaura cross-coupling reaction to give compound **2.2.22**. This Suzuki-Miyaura reaction

proceeded in low yield (14%) and therefore, optimisation of the reaction conditions for this step is required in the future in order to isolate a higher yield of compound **2.2.22**. The methoxy-protected bis-tetradentate proligand was deprotected via reaction with pyridine hydrochloride at 250 °C to give the desired bis-tetradentate proligand (**2.2.23**).

The final bis-tetradentate ligand consists of two O^N^C^N binding sites linked by a 4,6-disubstituted pyrimidine heterocycle. Pyrimidine was selected as the central heterocycle as a result of previous reports, by Kozhevnikov and co-workers, of highly luminescent dinuclear complexes of platinum(II) and iridium(III). *Tert*-butyl and *n*-butyl groups have been incorporated into the structure of the bis-tetradentate ligand in order to improve the solubility of the final dinuclear platinum(II) complex whilst decreasing the likelihood of excimer formation as discussed by Che and co-workers.[165]

Following the successful synthesis of bis-tetradentate ligand **2.2.23**, this ligand was utilised in the synthesis of a dinuclear platinum(II) complex as shown in Figure 81.[164]

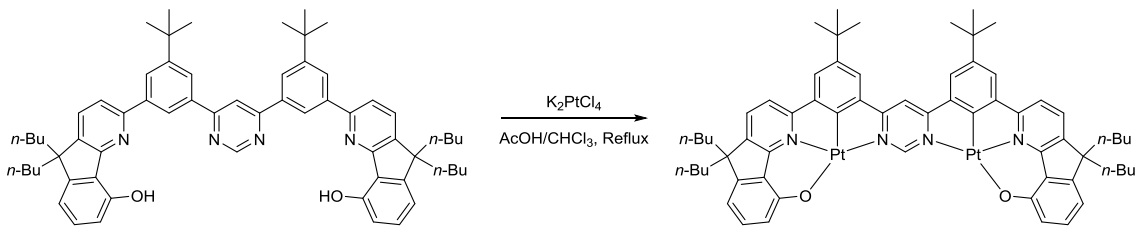

2.2.23 **2.2.24**

Figure 81: A scheme to show the synthesis of a rigidly-linked bis-tetradentate dinuclear platinum(II) complex (**2.2.24**) via the reaction of bis-tetradentate ligand **2.2.23** with K_2PtCl_4 in 9:1 mixture of acetic acid:chloroform.

The synthesis of this bimetallic Pt(II) complex proceeded under the same reaction conditions as those reported in the literature by Che *et. al.* in the synthesis of analogous monometallic, tetradentate platinum(II) complexes.[164] The bis-tetradenate ligand was heated to reflux with K_2PtCl_4 in a 9:1 mixture of acetic acid and chloroform. The desired dinuclear platinum(II) complex was isolated following purification by column chromatography and recrystallization

from methanol. The complex was isolated in very low yield (21%) and therefore, optimisation of the reaction procedures is required in the future.

The di-platinum(II) complex was characterised by ^{1}H and ^{13}C NMR spectroscopy and high-resolution mass spectrometry. The aromatic region of the ^{1}H NMR spectrum of **2.2.24** is shown in Figure 82. The peak at δ 10.2 ppm corresponds to proton environment 1 on the central pyrimidine ring and shows evidence of the ligand binding to the platinum(II) centres through observation of platinum(II) satellites.

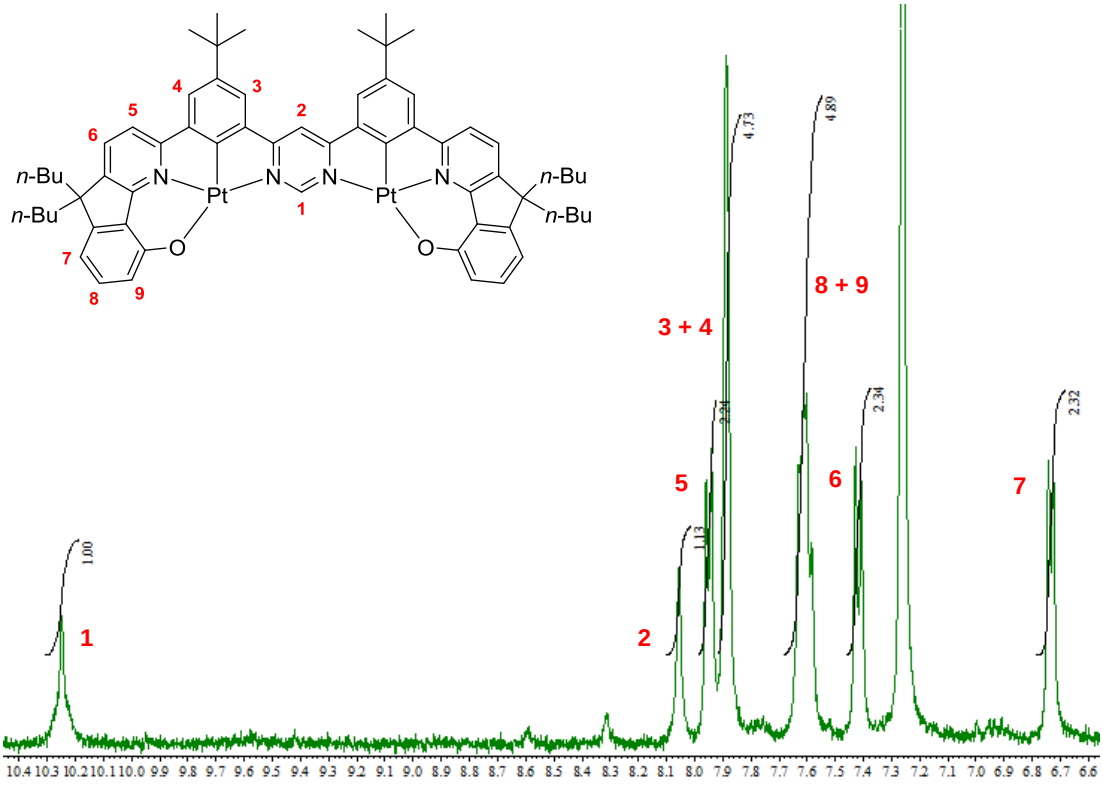

Figure 82: Aromatic region of the ^{1}H NMR spectrum of the di-platinum(II) complex **2.2.24**, in which the metal centres are rigidly-linked by a highly conjugated bis-tetradentate ligand.

The identity of the dinuclear platinum(II) complex was further confirmed by high-resolution mass spectrometry. The spectrum recorded is shown in Figure 83. The peak observed at m/z 1318.4860 corresponds to the ion $[M+H]^{+}$ and is a close match to the calculated value m/z 1318.4884.

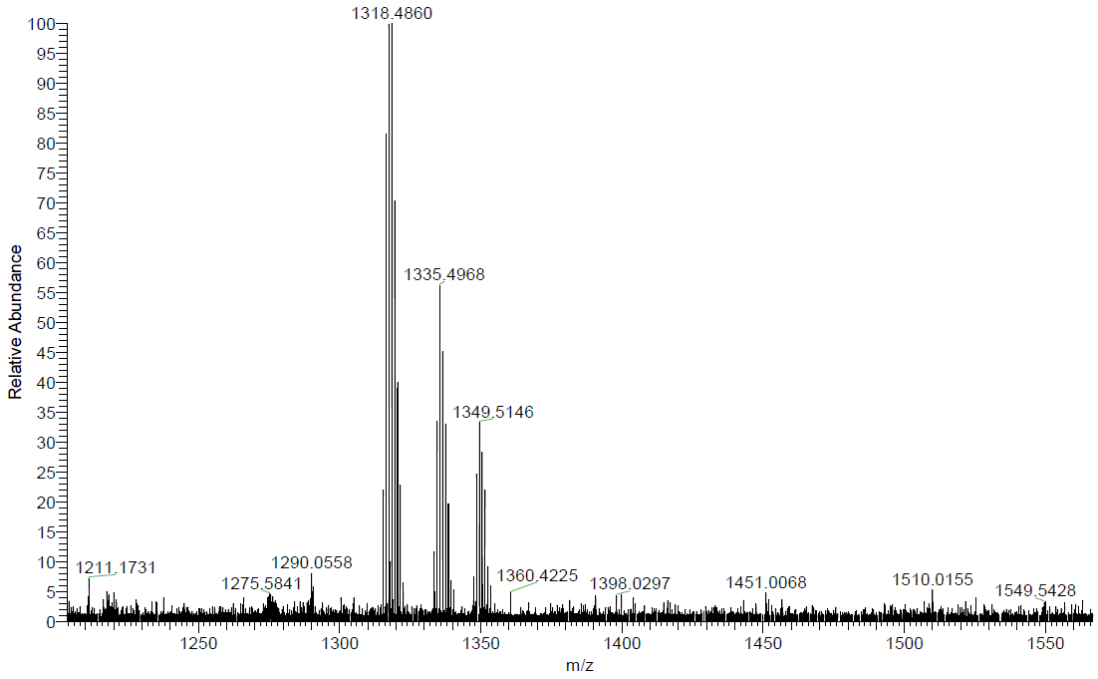

Figure 83: High resolution mass spectrum obtained for **2.2.24**, showing a peak for $[M+H]^+$ at m/z 1318.4860 (calc'd m/z 1318.4884).

In this section, we have successfully prepared a novel di-platinum(II) complex in which the metal centres are linked through a rigid, ditopic bis-tetradentate ligand. To the best of our knowledge, this is the first example of a bimetallic complex linked by a rigid, cyclometallating bis-tetradentate ligand of this type. The photophysical properties of this dinuclear platinum(II) complex, **2.2.24**, in which the metal centres are linked through a rigid bis-tetradentate ligand, will now be fully investigated in the group of Dr Fernando Dias at Durham University. The incorporation of **2.2.24** in an OLED device will also be investigated. The results of this study will be published in due course.

2.3 Experimental Section for Chapter 2

2.3.1 Bis-Thiophene Di-Platinum(II) Complex

Compound 2.1.5 – 4,6-di(5-hexylthiophenyl)pyrimidine[173]

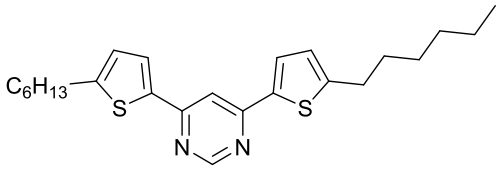

5-Hexyl-2-thiopheneboronic acid pinacol ester (1.96 g, 6.80 mmol), 4,6-dichloropyrimidine (0.392 g, 2.61 mmol), potassium carbonate (2.16 g, 15.6 mmol) and 1,4-dioxane (20 mL) were placed in a round bottomed flask and the reaction mixture degassed with argon for 10 min. Tetrakis(triphenylphosphine)palladium (0.183 g, 0.157 mmol) was added and the reaction mixture degassed for a further 10 minutes. The reaction mixture was then heated to reflux for 24 h. Toluene (15 mL) was added and the solution washed with water (3 x 10 mL). The organic layer was dried over $MgSO_4$ and the solvent evaporated under reduced pressure. The residue was recrystallised from ethyl acetate to give the product as a grey solid.

Yield: 0.908 g, 2.20 mmol, 84%

^{1}H NMR (400 MHz, $CDCl_3$): δ 8.98 (d, 1H, *J* = 1.4), 7.68 (d, 1H, *J* = 0.8), 7.65 (d, 2H, *J* = 3.7), 6.86 (d, 2H, *J* = 3.7), 2.87 (t, 4H, *J* = 7.8), 1.72-1.69 (m, 4H), 1.43-1.29 (m, 12H), 0.89 (t, 6H, *J* = 7.1).

^{13}C DEPT135 NMR (100 MHz, $CDCl_3$): δ 159.06 (C), 158.97 (CH), 151.71 (C), 139.32 (C), 127.37 (CH), 125.78 (CH), 107.85 (CH), 31.54 (CH_2), 31.44 (CH_2), 30.54 (CH_2), 28.72 (CH_2), 22.56 (CH_2), 14.09 (CH_3).

Compound 2.1.8 – 4,6-di(5'-hexyl-bithiophenyl)pyrimidine

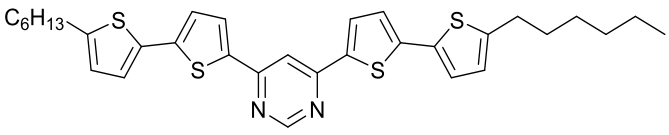

5′-Hexyl-2,2′-bithiophene-5-boronic acid pinacol ester (0.875 g, 2.32 mmol), 4,6-dichloropyrimidine (0.139 g, 0.923 mmol), potassium carbonate (0.771 g, 5.58 mmol) and 1,4-dioxane (20 mL) were placed in a round bottomed flask and the reaction mixture degassed with argon for 10 min. Tetrakis(triphenylphosphine)palladium (0.0645 g, 0.0558 mmol) was added and the reaction mixture degassed for a further 10 minutes. The reaction mixture was then heated to reflux for 24 h. Toluene (20 mL) was added and the solution washed with water (3 x 10 mL). The organic layer was dried over $MgSO_4$ and the solvent evaporated under reduced pressure. The residue was treated with methanol (20 mL) and the product collected as a dark green solid by filtration.

Yield: 0.478 g, 0.829 mmol, 90%

^{1}H NMR (400 MHz, $CDCl_3$): δ 9.00 (s, 1H, *J* = 0.9), 7.72-7.71 (m, 3H), 7.16 (d, 2H, *J* = 4.1), 7.13 (d, 2H, *J* = 3.7), 6.73 (d, 2H, *J* = 3.7), 2.82 (t, 4H, *J* = 7.8), 1.73-1.66 (m, 4H), 1.43-1.30 (m, 12H), 0.90 (t, 6H, *J* = 6.9).

^{13}C DEPT135 NMR (100 MHz, $CDCl_3$): δ 159.02 (CH), 158.67 (C), 147.03 (C), 142.76 (C), 139.51 (C), 134.16 (C), 128.14 (CH), 125.17 (CH), 124.65 (CH), 123.89 (CH), 107.91 (CH), 31.55 (CH_2), 30.23 (CH_2), 28.75 (CH_2), 22.58 (CH_2), 14.09 (CH_3).

Compound 2.1.1 (via 2.1.9 & 2.1.10)

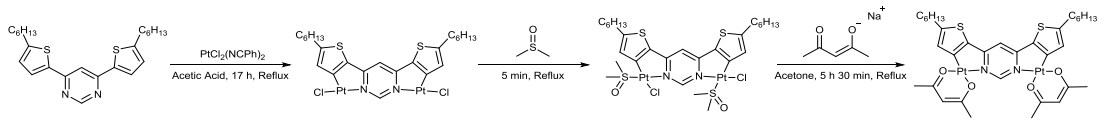

To a solution of 4,6-bis(5-hexylthiophen-2-yl)pyrimidine (0.134 g, 0.325 mmol) in acetic acid (80 mL), N-[dichloro(phenylformonitrile)platinio]benzonitrile (0.338 g, 0.714 mmol) was added. The reaction mixture was heated to reflux under argon for 17 h. The reaction mixture was cooled to room temperature and the solvent removed under reduced pressure. The dark red solid was filtered and washed with methanol (10 mL), water (15 mL) and methanol (10 mL).

Yield: 0.283 g, 0.324 mmol, 99%.

To the di-chlorobridged dimer (0.283 g, 0.324 mmol), DMSO (5 mL) was added and the reaction mixture was heated to reflux for 5 min. The reaction mixture was cooled slightly before methanol (10 mL) was added. Further methanol (30 mL) was added to aid in precipitation of the product. The precipitated solid was filtered and washed with methanol to give a dark red solid.

Yield: 0.201 g, 0.195 mmol, 60%.

The DMSO complex (0.198 g, 0.192 mmol) and acetone (100 mL) were added to a round-bottomed flask. To this, sodium acetylacetonate (0.235 g, 1.92 mmol) was added. The reaction mixture was heated to 100 °C under argon for 5 h 30 min. The reaction mixture was cooled to room temperature and water (100 mL) was added. The dark red solid formed was filtered and washed with water and acetone. The crude product was purified by column chromatography (silica gel) using DCM 100%.

Yield: 0.0821 g, 0.0822 mmol, 43%

^{1}H NMR (400 MHz, $CDCl_3$): δ 9.37 (s, 1H), 6.87 (s, 2H), 6.70 (s, 1H), 5.45 (s, 2H), 2.91 (t, 4H, *J* = 7.6), 1.75-1.67 (m, 4H), 1.42-1.29 (m, 12H), 0.88 (t, 6H, *J* = 6.8).

^{13}C DEPT135 NMR (100 MHz, $CDCl_3$): δ 185.02 (C), 183.58 (C), 167.64 (C), 157.35 (C), 128.31 (CH), 102.52 (CH), 100.59 (CH), 31.61 (CH_2), 31.53 (CH_2), 31.09 (CH_2), 28.89 (CH_2), 27.98 (CH), 26.75 (CH), 22.60 (CH), 14.12 (CH_2).

HRMS (FTMS^{+}): for $[M]^{+}$ calc'd 998.2027, found 998.2031.

Compound 2.1.2 (via 2.1.11 & 2.1.12)

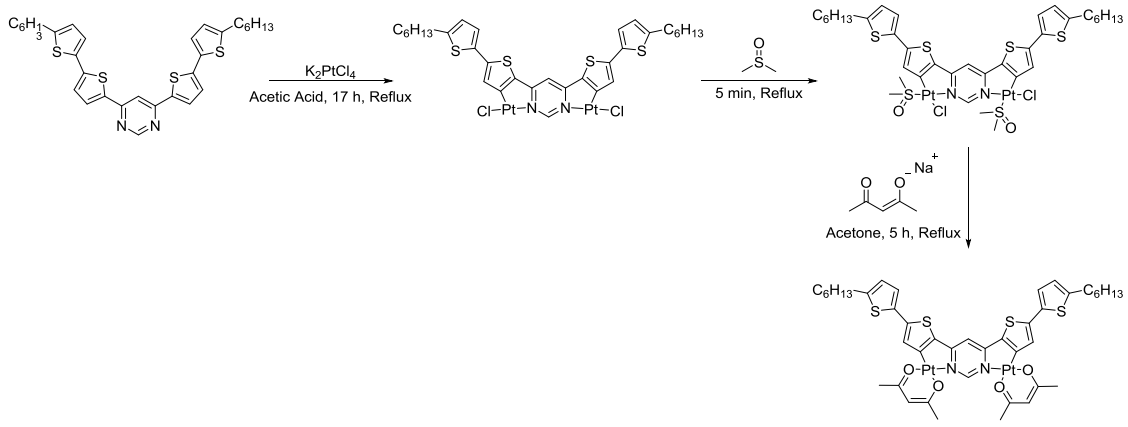

To a solution of 4,6-bis[5-(5-hexylthiophen-2-yl)thiophen-2-yl]pyrimidine (0.153 g, 0.265 mmol) in acetic acid (120 mL), potassium tetrachloroplatinate (0.242 g, 0.583 mmol) was added. The reaction mixture was heated to reflux under argon for 3 d. The reaction mixture was cooled to room temperature. The precipitated solid was filtered and washed with methanol (10 mL), water (15 mL) and methanol (10 mL).

Yield: 0.242 g, 0.233 mmol, 88%.

To the dichloro-bridged dimer (0.242 g, 0.233 mmol), DMSO (2 mL) was added. The reaction mixture was stirred at 110-120 °C for approximately 5 min and allowed to cool to room temperature. Methanol (10 mL) was added and the mixture was filtered. The solid collected was washed with methanol. This solid was re-dissolved in DMSO (2 mL) and stirred at 120-130 °C for 1 hour. The reaction mixture was cooled to room temperature and again methanol was added. The resulting solid was filtered. This product was purified by column chromatography (silica gel, DCM → DCM:MeOH). This product was further purified by column chromatography (fine silica gel, DCM → DCM:EtOAc 4:1 → DCM:MeOH 20:1) to give the DMSO intermediate, **2.1.12**.

Yield: 0.0950 g, 0.0797 mmol, 30%.

The DMSO complex (0.0950 g, 0.0797 mmol) and acetone (40 mL) were added to a round-bottomed flask. To this solution, sodium acetylacetonate (0.0973 g, 0.797 mmol) was added. The reaction mixture was heated to reflux under argon for 5 h. The reaction mixture was then cooled to room temperature and water (100 mL) was added. The precipitated dark red solid was filtered and washed with water (5 mL) and acetone (5 mL). The crude product was purified by column chromatography (silica gel, DCM:MeOH, 20:1) to give the desired product.

Yield: 0.0446 g, 0.0383 mmol, 48%

^{1}H NMR (400 MHz, $CDCl_3$): δ 9.27 (s, 1H), 7.11-7.09 (m, 4H), 6.70 (d, 2H, *J* = 3.7), 6.60 (s, 1H), 5.41 (s, 2H), 2.81 (t, 4H, *J* = 7.6), 1.74-1.66 (m, 4H), 1.42-1.32 (m, 12H), 0.91 (t, 6H, *J* = 6.7).

HRMS (FTMS^{+}): for $[M]^{+}$ calc'd 1162.1782, found 1162.1794.

2.3.2 Bis-Tetradentate Platinum(II) Complex

Compound 2.2.16 – 1-(3-bromo-5-tert-butylphenyl)ethan-1-one[167]

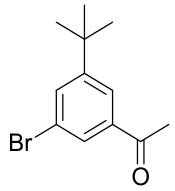

To a stirring solution of 1,3-dibromo-5-*tert*-butylbenzene (5.01 g, 17.2 mmol) in anhydrous diethyl ether, BuLi (12.9 mL, 20.6 mmol, 1.6 M) was added dropwise under argon at -78 °C. The mixture was stirred at -78 °C for 30 min. N-methoxy-N-methylacetamide (2.74 mL, 25.8 mmol) was added dropwise. The reaction mixture was stirred for 12 h and allowed to warm to room temperature. The reaction mixture was quenched with saturated NH_4Cl solution. Water was added and the mixture was extracted with diethyl ether (2 x 150 mL). The combined organic extracts were washed with water (2 x 200 mL), separated and dried with $MgSO_4$. The solvent was evaporated to dryness under reduced pressure/ The crude product was purified by column chromatography (silica gel, hexane:ethyl acetate, 10:1) to give the desired product as a yellow oil. Yield: 3.95 g, 15.4 mmol, 90%

^{1}H NMR (400 MHz, $CDCl_3$): δ 7.91 (t, 1H, *J* = 1.6), 7.88 (t, 1H, *J* = 1.6), 7.71 (t, 1H, *J* = 1.6), 2.60 (s, 3H), 1.34 (s, 9H).

^{13}C DEPT135 NMR (100 MHz, $CDCl_3$): δ 197.12 (C), 154.15 (C), 138.66 (C), 133.35 (CH), 128.88 (CH), 123.87 (CH), 122.77 (C), 35.18 (C), 31.20 (CH_3), 26.83 (CH_3).

Compound 2.2.18 – (2Z)-2-[(dimethylamino)methylidene]-7-methoxy-2,3-dihydro-1H-inden-1-one[166, 167]

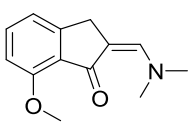

7-Methoxy-1-indanone (2.40 g, 14.8 mmol) and N,N-dimethylformamide dimethyl acetal (9.90 mL, 74.1 mmol) were added to a round-bottomed flask. The reaction mixture was heated to reflux

for 18 h. The reaction mixture was cooled to room temperature and the precipitated solid was filtered *in vacuo* and washed with petroleum ether 60-80°C. The product was isolated as a brown solid.

Yield: 2.99 g, 13.8 mmol, 93%

^{1}H NMR (400 MHz, $CDCl_3$): δ 7.42-7.38 (m, 2H), 7.00 (dd, 1H, *J* = 7.3, 0.9), 6.80 (d, 1H, *J* = 8.2), 3.95 (s, 3H), 3.85 (s, 2H), 3.14 (s, 6H).

^{13}C DEPT135 NMR (100 MHz, $CDCl_3$): δ 191.35 (C), 157.79 (C), 150.59 (C), 146.05 (CH), 133.14 (CH), 127.97 (C), 117.49 (CH), 108.85 (CH), 104.06 (C), 55.87 (CH_3), 31.32 (CH_2).

Compound 2.2.19 – 2-(3-bromo-5-tert-butylphenyl)-9-methoxy-5H-indeno[1,2-b]pyridine

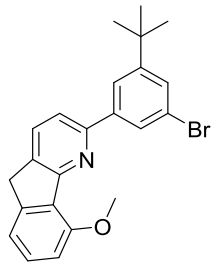

1-(3-bromo-5-*tert*-butylphenyl)ethan-1-one (3.65 g, 14.3 mmol), (2Z)-2-[(dimethylamino)methylidene]-7-methoxy-2,3-dihydro-1H-inden-1-one (3.11 g, 4.3 mmol) and KO^{t}Bu (1.93 g, 17.2 mmol) were added to a dry, argon-flushed round-bottomed flask. Anhydrous THF (100 mL) was added and a red suspension was formed. A solution of NH_4OAc in acetic acid (55.0 g, 73 mL) was added. The red solution was heated to reflux for 16 h. The reaction mixture was cooled to room temperature. Water was added and the mixture extracted with dichloromethane. The organic phase was separated, dried with $MgSO_4$ and the solvent evaporated to dryness under reduced pressure. The crude residue was purified by column chromatography (silica gel, hexane:ethyl acetate, 10:1) and the desired product isolated as a yellow solid.

Yield: 4.80 g, 11.8 mmol, 83%

^{1}H NMR (400 MHz, $CDCl_3$): δ 8.19 (t, 1H, *J* = 1.6), 8.06 (t, 1H, *J* = 1.6), 7.85 (d, 1H, *J* = 8.0), 7.60 (d, 1H, *J* = 7.6), 7.55 (t, 1H, *J* = 1.8), 7.39 (t, 1H, *J* = 7.8), 7.20 (d, 1H, *J* = 7.6), 6.98 (d, 1H, *J* = 8.4), 4.11 (s, 3H), 3.92 (s, 2H), 1.40 (s, 9H).

^{13}C DEPT135 NMR (100 MHz, $CDCl_3$): δ 160.72 (C), 156.49 (C), 154.95 (C), 153.60 (C), 146.47 (C), 141.66 (C), 135.23 (C), 132.33 (CH), 130.03 (CH), 128.78 (CH), 128.65 (C), 127.13 (CH), 122.92 (CH), 122.77 (C), 117.63 (CH), 116.96 (CH), 109.80 (CH), 56.06 (CH_3), 35.10 (C), 34.65 (CH_2), 31.25 (CH_3).

Compound 2.2.20 – 2-(3-bromo-5-tert-butylphenyl)-5,5-dibutyl-9-methoxy-5H-indeno[1,2-b]pyridine

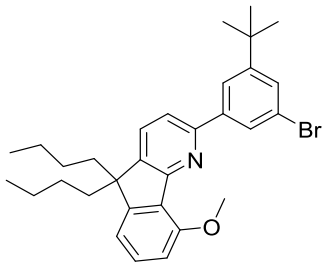

2-(3-bromo-5-*tert*-butylphenyl)-9-methoxy-5H-indeno[1,2-b]pyridine (4.80 g, 11.8 mmol) was added to a dry round-bottomed flask flushed with argon. Anhydrous THF (150 mL) was added and the mixture stirred. 1-bromobutane (3.16 mL, 29.4 mmol) was added and the mixture was further stirred. KO^{t}Bu (3.30 g, 29.4 mmol) was added. The reaction mixture was heated to reflux for 15 h under argon. The reaction mixture was cooled to room temperature. Water was added and the reaction mixture was extracted with dichloromethane. The organic phase was separated, dried with $MgSO_4$ and the solvent evaporated to dryness. The crude product was purified by column chromatography (silica gel, hexane:ethyl acetate 10:1) and the desired product was isolated as a brown solid.

Yield: 8.62 g, 16.6 mmol, 93%

^{1}H NMR (400 MHz, $CDCl_3$): δ 8.30 (t, 1H, *J* = 1.6), 8.07 (t, 1H, *J* = 1.6), 7.63 (q, 2H, *J* = 8.0, 6.4), 7.54 (t, 1H, *J* = 1.8), 7.40 (t, 1H, *J* = 7.8), 7.01 (d, 1H, *J* = 7.3), 6.93 (d, 1H, *J* = 8.2), 4.11 (s, 3H), 2.03-1.95 (m, 4H), 1.41 (s, 9H), 1.11-1.02 (m, 4H), 0.67-0.55 (m, 10H).

^{13}C DEPT135 NMR (100 MHz, $CDCl_3$): δ 160.59 (C), 156.40 (C), 154.79 (C), 154.26 (C), 153.78 (C), 142.96 (C), 141.55 (C), 130.68 (CH), 130.47 (CH), 128.91 (CH), 127.97 (C), 127.03 (CH),

122.85 (CH), 117. 09 (CH), 115.12 (CH), 109.62 (CH), 56.04 (CH_3), 53.20 (C), 40.13 (CH_2), 35.28 (C), 31.40 (CH_3), 26.20 (CH_2), 23.19 (CH_2), 13.98 (CH_3).

Compound 2.2.21 - 5,5-dibutyl-2-[3-tert-butyl-5-(4,4,5,5-tetramethyl-1,3,2-dioxaborolan-2-yl)phenyl]-9-methoxy-5H-indeno[1,2-b]pyridine

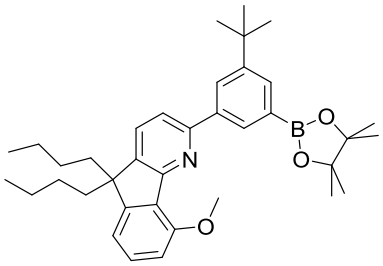

2-(3-bromo-5-tert-butylphenyl)-5,5-dibutyl-9-methoxy-5H-indeno[1,2-b]pyridine (1.26 g, 2.42 mmol) was added to a dry round-bottomed flask flushed with argon. Anhydrous 1,4-dioxane (50 mL) was added. The reaction mixture was stirred. Bis(pinacolato)diboron (0.920 g, 3.62 mmol) and potassium acetate (0.494 g, 5.03 mmol) were added and the reaction mixture was degassed under argon for 15 min. [1,1′-Bis(diphenylphosphino)ferrocene]dichloropalladium(II) (0.0986 g, 0.121 mmol) was added and the reaction mixture was degassed for a further 10 min. The reaction mixture was heated to 90 °C for 18 h. The reaction mixture was cooled to room temperature. The reaction mixture was extracted with diethyl ether and washed with water. The organic phase was separated and dried with $MgSO_4$. The solvent was evaporated to dryness under reduced pressure. The crude mixture was purified by column chromatography (silica gel, gradient elution with hexane:ethyl acetate 100:0 to 10:1) and the product was isolated as a brown oil.

Yield: 1.20 g, 2.11 mmol, 87%

^{1}H NMR (400 MHz, $CDCl_3$): δ 8.65 (t, 1H, *J* = 2.1), 8.30 (s, 1H), 7.87 (m, 1H), 7.78 (d, 1H, *J* = 7.8), 7.62 (d, 1H, *J* = 7.8), 7.38 (t, 1H, *J* = 7.8), 7.00 (d, 1H, *J* = 6.9), 6.92 (d, 1H, *J* = 8.2), 4.11 (s, 3H), 2.01-1.96 (m, 4H), 1.46 (s, 9H), 1.38 (s, 12H), 1.06 (sext, 4H, *J* = 22.0, 14.8, 7.3), 0.66-0.55 (m, 10H).

^{13}C DEPT135 NMR (100 MHz, $CDCl_3$): δ 171.17 (C), 160.26 (C), 156.22 (C), 156.03 (C), 154.06 (C), 150.65 (C), 142.01 (C), 138.58 (C), 131.95 (CH), 130.27 (CH), 130.18 (CH), 130.11 (CH),

128.28 (C), 127.00 (CH), 116.98 (CH), 114.94 (CH), 109.48 (CH), 55.87 (CH_3), 53.00 (C), 40.03 (CH_2), 34.94 (C), 31.45 ((CH_3)$_3$), 26.07 (CH_2), 24.95 (CH_3), 23.06 (CH_2), 21.07 (C), 13.84 (CH_3).

Compound 2.2.22

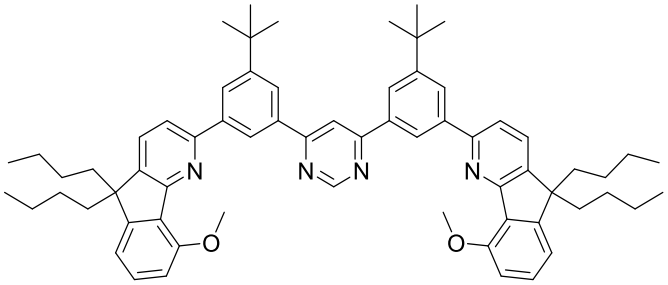

5,5-dibutyl-2-[3-tert-butyl-5-(tetramethyl-1,3,2-dioxaborolan-2-yl)phenyl]-9-methoxy-5H-indeno[1,2-b]pyridine (4.38 g, 7.72 mmol) was added to a dry round-bottomed flask flushed with argon. Anhydrous 1,4-dioxane (100 mL) was added and the reaction mixture was stirred. 4,6-Dichloropyrimidine (0.460 g, 3.09 mmol) and 2M K_2CO_3 solution (2.56 g, 18.5 mmol, 9.50 mL) were added and the reaction mixture was degassed under argon for 10 min. Tetrakis(triphenylphosphine)palladium(0) (0.214 g, 0.185 mmol) was added and the reaction mixture degassed for a further 10 min. The reaction mixture was heated at 95 °C for 24 h. The reaction mixture was cooled to room temperature and extracted with ethyl acetate. The organic phase was washed with water, separated and dried with $MgSO_4$. The solvent was evaporated to dryness. The crude product was purified by column chromatography (silca gel, gradient elution with hexane:ethyl acetate) to give the product as a pale yellow oil

Yield: 0.400 g, 0.417 mmol, 14%

^{1}H NMR (400 MHz, $CDCl_3$): δ 9.43 (d, 1H, *J* = 0.9), 8.69 (s, 2H), 8.61 (t, 2H, *J* = 1.6), 8.38 (d, 1H, *J* = 0.9), 8.32 (t, 2H, *J* = 1.6), 7.83 (d, 2H, *J* = 7.8), 7.69 (d, 2H, *J* = 7.8), 7.37 (t, 2H, *J* = 8.2, 7.8), 7.01 (d, 2H, *J* = 7.8), 6.86 (d, 2H, *J* = 8.2), 4.03 (s, 6H), 2.04-1.98 (m, 8H), 1.54 (s, 18H), 1.08 (sext, 8H, *J* = 22.2, 14.7, 7.3), 0.68-0.59 (m, 20H).

^{13}C DEPT135 NMR (100 MHz, $CDCl_3$): δ 165.51 (C), 160.52 (C), 159.10 (CH), 156.24 (C), 155.47 (C), 154.08 (C), 152.43 (C), 142.60 (C), 140.22 (C), 137.46 (C), 130.86 (C), 130.42 (CH),

130.33 (CH), 128.98 (C), 127.93 (C), 127.24 (C), 126.70 (CH), 124.85 (CH), 124.57 (C), 122.85 (C), 122.76 (CH), 117.09 (CH), 114.94 (CH), 113.72 (CH), 113.19 (C), 109.46 (CH), 55.94 (CH), 53.03 (C), 39.99 (CH_2), 35.23 (C), 31.46 (CH), 26.08 (CH_2), 23.04 (CH_2), 13.83 (CH).

Compound 2.2.23

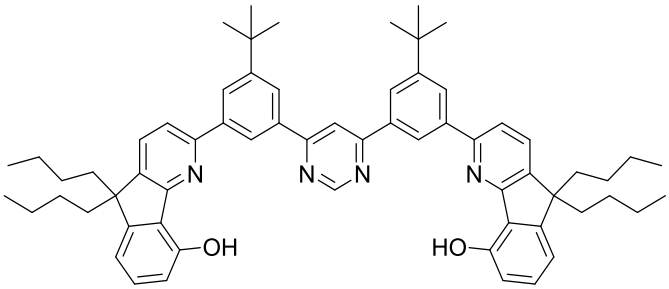

2.2.22 (0.360 g, 0.375 mmol) was added to a round-bottomed flask. Pyridine hydrochloride (0.867 g, 7.50 mmol) was added and the reaction mixture was heated to 250 °C under argon for 12 h. The reaction mixture was cooled to room temperature. Water was added and the resulting precipitate was filtered *in vacuo* and washed with water to give the desired product as a grey solid Yield: 0.243 g, 0.261 mmol, 70%

^{1}H NMR (400 MHz, $CDCl_3$): δ 9.43 (s, 1H), 8.60 (s, 2H), 8.32-8.31 (m, 5H), 7.80-7.74 (m, 4H), 7.34 (t, 2H, *J* = 7.8), 6.95 (d, 2H, *J* = 7.3), 6.90 (d, 2H, *J* = 7.8), 2.07-1.95 (m, 8H), 1.53 (s, 18H), 1.13 (sext, 8H, *J* = 22.2, 14.7, 7.3), 0.78-0.69 (m, 16H).

^{13}C DEPT135 NMR (100 MHz, $CDCl_3$): δ 165.14 (C), 161.28 (C), 159.26 (CH), 154.81 (C), 154.47 (C), 152.79 (C), 152.46 (C), 142.25 (C), 139.43 (C), 137.47 (C), 131.15 (CH), 131.01 (CH), 126.53 (CH), 124.93 (CH), 124.28 (C), 123.09 (CH), 117.98 (CH), 114.30 (CH), 113.43 (CH), 54.32 (C), 39.46 (CH_2), 35.24 (C), 31.46 (CH_3), 26.25 (CH_2), 23.03 (CH_2), 13.83 (CH_3).

HRMS (FTMS^{+}): for $[M+H]^{+}$ calc'd 931.5885, found 931.5873.

Compound 2.2.24

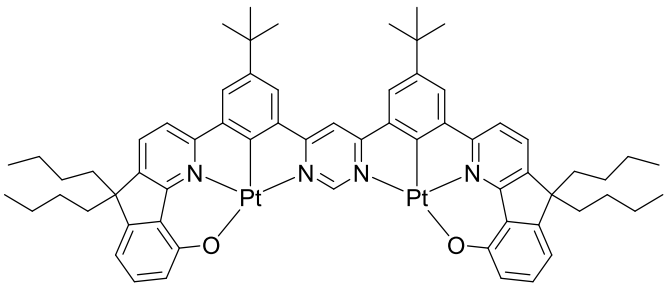

2.2.23 (0.103 g, 0.110 mmol) was added to a round-bottomed flask. Potassium tetrachloroplatinate (0.114 g, 0.275 mmol) was added. A 9:1 mixture of acetic acid and chloroform (50 mL) was added and the reaction was heated to reflux for 3 d. The mixture was cooled to room temperature and neutralised with a saturated solution of Na_2CO_3. The reaction mixture was then extracted with dichloromethane. The organic phase was separated and dried with MgSO4. The solvent was evaporated to dryness and the crude red residue purified by column chromatography (silica gel, DCM 100:0). The solid obtained was further purified by recrystallisation from methanol to give the desired product as a dark red solid.

Yield: 0.0301 g, 0.0228 mmol, 21 %

^{1}H NMR (400 MHz, $CDCl_3$): δ 10.25 (br s, 1H), 8.06 (br s, 1H), 7.95 (d, 2H, *J* = 7.3), 7.89 (br s, 4H), 7.61-7.58 (m, 4H), 7.42 (d, 2H, *J* = 8.2), 6.73 (d, 2H, *J* = 7.3), 2.07-2.05 (m, 8H), 1.53 (s, 18H), 1.14-1.11 (m, 8H), 0.72-0.68 (m, 16H).

HRMS (FTMS$^+$): for $[M+H]^+$ calc'd 1318.4884, found 1318.4860.

Chapter 3

Dinuclear Iridium(III) Complexes

3.0 Dinuclear Iridium(III) Complexes

The aim of this research was to prepare multimetallic complexes, for example dinuclear iridium(III) complexes, in which the two metal centres are rigidly linked by cyclometallating bridging ligands. As previously discussed in section 1.3, multinuclear complexes have become widely investigated as a consequence of their advantageous photophysical and electrochemical properties.

The bridging ligand used to link metal centres has an important role in the modulation of both the chemical and photophysical properties of the final multimetallic complex. In section 1.3, a large range of the bridging ligands previously reported in the preparation of polynuclear complexes were discussed.

The majority of dinuclear iridium(III) complexes reported to date are those in which the two metal centres are linked via polypyridine bridging ligands incorporating partially insulating spacer groups. Therefore, the two metal-containing units are electronically isolated from one another and retain the characteristics of their analogous monometallic components.[15, 71, 102-104, 106, 118, 120, 122, 123, 175] Tsuboyama *et. al.* reported, in 2004, the preparation of a dinuclear iridium(III) complex linked by a cyclometallating bis-bidentate bridging ligand, 1,4-bis(pyridine-2-yl)benzene (dpb). This complex exhibits intense red phosphorescence that is not observed for the analogous mononuclear complexes. This is one of the first and only examples of a di-iridium(III) complex in which the metal centres are rigidly-linked via a cyclometallating bridging ligand.[112]

Additionally, the preparation of multinuclear complexes as a single, pure isomer can be difficult. Despite showing red luminescence, the dinuclear iridium(III) complex synthesised by Tsuboyama and co-workers could only be isolated in a 3% yield following purification by column chromatography and recrystallisation from DMF.[112] Tris-bidentate Ir(III) complexes of the type $Ir(C\text{^}N)_3$ or $Ir(C\text{^}N)_2(L\text{^}X)$ have D_3 or C_2 symmetry meaning that they are chiral and are formed as a racemic mixture of enantiomers (Λ and Δ). In the case of monometallic complexes, this is not a problem as they have identical linear optical properties. However, when two chiral iridium(III) centres are brought together into one molecule, a mixture of diastereoisomers is formed. These diastereoisomers have different properties and must be separated. This separation

can be laborious, time consuming and result in low yields or difficulty in isolating any pure multinuclear complexes.[107, 112]

The design of the highly luminescent dinuclear iridium(III) complexes described in this work is such that the issues described above have been alleviated.

Previously, ligands based around the nitrogen-containing heterocycles pyrimidine, pyrazine and pyridazine that are capable of binding two transition metal centres were reported in the 1990s by Steel and co-workers and Rourke *et. al*.[176, 177] Similar bridging ligands were also used in the preparation of luminescent dinuclear platinum(II) complexes published by Kozhevnikov *et. al*.[85, 176-178] In the bimetallic iridium(III) complexes prepared here, the two iridium(III) centres are rigidly-linked using cyclometallating, bis-bidentate bridging ligands, incorporating the same range of N-containing heterocycles as reported in the literature. Linking two Ir(III) centres in this way facilitates electronic communication between the two metal centres leading to formation of a dinuclear complex with distinctly different properties compared with the corresponding monometallic complexes.[84]

Secondly, the formation of diastereoiomsers is avoided through the use of symmetrical, cyclometallating, terdentate N^C^N ligands as the use of these ligands leads to achirality in the final bimetallic Ir(III) complex. The use of such ligands in the preparation of achiral metal complexes has been previously reported in the literature. Bis-terpyridyl metal complexes have C_{2v} symmetry and are achiral. This class of complexes has been widely studied whereas the corresponding cyclometallated Ir(III) complexes have had significantly less investigation. Williams *et. al.* reported the synthesis of achiral monometallic iridium(III) complexes of the general formula Ir(N^C^N)(N^C)X. These complexes are comprised of a derivative of 1,3-dipyridylbenzene as a terdentate cyclometallating N^C^N ligand, a 2-phenylpyridine derivative as an N^C-coordinating bidentate ligand and an anionic monodentate ligand, for example a halide. These Ir(III) complexes showed strong luminescence with high quantum yields (ϕ = 0.20–0.71) and have been shown to perform well in OLED devices.[30]

Consequently, dinuclear iridium(III) complexes synthesised in this work comprise two iridium(III) centres linked by a bis-N^C-coordinating bridging ligand. The coordination of each Ir(III) centre is completed with a terdentate N^C^N-coordinating ligand and a monodentate chloride ligand. Combining both symmetrically-substituted bis-N^C-coordinating bridging ligands and terdentate N^C^N-coordinating auxiliary ligands is an attractive route to achiral dinuclear complexes that exhibit exciting photophysical properties.[30, 173]

In the following sections, the synthesis of the auxiliary terdentate N^C^N ligands, bis-bidentate bridging ligands and their corresponding dinuclear iridium(III) complexes will be discussed. Variation of the monodentate ligands from chloride to alternatives ligands, both anionic and neutral, will also be considered.

3.1 Auxiliary Terdentate N^C^N Ligands

In 2003, Williams *et. al.* reported on the use of N^C^N-coordinating cyclometallating ligands in the preparation of highly luminescent platinum(II) complexes with quantum yields of ϕ = 0.58–0.68.[18] This was the first investigation of luminescence of this class of platinum(II) complexes following the synthesis of the first example of a platinum(II) dipyridylbenzene complex in 1999.[65] Williams and co-workers have also synthesised and studied the luminescence of iridium complexes incorporating terdentate ligands. A range of bis-terdentate iridium(III) complexes, containing the N^C^N ligand 1,3-di(2-pyridyl)-4,6-dimethylbenzene (dpyx) were reported in 2006.[5] Haga *et. al.* have also prepared bis-terdentate iridium(III) complexes incorporating 1,3-bis(1-methyl-benzimidazol-2-yl)benzene ligands.[69] Previously, despite their structural advantages, iridium(III) complexes of terdentate ligands had been largely overlooked.[27, 30]

Terdentate ligands are known to have structural advantages over analogous bidentate ligands and complexes of such ligands often have outstanding performance. The higher degree of rigidity offered by terdentate ligands means that there is less molecular distortion on excitation from the ground state to the excited state and therefore, less excited stated energy is lost through non-radiative decay. Additionally, terdentate N^C^N ligands are likely to afford a complex with

increased chemical stability and have beneficial effects on chirality with respect to eliminating the formation of diastereoisomers in multimetallic systems.[5, 25, 27, 30, 179]

In this project, terdentate N^C^N-coordinating ligands were selected for use as auxiliary ligands based on the studies discussed above. Initially, only ligands based on 1,3-dipyridylbenzene were prepared. These ligands were synthesised in high yield via traditional cross-coupling methods such as Stille and Suzuki-Miyaura reactions as shown in Figure 84.

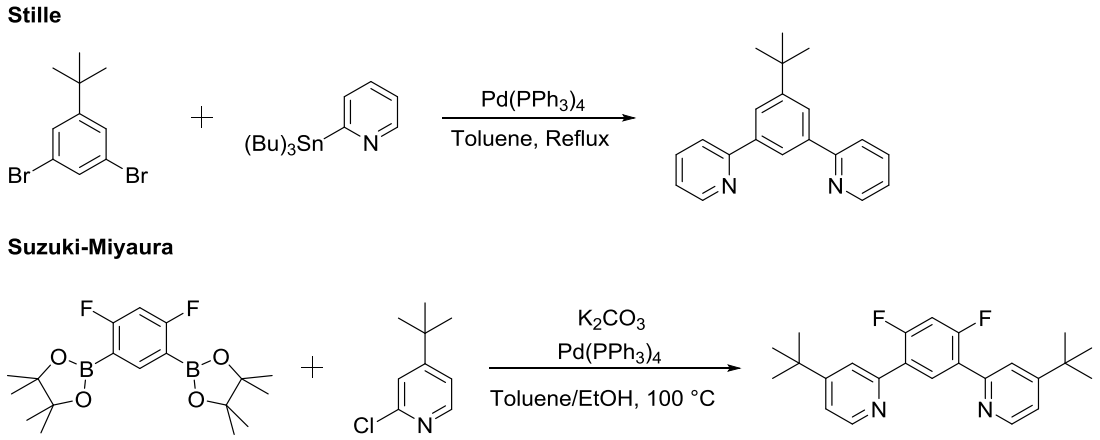

Figure 84: A scheme to illustrate the cross-coupling reactions used to synthesise a selection of terdentate N^C^N ligands.

Figure 85 shows the range of terdentate N^C^N-coordinating ligands prepared by cross-coupling methods. Ligands **3.1.1** to **3.1.3** were prepared via Suzuki-Miyaura reactions as described in the literature.[68, 70, 180] The synthesis of compounds **3.1.4** and **3.1.5** was reported by Chou *et. al.* in 2015, again utilising the Suzuki-Miyaura synthetic method. Alternatively, in this project, these ligands were prepared via the Stille cross-coupling route (Figure 84).

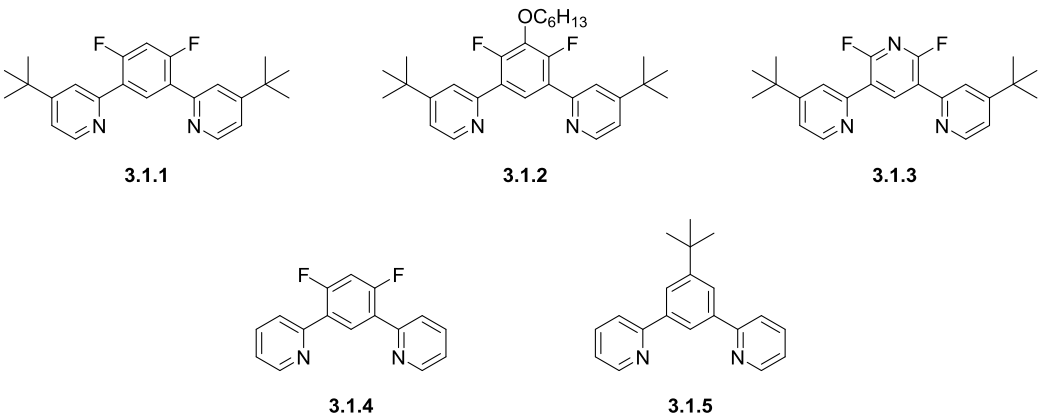

Figure 85: A figure to show the terdentate N^C^N-coordinating ligands prepared using traditional cross-coupling methods, Suzuki-Miyaura and Stille reactions.

When reacting terdentate cyclometallating ligands such as 1,3-dipyridylbenzene with a metal centre, the metal centre can bind in two possible modes, terdentate or bidentate (Figure 86). In this project, terdentate binding is desired and has been previously observed with Ru(II), Os(II) and Pt(II). In the reaction of iridium(III) with 1,3-dipyridylbenzene, the Ir(III) primarily binds in a bidentate mode with cyclometallation occurring at the C4 position. Williams and co-workers reasoned that cyclometallation at the 4-position on the central phenyl ring must be kinetically favoured over the analogous reaction at the more sterically hindered 2-position.[5, 17, 25, 27, 179]

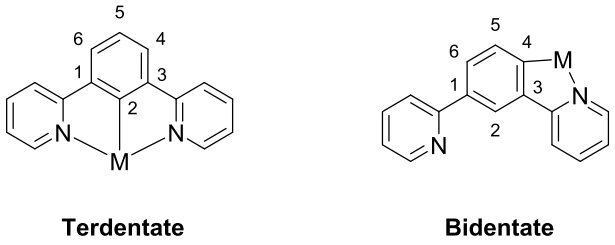

Figure 86: A figure to show the possible binding modes of a metal centre with a terdentate NCN ligand.

In order to direct cyclometallation to 2-position and ensure terdentate binding of the ligands with an iridium(III) metal centre, Williams *et. al.* showed that it is necessary to block the C4/C6 positions through the addition of substituents such as methyl, fluoro and trifluoromethyl. As shown in Figure 85, ligands **3.1.1** to **3.1.4** have fluoro substituents at C4 and C6 to block the competitive metallation. Alternatively, in the case of compound **3.1.5**, a single *tert*-butyl

substituent at the 5-position was used in an attempt to block bidentate chelation of the metal centre. We found this strategy to be successful in the synthesis of Ir(III) complexes of this ligand with binding going via a terdentate mode as will be discussed in section 3.2. This was also demonstrated by Chou *et. al.*[70]

As a result of the success of the *tert*-butyl substituent in blocking competitive metallation, a wider variety of terdentate N^C^N ligands also bearing this substituent were prepared via alternative synthetic routes utilising heterocyclic chemistry.

The first class of alternative terdentate N^C^N ligands we considered was those with the general structure 1,3-bis(benzimidazol-2-yl)benzene. Ligands of this type have been used in the preparation of luminescent complexes of transition metals such as Ir(III), Pt(II) and Au(III).[28, 69, 155, 162, 181-184] The five-membered imidazole rings present in these ligands are electron rich and push more electron density onto a metal centre when compared with ligands such as 1,3-dipyridylbenzenes. The increased electron density on the metal centre leads to a destabilisation of the metal-centred d-d states and as previously mentioned, this is one way to reduce non-radiative decay and increase the quantum yield.

Yam and co-workers reported the first examples of a platinum(II) complex incorporating 1,3-bis(N-alkylbenzimidazol-2'-yl)benzenes (bzimb) in 2011. This complex showed strong green luminescence (508-587 nm) with a quantum yield of $\phi = 0.19$ at room temperature.[185] Haga *et. al.* reported the first examples of the preparation of mononuclear iridium complexes incorporating these benzimidazole-type ligands as is shown in Figure 87.[28, 69] These complexes show high quantum yields, $\phi = 0.10–0.95$, with the mixed terdentate-bidentate complex [Ir(Phbib)(ppy)Cl] showing the highest quantum yield of 0.95.

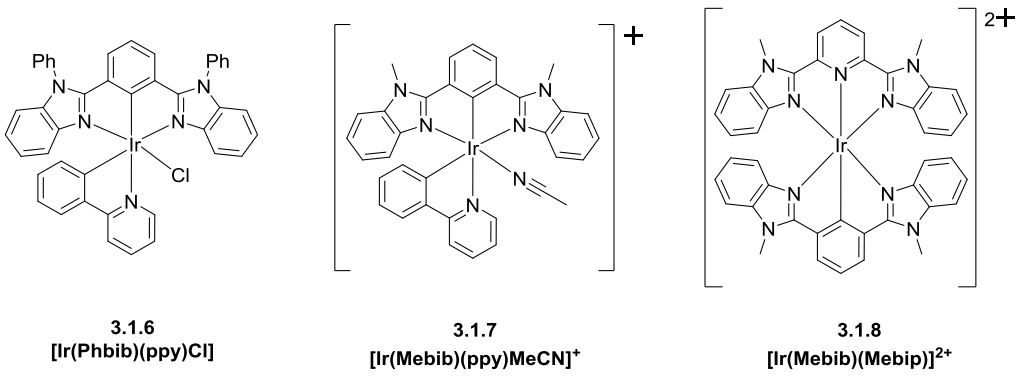

Figure 87: A figure to illustrate the iridium(III) complexes **3.1.6**-**3.1.8** prepared by Haga *et. al*. incorporating terdentate NCN ligands containing benzimidazole moieties.

Based on this literature precedent for highly luminescent complexes of N^C^N 1,3-bis(benzimidazol-2-yl)benzene ligands, a small selection of this class of ligands bearing different N-substituents was prepared.

The synthetic routes to the benzimidazole-type ligands prepared in this work are shown in Figure 88. These compounds were prepared via the condensation reaction of either 5-*tert*-butyl isophthalic acid or the corresponding acid chloride with a diamine as shown below. [182, 184] [162, 186] Compounds **3.1.11** and **3.1.12** were isolated in good yields, 76% and 77% respectively, following purification by column chromatography.

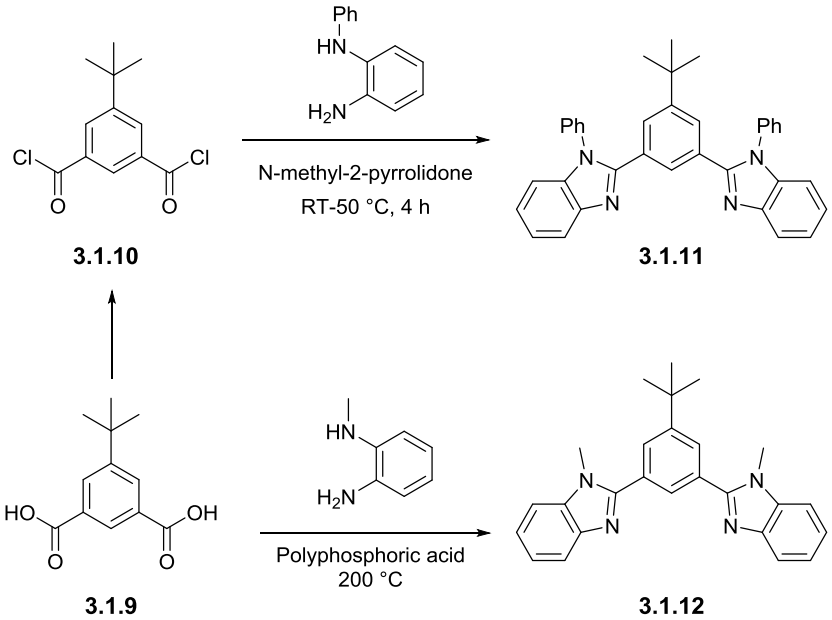

Figure 88: A figure to show the structures of the benzimidazole ligands **3.1.11** and **3.1.12** prepared through the condensation reactions.

The incorporation of these compounds as ligands in dinuclear iridium(III) complexes and the effects of the benzimidazole moieties on their photophysical properties will be discussed in sections 3.2 and 3.3.

The second type of alternative N^C^N ligands considered in this work were those with the general structure 1,3-bis(pyrazolyl)benzene. Cyclometallating N^C^N ligands in which the heterocycle used is a pyrazole have been widely investigated for the preparation of blue-emitting iridium(III) complexes. When compared with pyridine, pyrazole is a poorer π-acceptor. Therefore, in a complex of a 1,3-bis(pyrazolyl)benzene ligand, the LUMO is raised relative to those in which dipyridylbenzenes are used as the terdentate ligand. This leads to emission that is blue-shifted in the pyrazole-containing complexes.[126]

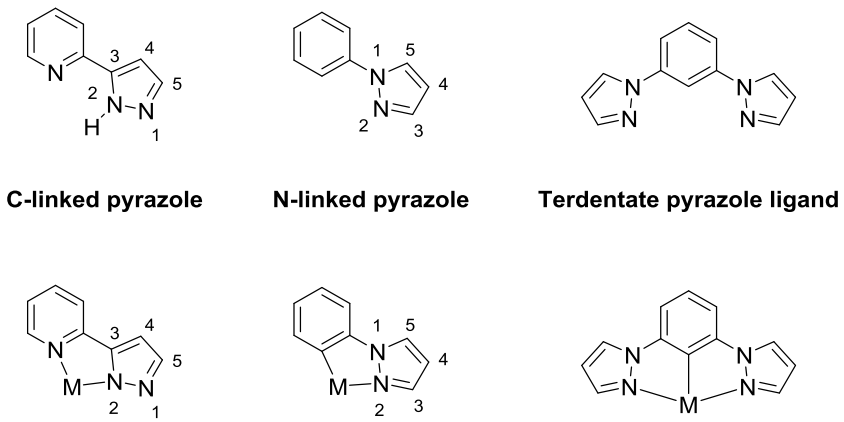

Figure 89: A figure to show the structures and binding modes both bidentate and terdentate pyrazole-containing ligands.

The majority of reports of luminescent complexes incorporating pyrazole-containing ligands are those with bidentate ligands. There has been less investigation into terdentate pyrazole ligands. Figure 89 shows the structures of pyrazole-containing ligands, both bidentate and terdentate. C-linked pyrazole ligands have been the most widely investigated for use in luminescent complexes. This type of structure has two tautomeric forms in which the proton can reside on N^1 or N^2. The N^2-deprotonated form can bind a metal centre as an anionic ligand and so can be considered an analogue of 2-phenylpyridine. N-linked 1-aryl pyrazoles were incorporated as ligands into some

of the earliest examples of room-temperature-emissive platinum(II) complexes and in this work, terdentate N^C^N analogues of this type of ligand will be used.[40] Terdentate ligands incorporating pyrazoles were first investigated for the preparation of luminescent Pt(II) complexes by Connick *et. al.*, initially reporting complexes of 1,3-bis(1-pyrazolyl)pyridines and secondly, the analogous cyclometallating ligands 1,3-bis(1-pyrazolyl)benzenes. Williams and co-workers also reported luminescent cyclometallated Pt(II) complexes of such pyrazole-containing ligands.[126, 187, 188]

Iridium(III) complexes of bis(pyrazolyl)benzene ligands (Figure 90) were reported by Haga *et. al.* in 2008. These complexes exhibit emission in the blue region (447-460 nm) at 77 K but only show weak room temperature emission with quantum yields ranging from ϕ = 0.4 x 10^{-3} to 8 x 10^{-3}. This weak emission under ambient conditions is thought to be due to a deactivation mechanism involving thermally accessible metal-centred d-d states.[189]

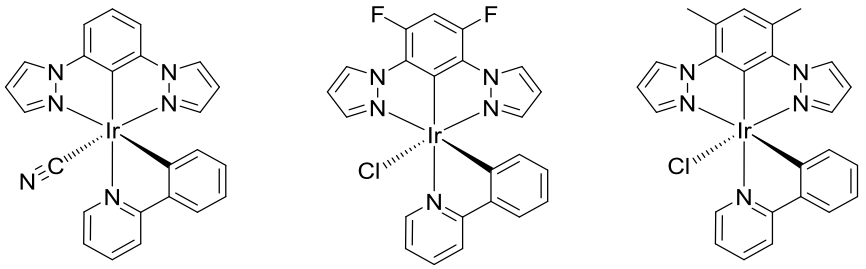

3.1.13 **3.1.14** **3.1.15**

Figure 90: Structures of iridium(III) complexes prepared by Haga and co-workers incorporating terdentate bis(pyrazolyl)benzene ligands. The quantum yields recorded for these complexes were (**3.1.13**) 5 x 10^{-3}, (**3.1.14**) 0.4 x 10^{-3} and (**3.1.15**) 0.5 x 10^{-3}.[189]

As previously mentioned, in this work ligands with the general structure 1,3-bis(pyrazolyl)benzene will be investigated for use in the preparation of bimetallic iridium(III) complexes. The structures and suggested syntheses of the target pyrazole-containing N^C^N ligands are shown in Figure 91. The synthetic route shown below is a modified Ullmann reaction. This type of copper-mediated aromatic nucleophilic substitution reaction was first reported by Ullmann and Goldberg in the early 1900's. Traditionally, these reactions required harsh reaction conditions and stoichiometric amounts of copper. More recently, the original reaction conditions

have been modified through the addition of organic additives capable of acting as a ligand for copper. This development has transformed these reactions into catalytic processes.

Compound **3.1.17** was successfully isolated in high yield (70%) using these modified reaction conditions and was subsequently used in the formation of a dinuclear iridium(III) complex as will be discussed in sections 3.2 and 3.3.

Compound **3.1.19** could not be isolated using this method. This is thought to be due to the low reactivity of the bromo- group. An alternative synthetic route is to go via the iodo-substituted compound following a bromo-iodo exchange reaction, however, due to time restraints this route was not attempted.[126]

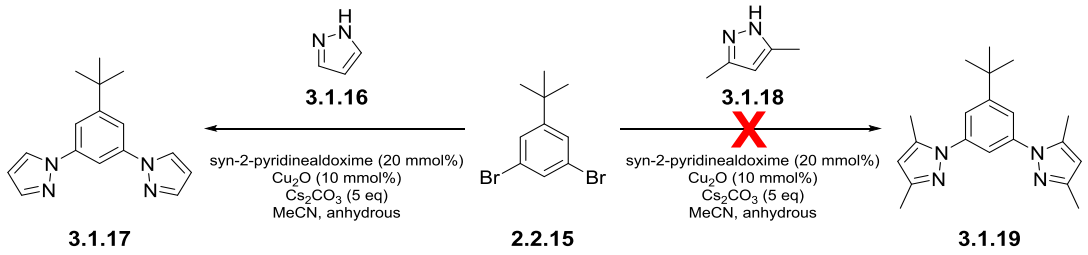

Figure 91: A scheme to show the structures and syntheses of two pyrazole-containing terdentate N^C^N ligands, **3.1.17** and **3.1.19**.

The cyclometallating, terdentate N^C^N ligands discussed here incorporate a range of heterocycles and substituents in order to assess the effects of such factors on the photophysical properties of resulting dinuclear complexes. The incorporation of these N^C^N ligands into bimetallic iridium(III) complexes will be discussed in the following sections of this work.

3.2 Di-Iridium(III) Complexes – Synthesis of Iridium Dichloro-bridged Dimers

Following the successful synthesis of the range of symmetrically-substituted cyclometallating, terdentate N^C^N ligands shown in Figure 92, the first step in the preparation of our target dinuclear iridium(III) complex is the formation of a dichloro-bridged iridium dimer.

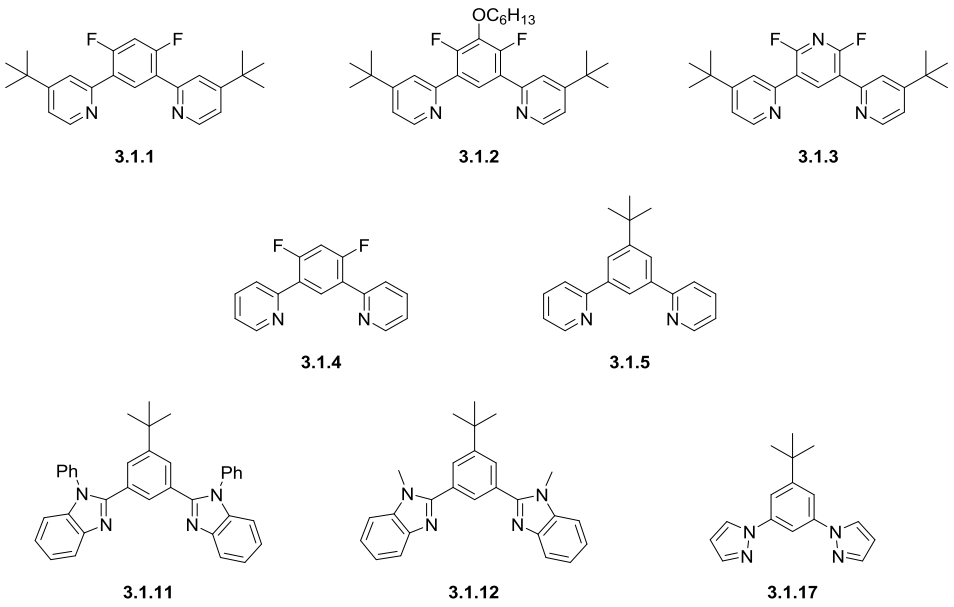

Figure 92: A figure to show the full range of terdentrate N^C^N-coordinating proligands synthesised for use in the preparation of dinuclear iridium(III) complexes.

As is widely reported in the literature, the preparation of the a dichloro-bridged iridium(III) dimer of this type involves the reaction of a terdentate N^C^N ligand with $IrCl_3.H_2O$ in a 3:1 solvent mixture of 2-ethoxyethanol and water as shown in the reaction scheme in Figure 93.[25, 27, 30, 70, 122, 123, 173]

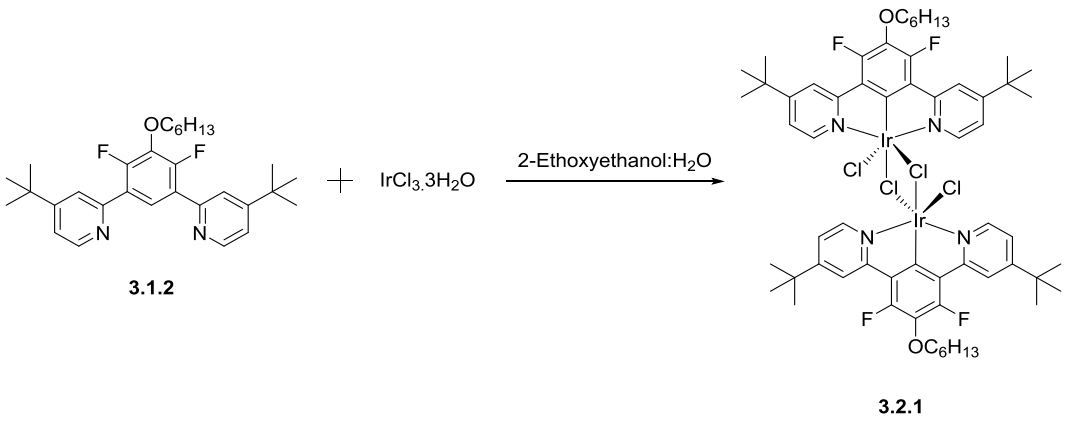

Figure 93: Reaction scheme to show the synthesis of a dichloro-bridged iridium(III) dimer of terdentate N^C^N ligand **3.1.2**. The proligand is mixed with $IrCl_3.H_2O$ in a 3:1 solvent mixture of 2-ethoxyethanol and water. This particular dichloro-bridged dimer, **3.2.1**, was isolated in a yield of 82%.

Using the synthetic route shown above, the dichloro-bridged iridium(III) dimers were isolated in high yields of 67-91% and, as a result of the solubilising functional groups present, the dimers can be characterised by ^{1}H, ^{19}F and ^{13}C NMR in $CDCl_3$ solution.

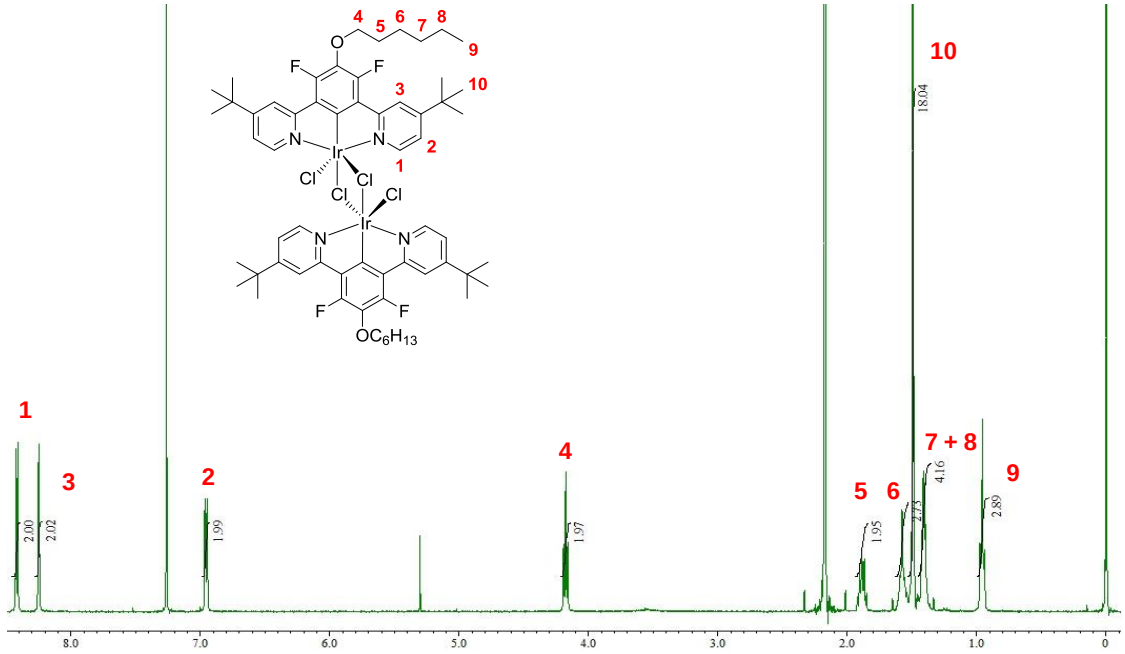

Figure 94: ^{1}H NMR spectrum of iridium dichloro-bridged dimer **3.2.1**. This spectrum shows 3 aromatic proton environments in the range of δ 8.4-6.9 ppm and 6 aliphatic peaks in the range of δ 4.2-0.9 ppm corresponding to the 7 aliphatic proton environments.

Figure 94 shows the ^{1}H NMR spectrum of the iridium(III) dichloro-bridged dimer **3.2.1**. The spectrum shows that there are 3 aromatic proton environments in the range of δ 8.4-6.9 ppm and 6 peaks in the aliphatic region that correspond to 7 proton environments. This spectrum matches the structure of **3.2.1**.

The isolated iridium(III) dichloro-bridge dimers were used in the synthesis of target dinuclear Ir(III) complexes without any further purification. The synthesis and photophysical properties of the resulting luminescent complexes will be discussed in the following sections of this chapter.

3.3 4,6-Pyrimidine-Linked Dinuclear Iridium(III) Complexes

The first bis-bidentate cyclometallating ligands investigated in this research were those containing a pyrimidine ring as the central heterocycle. This class of bridging ligands, based around a 4,6-disubstituted pyrimidine ring, have been previously reported by Kozhevnikov *et. al.* in the preparation of both homo- and hetero- multimetallic complexes of Pt(II) and Ir(III). Using the same, Suzuki-Miyaura cross-coupling reactions as reported in these earlier works (Figure 95), these ligands were synthesised in moderate to good yields.

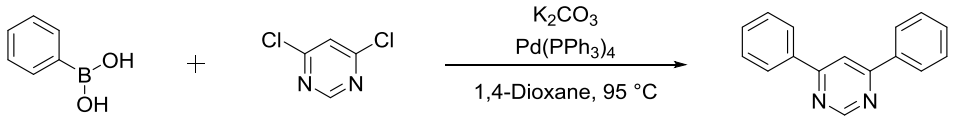

3.3.1 **3.3.2** **3.3.3**

Figure 95: A scheme to illustrate the Suzuki-Miyaura cross-coupling reaction used to synthesise the pyrimidine-based C^N^N^C bridging ligands.

The range of pyrimidine-based bis-bidentate C^N^N^C ligands prepared using this method is shown in Figure 96. A range of electron-donating and –withdrawing substituents were incorporated in order to vary the electronic properties of the bridging ligands used. As discussed previously 1.2.3, addition of substituents can be used as a strategy for the tuning of photophysical properties of the final luminescent complex. In **2.1.5**, the terminal phenyl rings were replaced with thiophene units. Thiophene rings are more electron-rich than phenyl rings and therefore, complexes of ligands containing thiophene units have emission that is red-shifted relative to those containing phenyl rings. This is an alternative strategy available for tuning of emission colour as was described in chapter 2.0.[163]

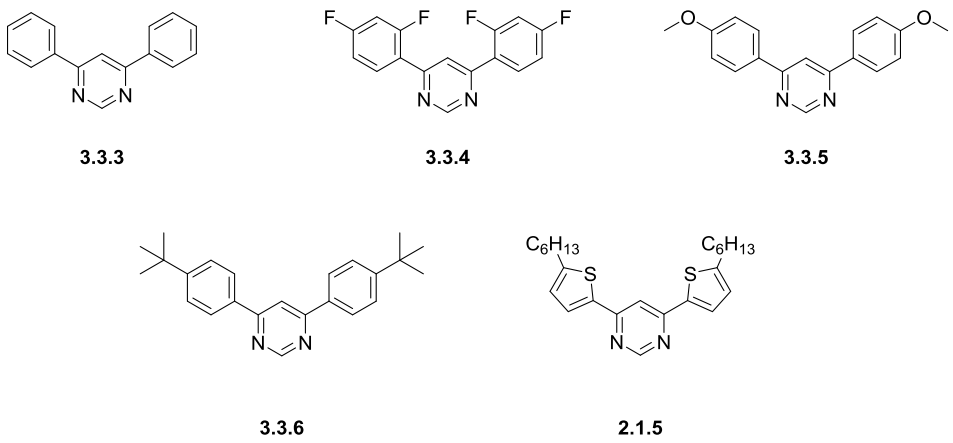

Figure 96: A figure to show the pyrimidine-containing bis-bidentate C^N^N^C-coordinating proligands prepared using Suzuki-Miyaura reactions.

Using the five bis-bidentate bridging ligands shown above, target dinuclear iridium(III) complexes were synthesised. In conjunction with these bridging ligands, a selection of three terdentate N^C^N-coordinating ligands based on 1,3-dipyrididylbenzene were incorporated; **3.1.2**, **3.1.1** and **3.1.3**. The preparation of these proligands was previously discussed in section 3.1. These N^C^N-coordinating ligands each comprise of lateral 4-*tert*-butylpyridine groups, however the substituents on the central ring were varied (Figure 85). In order to block competitive bidentate metalations, the 4- and 6- positions of the central phenyl rings are substituted with fluorine atoms. The synthetic route used to prepare the final dinuclear iridium(III) complexes allows the separate introduction of terdentate N^C^N auxiliary ligands and bis-bidentate bridging ligands.[30] As a result, a series of eight dinuclear pyrimidine-linked iridium(III) complexes were prepared, as is shown in Figure 97, and the influence of the substitution pattern of both the bis-N^C bridging and N^C^N auxiliary ligands was independently investigated. As part of this series of eight dinuclear complexes, monodentate ligand metathesis of the chloride ligand to a cyano-ligand and this will be discussed in a later section of this chapter (section 3.7).

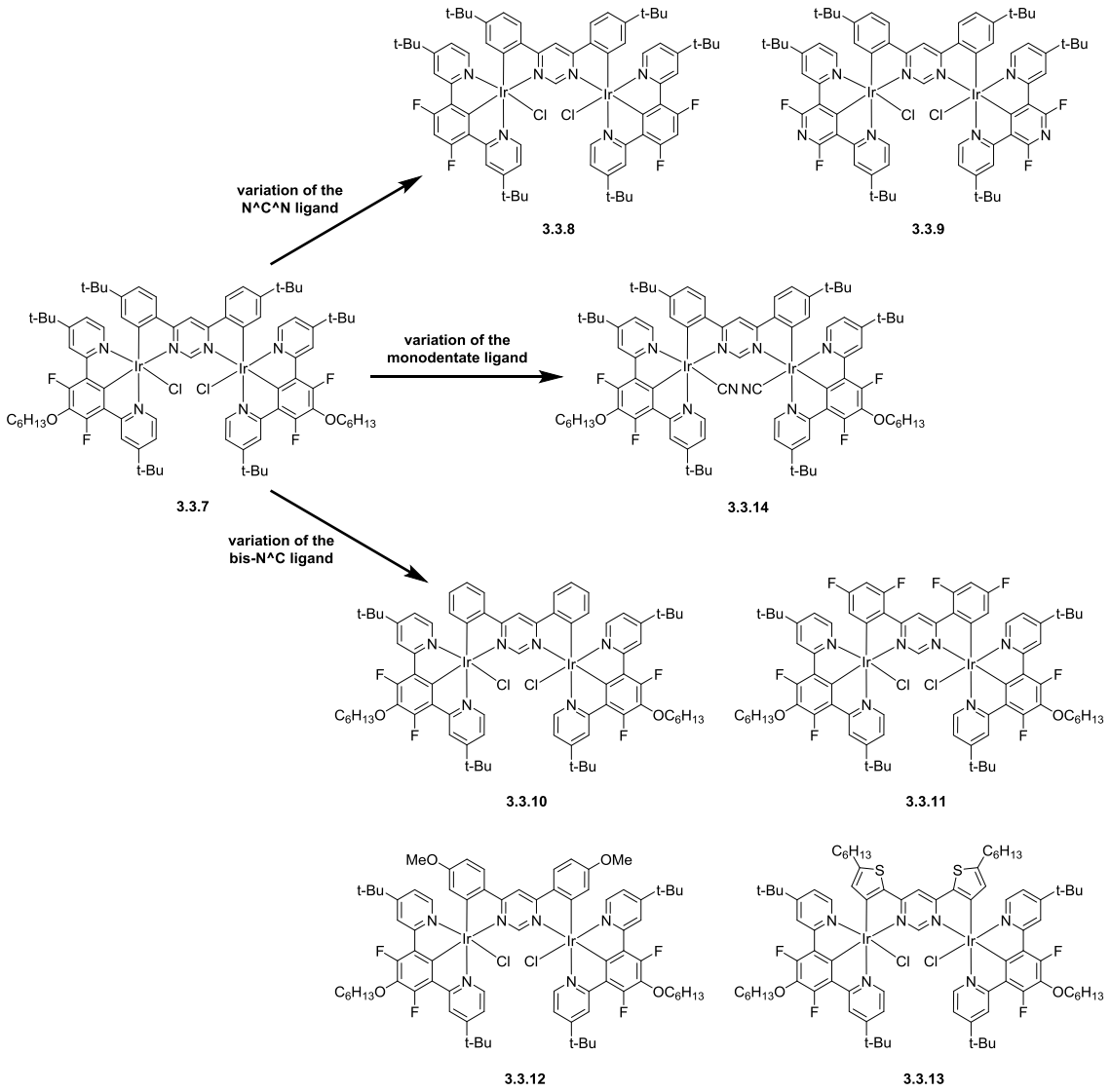

Figure 97: Scheme to show the range of pyrimidine-linked di-iridium(III) complexes synthesised through variation of the substitution pattern on the bis-bidentate bridging ligand, the terdentate auxiliary ligand and the monodentate ligand.

The synthetic route utilised for the isolation of the target dinuclear complexes is a two-step procedure and is similar to that previously developed for related mononuclear complexes.[27, 30] The first step is that described in section 3.2, the preparation of the dichloro-bridged iridium(III) dimer. Secondly, the dichloro-bridged dimers were reacted with the bis-N^C-coordinating proligands **3.3.3**-**3.3.6** and **2.1.5** under reflux in toluene, in the presence of silver triflate as a chloride scavenger. Following completion of the reaction, the mixture was treated with excess HCl (2M, aq.) in order to ensure that the monodentate ligands in the final products are exclusively chloride. The target complexes were isolated in good yields (50-80%) following treatment with methanol.

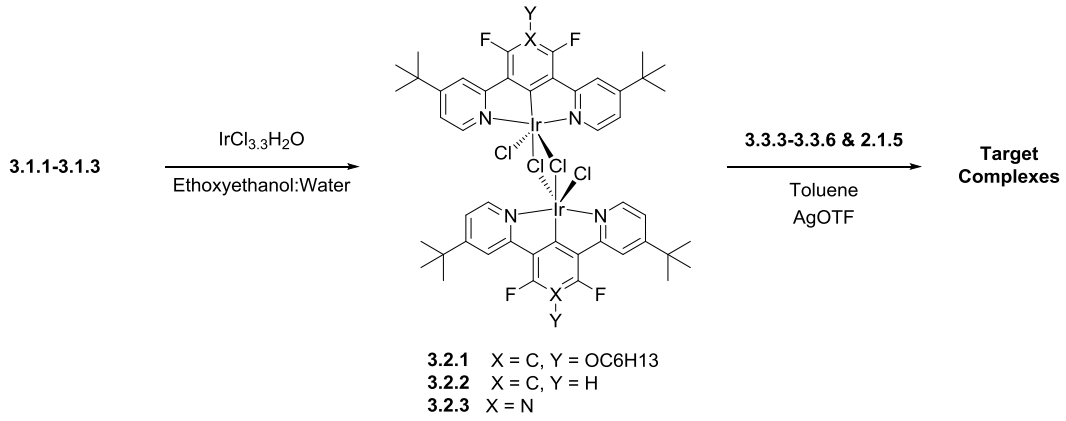

Figure 98: Synthetic route to the final dinuclear iridium(III) complex starting from terdentate N^C^N proligands. The reaction of the N^C^N-coordinating proligands with $IrCl_3.3H_2O$ in leads to formation of the iridium(III) dichloro-bridged dimer. Further reaction of this dimer with a bis-N^C bridging ligand in toluene and in the presence of AgOTf results in formation of the target dinuclear iridium(III) complexes.

Characterisation of the resulting dinuclear iridium(III) complexes was carried out by ^{1}H, ^{19}F and ^{13}C NMR spectroscopy and high-resolution mass spectrometry.

A critical point to note is that, due to the strong *trans*-influence of the formally anionic, metallated carbon atoms, the product that is formed is exclusively that in which the pyrimidine ring of the bridging ligand is *trans* to the central aryl ring of the N^C^N terdentate ligand. In each case, there is no evidence for the formation of isomers in which the cyclometallated aryl rings of the N^C and N^C^N units are *trans* to one another. This observation concurs with earlier studies of similar mononuclear systems.[27, 28, 30, 179, 190] Therefore, in contrast to the majority of bimetallic complexes previously studied, only one stereoisomer is formed for these dinuclear iridium(III) complexes.[83, 84, 106, 107, 112, 118, 191-194]

Below is the ^{1}H NMR spectrum of the target bimetallic complex **3.3.7**. The ^{1}H NMR spectra of these dinuclear complexes show characteristic features that can be used in conjunction with other data to confirm their identities. Firstly, a singlet at very high chemical shift between δ 11-12 ppm, assigned to the proton at the 2-position of the pyrimidine ring. Secondly, a low-frequency multiplet at chemical shifts between δ 5.6-6.8 ppm, assigned to the protons *ortho* to the cyclometallated carbon in the aryl ring of the bridging ligand.

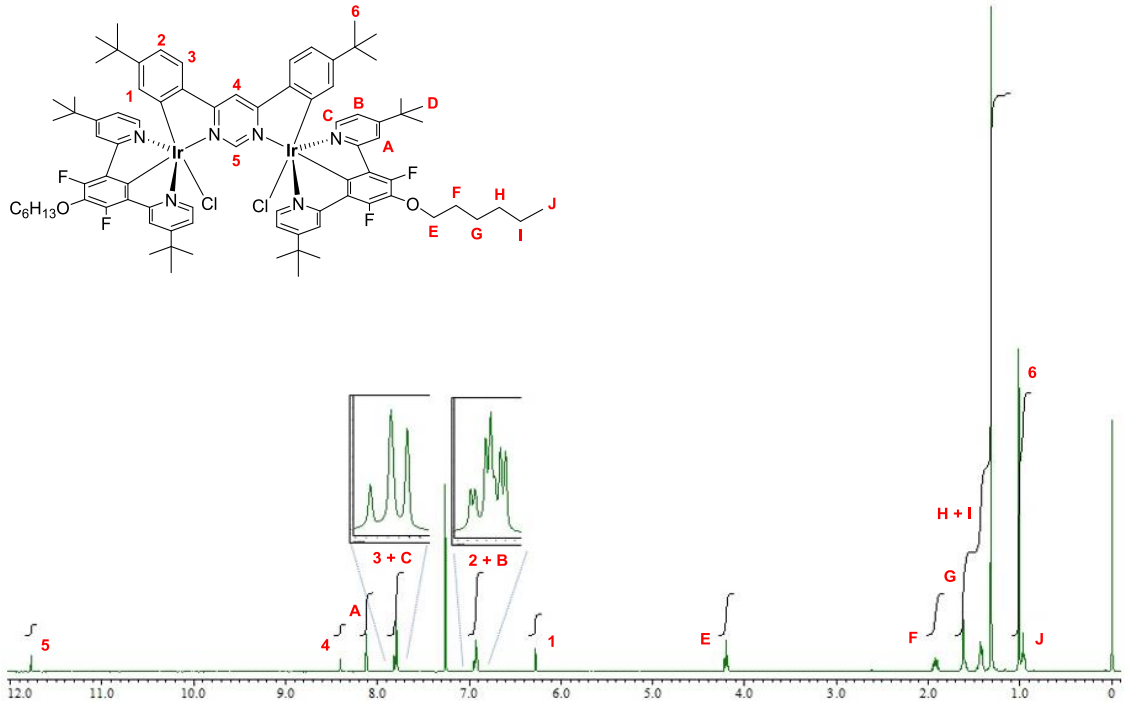

Figure 99: ^{1}H NMR spectrum of dinuclear iridium(III) complex **3.3.7** illustrating the presence of characteristic proton signals used to indicate the formation of the pure dinuclear iridium(III) complex.

In addition to NMR spectroscopy and mass spectrometry, X-ray crystallography can also be used to characterise our dinuclear iridium(III) complexes. Crystals of **3.3.11** suitable for X-ray diffraction were obtained by slow evaporation of a solution of the bimetallic complex in CH_2Cl_2/MeOH (3:1 v/v). The molecular structure of **3.3.11** was solved using X-ray crystallography by Dr M. Probert and Prof. W. Clegg at Newcastle University. The crystal structure obtained is shown below in Figure 100 with important bond angles and lengths shown in

Table 3. The complex has a crystallographic mirror plane passing through atoms C38 and C39. Two-fold disorder was modelled on atoms C28-C30 (and their H atoms) of the hexyl chain. Parameters determined using X-ray crystallography suggest further disorder of this hexyl chain and of the *t*-butyl groups, however this was not modelled.[173]

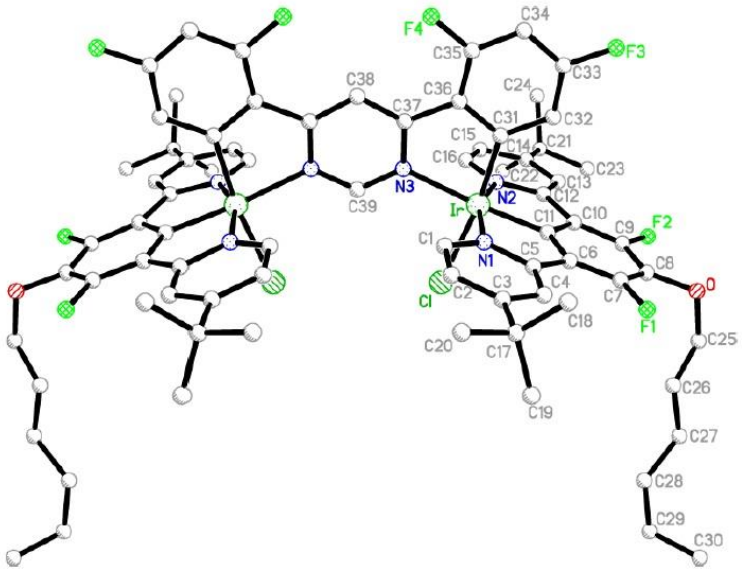

Figure 100: The molecular structure of **3.3.11** obtained using X-ray diffraction of a single crystal. The single crystal was grown by the slow evaporation of a solution of the dinuclear complex in CH_2Cl_2/MeOH (3:1 v/v).

Table 3: Selected bond lengths (Å) and angles (°) for complex **3.3.11** as determined by X-ray diffraction and the corresponding values in the energy-minimised structure obtained by DFT calculations. (a) DFT-derived values in square parentheses are for the geometry with imposed mirror symmetry about the central ligand (see text).

Bond Length (Å) or Angle (°)	**X-Ray Data**	**DFT Data[(a)]**
Ir-N1	2.049(5)	2.090 [2.085]
Ir-N2	2.048(5)	2.081 [2.085]
Ir-N3	2.157(5)	2.208 [2.215]
Ir-C11	1.926(7)	1.936 [1.936]
Ir-C31	1.996(5)	2.024 [2.024]
Ir-Cl	2.4406(15)	2.483 [2.479]
N1-Ir-N2	160.4(2)	159.9 [159.9]
N1-Ir-Cl11	80.3(2)	79.9 [80.0]
N2-Ir-C11	80.1(2)	80.1 [80.0]
N3-Ir-C11	173.4(2)	176.1 [176.5]
N2-Ir-C31	78.9(2)	78.3 [78.5]
N3-Ir-C1	93.66(12)	92.2 [92.7]
C31-Ir-C1	172.6(2)	170.1 [171.1]
C11-Ir-C31	95.3(3)	97.9 [98.0]

The crystal structure obtained for **3.3.11**, when compared with structurally related mononuclear complexes bearing terpyridine terdentate ligands rather than cyclometallating N^C^N ligands, provides further evidence for the strong *trans* influence associated with the central metallated aryl ring of the N^C^N ligand. As shown in Figure 101, the Ir-N3 bond length of 2.157(5) Å is elongated when compared with the Ir-N bond of the N^C ligand of $[Ir(tpy)(MeOmppy)Cl]^+$ (for which the value is 2.068(2) Å) and for the N^N ligand in $[Ir(tpy)(bpy)Cl]^{2+}$ (for which the value is 2.081(1) Å).[195] In the mononuclear iridium(III) complexes shown in Figure 101, these Ir-N bonds are *trans* to another Ir-N bond as opposed to Ir-C bonds. The strong *trans* influence of the metallated carbon atoms of the diarylpyrimidine ligand is also evidenced by the elongation of the Ir-Cl bonds. For example, in our dinuclear iridium(III) complex **3.3.11**, the Ir-Cl bond length is 2.4406(15) Å whereas the value is 2.334(5) Å in the complex $[Ir(tpy)(bpy)Cl]^{2+}$, where the chloride is *trans* to a pyridine rather than a metallated aryl ring.

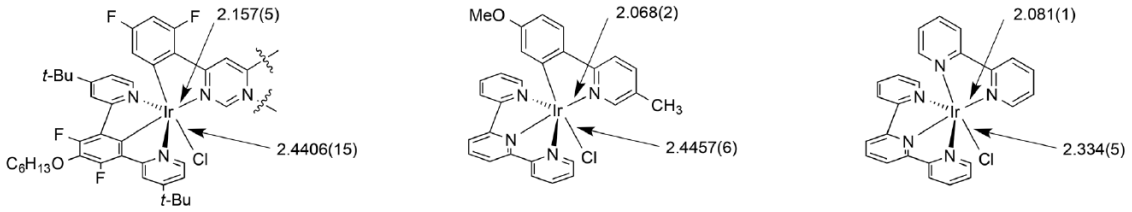

3.3.11 **[Ir(tpy)(MeOmppy)Cl]$^+$** **[Ir(tpy)(bpy)Cl]$^{2+}$**

Figure 101: A figure to illustrate the *trans* influence of the metallated carbon atoms in elongating *trans*-positioned bonds. The Ir-N and Ir-Cl bond lengths in both **3.3.11** and related mononuclear complexes highlight this point.

Further investigation of the structures of these new dinuclear iridium(III) complexes was carried out using density functional theory (DFT) calculations, as performed by Dr M. Durrant at Northumbria University. In order to decrease the duration of the DFT calculations, the *t*-butyl and OC_6H_{13} substituents of the terdenatate N^C^N ligands and the thienyl groups of the bis-N^C bridging ligand **2.1.5** in **3.3.13** were truncated to Me, OMe and Me respectively. The *t*-butyl groups of **3.3.6** were retained in full. The dinuclear complexes were subjected to full geometry optimisation although, due to the large size of these bimetallic iridium(III) complexes, frequency calculations proved difficult and therefore have been omitted.

The optimised geometries calculated for the full series of eight dinuclear iridium(III) complexes showed a twist about the central pyrimidine bridging ligand, giving dihedral angles between the two phenyl rings between 7.9° for **3.3.10** and 22.8° for **3.3.7**. The dihedral angle between the thiophene rings in **3.3.13** was much smaller, at 1.0°. In all cases, the twisting results in rotational symmetry about the central pyrimidine ring of the bis-N^C ligand. This contrasts with the X-ray crystal structure obtained for **3.3.11**, in which mirror symmetry about the pyrimidine ring is observed (Figure 100) such that the central bridging ligand remains planar rather than twisted. Consequently, there are different distances between the equivalent N atoms of the pyridine rings of the auxiliary N^C^N ligands in the experimental structure (6.293 and 7.433 Å), whereas in the calculated structures these distances are equal (7.104 Å). To investigate this further, a geometry optimisation starting from the X-ray crystal structure was carried out. This produced the same calculated structure and therefore, suggests that these two slightly different conformations are similar in energy. This conclusion was confirmed through re-optimising the geometry of **3.3.11** with imposed mirror symmetry. This gave an optimised structure for the dinuclear complex that was closer to the experimental structure and only 0.3 kJ mol^{-1} higher in energy compared with the rotationally symmetric conformer. Therefore, it is possible to conclude that deformation about the central bis-N^C bridging ligand is a very low energy process within the margin of error of the calculations and the effects of molecular packing within the crystal structure.

In all other respects, the calculated structures of our dinuclear iridium(III) complexes are as expected, giving good agreement between the calculated and experimental bond lengths and angles (Table 2). In each case, the metal centre has a distorted octahedral geometry. The Ir-N(pyridine) bond lengths (2.079-2.096 Å) are shorter than the Ir-N(pyrimidine) bond lengths (2.208-2.263 Å). In addition, the Ir-C bond lengths (1.917-1.936 Å) for the terdentate auxiliary ligands are shorter than the equivalent Ir-C bond lengths (2.017-2.085 Å) for comparable bidentate cyclometallating ligands. These results are consistent with the expected *trans* influence of the various donor atoms involved and mirror the differences observed for related mononuclear complexes.[30, 179] The Ir-Cl bond lengths range between 2.478-2.489 Å.

The next step in the study of this series of dinuclear iridium(III) complexes was to measure their absorption and emission properties. All of the photophyiscal measurements for these complexes were performed by Prof. J. A. Gareth Williams at Durham University. In order to discuss the photophysical properties of these complexes, we will divide them into two series with **3.3.7** common to both series. In the first series, the bis-bidentate ligand remains constant in each complex and therefore, the changes in the photophysical properties can only be attributed to the variation of substituents on the terdentate N^C^N ligand. In the second series, the terdentate N^C^N ligand **3.1.2** is common to each complex and so only the influence of the variation of substituents on the bis-N^C bridging ligand account for the changes in optical properties.

The UV-visible absorption spectra of the dinuclear iridium(III) complexes recorded in dichloromethane solution at room temperature are shown in Figure 102, with the absorption maxima and molar extinction coefficients tabulated in Table 4. All of the bimetallic complexes show a series of intense bands in the UV region of the spectrum ($\varepsilon \approx 30\text{-}80 \times 10^3$ M^{-1} cm^{-1}) as well as intense bands in the visible region to around 500-530 nm ($\varepsilon \approx 5\text{-}30 \times 10^3$ M^{-1} cm^{-1}). With increasing wavelengths, there is a trend to decreasing molar absorptivities. The absorption spectra recorded are typical of cyclometallated iridium(III) complexes, but with higher extinction coefficients than those of related mononuclear complexes, for example, those with the general structure Ir(N^C^N)(N^C)Cl as reported by Williams *et. al*.[29-31, 88, 134, 136, 148, 158, 196-213] The observation of higher molar absorption coefficients for multimetallic complexes is consistent with previous examples investigated by Kozhevnikov and co-workers.[83-85]

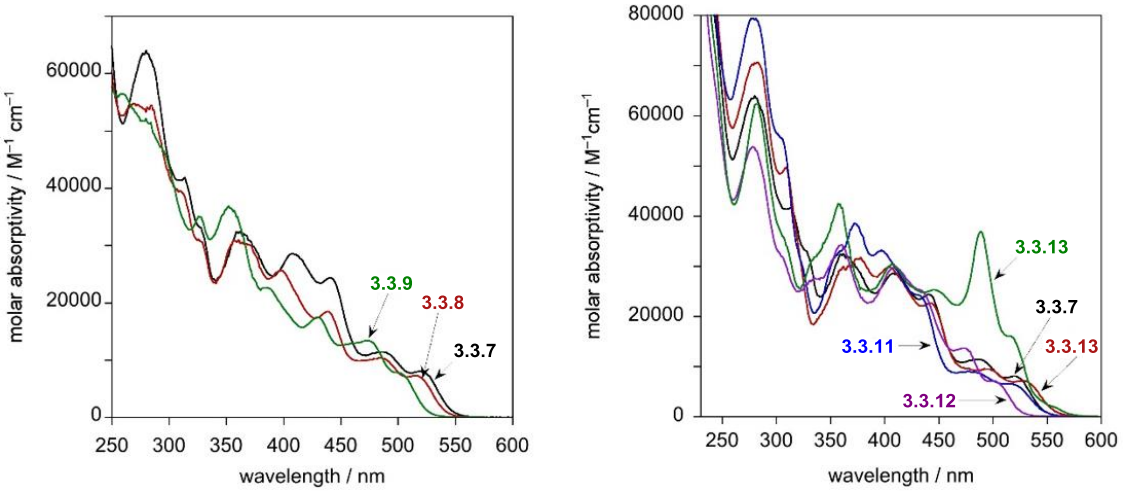

Figure 102: UV-visible absorption spectra recorded for the pyrimidine-linked dinuclear iridium(III) complexes in CH_2Cl_2 at 298 K ± 3 K (left) the first series **3.3.7**-**3.3.9** in which the terdentate N^C^N ligand is varied (right) the second series **3.337** and **3.3.10**-**3.3.13** in which the bis-N^C bridging ligand is varied.

Table 4: UV-visible absorption data for the pyrimidine-linked dinuclear Ir(III) complexes in CH_2Cl_2 at 298 K ± 3 K.

Complex[(a)]	**λ_{max} / nm (ε / M^{-1} cm^{-1})**
3.3.7	279 (63400), 312 (41500), 360 (32300), 408 (28600), 441 (24400), 484 (11400), 520 (8080)
3.3.8	270 (54700), 310sh (39500), 326sh (31100), 363 (30400), 398 (25600), 438 (18500), 484 (10300), 514 (7300)
3.3.9	260 (56500), 281 (51500), 327 (34900), 354 (36500), 385 (22500), 430 (17500), 474 (13400), 500 (7800)
3.3.10	281 (70400), 309 (49600), 376 (31500), 4040 (29800), 442 (22600), 494 (9150), 526 (7120)
3.3.11	279 (79300), 3030sh (55800), 358sh (32700), 372 (38600), 397 (33200), 430 (24300), 477 (8970), 514 (6560)
3.3.12	277 (53600), 335 (27600), 360 (34300), 409 (29700), 433sh (25200), 473 (13700), 498 (7070)
3.3.13	281 (62300), 305sh (36200), 337sh (31800), 358 (42200), 407 (30300), 446 (25300), 489 (36800), 514 (16100), 554 (2100)

(a) For comparison, data for the related mononuclear complex Ir(F_2dpyb)(ppy)Cl are as follows: λ_{max} / nm (ε = M-1 cm-1) = 260 (44800), 280 (40300), 358 (9100), 381 (11300), 402 (14000), 438 (3640), 473 (1540).[30]

From the UV-visible absorption spectra shown in Figure 102 and the corresponding data in Table 4, it is possible to see that the spectra for the **3.3.7**-**3.3.9** series have very similar profiles, but with the bands at $\lambda > 370$ nm becoming increasingly blue-shifted on going from **3.3.7** to **3.3.8** to **3.3.9**. In **3.3.9**, the difluorophenyl ring of **3.3.8** is replaced with a difluoropyridyl ring. This leads to a more electron-withdrawing N^C^N ligand and shifts the absorption bands to higher energy by approximately 500 cm^{-1}. Conversely, going from **3.3.8** to **3.3.7** the addition of the alkoxy

substituent leads to a terdentate auxiliary ligand with more electron-donating character and therefore the absorption bands of **3.3.7** are shifted to lower energy by around 200 cm^{-1}. For the series **3.3.7** and **3.3.10**-**3.3.13**, in which the bis-bidentate bridging ligand is varied, the absorption spectra of **3.3.7** and **3.3.10**-**3.3.12** are similar to one another in profile, with the lowest-energy absorption bands increasing in energy in the order **3.3.10** < **3.3.7** < **3.3.11** < **3.3.12**. The spectra recorded for the bis-thienylpyrimidine complex, **3.3.13**, is very different to those obtained for the rest of the series at wavelengths above 450 nm. The appearance of two bands in this region have much higher extinction coefficients than those of the other complexes. Additionally, there is a weakly-absorbing band at low energy (λ_{max} = 554 nm, ε = 2100 M^{-1} cm^{-1}) in the absorption spectra of **3.3.13**. This band has no observable counterpart in the spectra of the other complexes in this series.

The seven pyrimidine-linked dinuclear iridium(III) complexes being discussed in this chapter are highly luminescent in deoxygenated solutions at room temperature. The emission spectra recorded for these complexes are shown in Figure 103 (subdivided into the same series as in Figure 102) with the corresponding emission data shown in Table 5. The majority of the spectra show a well-defined emission maximum accompanied by a shoulder on the lower-energy side. Literature suggests that this type of emission profile is typical of rigid chromophores with a small Huang-Rhys factor, in which the emission is concentrated in the highest-energy 0,0 vibrational component band.[20] At 77 K, the vibrational structure of the emission spectra becomes more pronounced with the emission spectra of all complexes exhibiting at least three components of a vibrational progression of 1400 cm^{-1}. This is typical of aromatic C=C vibrational modes. The thienyl complex, **3.3.13**, shows additional bands due to a second, lower-frequency vibrational progression. The emission spectra recorded for the two series of dinuclear iridium(III) complexes show two main trends. Firstly, for the series **3.3.7**-**3.3.9**, the energy of the emission maxima increases in the order **3.3.7** < **3.3.8** < **3.3.9**, equal to the trend observed for the absorption spectra. In addition, from the 0,0 maxima, the differences in emission energy on going from **3.3.7** to **3.3.8** (≈ 200 cm^{-1}) and from **3.3.8** to **3.3.9** (≈ 500 cm^{-1}) are similar to the differences observed for the lowest-energy absorption band. Secondly, for the series **3.3.7** and **3.3.10**-**3.3.13**, the trend in

emission energy at room temperature is **3.3.13** ≈ **3.3.11** ≈ **3.3.10** < **3.3.7** < **3.3.12**. At 298 K, the vibrational shoulder in the emission spectra is only just detectable for **3.3.11** and is not observed at all for **3.3.10**. When recorded at 77 K, all of the emission spectra for this series show clearly resolved 0,0 components although the order of emission energy varies to **3.3.13** < **3.3.11** < **3.3.10** < **3.3.7** < **3.3.12**.

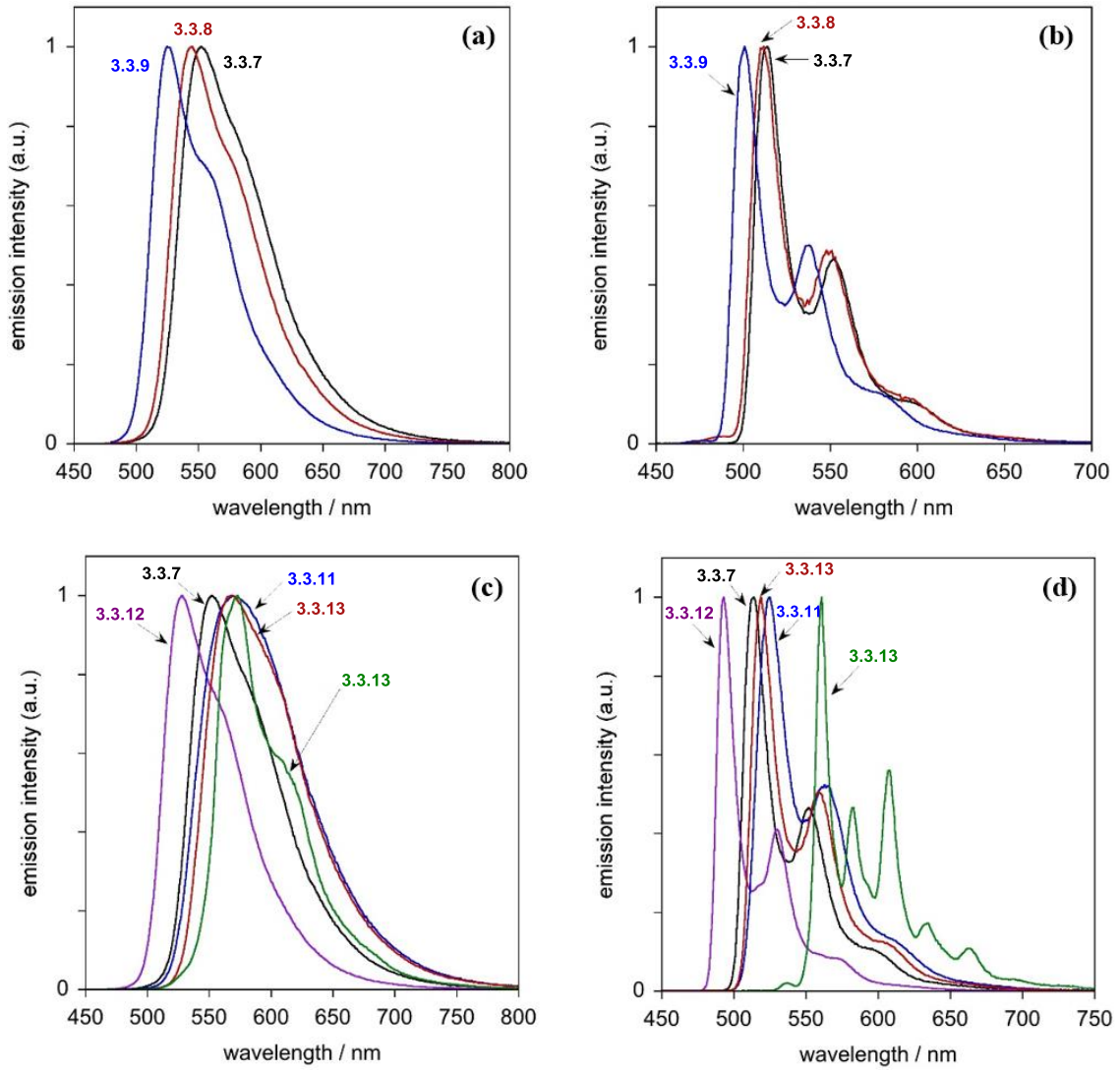

Figure 103: Luminescence spectra of the dinuclear iridium(III) complexes. (Top) Emission spectrum of series **3.3.7**-**3.3.9** (a) in CH_2Cl_2 at 298 K ± 3 K and (b) in diethyl ether / isopentane / ethanol (2:2:1) at 77 K. (Bottom) Emission spectra of **3.3.7** and **3.3.10**-**3.3.13** (c) in CH_2Cl_2 at 298 K ± 3 K and (d) in diethyl ether / isopentane / ethanol (2:2:1) at 77 K.

Table 5: Emission data for the pyrimidine-linked dinuclear iridium(III) complexes in degassed CH_2Cl_2 at 298 K and in EPA[(a)] at 77 K.

Complex	λ_{max} / nm	Φ_{lum}[(b)]	τ / ns[(c)]	k_r[(d)] / 10^6 s^{-1}	Σk_{nr}[(d)] / 10^6 s^{-1}	k_Q^{O2} [(e)] / 10^9 M^{-1} s^{-1}	Emission at 77K[(f)]	
							λ_{max} / nm	τ / ns
3.3.7	552, 582sh	0.94	440 [210]	2.14	0.14	1.13	513, 552, 594	6650
3.3.8	544, 576sh	1.0	550 [160]	1.82	--[(g)]	2.01	512, 549, 593sh	7500
3.3.9	526, 557sh	1.0	590 [230]	1.69	--[(g)]	1.21	501, 538, 578	7800
3.3.10	568, 599sh	0.88	570 [230]	1.54	0.21	1.18	519, 559, 602	4200
3.3.11	570	0.91	590 [220]	1.54	0.15	1.30	525, 563, 610sh	1300
3.3.12	528, 557sh	1.0	360 [160]	2.78	--[(g)]	1.58	493, 530, 569	2400
3.3.13	572, 611sh	0.94	4000 [380]	0.24	0.015	1.08	560, 582, 608, 633, 663, 695, 728	23000

(a) EPA = diethyl ether / isopentane / ethanol (2:2:1 v/v). (b) Measured using $Ir(ppy)_3$ in 2-MeTHF as the standard, for which the $\Phi = 0.97$. (c) Values in air-equilibrated solution in parentheses. (d) k_r and Σk_{nr} are the radiative and non-radiative decay rate constants, estimated from the quantum yield and lifetime assuming that the emissive state is formed with unitary efficiency. (e) Bimolecular rate constant for quenching by O_2, estimated from the luminescence lifetimes in degassed and air-equilibrated solutions, and taking $[O_2] = 2.2$ mM in CH_2Cl_2 at $p = 1$ atm air and T = 298 K. (f) In EPA: see footnote a. (g) Since the measured quantum yield is unity within the error of measurement, it is not possible to make a meaningful estimate of k_{nr}. (h) For comparison, data for the related mononuclear complex $Ir(F_2dpyb)(ppy)Cl$ are as follows: At 298 K, λ_{max} = 487, 516 nm; $\Phi_{lum} = 0.20$; τ = 390 ns; $k_r = 0.5 \times 10^6$ s^{-1}; $\Sigma k_{nr} = 2.1 \times 10^6$ s^{-1}. At 77 K, λ_{max} = 471, 508, 537, 548, 593 nm; $\tau = 2.5$ μs.[30]

The excitation spectra measured closely match the absorption spectra for all seven of the bimetallic Ir(III) complexes investigated in this section. This indicates that the same emissive state is formed with high efficiency, irrespective of the excitation wavelength. This is typical for cyclometallated complexes of third-row transition metals such as Ir(III). For such complexes, the processes of internal conversion and intersystem crossing to the lowest-lying triplet state are faster than the rate of fluorescence from the lowest-lying singlet state by several orders of magnitude.[214-216] The luminescence quantum yields in solution at room temperature are very high for all of the complexes, approaching unity, within the uncertainty of the measurement. The quantum yields measured are higher than those of related mononuclear Ir(III) complexes of the Ir(N^C^N)(N^C)Cl series previously studied by Williams *et. al* (see footnote to Table 5).[30] The values obtained for the quantum yields are comparable to *fac*-$Ir(ppy)_3$, despite the emission being significantly red-shifted in comparison.[217] The luminescence lifetimes recorded for these dinuclear complexes are in the range of 360-590 ns at room temperature, except for **3.3.13** which

has a longer lifetime of 4000 ns under the same conditions. These lifetimes are much shorter than that of *fac*-Ir(ppy)$_3$, for which a value of 1.6 μs has been reported under comparable conditions.[217] Given that the quantum yields are comparable to *fac*-Ir(ppy)$_3$, the observation of much shorter luminescence lifetimes suggests a significantly higher rate of radiative decay in the dinuclear complexes. The radiative and non-radiative rate constants, k_r and Σk_{nr} respectively, can be estimated using the equations below, assuming that the emissive state is formed with unitary efficiency upon excitation.

$$k_r = \frac{\Phi}{\tau} \quad \text{and} \quad \sum k_{nr} = \frac{1-\Phi}{\tau}$$

The values for the radiative and non-radiative rate constants shown in Table 5 were estimated using this method. For *fac*-Ir(ppy)$_3$, the value of k_r has been estimated as 6 x 10^5 s^{-1}.[217] Therefore, it can be seen that, with the exception of **3.3.13**, the values for k_r for the dinuclear iridium(III) complexes are increased by a factor of 2-5.

The luminescence observed for these complexes is quenched by oxygen with a bimolecular rate constant of the order of 10^9 M^{-1} s^{-1}. This is typical for cyclometallated complexes of third-row transition metals such as Ir(III) and Pt(II). However, due to the high k_r values and the very short luminescence lifetimes (except for **3.3.13**), the effect of oxygen on the reduction of lifetimes and emission intensities is unusually small at atmospheric pressure. Only a reduction by around a factor of 2 is observed. As a consequence of the much longer lifetime of **3.3.13**, both at 298 and 77 K (4 and 23 μs respectively), the emission of this complex in solution is much more sensitive to quenching by O_2.

The photophysical properties observed for the seven pyrimidine-linked dinuclear iridium(III) complexes can be rationalised further with the aid of time-dependent DFT (TD-DFT) calculations. The optimised geometries of the dinuclear complexes, calculated as described previously, were utilised to obtain main excitation energies, oscillator strengths and the predominant molecular orbital contributions. UV-visible spectra were calculated in vacuum, and in dichloromethane solution. In all cases the general effect of the solvent is to blue-shift the frequency of the highest

energy singlet band by 15 to 38 nm and to increase its intensity. The simulated absorption spectra show less vibrational structure than the spectra obtained experimentally. Vibrational structure in the experimental absorption spectra likely arises as a result of excitation to vibrationally excited levels of the electronic excited states. This is not modelled theoretically and therefore does not appear in the simulated spectra.

The data obtained from the calculation is extremely useful in providing further insight into the trends in absorption and emission energies. For all of the dinuclear complexes, both the experimental trends in the energy of the lowest-energy absorption band and the emission energy correlate well with the calculated HOMO-LUMO gap, as is shown in Figure 105. Plots of the calculated S_1 and T_1 energies both in vacuum and in solvent also show good correlation with the experimental data.

Using the TD-DFT data, it is appropriate to attempt to understand the influence of the substituents on the cyclometalling ligands in terms of their effects on the energies of the HOMO and LUMO. Frontier orbital plots of the HOMO and LUMO of the dinuclear complex **3.3.7** are shown in Figure 104 with frontier orbital plots and related TD-DFT data of all the dinuclear iridium(III) complexes within this series shown in section 5.2. As discussed previously in section 1.2.3, it has been reported that for mononuclear complexes of Ir(III) and Pt(II) of cyclometallated ligands such as 2-phenylpyridine, the LUMO is based on the heterocycle with the HOMO localised on the metallated aryl ring and the metal atom.[51] In the case of our dinuclear iridium(III) complexes, the calculations show that the LUMO is located predominantly on the pyrimidine ring of the bis-N^C ligand. This is as expected as the pyrimidine ring of the bridging ligand is more electron-deficient than the pyridine rings of the terdentate N^C^N ligand and therefore offers lower-energy π^* orbitals. On the other hand, the calculations show that the HOMO for each complex is localised on the metal atom and the metallated aryl ring of either the N^C^N or the bis-N^C ligand depending on the identity of the two ligands.

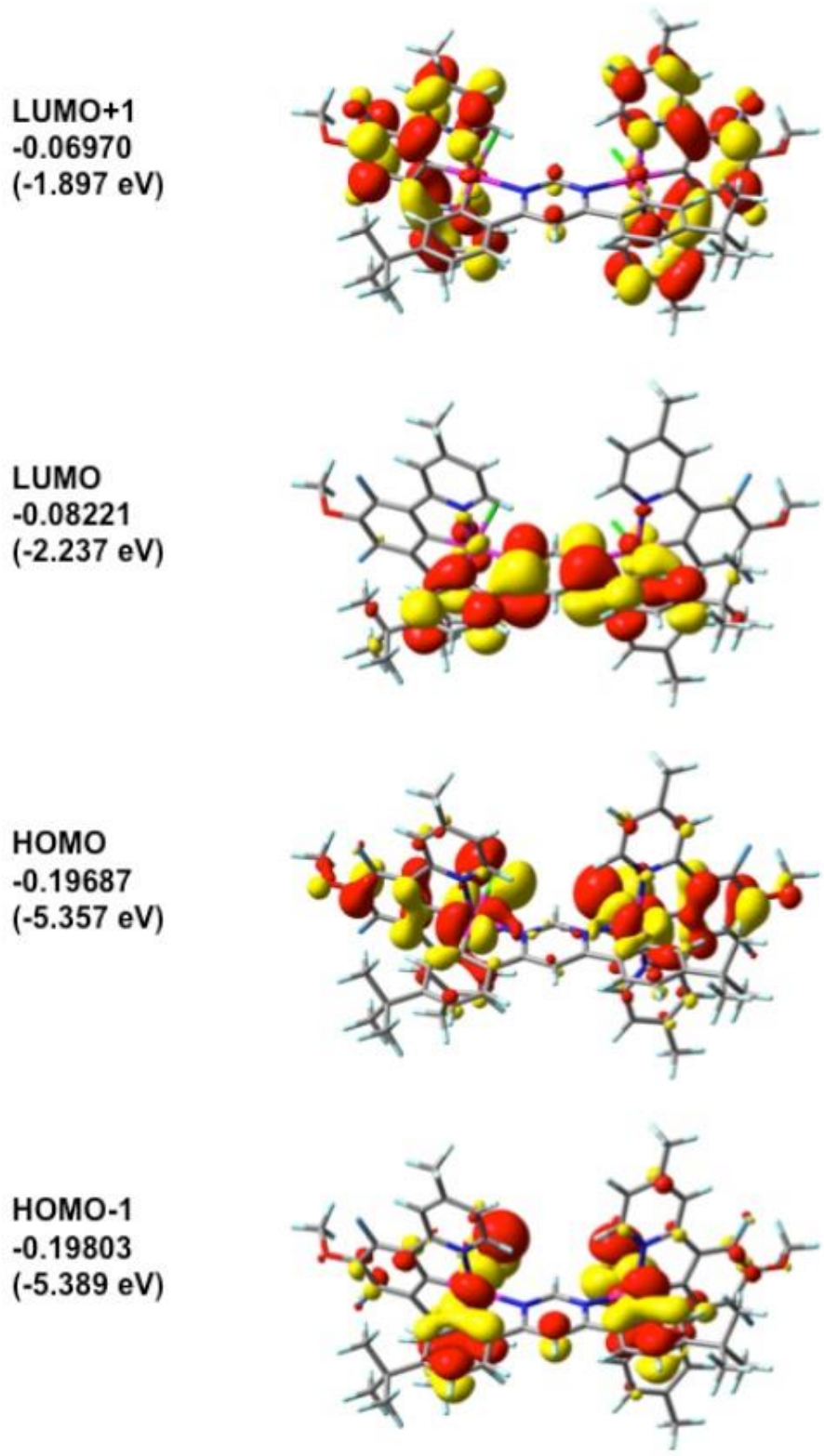

Figure 104: Frontier orbital plots of dinuclear iridium(III) complex **3.3.7**, with their energies in Hartree (energies in eV in parenthesis).

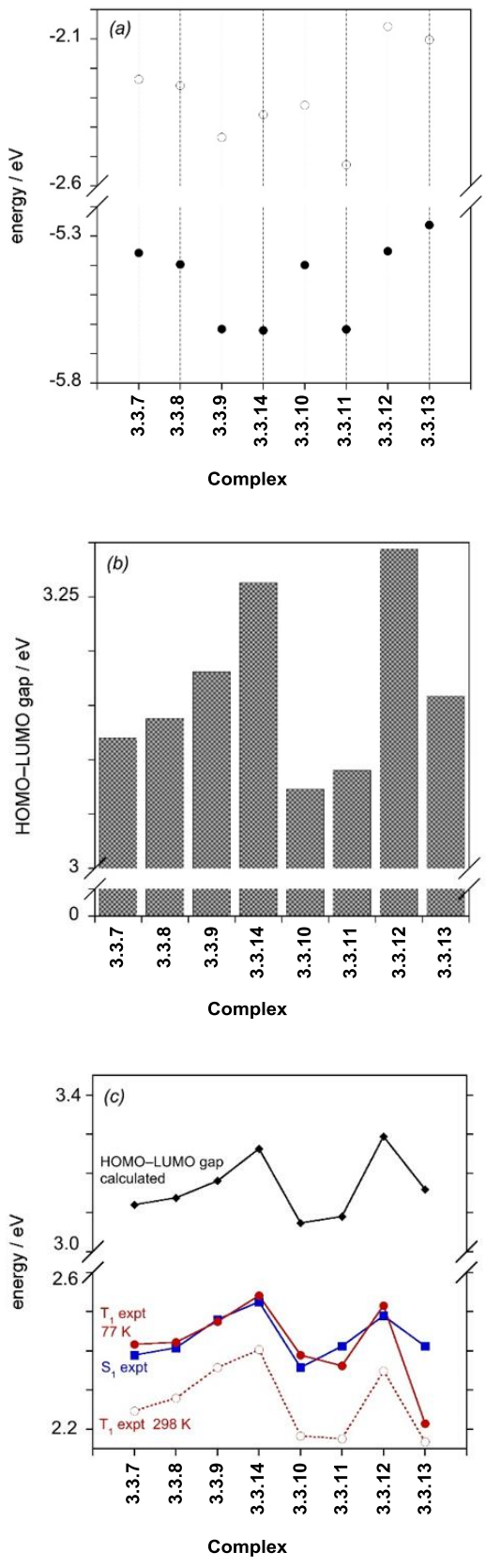

Figure 105: (a) Calculated HOMO and LUMO energies for the complexes in vacuo, in eV (filled and empty circles respectively). (b) The HOMO-LUMO gap (eV) calculated from the respective energies in (a). (c) Plot of experimental S_1 energy (blue squares), estimated based on λ_{max} of the lowest-energy absorption band (excluding the weak band at 554 nm for **3.3.13**, which is concluded to be a direct excitation to $^3\pi$-π^* state); the T_1 energy estimated from experimental λ_{max} (0,0) values in the emission spectra at 298 K (open red circles) and at 77 K (filled red circles); and the calculated HOMO-LUMO gap (black diamonds). The lines between points are provided solely as a guide for the eye.

The plots above (Figure 105) show the calculated HOMO and LUMO energies of the dinuclear complexes as well as the magnitude of the resulting energy gap.

For the first series of complexes, it can be seen that the blue-shift in absorption and emission on going from **3.3.7** to **3.3.8** and to **3.3.9** is due to a larger stabilisation of the HOMO than the LUMO. In **3.3.7**, the HOMO is mainly localised on the aryl ring of the N^C^N ligand with a minor contribution from the metallated ring of the bis-N^C ligand. In **3.3.8**, in which the electron-donating alkoxy group is absent, the HOMO now involves primarily the bis-N^C aryl ring with only a minor contribution from the terdentate ligand. Replacement of the central aryl ring of the N^C^N ligand with a pyridine ring in **3.3.9** leads to a HOMO almost wholly localised on the aryl ring of the bridging ligand with the contribution of the terdentate ligand becoming negligible.

For the second series of dinuclear iridium(III) complexes, the shifts in absorption and emission depend on the variation in both the HOMO and LUMO energies. Moving from **3.3.7** to **3.3.10**, there is a small red-shift in the absorption and emission maxima arising primarily from stabilisation of the LUMO due to removal of the *t*-butyl substituents. In this case, the effect on the LUMO is larger than that on the HOMO. Figure 105 suggests that **3.3.11** should be fairly similar to **3.3.10** and this is indeed what is observed experimentally (only a small blue-shift is observed in the absorption spectra). At first, the similarity of these two complexes is surprising as, from the literature, it is known that *fac*-Ir(dfppy)$_3$ is significantly blue-shifted relative *fac*-Ir(ppy)$_3$ as a result of stabilisation of the HOMO by the fluoro- groups.[24] However, Figure 105 shows that the electron-withdrawing fluoro- groups present in **3.3.11** stabilise both the HOMO and LUMO to similar extents and this is the reason for the lack of significant effect on the photophysical properties. In the methoxy-substituted complex, **3.3.12**, a large blue-shift is observed in the absorption and emission spectra when compared with **3.3.7**. It can be seen, using Figure 105, that this is exclusively due to destabilisation of the LUMO based on the bis-N^C bridging ligand. The electron-donating methoxy substituents on **3.3.12** are located *para* to the electron-deficient pyrimdine ring on which the LUMO is located and additionally are sufficiently electron-rich to shift the HOMO from the N^C^N ligand to the aryl ring of the bis-N^C ligand. Finally, for **3.3.13**, this complex is predicted to have the lowest-energy emission of the bimetallic

iridium(III) complexes prepared as observed experimentally at 77 K. **3.3.13** has an anomalously long luminescence lifetime of 4 μs at 298 K and 23 μs at 77 K. Combining the observation of a long luminescence lifetime with the highly vibrationally-structured emission spectra of this complex at 77 K, it is appropriate to consider that the excited state of **3.3.13** may have more ligand-centred π-π* character.[163] Based on the emission spectra of this complex both at 298 K and 77 K, it seems likely that at room temperature the ^{3}MLCT and ^{3}π-π* states are close in energy whereas at 77 K, the former is displaced to higher energy leading to the ^{3}π-π*-like emission spectrum at 77 K.

Following this analysis of the photophysical properties of this series of seven dinuclear iridium(III) complexes, we can draw some conclusions about the influence of the second metal ion. From the emission data in Table 5, we can see that the radiative decay constants for these complexes is enhanced relative to related mononuclear complexes whilst the non-radiative decay is suppressed. The dinuclear complexes have significantly lower excited state energies than corresponding mononuclear complexes and therefore, considering the energy gap law, the observation of reduced non-radiative decay for our di-iridium(III) complexes is remarkable. The energy gap law says that for a given class of complex, non-radiative decay processes increase with decreasing excited state energy with possible decreases in k_r to be anticipated also. The fact that k_r is increased consistently for our multimetallic complexes supports the idea that a second heavy metal ion may enhance the spin-orbit coupling pathways. The same increase in k_r has also been observed with multimetallic complexes previously investigated by Kozhevnikov *et. al*. The suppression of the non-radiative decay, is thought to be due to the greater conformational rigidity of the dinuclear systems.[83-85]

Following on from this research into pyrimidine-linked dinuclear iridium(III) complexes bearing auxiliary terdentate N^C^N ligands derivatised from 1,3-dipyridylbenzene, we prepared a further series of pyrimidine-linked di-iridium(III) complexes incorporating the alternative N^C^N-coordinating auxiliary ligands as discussed in section 3.1.

Firstly, the influence of the substituents attached to the N^C^N-coordinating ligand was investigated. The importance of blocking the competitive bidentate coordination of terdentate ligands through incorporation of substituents was discussed in section 3.1. Traditionally substituents have been added at positions 4- and 6- of the central phenyl ring of the N^C^N-coordinating ligand, however, more recently the use of a single substituent at the 5-position has been reported.[70] As a result, we prepared a terdentate ligand incorporating a single *t*-butyl substituent at the 5-position of central phenyl ring. In the synthesis of the dichloro-bridged iridium(III) dimer, this ligand **3.2.4** showed terdentate coordination to the metal centre. The corresponding dinuclear iridium(III) complex was prepared using the same two-step synthetic procedure as described previously in Figure 98, with the bis-N^C-coordinating bridging ligand **3.3.6** selected. The desired pure bimetallic complex **3.3.15**, as shown in Figure 106 was isolated in a relatively low yield of 15%, following purification by column chromatography.

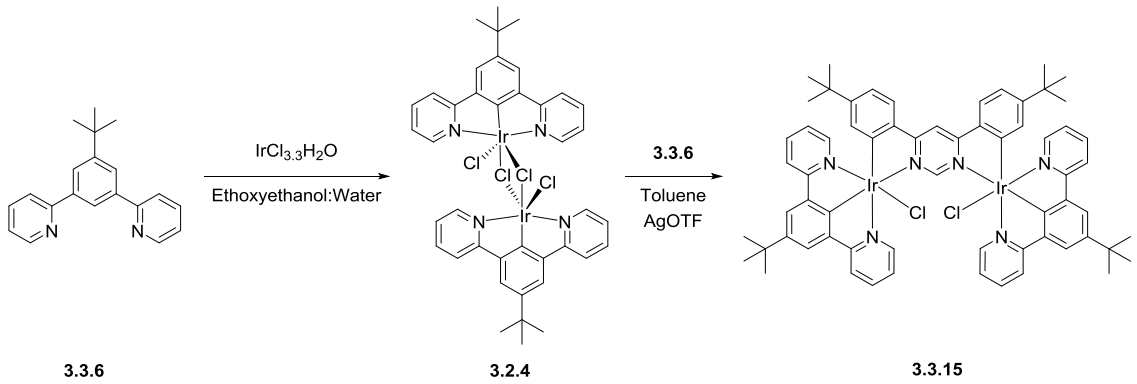

Figure 106: A reaction scheme to show the synthetic method used for the preparation of **3.3.15**. The dinuclear complex was isolated as a red-orange solid in a yield of 15%.

The identity of this dinuclear iridium(III) complex was confirmed using ^{1}H and ^{13}C NMR spectroscopy and using mass spectrometry. The aromatic region of the ^{1}H NMR spectrum of **3.3.15** is shown in Figure 107 and shows the characteristic features of the desired final dinuclear complex. The singlet at δ 11.8 ppm corresponds to the proton at the 2-position of the pyrimidine ring. This signal has a high chemical shift due to the proximity of this proton to the two monodentate chloro ligands. The doublet at δ 6.00 ppm corresponds to the two protons *ortho* to the metallated carbon atoms in the aryl rings of the bis-bidentate bridging ligand.

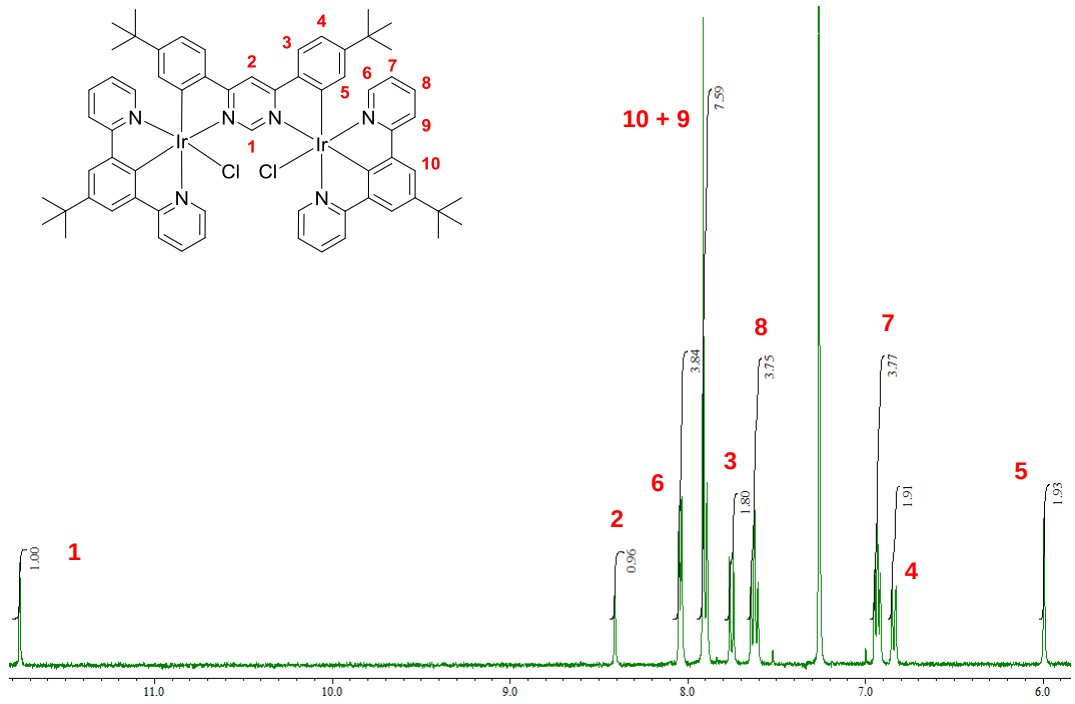

Figure 107: A figure to show the aromatic region of the ^{1}H NMR spectrum of **3.3.15**. The NMR shows characteristic features indicative of the final dinuclear iridium(III) complex. The singlet at δ 11.8 ppm corresponds to the proton at the 2-position of the pyridmidine ring and the doublet at δ 6.00 ppm corresponds to the two protons *ortho* to the metallated carbon atoms in the aryl rings of the bis-bidentate bridging ligand. Additionally, this NMR spectrum shows no evidence for the formation of diastereoisomers.

Successful utilisation of terdentate auxiliary ligand **3.1.5** in a pyrimidine-linked dinuclear iridium(III) complex led to the preparation of further bimetallic iridium(III) complexes incorporating N^C^N ligands also bearing a single *t*-butyl substituent on the central aryl ring. In order to investigate the effect of the heterocycle of the terdentate ligand, the pyridine rings were replaced with alternative heterocycles; benzimidazole and pyrazole, as shown in Figure 88 and Figure 91 in section 3.1. This series of dinuclear complexes synthesised using these alternative N^C^N-coordinating auxiliary ligands are shown in Figure 108.

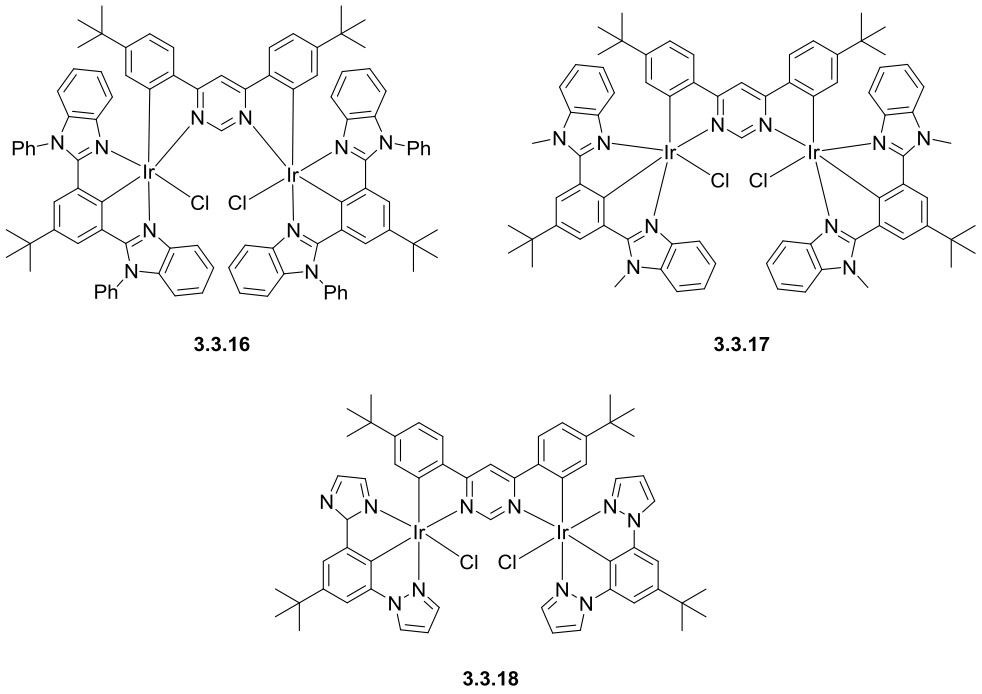

Figure 108: A figure to illustrate the structures of dinuclear iridium(III) complexes incorporating terdentate N^C^N-coordinating ligands in which the N-coordinating moiety is a benzimidazole or a pyrazole. The complexes were isolated in moderate to good yields (33-83%).

The target complexes in this case were isolated in moderate to good yield (33-83%) following purification by column chromatography.

Again, each of the final complexes were characterised by ^{1}H and ^{13}C NMR spectroscopy and by mass spectrometry. In addition, a crystal suitable for X-ray diffraction was obtained for **3.3.16**. The crystallographic analysis was performed by Marsel Shafikov in the group of Professor Hartmut Yersin at Regensburg University. The molecular structure is shown in Figure 109 and the corresponding crystallographic data is shown in Table 6. The crystal structure shows the two iridium(III) centres, each with distorted octahedral geometry, rigidly-linked via the bis-bidentate bridging ligand. Each iridium centre is bound to one auxiliary terdentate N^C^N ligand, **3.1.11**, and the coordination sphere of each metal ion is completed by a monodentate chloride ligand. The crystal structure below shows that the unit cell contains three molecules of methanol originating from the crystallisation procedure.

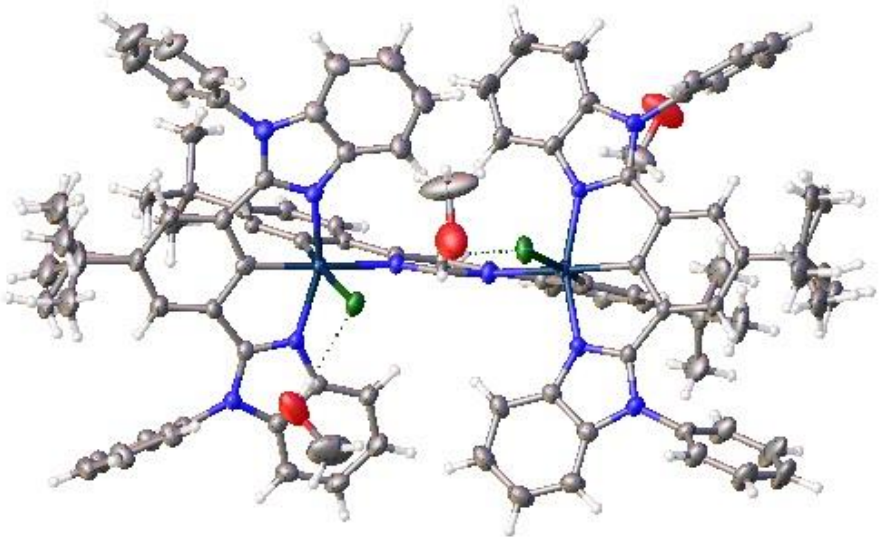

Figure 109: The crystal structure of **3.3.16·3MeOH**, obtained by X-ray crystallography.

Table 6: Selected bond lengths (Å) for the complex **3.3.16·3MeOH** as determined by X-ray crystallography.

Bond Length (Å)	**X-Ray Data**
Ir-N(benzimidazole)	2.057(2)
Ir-N(benzimidazole)	2.058(2)
Ir-N(pyrimidine)	2.143(2)
Ir-C(N^C^N)	1.946(3)
Ir-C(bis-N^C)	2.018(3)
Ir-Cl	2.477(7)

The crystallographic data show in Table 6 illustrates that, like the series of pyrimidine-linked dinuclear iridium(III) complexes discussed previously in this section, there is a strong *trans* influence associated with the metallated carbon atoms of both the terdentate N^C^N and bis-N^C ligands. This is evidenced by the elongated bonds lengths of the Ir-N(pyrimidine) bond with a length of 2.143(2) Å and the Ir-Cl bond with a length of 2.477(7) Å. Similar elongated bond lengths were observed in the crystal structure of **3.3.11** (Table 3).

Full investigation of the photophysical properties for this series of pyrimidine-linked complexes, **3.3.15**-**3.3.18** is still required, however, luminescence measurements of **3.3.16** were carried out by Marsel Shafikov in the group of Professor Hartmut Yersin at Regensburg University. It was

observed that **3.3.16** exhibits a photoluminescence quantum yield of 100% and a luminescence lifetime of 450 ns, both measured in degassed CH_2Cl_2 solution at 300 K.

In summary, in this section we have shown that 4,6-diarylpyrimdines can be used as bis-cyclometallating bridging ligands, binding to two iridium centres via N^C-coordination to each metal. We have also shown that incorporation of a terdentate N^C^N ligand ensures that the resulting dinuclear complexes are achiral, contrasting with the mixtures of stereoisomers that form in the case of tris-bidentate metal complexes. In addition, the strong *trans* influence of the cyclometallated aryl rings of both the bis-bidentate and terdentate ligands lead to the formation of only one unique product, in which the pyrimidine ring is *trans* to the central aryl ring of the N^C^N ligand at both iridium centres. The final dinuclear iridium(III) complexes are intensely luminescent, with quantum yields close to unity and the emission energies tuneable through the variation of substituents on bis-N^C bridging ligand or the terdentate N^C^N ligand. In addition to the strong light absorption and intense emission in the visible region, these bimetallic complexes offer huge potential for structural diversity. This structural diversity is possible as a result of the versatility of the design strategy and the ease of synthesis of suitable of terdentate and bis-bidentate ligands. These numerous advantages to these pyrimidine-linked dinuclear iridium(III) complexes have led to further investigation into new compounds as will be discussed in the following sections of this chapter. These new complexes may be applied to a variety of applications in which multinuclear complexes are already recognised to offer unique opportunities, for example, as water splitting catalysts or for interaction with biomolecules.

3.4 2,5-Pyrazine- vs. Thiazole-Linked Dinuclear Iridium(III) Complexes

As has been stated previously, the bridging ligand linking the metal centres in a multinuclear complex is important in the modulation of both the chemical and photophysical properties of the final compound.[84] Research into dinuclear iridium(III) complexes linked by cyclometallating bis-N^C-coordinating 4,6-diphenylpyrimidine-based bridging ligands was described in section 3.3. The complexes studied were highly luminescent, displayed advantageous optical properties and

have enormous potential in terms of routes for structural variation. One fundamental way in which the structure of such bimetallic iridium(III) complexes can be altered is through variation of the bis-N^C-coordinating bridging ligand.

Bridging ligands utilising pyrazine as a central heterocycle have been previously employed in the synthesis of multinuclear complexes. Zysman-Colman and co-workers reported the preparation of a cationic dinuclear iridium(III) complex in which the cyclometallated $Ir(ppy)_2$ fragments are linked by 2,5-dipyridylpyrazine. This multinuclear complex shows no room temperature luminescence, unlike the related mononuclear complex and analogous dinuclear Ru(II) complexes.[106, 218] In addition, previous work by Kozhevnikov *et. al.* used 2,5-diphenylpyrazine as a cyclometallating bridging ligand in the synthesis of a highly luminescent bimetallic platinum(II) complex.[85] This complex showed room temperature phosphorescence with a quantum yield of $\phi = 0.41$.[85] In these cases, the pyrazine-based bis-bidentate bridging ligands offer a linear geometry with *para*-coordination of the two metal centres across the central pyrazine ring. Following on from previous reports and its favourable structural characteristics, we decided to investigate a derivative of 2,5-diphenylpyrazine as a bis-N^C-coordinating bridging ligand in our rigidly-linked dinuclear iridium(III) complexes. This allowed the study of the influence of bridging ligand structure on the chemical and photophysical properties of the final multinuclear complex.

Consequently, using the same synthetic method as previously described in section 3.3, a dinuclear iridium(III) complex was prepared incorporating the linear bridging ligand 2,5-bis(4-*tert*-butylphenyl)pyrazine. The bimetallic complexes are composed of two iridium metal centres rigidly-linked via a bis-N^C-coordinating ligand, in this case 2,5-bis(4-*tert*-butylphenyl)pyrazine. Each iridium(III) centre is also bound to a terdentate N^C^N ligand and a monodentate chloro ligand. In the design of this dinuclear complex, the N^C^N-coordinating ligand **3.1.2** was selected. Therefore, the pyrazine-linked complex prepared here is analogous to the pyrimidine-linked dinuclear iridium(III) complex **3.3.7,** discussed in section 3.3.

Firstly, the preparation of the bis-bidentate bridging ligand, 2,5-bis(4-*tert*-butylphenyl)pyrazine (**3.4.1**) was carried out via the Suzuki-Miyaura cross-coupling reaction of 2,5-dibromopyrazine

and 5-*tert*-butylphenylboronic acid, as shown in Figure 110. The *tert*-butyl substituents present on the final ligand increase the solubility of the final mulitmetallic complex. Using this method, the bis-N^C-coordinating ligand was prepared in high yield (85%).

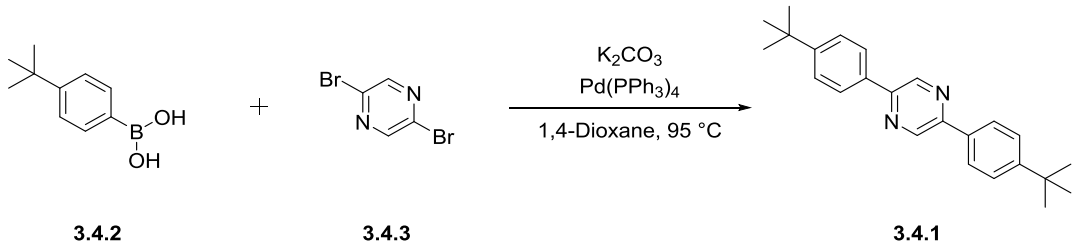

3.4.2 **3.4.3** **3.4.1**

Figure 110: A reaction scheme to show the synthesis of compound **3.4.1** via a Suzuki-Miyaura cross-coupling reaction.

The terdentate proligand **3.1.2** was synthesised as described previously in section 3.1. The fluoro-groups on the phenyl ring facilitate the synthesis of this ligand by *ortho*-directing the lithiation reactions involved in its preparation. Additionally, these fluoro- groups, at the 4- and 6- positions of the aryl ring, block the competitive bidentate binding of the iridium centre. Meanwhile, the hexyloxy- and *tert*-butyl substituents increase solubility of the proligands and the corresponding iridium complexes.[173]

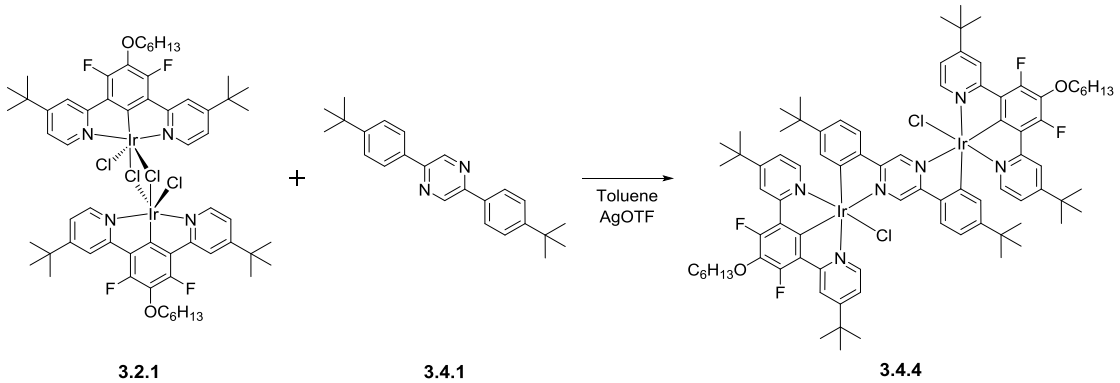

3.2.1 **3.4.1** **3.4.4**

Figure 111: A figure to show the synthesis of dinuclear Ir(III) complex, **3.4.4**. The target complex was isolated as a red solid in a good yield of 64%.

The synthetic procedure used for the preparation of the target dinuclear complex, **3.4.4** is shown in Figure 111. The first step involves the reaction of the terdentate proligand with $IrCl_3.H_2O$ at reflux in a mixture of 2-ethoxyethanol and water to yield the dichoro-bridged iridium(III) dimer

$[Ir(N^C^N)Cl(\mu\text{-}Cl]_2$ as a bright orange solid. The iridium dimer was isolated in high yield and fully characterised by ^{1}H, ^{19}F and ^{13}C NMR spectroscopy. As stated previously, the *tert*-butyl and hexyloxy-substituents present on the terdentate ligand increase the solubility of the dichloro-bridged iridium dimer, allowing characterisation in $CDCl_3$.

The iridium(III) dimer was then reacted with the bis-bidentate proligand, **3.4.1**, in toluene in the presence of silver triflate as a chloride scavenger. At completion of the reaction, the mixture was treated with an excess of HCl (3M, aq.) in order to ensure that the only monodentate ligand present on the iridium centres was chloride. Purification was carried out via column chromatography to give the final dinuclear complex in a good yield of 64%.[173]

As with the series of pyrimidine-linked complexes discussed in section 3.3, **3.4.4** was fully characterised by ^{1}H, ^{19}F and ^{13}C NMR spectroscopy and mass spectrometry. The ^{1}H NMR spectra of **3.4.4** (Figure 112) shows a characteristic signal at high chemical shift, δ 10.8 ppm, that corresponds to the two protons at the 2- and 5-positions of the pyrazine ring. This is, again, explained by the proximity of the electronegative chlorides to these protons. A second characteristic signal observed at δ 6.20 ppm can be assigned to the two protons *ortho* to the metallated carbon atoms of the bis-bidentate bridging ligand.

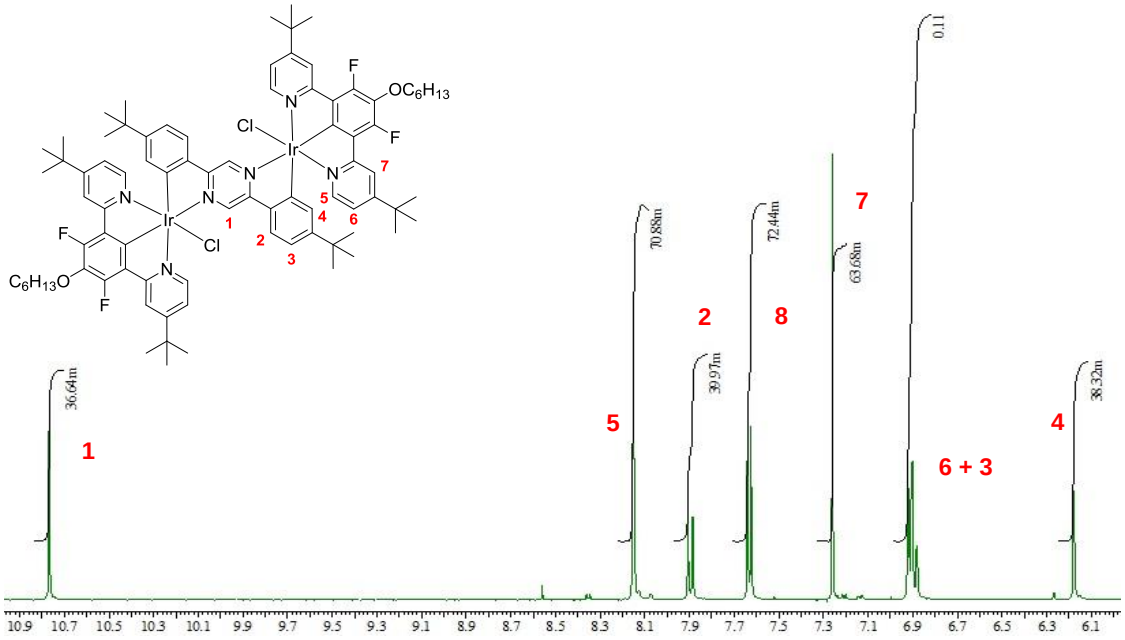

Figure 112: A figure to show the aromatic region of the ^{1}H NMR spectrum of **3.4.4**, recorded in $CDCl_3$. Like the pyrimidine-linked complexes, the NMR spectrum shows characteristic features indicative of the final dinuclear iridium(III) complex. The singlet at δ 10.8 ppm corresponds to the two protons of the pyrazine ring and the doublet at δ 6.20 ppm corresponds to the two protons *ortho* to the metallated carbon atoms in the aryl rings of the bis-bidentate bridging ligand.

The ^{1}H NMR spectrum shown above was recorded in $CDCl_3$. It was observed that the NMR sample of **3.4.4** degraded upon exposure to daylight, with the first signs of degradation noticeable after only a few minutes. This degradation of the $CDCl_3$ sample of **3.4.4** was not observed when the sample was stored in the dark and additionally, no degradation of the dinuclear complex was observed when dissolved in d^{6}-DMSO. Therefore, the degradation of **3.4.4** appears to occur only in chlorinated samples when exposed to light. In order to further study the degradation of this dinuclear iridium(III) complex, NMR spectra were recorded at time intervals of 0, 10, 60, 120, 180 and 600 minutes, following exposure of the sample to sunlight. The NMR spectra obtained at each of these time intervals are shown in Figure 113. After just 10 minutes of exposure to sunlight, there is evidence in the ^{1}H NMR spectrum for the formation of new species. Over time, the signals of several new species increase in intensity while the NMR signals corresponding to the dinuclear iridium(III) complex **3.4.4** decrease in intensity. After approximately 10-15 h, the sample is stable and no further degradation is observed.

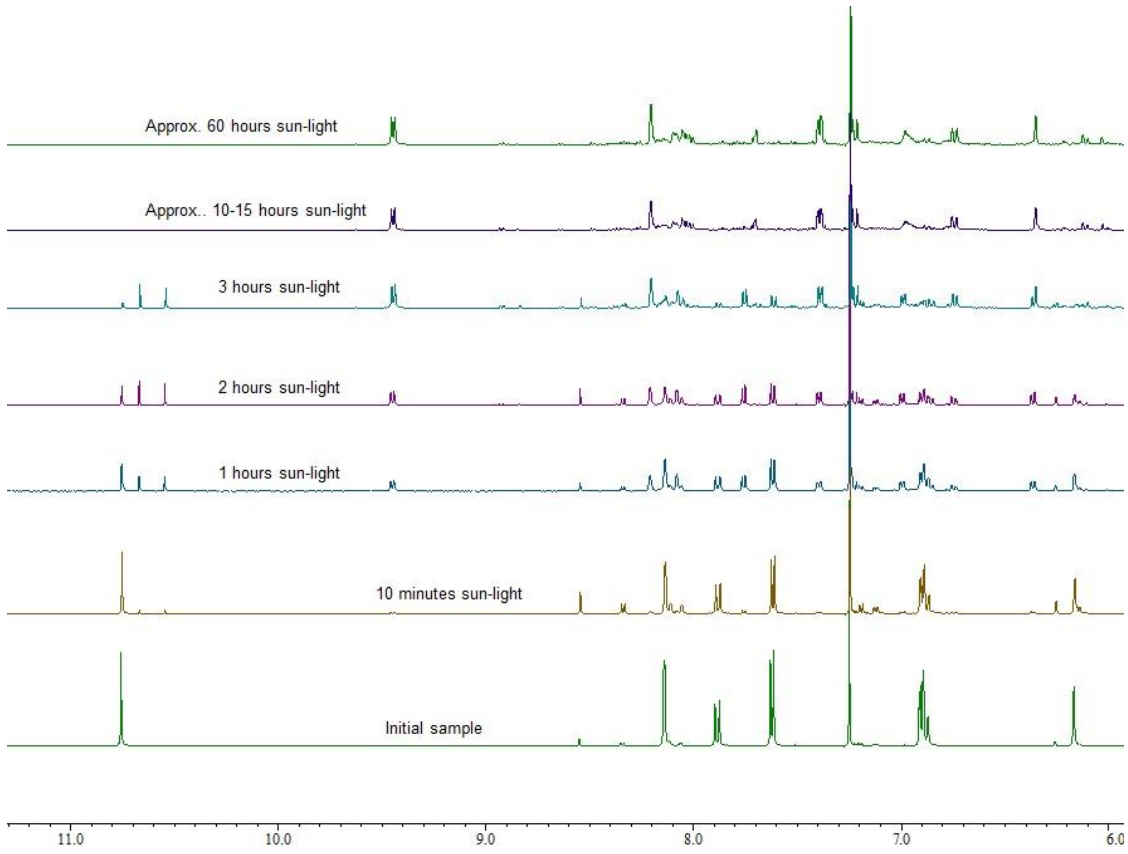

Figure 113: A figure to illustrate the degradation of dinuclear iridium(III) complex, **3.4.4** in $CDCl_3$ over a period of approximately 60 h. The NMR spectra were recorded at time intervals of 0 min, 10 min, 1 h, 2 h, 3 h, 10-15 h and approximately 60 h, following exposure of the NMR sample to sunlight.

Following the degradation of the sample of **3.4.4** as shown in Figure 113, the final species was recovered and analysed by mass spectrometry. The mass spectrum obtained for the degraded material is shown in Figure 114. The spectrum shows intense peaks at m/z 1695.6596, 847.3734 and 487.1942. The mass of fragment ions possible following ionisation of the initial pyrazine-linked dinuclear iridium(III) complex were calculated, however, there were no close matches for the peaks observed on the mass spectrum of the degraded material.

The fact that **3.4.4** was observed to degrade only in chlorinated solvents and only on exposure to light is suggestive of a photodegradation pathway, possibly involving radicals. Further investigation into the degradation of our pyrazine-linked dinuclear iridium(III) complex, **3.4.4**, is required in order to fully understand the reasons for its instability. It appears that the *para*-coordination of the two metal centres across the central pyrazine of the bis-bidentate bridging ligand incorporated has resulted in the final bimetallic complex being unstable.

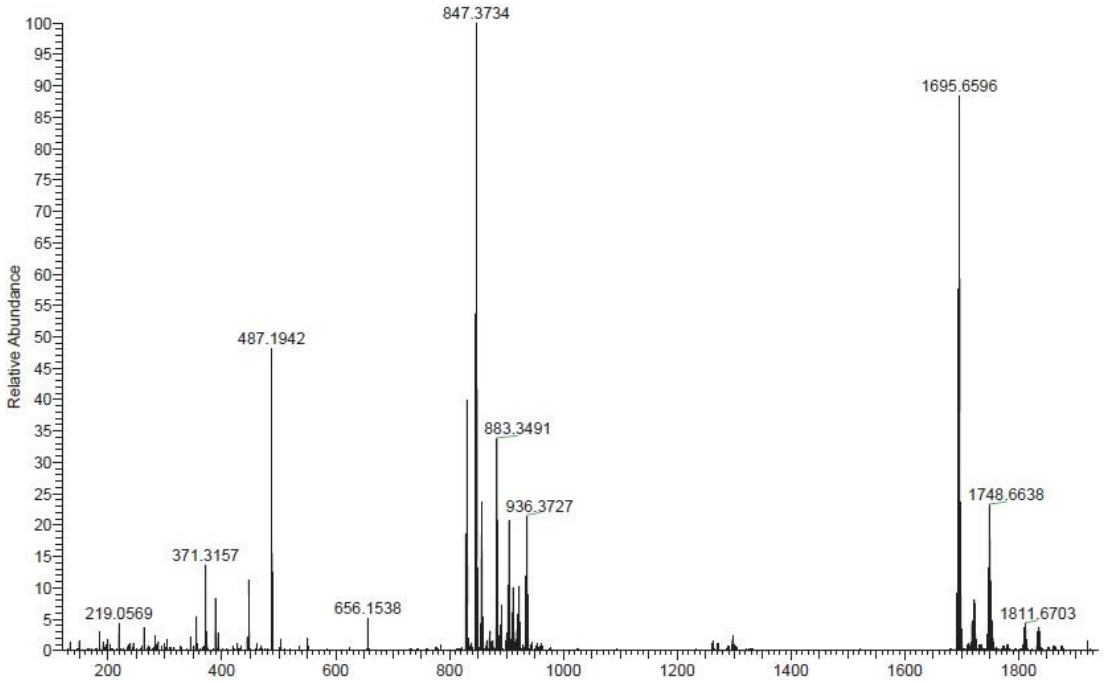

Figure 114: The mass spectrum for the degraded material recovered from a sample of **3.4.4** that was degraded on exposure to light.

In an attempt to increase the stability of the final dinuclear iridium(III) complex, an alternative bridging ligand, bis(4-*tert*-butylphenyl)-[1,3]thiazolo[5,4-d][1,3]thiazole, was prepared. The synthetic route used to prepare this bis-N^C-coordinating ligand, **3.4.5**, is shown in Figure 115 as reported by Reginato *et. al*. A condensation reaction of dithiooxamide and 4-*tert*-butylbenzaldehyde gave the desired compound in moderate yield of 36%.[219] 4-*tert*-Butylbenzaldehyde was selected in order to incorporate *tert*-butyl substituents at the 4-positions of the phenyl groups of the final bis-bidentate ligand. This allows direct comparison between the bridging ligands **3.4.1** and **3.4.5** and an evaluation of the effects of the two central heterocyclic cores on the properties of the final dinuclear complexes can be carried out.

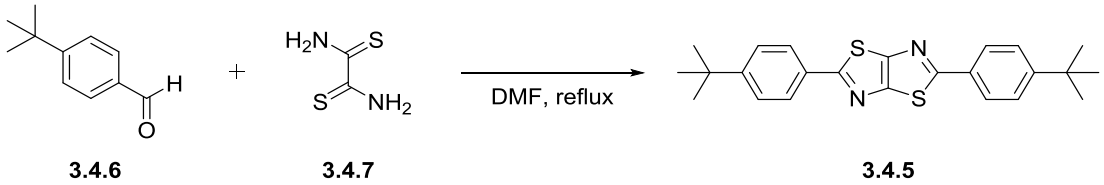

3.4.6 **3.4.7** **3.4.5**

Figure 115: A reaction scheme to show the synthesis of compound **3.4.5** via a condensation reaction of dithiooxamide and 4-*tert*-butylbenzaldehyde. The desired compound was isolated in a moderate yield (36%).

Thiazolo[5,4-d]thiazoles are an important class of bicyclic aromatic molecule containing two fused thiazole rings. The first compound containing this core structure was first discovered in 1891 by Ephraim.[220] Further research by Johnson *et. al.* in 1960 reported both the correct structure of the bicyclic core and a series of analogues.[221] Many research groups have studied the synthesis of this class of compounds to optimise the reaction conditions and expand the range of substrates available.[222] Reginato *et. al*. further investigated the synthesis, designing a microwave-assisted method for the preparation of symmetrically-substituted the thiazolo[5,4-d]thiazoles. Compounds containing the thiazolo[5,4-d]thiazoles core have been investigated as a result of their potential biological activity and possible inclusion in materials, for example, semiconducting polymer and optical devices. There have been few reports related to the coordination chemistry of these compounds.[223, 224] Steel and co-workers investigated the utilisation of 2,5-di(2-pyridyl)thiazolo[5,4-d]thiazole in the preparation of metal complexes of both copper and ruthenium.[224]

Compound **3.4.5**, containing a thiazolo[5,4-d]thiazole core, was selected as an appropriate alternative bis-bidentate bridging ligand to replace **3.4.1** as it is a coplanar molecule with a rigid, bicyclic core giving rise to an extended π-electron system capable of maintaining conjugation between the two binding sites.

The preparation of the dinuclear iridium(III) complex **3.4.8** was carried out using the same synthetic route as previously described for **3.4.4** as shown in Figure 111.[173] The final bimetallic complex was isolated in a moderate yield (55%) following purification by column chromatography. The identity of **3.4.8** was confirmed by ^{1}H, ^{19}F and ^{13}C NMR spectroscopy and mass spectrometry. The aromatic region of the ^{1}H NMR spectrum of **3.4.8** is shown in Figure 116. The spectrum shows 6 aromatic proton environments; 3 signals corresponding to protons on the pyridyl rings of the terdentate N^C^N ligands and 3 signals corresponding to protons on the aryl rings of the bis-bidentate bridging ligand. Comparable with **3.4.4**, the signal at δ 6.08 ppm can be assigned to the two protons *ortho* to the metallated carbon atoms of the aryl ring of the bis-N^C-coordinating bridging ligand. This is a characteristic signal for our dinuclear iridium(III) complexes.

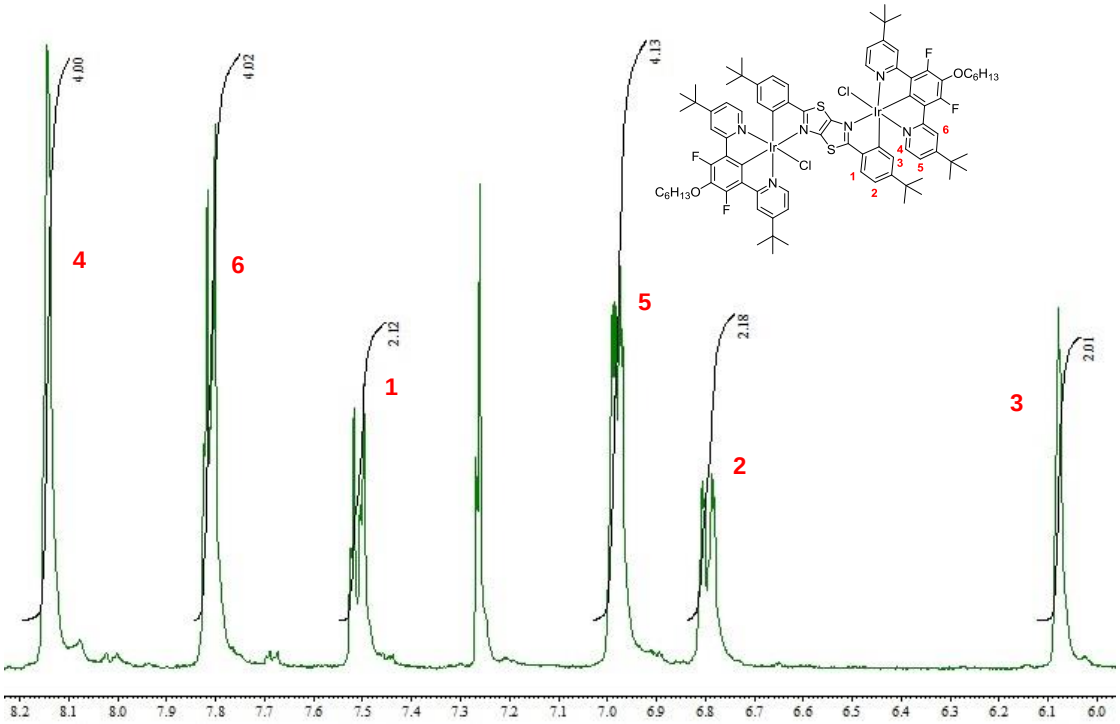

Figure 116: A figure to show the aromatic region of the ^{1}H NMR spectrum of **3.4.8** recorded in $CDCl_3$. The spectrum shows 6 aromatic proton signals; 3 signals corresponding to protons on the pyridyl rings of terdentate N^C^N ligands and 3 corresponding to protons on the aryl rings of the bis-bidentate bridging ligand, **3.4.5**. The signal at δ 6.08 ppm is a characteristic signal for our dinuclear iridium(III) complexes, corresponding to the two protons *ortho* to the metallated carbon atoms of the aryl rings of the bridging ligands.

The stability of the thiazolo[5,4-d]thiazole-linked bimetallic complex, **3.4.8**, was investigated under conditions comparable to those employed in the case of **3.4.4**. A solution of **3.4.8** in $CDCl_3$ was exposed to sunlight and ^{1}H NMR spectra were obtained at time intervals of 0, 10, 60, 120, 180 and 600 minutes. An additional NMR spectrum was recorded after the sample had been exposed to sunlight for 2 weeks. The eight ^{1}H NMR spectra recorded to study the possible degradation of **3.4.8** are shown in Figure 117. This series of NMR spectra show that over the time period studied, there is no photodegradation of the initial sample of this dinuclear complex in chlorinated solvents. Therefore, varying the central heterocyclic core of the bis-N^C-coordinating bridging ligand from a 2,5-disubstituted pyrazine to thiazole[5,4-d]thiazole results in the formation of rigidly-linked dinuclear iridium(III) complex that is much more stable with respect to photodegradation in chlorinated solvents. Further investigation of the degradation mechanism of **3.4.4** may offer further insight into the reasons for the increased stability of **3.4.8**.

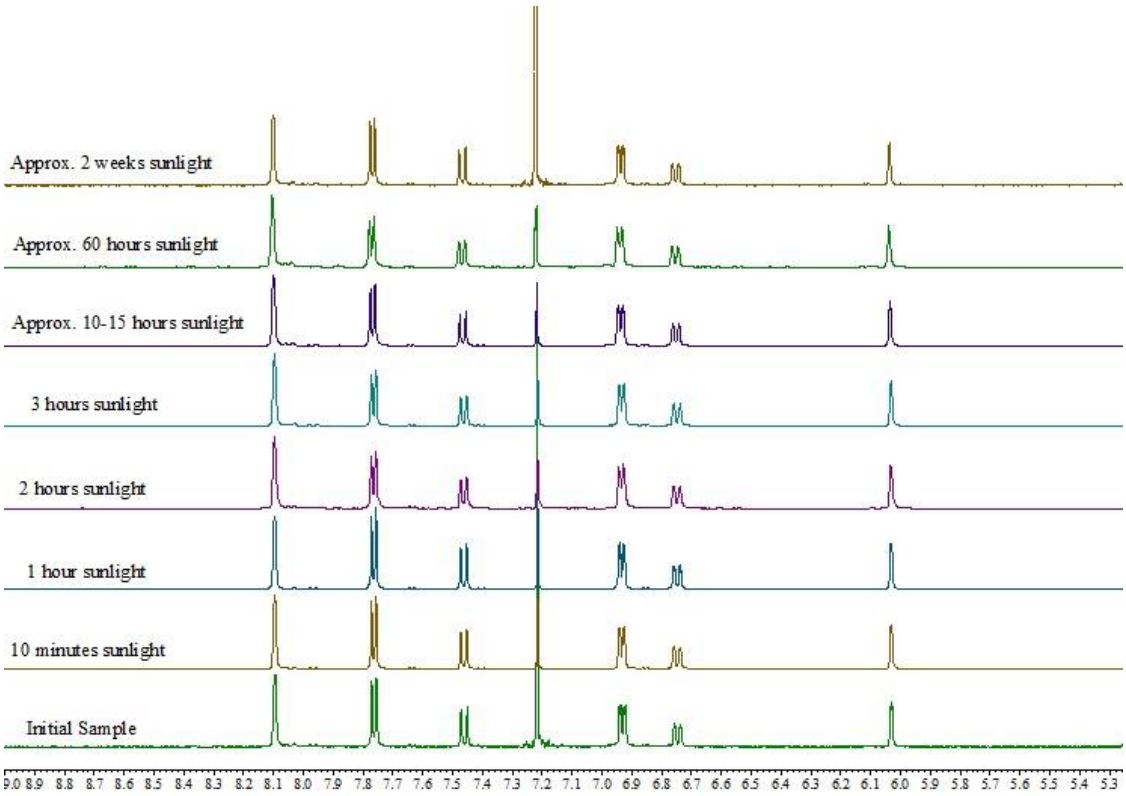

Figure 117: A figure to illustrate the stability of dinuclear iridium(III) complex, **3.4.8** in $CDCl_3$ over a period of approximately 60 h. The NMR spectra were recorded at time intervals of 0 min, 10 min, 1 h, 2 h, 3 h and approximately 10 h, following exposure of the NMR sample to sunlight. An additional NMR spectrum was recorded after the sample had been exposed to sunlight for 2 weeks. The $CDCl_3$ sample of **3.4.8** shows no degradation over this time period.

The photophysical properties of both **3.4.4** and **3.4.8** were measured in order to further investigate the effects of the bridging heterocyclic system on the optical properties.

The UV-visible absorption spectra of **3.4.4** and **3.4.8**, measured in dichloromethane solution at room temperature are shown in Figure 118 with the absorption maxima and molar extinction coefficients being tabulated in Table 7. The UV-visible absorption data for the bis-bidentate bridging ligands are also included. The absorption spectra of both complexes display intense bands in the UV region of the spectrum (< 400 nm) ($\varepsilon \approx 30\text{-}55 \times 10^3$ M^{-1} cm^{-1}) and relatively intense bands in the visible region (> 400 nm) ($\varepsilon \approx 6\text{-}30 \times 10^3$ M^{-1} cm^{-1}). The pyrazine-linked complex, **3.4.4**, has a similar absorption profile to that observed for the related pyrimidine-linked dinuclear iridium(III) complex, **3.3.7** (section 3.3). The molar extinction coefficients for **3.4.4** are also similar to those of the analogous pyrimidine-linked complex. For the thizolo[5,4-d]thiazole-linked complex, **3.4.8**, the spectral profile above ≈ 450 nm is very different to that of **3.4.4**, with two peaks appearing exhibiting molar extinction coefficients much higher than for **3.4.4**.

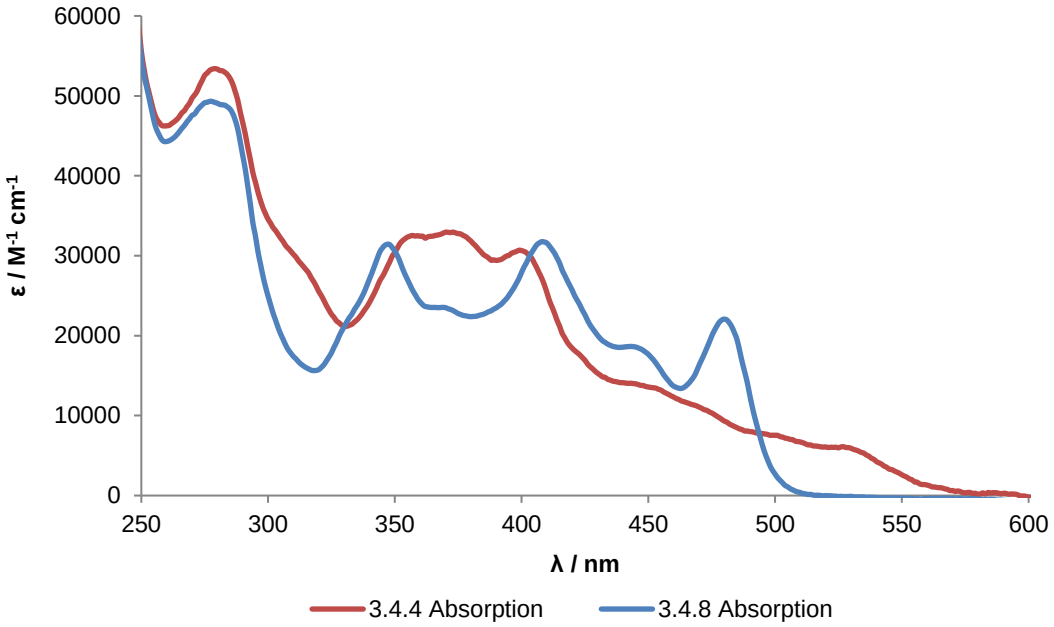

Figure 118: UV-visible absorption spectra recorded for the dinuclear iridium(III) complexes, **3.4.4** (red) and **3.4.8** (blue), in CH_2Cl_2 at room temperature.

Table 7: UV-visible absorption data for the dinuclear Ir(III) complexes, **3.4.4** and **3.4.8**, in CH_2Cl_2 at room temperature.

Complex[a]	**λ_{max} / nm (ε / M^{-1} cm^{-1})**
3.4.1	278 (50000), 291 sh (45000), 335 (31000)
3.4.5	276 (240000), 354 sh (40000), 366 (43000), 382 sh (27000)
3.4.4	281 (53000), 316 sh (28000), 359 (33000), 376 (33000), 400 (31000), 449 (14000), 475 sh (10000), 501 sh (7500), 530 (5900)
3.4.8	279 (49000), 349 (31000), 372 sh (23000), 410 (32000), 448 sh (18000), 482 (22000)

As is shown in the absorption spectra, the lowest energy absorption bands become more blue-shifted on going from **3.4.4** to **3.4.8**. Varying the central heterocycle of the bis-N^C bridging ligand from 2,5-substituted pyrazine to thiazole[5,4-d]thiazole results in a substantial shift of the lowest-energy absorption bands of 1900 cm^{-1}. The higher energy part of the absorption spectrum is largely unaffected upon changing the bridging ligand.

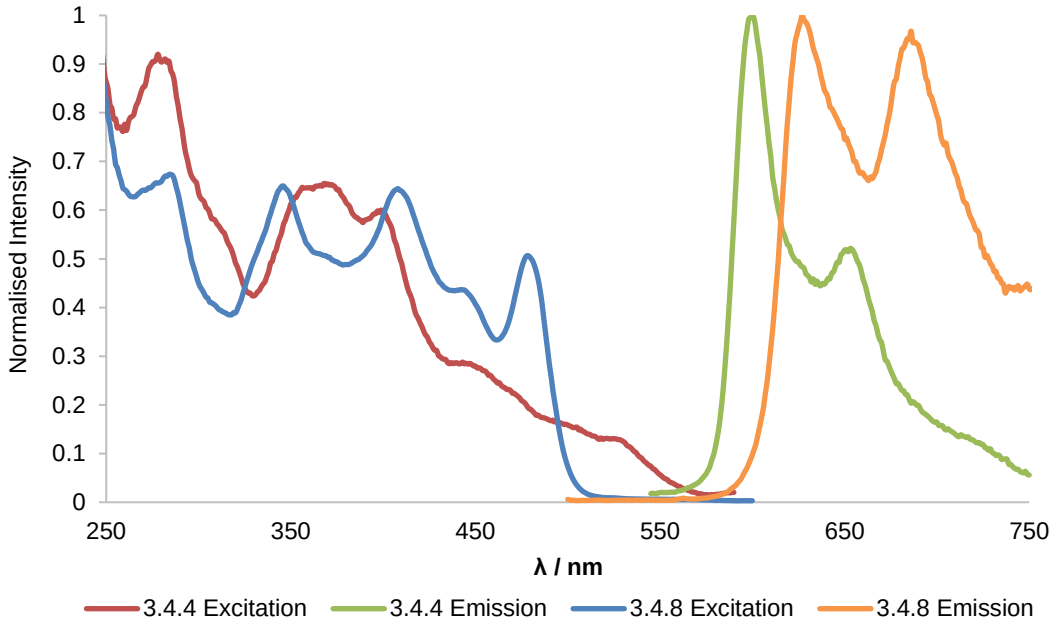

Figure 119: Excitation and emission spectra recorded for **3.4.4** and **3.4.8** in deoxygenated CH_2Cl_2 at room temperature. Emission maxima are observed at 600 and 655 nm for **3.4.4** and at 628 and 686 nm for **3.4.8.**

The excitation and emission spectra of **3.4.4** and **3.4.8** were recorded in deoxygenated CH_2Cl_2 solutions at room temperature and are shown in Figure 119. The excitation spectra recorded for the dinuclear iridium(III) complexes closely resemble the absorption spectra shown in Figure 118. The emission maximum for **3.4.4** is observed at 600 nm with a shoulder at lower energy (655 nm). For **3.4.8**, the emission is red-shifted relative to **3.4.4** with maxima observed at 628 and 686 nm. The tail of the emission spectrum of **3.4.8** extends into the NIR region with the detection of this emission being limited by the instrument used. Further investigation of the photophysical properties of these dinuclear complexes is required in order to assess the luminescence quantum yields and lifetimes.

In summary, we have shown that on variation of the central heterocycle of the bis-bidentate bridging ligand to a 2,5-substituted pyrazine ring, the final dinuclear iridium(III) complex is unstable in chlorinated solvents upon exposure to daylight. More investigation is required in order to understand the origin of the reduced stability and the mechanism of degradation. As a result of the observed degradation, an alternative dinuclear iridium(III) complex was prepared, incorporating a bis-bidentate bridging ligand with a thaizolo[5,4]thiazole core. Using this bis-

bidentate bridging ligand, a more stable dinuclear complex was isolated. The photophysical properties of both the 2,5-substituted pyrazine and the thaizolo[5,4]thiazole based di-iridium(III) complexes were investigated with emission observed in the orange and red regions of the spectrum respectively.

3.5 2,3-Pyrazine-Linked Dinuclear Iridium(III) Complexes

The research into rigidly-linked iridium(III) complexes discussed so far in this work has provided further evidence for the importance of the bridging ligand and the extent of its influence on the chemical and photophysical properties on the final multinuclear complex. The rigid, bis-bidentate bridging ligands incorporated in the bimetallic iridium(III) complexes described so far have been based on 4,6-disubstituted pyrimidines and 2,5-disubstituted pyrazines. Variation of the central heterocycle to a 2,3-disubstituted pyrazine ring was also investigated in order to study the effect this would have on the properties of the corresponding dinuclear iridium(III) complex.

Bridging ligands incorporating 2,3-disubstituted pyrazines, such as 2,3-dipyridylpyrazine (2,3-dpp) have previously been utilised in the synthesis of rigid multinuclear complexes of transition metals such as Ru(II), Os(II) and Pt(II), amongst others.[82, 191, 218, 225-227] The mono-, di-, tri- and tetranuclear ruthenium(II) complexes of the bridging ligand 2,3-dpp, reported by Denti *et. al.* all displayed luminescence, both in fluid solution at room temperature and in a rigid matrix at 77 K, with quantum yields in the range $\phi = 0.041$ to $\phi = 0.001$ and luminescence lifetimes ranging from 60 to 620 μs in degassed solutions at room temperature.[218] In 1990, the cyclometallating analogue of 2,3-dpp, 2,3-diphenylpyrazine, was utilised by Steel and co-workers in the synthesis of a di-palladium complex. Structural analysis using the X-ray crystal structure was carried out but the photophysical properties of this complex were not investigated.[178] In addition, previous work by Kozhevnikov *et. al.* used 2,3-diphenylpyrazine as a cyclometallating bridging ligand in the synthesis of a highly luminescent bimetallic platinum(II) complex. The optical properties of this di-platinum(II) complex were studied and the phosphorescence quantum yield was recorded to be $\phi = 0.37$ in degassed solution at room temperature.[85]

In this section, the investigation of the bis-N^C-coordinating ligand, 2,3-diphenylpyrazine, as a bridging ligand in a rigid, dinuclear iridium(III) complex is described. The incorporation of 2,3-diphenylpyrazine in our bimetallic iridium(III) complexes facilitated further study of the effects of the bridging ligand on the properties of the final multinuclear complex.

Following on from the dinuclear iridium(III) complexes discussed in earlier sections of this work (3.3 and 3.4), a *tert*-butyl-substituted derivative of 2,3-diphenylpyrazine, 2,3-bis(4-*tert*-butylphenyl)pyrazine, was selected to link the iridium(III) centres in our multinuclear complex. The use of this bis-bidentate bridging ligand, bearing identical substituents to those of **3.3.6** and **3.4.1**, allows direct comparison between the corresponding dinuclear complexes and evaluation of the effects of the central heterocycle of the bridging ligand.

Firstly, the bis-bidentate ligand, 2,3-bis(4-*tert*-butylphenyl)pyrazine, was synthesised from the commercially available 4-*tert*-butylbenzaldehyde. As shown in Figure 120, this is converted into the diketone, bis(4-tert-butylphenyl)ethane-1,2-dione, before undergoing a condensation reaction with ethylene diamine. Using this method, the desired bis-N^C-coordinating ligand was isolated in moderate yield (35%).

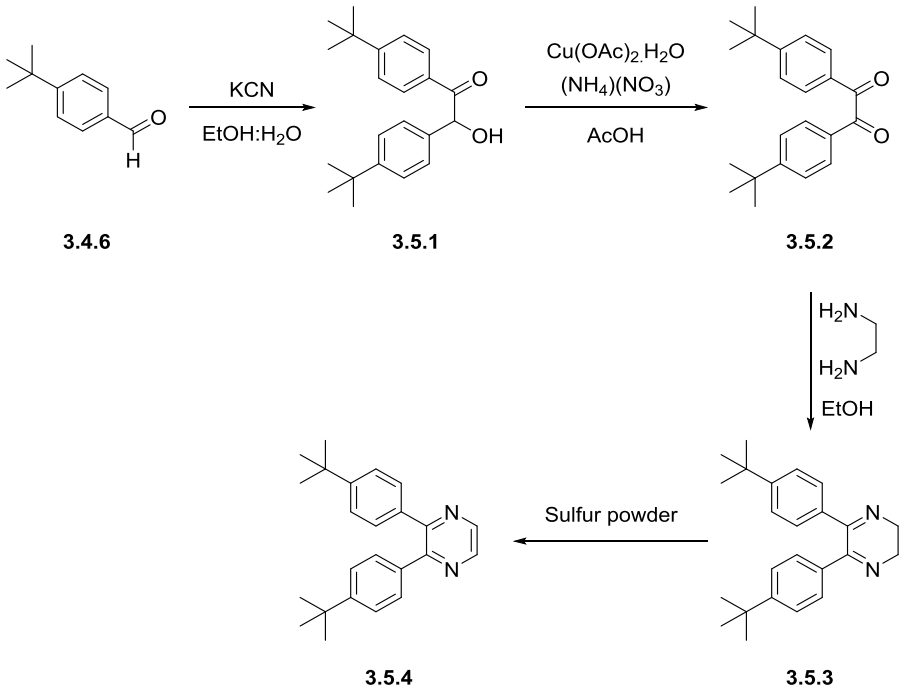

Figure 120: A reaction scheme to show the synthesis of the bis-N^C-coordinating ligand 2,3-bis(4-*tert*-butylphenyl)pyrazine.

To prepare the dinuclear iridium(III) complex, the same synthetic procedure was used as that described previously in sections 3.3 and 3.4 and is as shown in Figure 121.[173] For this complex, the N^C^N-coordinating compound, **3.1.5**, was selected as the auxiliary ligand. This terdentate ligand bears a single *tert*-butyl substituent at the 5-position of the central phenyl ring. This substituent acts to block the competitive bidentate binding of the iridium(III) ion with the terdentate ligand whilst also increasing the solubility of the target dinuclear complex. Following the reaction of the terdentate ligand with $IrCl_3.H_2O$, the resulting iridium dichloro-bridged dimer, **3.2.4** was reacted with the bis-N^C-coordinating ligand **3.5.4**. This reaction was carried out in refluxing toluene and in the presence of silver triflate as a chloride scavenger. The final dinuclear complex, **3.5.5**, was isolated in a low yield (11%) following purification by column chromatography.

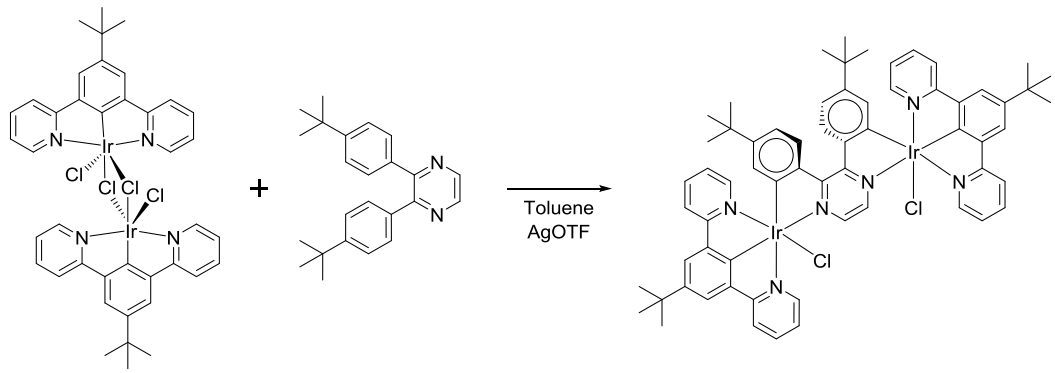

Figure 121: Reaction scheme to illustrate the synthesis of **3.5.5**, in which the two iridium(III) centres are linked by the bis-N^C-coordinating bridging ligand 2,3-bis(4-*tert*-butylphenyl)pyrazine.

The dinuclear iridium(III) complex linked by 2,3-bis(4-*tert*-butylphenyl)pyrazine was fully characterised by ^{1}H and ^{13}C NMR spectroscopy and mass spectrometry. Figure 122 shows the aromatic region of the ^{1}H NMR spectrum of **3.5.5** recorded in d^6-DMSO at room temperature.

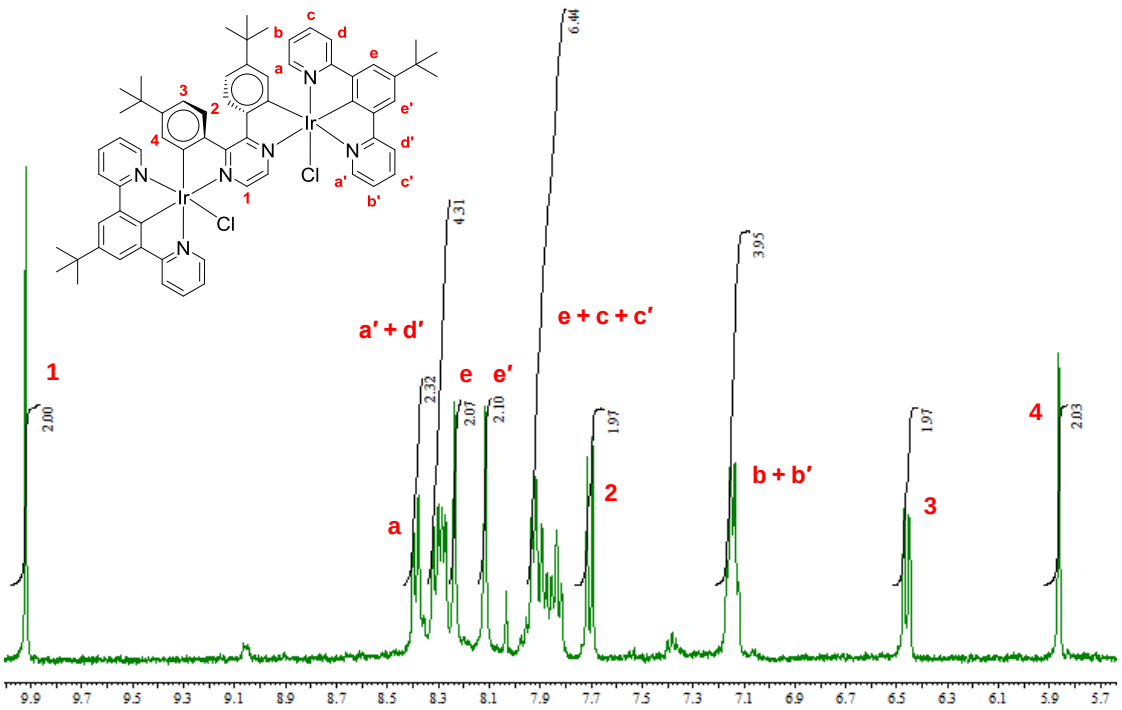

Figure 122: The aromatic region of the ^{1}H NMR spectrum of **3.5.5** recorded in d^{6}-DMSO. This NMR spectrum shows the same characteristic signals as expected for our dinuclear iridium(III) complexes; the singlet at δ 9.92 ppm corresponding to the two protons on the 2,3-substituted pyrazine ring and the peak at δ 5.87 ppm corresponding to the two protons *ortho* to the metallated carbon atoms of the bridging ligand. The NMR spectrum of this dinuclear iridium(III) complex linked by 2,3-bis(4-*tert*-butylphenyl)pyrazine also shows evidence of twisting within structure of the bimetallic complex.

This ^{1}H NMR spectrum shows the same characteristic signals as discussed previously this type of di-iridium(III) complex. The singlet at δ 9.92 ppm corresponds to the two protons on the 2,3-disubstituted pyrazine ring and the peak at δ 5.87 ppm corresponds to the two protons *ortho* to the metallated carbons of the bis-bidentate bridging ligand. The NMR spectrum of **3.5.5** also exhibits evidence of twisting in the structure of the dinuclear complex, about the bis-bidentate bridging ligand. This is shown by the presence of two sets of signals corresponding to the terdentate N^C^N auxiliary ligands.

Twisting about the bridging ligand 2,3-diphenylpyrazine was also observed in the dipalladium(II) complex reported by Steel *et. al*. The X-ray crystal structure of this complex and a representation of the twist observed is shown in Figure 123. With two Pd(II) centres bound to the 2,3-diphenylpyrazine bridging ligand, both metallated phenyl rings are constrained to be approximately coplanar with the pyrazine ring. This leads to a large steric interaction between the two protons on carbons C16A and C16B (Figure 123) and as a result the metallated phenyl rings

of the bis-N^C-coordinating bridging ligand twist in an attempt to relieve the steric strain. In the dinuclear palladium(II) complex shown in Figure 123, the twisting results in an angle of 19.6(5) ° between the planes of the two metallated phenyl ring and a C11A-C1A-C1B-C11B torsion angle of 18.0(1) °.[178]

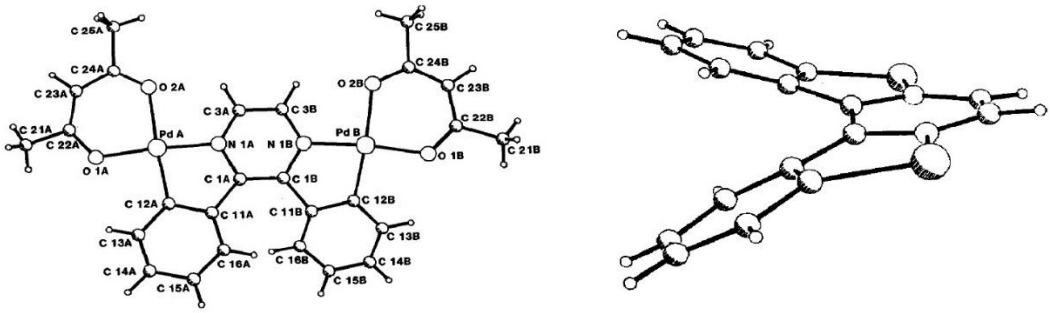

Figure 123: A figure to show the X-ray crystal structure of the 2,3-diphenylpyrazine-linked dinuclear palladium(II) complex reported by Steel and co-workers. Also shown is the view of this complex with the two cyclometallated rings twisted. In this view, the acac ligands have been omitted for clarity.[178]

The twist of the 2,3-bis(4-*tert*-butylphenyl)pyrazine bridging ligand results in the final dinuclear iridium(III) complex being a chiral molecule and therefore, leads to the formation of this complex in a racemic mixture of two enantiomers. In order to further investigate the properties of these enantiomers and attempt separation, a sample of **3.5.5** was sent to Durham University for analysis by chiral HPLC in the group of Professor J. A. Gareth Williams and the results will be described in due course.

In addition, properties of the twist in our dinuclear iridium(III) complex **3.5.5** were studied by a variable temperature NMR experiment, as previously carried out for octahedral platinum(IV) complexes.[228] The ^{1}H NMR spectrum of **3.5.5** was recorded at intervals of 5 °C across a temperature range of 25-90 °C. As is shown in Figure 124, at 25 °C the ^{1}H NMR of **3.5.5** shows two sets of signals corresponding to the terdentate N^C^N ligands as a result of the twist in the structure. As the temperature is increased, the NMR signals corresponding to the N^C^N-coordinating ligands coalesce. Coalescence of these signals occurs at approximately 50 °C whilst the NMR signals assigned to the bis-N^C bridging ligand remain well-resolved. Increasing the temperature further, to 80 °C, leads to the formation of well-resolved proton signals which

correspond to the terdentate N^C^N ligands. The NMR spectrum of **3.5.5** was measured up to 100 °C with the new signals remaining stable at this temperature.

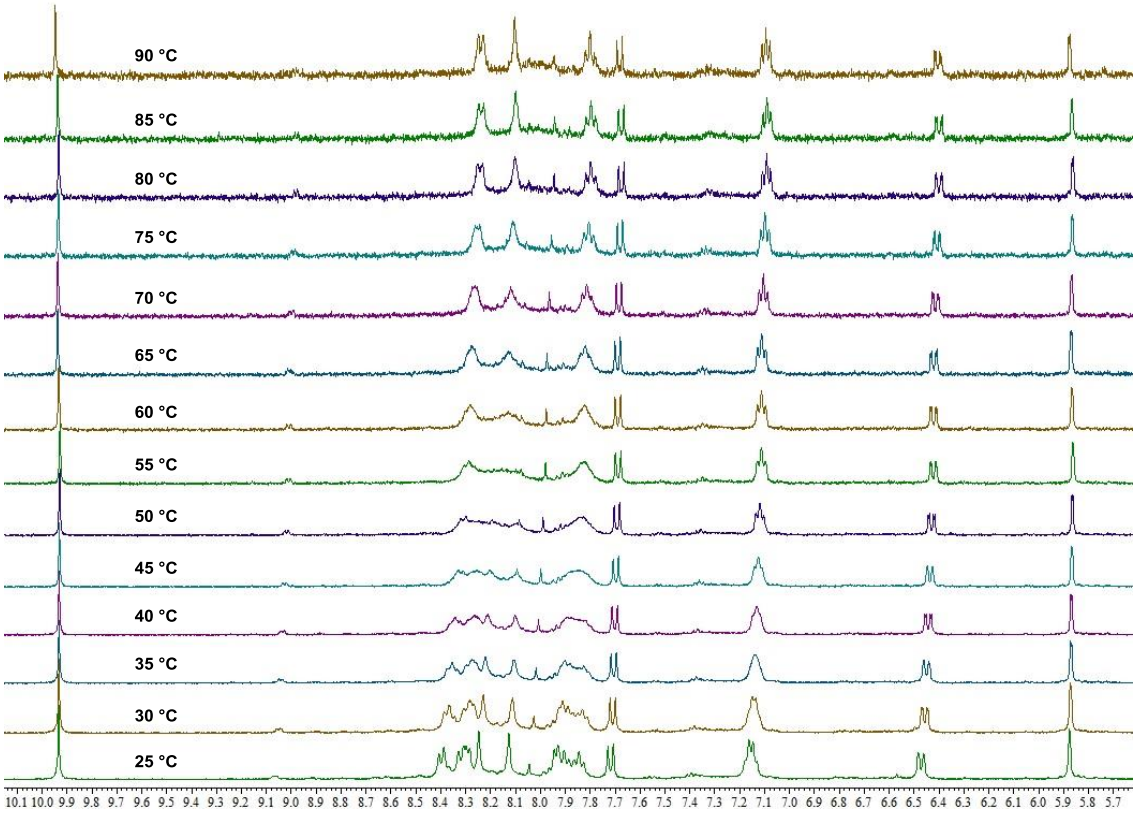

Figure 124: A figure show the change in the ^{1}H NMR spectrum of **3.5.5** with varying temperature in the range of 25 °C to 90 °C. The NMR spectrum was recorded at temperature intervals of 5 °C.

To investigate the effect that the linking of the two metallated phenyl rings of the bis-N^C-coordinating bridging ligand has on the twist observed within our 2,3-pyrazine-linked complex, we prepared a dinuclear iridium(III) complex in which the two metal centres are linked via the bis-bidentate bridging ligand, **3.5.6**, shown in Figure 125. The use of this bridging ligand, 1,4-diazatriphenylene, was previously used in the preparation of dipalladium(II) complexes by Steel and co-workers.[178]

The preparation of the bis-N^C-coordinating bridging ligand **3.5.6** was carried out using a condensation reaction under the same conditions as that used in the synthesis of **3.5.4**. The commercially available diketone, 9,10-phenanthrenequinone, was reacted with ethylene diamine

in refluxing ethanol. The desired compound was isolated in moderate yield (36%) without the need for oxidation using sulfur powder. The reaction scheme for this synthesis is shown in Figure 125.

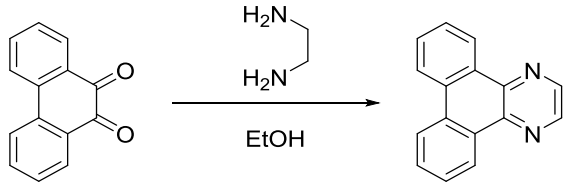

3.5.7 **3.5.6**

Figure 125: A reaction scheme to show the preparation of compound via the condensation reaction of 9,10-phenanthrenequione and ethylene diamine. The target compound was isolated as an off-white solid in a moderate yield of 36%.

Of the 2,3-substituted pyrazine bridging ligands prepared in this work, compound **3.5.6** is the only one not to bear a *tert*-butyl substituent. The preparation of the analogous *tert*-butyl-substituted ligand was attempted via oxidative aryl-aryl coupling reactions of bis(4-tert-butylphenyl)ethane-1,2-dione and 2,3-bis(4-tert-butylphenyl)pyrazine, using VOF_3 in the presence of boron trifluororide diethyl ether, as shown in Figure 126. These reactions were unsuccessful and did not yield the desired product.

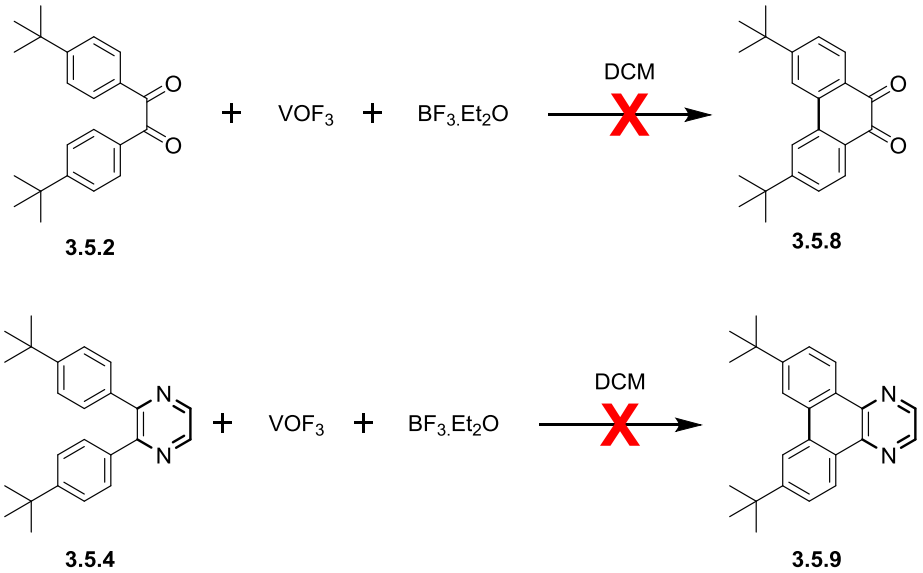

3.5.2 **3.5.8**

3.5.4 **3.5.9**

Figure 126: Reaction schemes to show the synthetic routes attempted to prepare a 1,4-diazatriphenylene-based bis-bidentate ligand bearing *tert*-butyl groups at the 4-positions of the phenyl rings.

The bis-N^C-coordinating bridging ligand, **3.5.6**, was utilised in the preparation of a dinuclear iridium(III) complex as shown in Figure 127. Using the same synthetic procedure as used in the preparation of **3.5.5**, the diiridium(III) complex **3.5.10** was synthesised. The target complex was isolated in a low yield (17%) following purification via column chromatography.

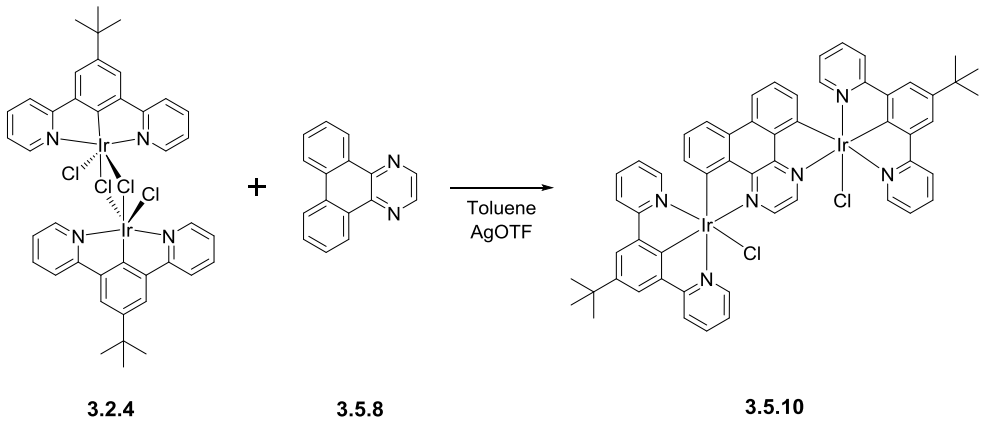

Figure 127: Figure to show the synthetic route used in the synthesis of the dinuclear iridium(III) complex, **3.5.10**.

The final dinuclear iridium(III) complex, **3.5.10**, was fully characterised by ^{1}H and ^{13}C NMR spectroscopy and mass spectrometry. Figure 128 shows the aromatic region of the ^{1}H NMR spectrum of **3.5.10** recorded in $CDCl_3$. This spectrum shows the same characteristic peaks as discussed for the ^{1}H NMR spectra of dinuclear iridium(III) complexes previously shown in this work. The singlet at δ 10.5 ppm corresponds to the two protons on the 2,3-substituted pyrazine ring and the doublet at δ 6.25 ppm corresponds to the two protons *ortho* to the metallated carbon atoms of the bridging ligand. In comparison with the proton spectrum of **3.5.5**, the ^{1}H NMR spectrum of **3.5.10** shows only one set of signals for both the terdentate N^C^N-coordinating ligand and the bis-N^C-coordinating bridging ligand. Therefore, this proton NMR shows no evidence of twisting within the structure of **3.5.10**.

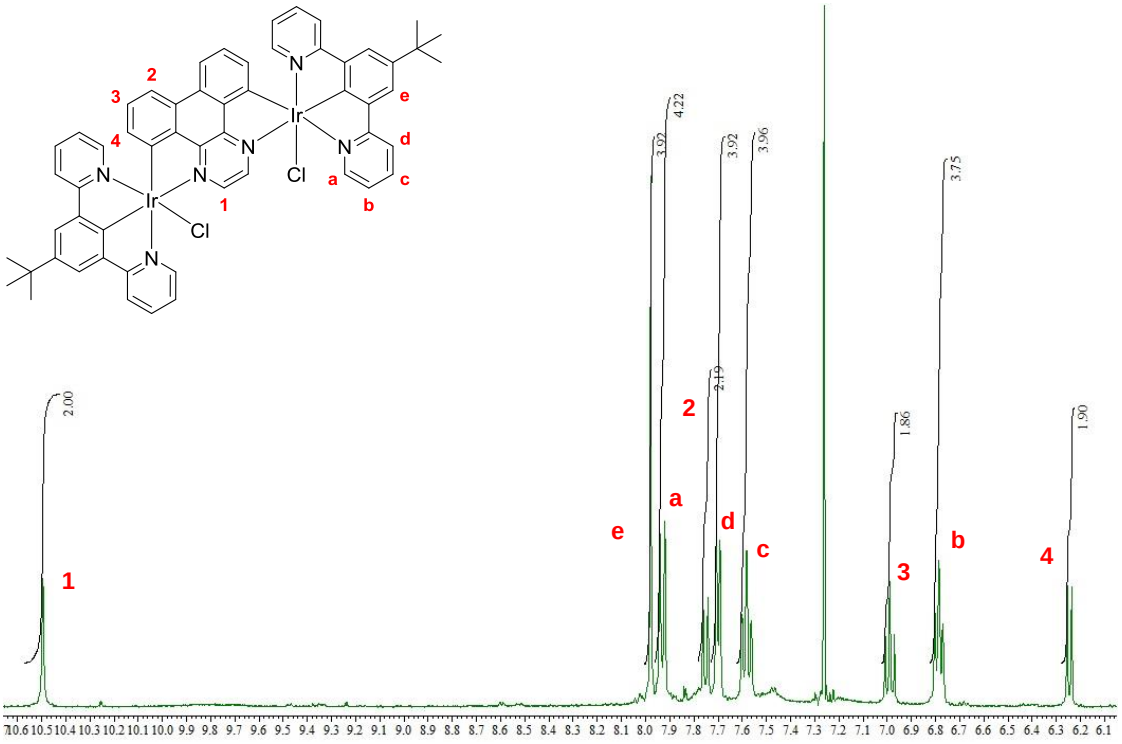

Figure 128: The aromatic region of the ^{1}H NMR spectrum of dinuclear iridium(III) complex, **3.5.10** recorded in $CDCl_3$. This NMR spectrum shows characteristic signals of a dinuclear iridium(III) complexes. The singlet at δ 10.5 ppm corresponds to the two protons on the 2,3-substituted pyrazine ring and the doublet at δ 6.25 ppm corresponds to the two protons *ortho* to the metallated carbon atoms of the bridging ligand. The NMR spectrum of this dinuclear iridium(III) complex linked by 1,4-diazatriphenylene shows no evidence for twisting of the bridging ligand.

In summary, dinuclear iridium(III) complexes linked via 2,3-pyrazine-based bis-bidentate bridging ligands have been successfully prepared and were observed to show better photostability than the related 2,5-isomers. The complex **3.5.5** has twisted geometry at room temperature and this has the potential for the preparation of an optically pure complex. However, the energy barrier for the twisted geometry can be overcome thermally. On linking the two phenyl rings of the 2,3-substituted pyrazine ring, the bis-bidentate bridging ligand forces a planar geometry and the twist is no longer observed. Further study of these complexes is required in order to investigate the photophysical properties of these 2,3-pyrazine-linked dinuclear iridium(III) complexes.

3.6 3,6-Pyridazine-Linked Dinuclear Iridium(III) Complexes

The final class of rigid bis-N^C-coordinating ligand investigated for incorporation into our dinuclear iridium(III) complexes was those in which the central heterocycle was a pyridazine ring. Pyridazines have previously been incorporated into cyclometallating ligands utilised in the

preparation of both monometallic and bimetallic iridium(III) complexes.[83, 130, 229-231] Rourke *et. al.* reported the preparation of dinuclear homometallic complexes of palladium(II) and platinum(II) in which the two metal centres were linked via a 3,6-bis[4-(alkoxy)phenyl]pyridazine bridging ligand. In the reaction between the pyridazine-based bridging ligand and potassium tetrachloroplatinate, the bimetallic complex was the only product formed. Analysis of the dimetallated species formed using ^{1}H NMR data, mass spectrometry and elemental analysis showed that the complex was composed of two platinums, three chlorides and one potassium atom per pyridazine unit. Further reaction of this cycloplatinated species with triphenylphosphine gives the final diplatinum(II) complex, as shown in Figure 129. Both these dinuclear complexes contain a chloride bridge between the two platinum(II) centres. Rourke and co-workers suggested that the formation of this chloride bridge, in conjunction with the nitrogen coordination, is the driving force of the second cyclometallation.[176, 177]

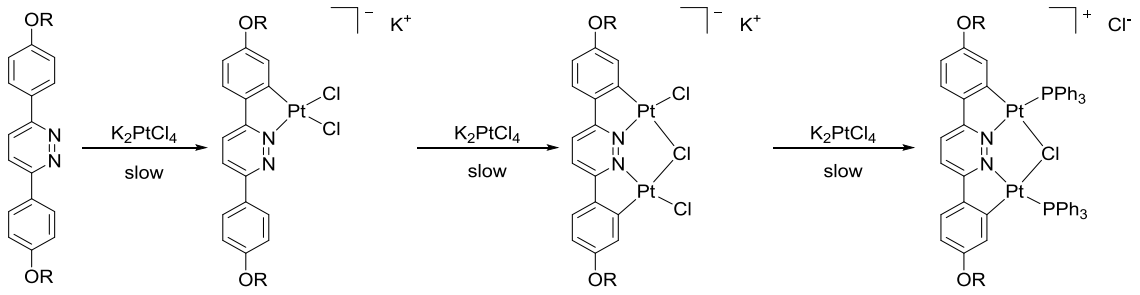

Figure 129: A reaction scheme to show the diplatinum(II) complex reported by Rourke *et. al.* in which the two metal centres are linked by both a bis-N^C-coordinating bridging ligand based on a 3,6-disubstituted pyridazine ring and a chloride bridge.

It was observed, from preliminary work within our research group, that the use of a bis-N^C-coordinating bridging ligand based on a 3,6-disubstituted pyridazine ring to link two iridium(III) centres resulted in the formation of a chloride bridge between the Ir(III) centres. This is consistent with that observed by Rourke *et. al.* as mentioned above. The sharing of a chloride by the two metal centres results in the final dinuclear complex being cationic. The ionic nature of the final complex leads to increased solubility in water which is advantageous for applications such as bio-imaging.

In comparison with traditional bio-imaging and photodynamic therapy (PDT) agents, transition metal complexes combine longer emission lifetimes and higher photostabilities with the relative ease of chemical modification.[232] During imaging, longer emission lifetimes permit the use of time-gating to reduce auto-fluorescence and can be utilised to detect biologically relevant analytes, for example, O_2 *in vitro* and *in vivo*.[232-234] For PDT applications, long emission lifetimes lead to high yields of $^1O_2$ and other reactive oxygen species, and thus efficient photo-induced cell death. Increased photostability favours longer term tracking during bioimaging and increases photosensitising activity of an agent during PDT.[146, 235]

In the field of transition metal complexes for use in bioimaging, ruthenium, rhenium and platinum complexes dominated the early literature. However, in the last decade iridium complexes with higher quantum yields and localisations to a wide variety of sub-cellular organelles have seen a surge in popularity.[109, 145, 147, 151, 236, 237] In PDT, ruthenium(II) complexes have dominated the field of transition metal photosensitisers with one Ru(II) complex having entered clinical trials in Canada.[238-244] In comparison, iridium complexes are yet to be fully explored with regard to PDT applications. Importantly, a few iridium(III) complexes have been recently shown to have phototoxicities with low light doses under both one- and two-photon excitation, suggesting that Ir(III) complexes hold future potential for PDT.[245-256]

As has been shown in the previous sections of this work, bimetallic complexes of transition metals such as Pt(II) and Ir(III) offer several advantages over monometallic analogues. These beneficial properties include red-shifted absorption and emission which would minimise the observed background autoluminescence. In addition, the increased molar extinction coefficient of the low-energy bands and high quantum yields leads to the high brightness of these complexes, making them good imaging agents. The red-shift is also advantageous for PDT as it allows a metal complex to be excited by and emit at wavelengths of light longer than those required for good tissue penetration (> 650 nm).

Dinuclear iridium(III) complexes formed from ditopic bis-N^C ligands in conjunction with symmetrically substituted terminal N^C^N ligands, as discussed in this chapter, show the highest quantum yields and are facile to synthesise with only one dinuclear product formed. The bimetallic Ir(III) complexes discussed so far in this work have all been designed for application in organic light-emitting diodes, however, there is huge potential for their utilisation in alternative applications such as bioimaging.

Motivated by the potential for the utilisation of iridium(III) complexes in bioimaging and PDT applications, the advantages that our dinuclear iridium(III) complexes offer and drawing from reports of pyridazine-linked multinuclear complexes published by Rourke and co-workers, we designed a dinuclear iridium(III) complex in which the two metal centres were linked via a rigid bis-N^C-coordinating bridging ligand based on 3,6-diphenylpyridazine.

In the preparation of our pyridazine-linked dinuclear iridium(III) complex, the first step was synthesis the bis-N^C-coordinating bridging ligand. Figure 130 shows the synthetic route utilised in the synthesis of the pyridazine-based bridging ligand, **3.6.5**. Using Suzuki-Miyaura cross-coupling methodology, 3,6-dichloropyridazine and 4-*tert*-butylphenylboronic acid were reacted together in 1,4-dioxane in the presence of 2M aqueous potassium carbonate and the palladium catalyst, $Pd(PPh_3)_4$. A similar synthetic route for the preparation of (**3.6.5**) was reported by Wang and co-workers.[257] The desired bis-bidentate bridging ligand was isolated in good yield (62%) following recrystallisation from dimethylformamide (DMF). Again, *tert*-butyl substituents were incorporated at the 4-postion of the phenyl rings of **3.6.5** in order to increase the solubility of the corresponding dinuclear complex. Addition of these *tert*-butyl groups also allows direct comparison of the dinuclear iridium(III) complexes of bis-N^C-coordinating bridging ligands, **3.3.6**, **3.4.1** and **3.5.4**.

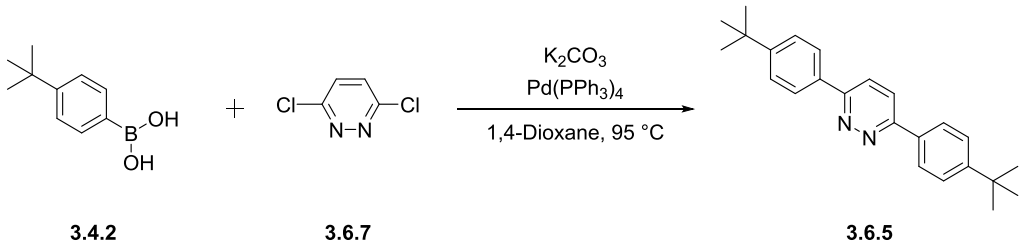

3.4.2 **3.6.7** **3.6.5**

Figure 130: A reaction scheme to show the synthesis of compound **3.6.5** via a Suzuki-Miyaura cross-coupling reaction.

Preparation of the corresponding dinuclear iridium(III) complex of **3.6.5** was carried out using the synthetic procedure shown in Figure 131 and adapted from that previously shown in earlier sections of this chapter.

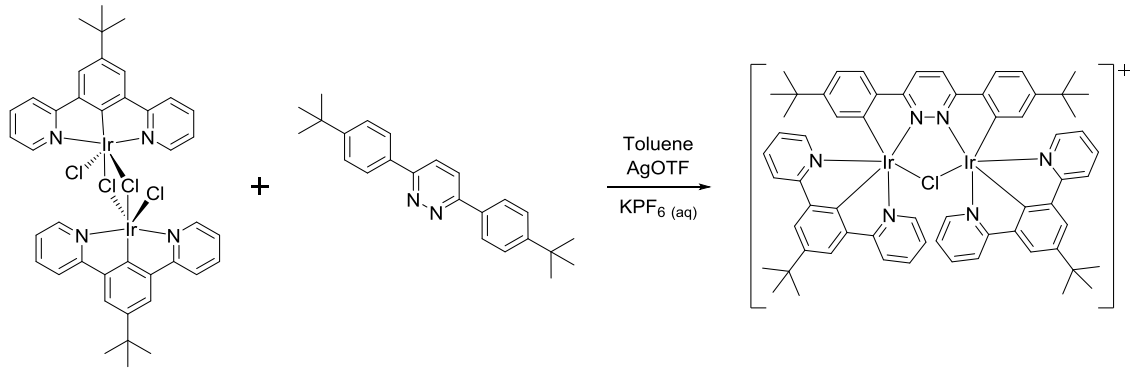

3.2.4 **3.6.5** **3.6.8**

Figure 131: Reaction scheme to show the synthesis of the cationic dinuclear iridium(III) complex, **3.6.8**, in which the two Ir(III) centres are linked via the bis-bidentate bridging ligand 3,6-(bis(4-*tert*-butylphenyl)pyridazine.

Firstly, the terdentate N^C^N- coordinating ligand, **3.1.5** was reacted with $IrCl_3 \cdot H_2O$ at reflux in a mixture of 2-ethoxyethanol and water to give the dichloro-bridged iridium(III) dimer, **3.2.4**. This dimer was then reacted with the bis-N^C-coordinating proligand, **3.6.5**, in toluene, using silver triflate as a chloride scavenger. At completion of the reaction, the mixture was treated with excess HCl (3M, aq.) in order to ensure that chloride was the only monodentate ligand present. Following this, a PF_6^- exchange was carried out using a saturated solution of KPF_6(aq). Purification was carried out using column chromatography to give the target dinuclear complex in 38% yield.

The dinuclear complex **3.6.8** was fully characterised by ^{1}H and ^{13}C NMR spectroscopy and high-resolution mass spectrometry. The aromatic region of the ^{1}H NMR spectrum is shown below in Figure 132. As with the dinuclear iridium(III) complexes previously discussed, this NMR spectrum shows characteristic signals of the target complex. The singlet at δ 8.72 ppm corresponds to the two protons on the pyridazine ring and the doublet at δ 6.00 ppm corresponds to the two protons *ortho* to the metallated carbon atoms of the bis-bidentate bridging ligand.

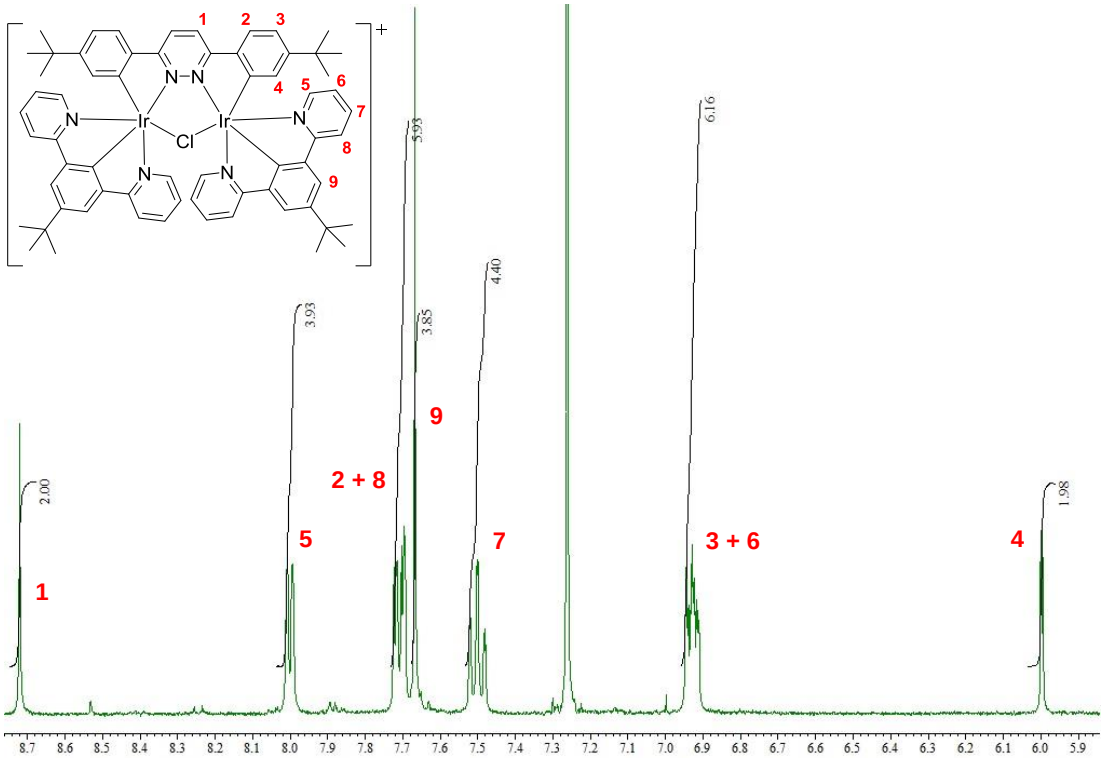

Figure 132: The aromatic region of the ^{1}H NMR spectrum of **3.6.8** recorded in $CDCl_3$. This NMR spectrum shows the same characteristic signals as expected for our dinuclear iridium(III) complexes; the singlet at δ 8.72 ppm corresponding to the two protons on the 3,6-substituted pyridazine ring and the peak at δ 6.00 ppm corresponding to the two protons *ortho* to the metallated carbon atoms of the bridging ligand.

As observed by Rourke *et. al.*, we observe the presence of a chloride bridge between the two iridium(III) centres in **3.6.8**. This is also consistent with preliminary work carried out within our research group. It is thought that the close proximity of the Ir atoms, following coordination to the pyridazine ring, causes the Cl atom to act as a bridging ligand. As a result, five-membered chelate rings form, providing the driving force for the reaction and leading to a rigid architecture. As a consequence of the chloride bridge, the final product is ionic in nature, bearing a PF_6^-

counterion. To confirm the presence of the chloride bridge in **3.6.8**, a ^{19}F NMR spectrum was obtained. This NMR spectrum showed a peak at δ -71.8 ppm corresponding to the PF_6^- counterion to **3.6.8**. High-resolution mass spectrometry was utilised to confirm the identity of the cation. The spectrum obtained is shown in Figure 133. The peak observed at m/z 1337.4144 corresponds to the molecular ion $[M]^+$ (calc'd m/z 1337.4129) and the peak at m/z 823.3359 corresponds to $[M-(Ir(NCN))-Cl]^+$ (calc'd m/z 823.0780). The observed data experimentally matches closely with the theoretical data and confirms the identity of the **3.6.8** as shown in Figure 131.

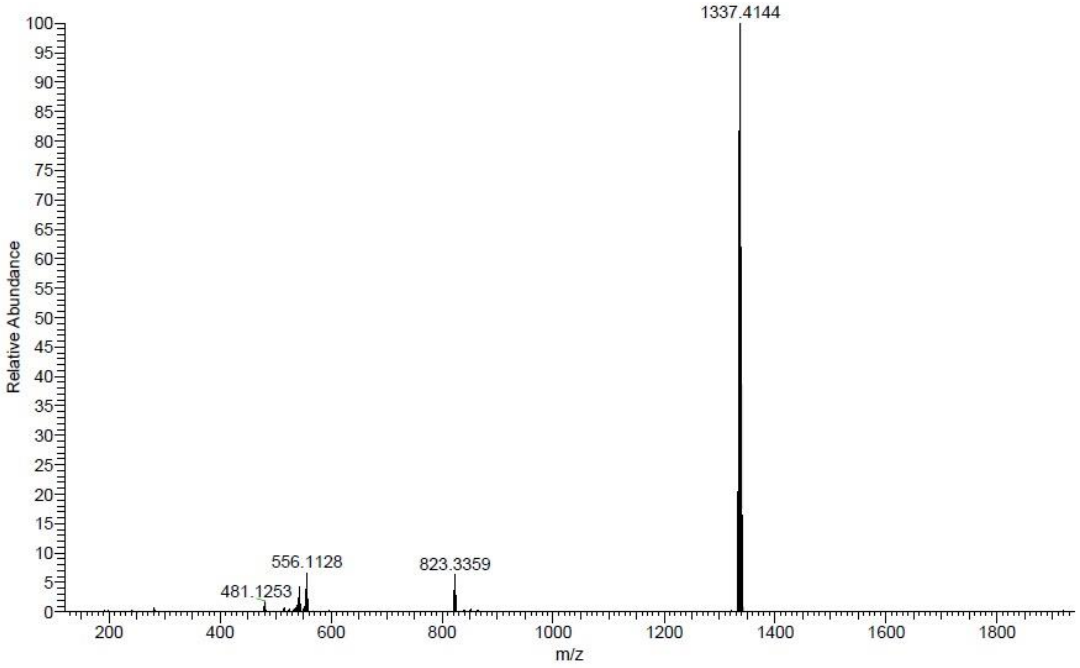

Figure 133: High resolution mass spectrum obtained for **3.6.8**, showing a peak for the molecular ion $[M]^+$ at m/z 1337.4144 (calc'd m/z 1337.4129) and a peak for $[M-(Ir(NCN))-Cl]^+$ at m/z 823.3359 (calc'd m/z 823.0780).

The photophysical properties of the pyridazine-linked dinuclear iridium(III) complex, **3.6.8** were investigated and the UV-visible absorption and emission spectra recorded at the University of Sheffield. Figure 134 shows the absorption and emission spectra recorded with the related data tabulated in Table 8. In acetonitrile solution, **3.6.8** shows broad UV excitation with appreciable absorption up to ~500 nm. Upon excitation (λ_{ex} = 400 nm) **3.6.8** shows broad emission (λ_{em} = ~520 – 720 nm). A luminescence lifetime of 1.892 μs was measured in degassed acetonitrile. A quantum yield of $\phi = 0.5 \pm 0.11$ was measured for the complex in degassed acetonitrile solution. The quantum yield measured in aerated acetonitrile solution is far lower in comparison ($\phi = 0.05$)

indicating significant quenching. The singlet oxygen yield, Φ_{Δ}, was determined to be 45% when measured in direct detection with UV excitation (λ_{ex} = 355 nm). The singlet oxygen yield clearly shows the potential for this class of compounds to be utilised as therapeutic agents as shown in Figure 135.

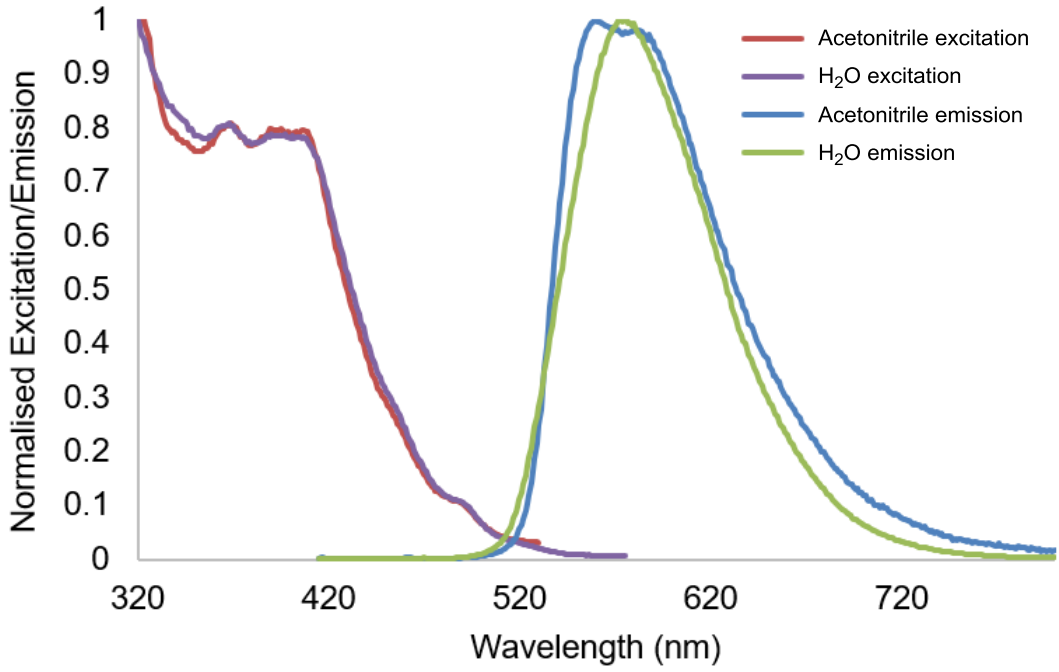

Figure 134: Normalised UV-visible absorption and emission spectra of **3.6.8** measured in both acetonitrile and H_2O solution at ambient temperature in air-equilibrated solvent.

Table 8: Summary of the photophysical data recorded for **3.6.8**. (a) Acetonitrile (b) λ_{ex} = 400 nm (c) τ_0 = degassed acetonitrile, τ_1 = acetonitrile, τ_2 = water from DMSO stock (d) Φ_0 = degassed, Φ_1 = aerated $[Ru(Bipy)_3]PF_6$ standard (e) λ_{ex} = 355 nm, perinapthenone standard.

Complex	**λ_{max} abs. / nm (ε / dm^3 mol^{-1} cm^{-1})[a]**	**λ_{max} em. / nm (ε / dm^3 mol^{-1} cm^{-1})[a, b]**	**τ_0, τ_1, τ_2 / ns[a, c]**	**Φ_0, Φ_1 / %[a, b, d]**	**Φ_{Δ} / %[a, e]**
3.6.8	235 (79,900) 284 (54,700) 397 (24,200)	576	1890, 226, 561/103	52, 5	45

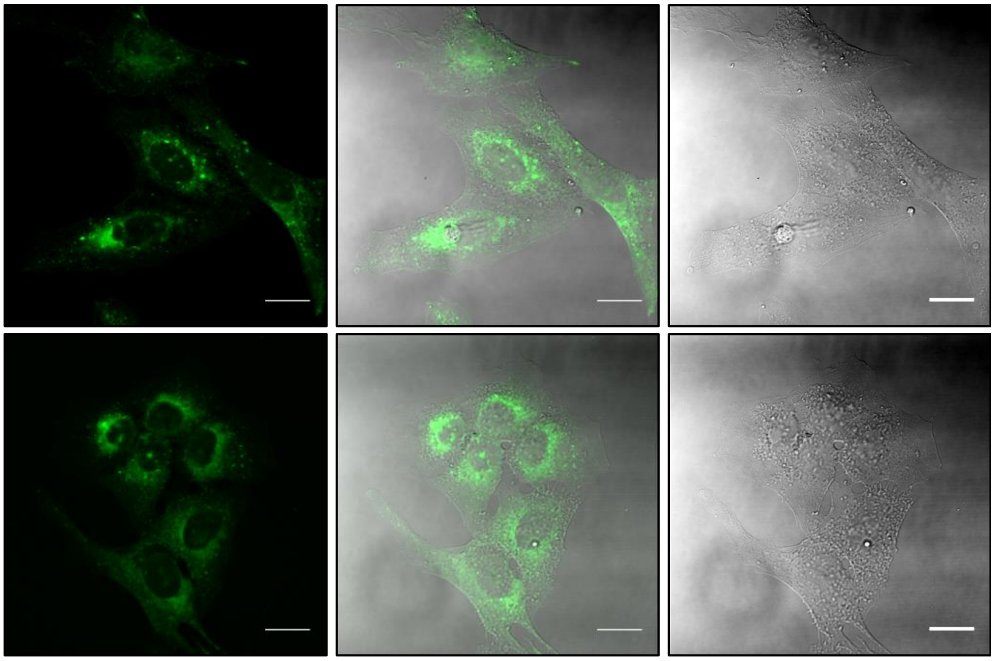

Figure 135: Multiphoton images of **3.6.8** in U2OS cells, 20 μM, 5 hours, emission (left), brightfield (right) and overlay (centre). Excitation at 800 nm and emission at 565-615 nm (green LUT chosen for clarity). Scale bars = 20 μm.

The cellular uptake and toxicity of **3.6.8** was then investigated. The pyridazine-linked dinuclear complex is moderately soluble in water, however, DMSO was used to assist with solubility. Using multiphoton excitation microscopy (λ_{ex} = 800 nm), **3.6.8** was observed to enter cells and localise in the cyctoplasm with distinct punctate staining. This is consistent with previously reported cationic metal complexes which are known to locate in mitochondrial and lysosomal or endosomal structures.[252] Co-localisation of **3.6.8** with mitochondria was confirmed using organelle-specific stains and confocal microscopy (λ_{ex} = 405 nm) as shown in Figure 136, giving a Pearson's correlation coefficient of R = 0.76 (averaged over 15 cells) for Mitotracker red. Co-localisation of **3.6.8** with Lysotracker red was not observed (Figure 136) indicating that the punctate staining may result from other endosomal structures (Pearson's correlation coefficient of R = 0.53 with Lysotracker red (averaged over 15 cells).

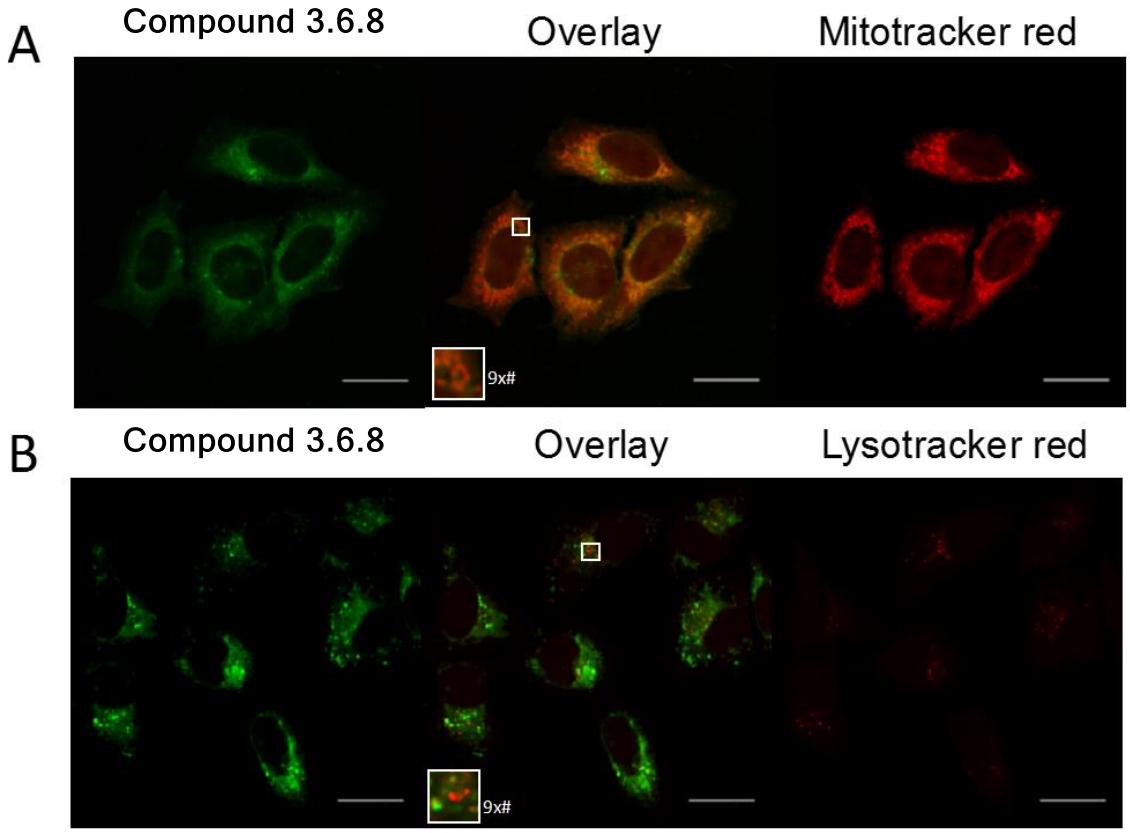

Figure 136: Sub-cellular localisation of **3.6.8**. HeLa cells following a 5 hour incubation with **3.6.8** (green), colocalised with (A) Mitotracker red (red) or (B) Lysotracker red (red). Zoomed sections (x9) are shown as insets. Scale bars = 20 μm.

Following a short incubation time of 5 hours, **3.6.8** induced a significant dose-dependent reduction in metabolic activity/cell viability in both U2OS and HeLa cancer cell lines as indicated by MTT assay. The toxicity of the associated ligands was also measured. The terdentate N^C^N-coordinating ligand, **3.1.5**, did not reduce cell viability whilst the bis-N^C-coordinating bridging ligand, **3.6.5**, induced a similar reduction in metabolic activity as **3.6.8** (Figure 137).

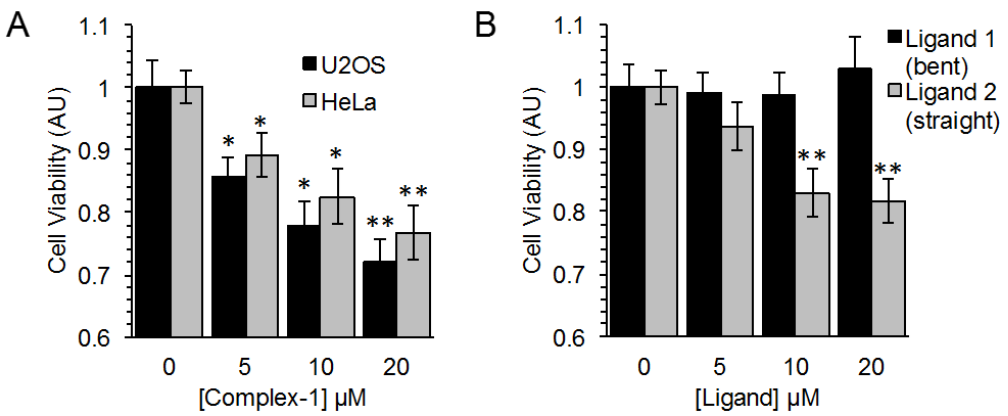

Figure 137: 3.6.8 and **3.6.5** induce a significant reduction in cell viability. Cell viability as measured by MTT assay after a 5 hour incubation with A. **3.6.8** and B. Ligands as indicated. Mean and SEM of 4 independent repeats is shown. Significance calculated by Student's T-test compared to respective untreated control is indicated, where * = $p < 0.05$ and ** = $p < 0.01$.

The MTT assay measures the metabolic activity of a cell, and therefore can be considered a read out of cell viability. Despite this it is not a measure of long term survival. A clonogenic survival assay was used in order to get a more accurate assessment of the cellular toxicity. In this assay, the cells were plated in a low density prior to a 5 hour incubation with **3.6.8** or the corresponding ligands. Subsequently the cells were left to recover and form colonies for 10 days. In this more reliable assay of cell toxicity, **3.6.8** showed significant toxicity (LD_{50} = 4.46 μM) while the associated ligand induced only a slight toxicity at the highest doses tested (LD_{50} > 20 μM) (Figure 138).

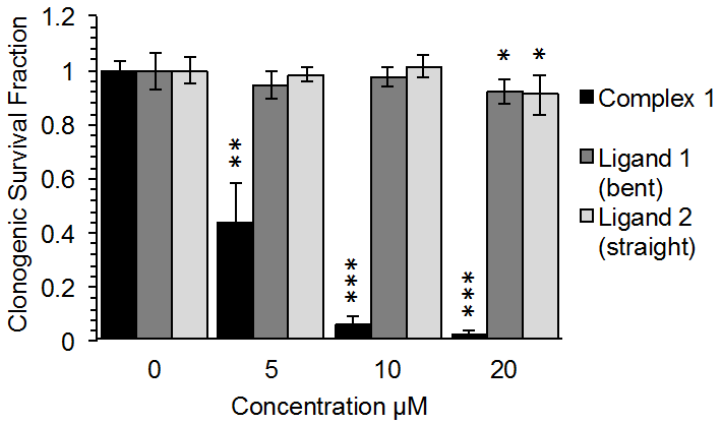

Figure 138: 3.6.8 reduces cell survival to a significantly greater degree than each ligand alone. Long term survival (10 days) as measured by clonogenic survival assay after a 5 hour incubation with **3.6.8** as indicated. Mean and SD of 2 independent repeats (each conducted in duplicate is shown). Significance calculated by Student's T-test compared to respective untreated control is indicated, where * = $p < 0.05$, ** = $p < 0.01$ and *** = $p < 0.001$.

Taken together, the MTT and clonogenic survival data reveal that although both **3.6.8** and **3.6.5** can reduce the metabolic activity of cells in the short term, **3.6.8** is significantly more toxic to cells than either of the ligands alone. This work also highlights the importance of assessing toxicity over a clinically-relevant period of time when considering the therapeutic use of any novel agent.

In this study, **3.6.8** was also investigated for suitability for use as a contrast agent in transmission electron microscopy (TEM). Cells were both incubated in the presence or absence of a 20 μM solution of **3.6.8** for 4 h. Following this, cells were processed for TEM imaging with or without standard contrasting agents as shown in Figure 139. Enhanced contrast was observed using **3.6.8** in comparison to unstained cells. Additionally, the dinuclear complex **3.6.8** did not interfere with the standard double contrast agents (uranyl acetate and lead citrate).

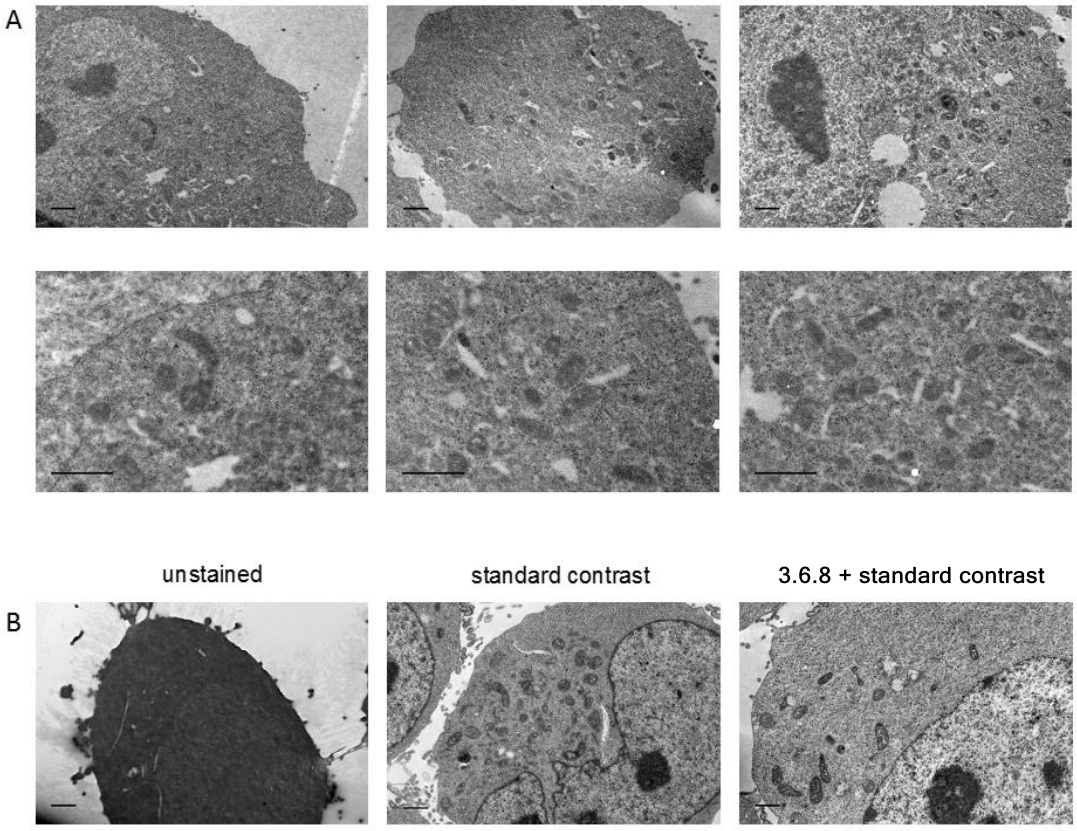

Figure 139: A figure to show transmission electron microscopy (TEM) images using **3.6.8** as a contrast agent. Cells were incubated with or without at 20 μM solution of **3.6.8** for 4 h. (A) Example images of staining with only **3.6.8**. (B) Example image of unstained cells, those stained with standard double contrast agents (uranyl acetate and lead citrate) and those stained with **3.6.8** in addition to standard agents. Scale bars = 1 μm.

In this section of this work, we have demonstrated that a novel pyridazine-bridged cationic dinuclear iridium(III) complex can enter cells, has favourable photophysics and shows appreciable singlet oxygen yield. However, due to the high cytotoxicity, this complex is likely unsuitable for PDT applications. Instead, the toxicity of the complex could be exploited in other applications where its intrinsic toxicity could be beneficial, such as in the development of new anticancer agents.

The photophysical properties of the complex are of interest for luminescent bio-imaging and the presence of two heavy atoms allows its use as a contrast reagent. Potentially the structure of the complex can be varied through modification of both bridging and auxiliary ligands as well as incorporating alternative metals.

Encouraged by these first results, more examples of such systems should be prepared in order to fine-tune the properties and reduce toxicity.

3.7 Variation of Monodentate Ligand

The work discussed in the previous sections of this chapter has showed that dinuclear iridium(III) complexes in which the metal centres are rigidly-linked via bis-N^C-coordinating bridging ligands are highly luminescent and exhibit advantageous structural and photophysical properties when compared with their monometallic counterparts.

The structure of the dinuclear iridium(III) complexes studied as part of this work offers multiple routes for modulation of the photophysical and structural properties of the complexes. In the previous sections of this chapter, we have discussed the effect of varying both the terdentate N^C^N ligand and the ditopic bridging ligand. The results obtained show that variation in the nature of the substituents on the ligands or the core structure of the ligand (for example, the central heterocycle of the bridging ligand) have a large effect on the properties of the final multinuclear complex.

In addition to the cyclometallating terdentate N^C^N ligand and the N^C-coordinating bridging ligand, each iridium(III) centre is also bound to a monodentate ligand. The synthetic procedure

followed in the preparation of the dinuclear iridium(III) complexes discussed so far in this chapter ensures, through addition of excess 2M HCl (aq.) during the work-up, that the monodentate ligands are exclusively chloride. The variation of this monodentate ligand may offer additional opportunities to tune the properties of our target bimetallic Ir(III) complexes.

In the literature, alternative monodentate ligands are routinely used in cyclometallated complexes of Pt(II) and Ir(III). These ligands are incorporated through metathesis reactions of the analogous chloro complex.

In 2009, Che *et. al.* utilised cyclometallated aryl acetylides bearing different R groups as shown in Figure 140. It was observed that the nature of the R group on the monodentate aryl acetylide ligand had a significant effect on the properties of the resulting complexes through altering the extent of Pt-Pt interactions between the mononuclear complexes.[258]

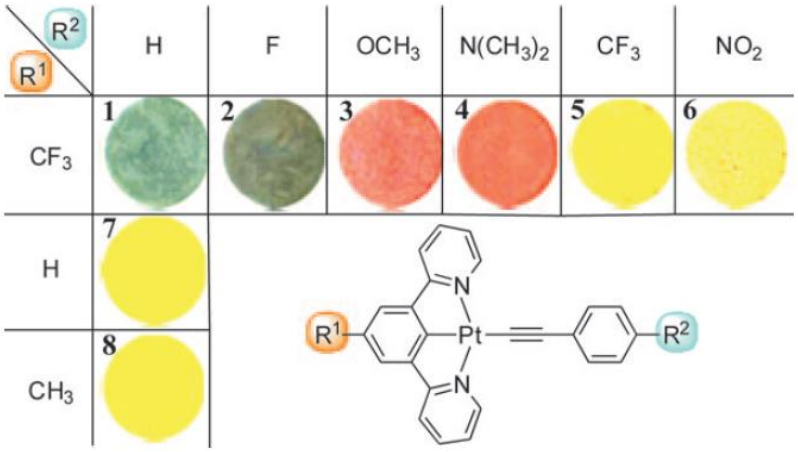

Figure 140: A figure to show the series of cyclometallated Pt(II) complexes prepared by Che *et. al.* in which cyclometallating aryl acetylides, bearing different R groups, were utilised as the monodentate ligands.[258]

In 2010, Li and co-workers demonstrated that the monodentate chloride ligand of Pt(N^C^N)X complexes could be displaced by an anionic phenoxide ligand. Through investigation of the photophysical properties of both the chloride and phenoxide complexes, it was concluded that the monodentate ligand has a large effect on the photophysical properties of the final Pt(N^C^N)X

complexes through Pt-X interactions. This occurs despite the excited state being localised on the Pt(N^C^N) fragment.[21]

Further monodentate ligands such as MeCN, OH_2 and halogens (Br^- and I^-) have also been reported by a number of research groups.[259-261]

Previously, in section 3.3, the preparation of a series of eight dinuclear iridium(III) complexes with the metal centres linked by a 4,6-disubstituted pyrimidine-based bridging ligand was discussed. As part of this work, it was demonstrated that facile metathesis reaction of the monodentate chloride ligands could be carried out in order to alter the identity of the monodentate ligand.

The first example of this type of reaction with our pyrimidine-linked dinuclear complexes is shown in Figure 141. **3.3.14**, in which the monodentate chloride ligands were replaced with cyanide ligands, was prepared by the reaction of **3.3.7** with excess KCN at room temperature. The target cyano complex was isolated in high yield (75%) following treatment of the crude product with methanol.

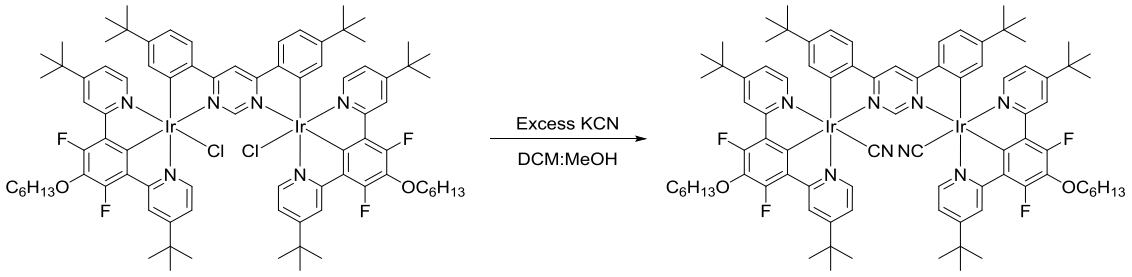

Figure 141: Reaction scheme to show the metathesis reaction of **3.3.7** to **3.3.14** in which the chloride ligands are replaced by cyanide ligands. The final cyano complex was isolated in high yield of 75%.

The final dinuclear iridium(III) complex was fully characterised by ^1H, ^{19}F and ^{13}C NMR spectroscopy and mass spectrometry. The aromatic region of the ^1H NMR spectrum of **3.3.14** is shown in Figure 142. The proton NMR spectrum shows the characteristic signals expected for a pyrimidine-linked dinuclear iridium(III) complex. The singlet at δ 11.5 ppm corresponds to the

proton at the 2-position of the pyrimdine ring with the doublet at δ 6.30 ppm corresponding to the two protons *ortho* to the metallated carbon atoms of the aryl rings of the bis-N^C bridging ligand. In addition to the NMR spectra recorded, the high-resolution mass spectrum can also be used to confirm the identity of the product **3.3.14**. The peak observed at m/z 1739.7240 matches well with the calculated value of m/z 1739.7252 for $[M+H]^+$.

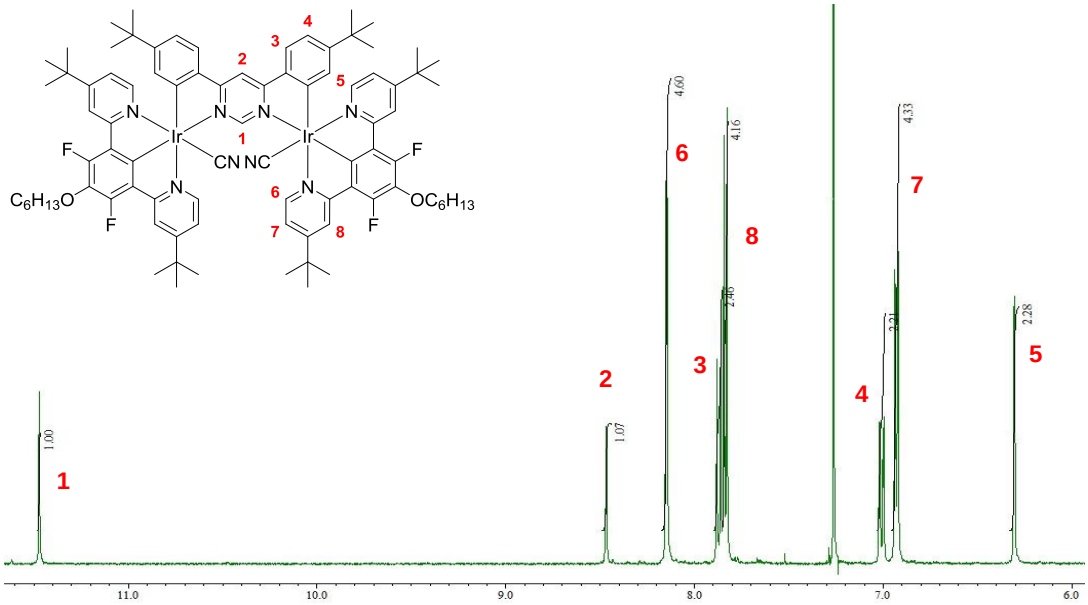

Figure 142: Aromatic region of the ^{1}H NMR spectrum of **3.3.14**. The NMR spectrum shows the characteristic signals expected for our pyrimidine-linked dinuclear iridium(III) complexes. The singlet at δ 11.5 ppm corresponds to the proton at the 2-position of the pyrimidine ring whilst the doublet at δ 6.30 ppm corresponds to the two protons *ortho* to the two metallated carbon atoms of the aryl rings of the bis-bidentate bridging ligand.

The photophysical properties of the dinuclear iridium(III) complex bearing cyanide monodentate ligands were measured and compared with the analogous di-iridium(III) complexes bearing monodentate chloride ligands.

The absorption spectrum recorded for **3.3.14** is shown below in Figure 143 with the related absorption data tabulated in Table 9. In each case, the data obtained for the chloride analogue, **3.3.7**, is included for comparison. On changing the monodentate ligand from chloride to cyanide, there is a relatively large blue-shift of the lowest-energy absorption bands of approximately 29 nm. The overall spectral profile remains largely the same with the higher-energy region (< 350 nm) of the absorption spectrum little affected.

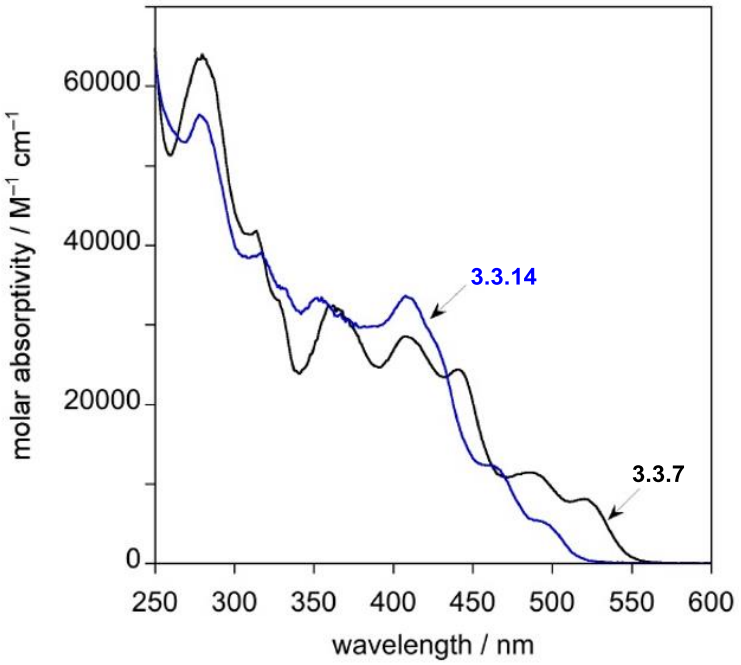

Figure 143: UV-visible absorption spectra for the dinuclear iridium(III) complex **3.3.14** in CH_2Cl_2 at 298 ± 3 K. The absorption spectra of **3.3.7**, recorded under the same conditions, is also shown for comparison with **3.3.14**.

Table 9: UV-visible absorption data for **3.3.14** and **3.3.7** in CH_2Cl_2 at 298 ± 3 K.

Complex[(a)]	**λ_{max} / nm (ε / M^{-1} cm^{-1})**
3.3.7	279 (63400), 312 (41500), 360 (32300), 408 (28600), 441 (24400), 484 (11400), 520 (8080)
3.3.14	279 (56300), 315 (38800), 353 (33000), 409 (33500), 460 (12300), 491 (5390)

The luminescence properties of the cyano di-iridium(III) complex, **3.3.14**, were also measured and the emission spectra and related emission data are shown in Figure 144 and Table 10 respectively. The bimetallic Ir(III) complex bearing monodentate cyanide ligands is highly luminescent in degassed CH_2Cl_2 solution at room temperature as was observed with the pyrimidine-linked complexes discussed in section 3.3. At 298 K, the emission spectrum of **3.3.14** shows a well-defined maximum with a shoulder to the low-energy side. When compared with room-temperature emission of **3.3.7**, the vibrational structure is more pronounced at 77 K with three peaks observed having a vibrational progression of approximately 1400 cm^{-1}. This is typical of aromatic C=C vibrational modes. From the emission spectra in Figure 144 it can be observed that replacement of the monodentate Cl ligands by CN, going from **3.3.7** to **3.3.14**, the emission is blue-shifted by ~ 1000 cm^{-1}. This shift is of a similar magnitude to that observed in the

absorption spectra of the two complexes. Using the HOMO and LUMO energies calculated by TD-DFT and discussed in section 3.3 (Figure 105), it can be seen that the replacement of the chloride ligands by cyanide has a much larger stabilising effect on the HOMO than the LUMO. Therefore, this accounts for the large blue-shift observed experimentally, in both the absorption and emission spectra. This is consistent with the observation that the metal centre makes a more significant contribution to the HOMO than the LUMO.

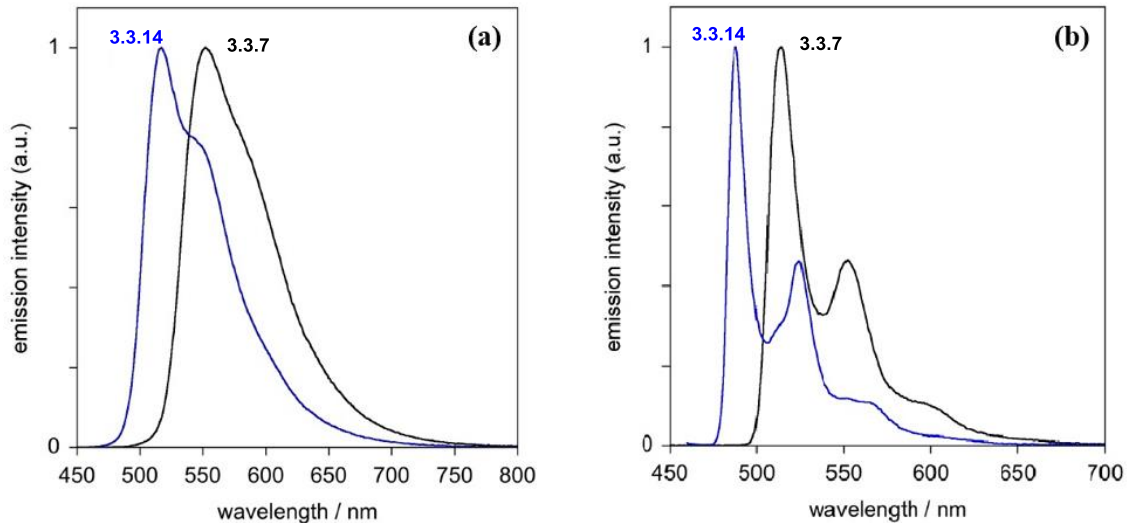

Figure 144: Luminescence spectra of the dinuclear iridium(III) complexes **3.3.14** and **3.3.7** (a) in CH_2Cl_2 at 298 ± 3 K and (b) in diethyl ether / isopentane / ethanol (2:2:1) at 77 K.

Table 10: Emission data for the dinuclear iridium(III) complexes **3.3.14** and **3.3.7** at 298 K and in EPA[a] at 77K.

Complex	λ_{max} / nm	Φ_{lum}[b]	τ / ns[c]	k_r[d] / 10^6 s^{-1}	Σk_{nr}[d] / 10^6 s^{-1}	k_Q^{O2} [e] / 10^9 M^{-1} s^{-1}	Emission at 77K[f]	
							λ_{max} / nm	τ / ns
3.3.7	552, 582sh	0.94	440 [210]	2.14	0.14	1.13	513, 552, 594	6650
3.3.14	517, 547sh	0.88	590 [240]	1.49	0.20	1.12	488, 523, 560	5100

(a) EPA = diethyl ether / isopentane / ethanol (2:2:1 v/v). (b) Measured using $Ir(ppy)_3$ in 2-MeTHF as the standard, for which the Φ = 0.97. (c) Values in air-equilibrated solution in parentheses. (d) k_r and Σk_{nr} are the radiative and non-radiative decay rate constants, estimated from the quantum yield and lifetime assuming that the emissive state is formed with unitary efficiency. (e) Bimolecular rate constant for quenching by O_2, estimated from the luminescence lifetimes in degassed and air-equilibrated solutions, and taking $[O_2]$ = 2.2 mM in CH_2Cl_2 at p = 1 atm air and T = 298 K. (f) In EPA: see footnote a. (g) Since the measured quantum yield is unity within the error of measurement, it is not possible to make a meaningful estimate of k_{nr}. (h) For comparison, data for the related mononuclear complex $Ir(F_2dpyb)(ppy)Cl$ are as follows: At 298 K, λ_{max} = 487, 516 nm; Φ_{lum} = 0.20; τ = 390 ns; k_r = 0.5 x 10^6 s^{-1}; Σk_{nr} = 2.1 x 10^6 s^{-1}. At 77 K, λ_{max} = 471, 508, 537, 548, 593 nm; τ = 2.5 μs.[30]

In order to demonstrate further versatility of our dinuclear iridium(III) complexes with respect to metathesis reactions of the monodentate chloride ligands, additional reactions were carried out to replace the chloride ligands with alternative monodentate ligands, both anionic and neutral, as shown in Figure 145. The use of anionic and neutral monodentate ligands results in the formation of both neutral and cationic dinuclear complexes. These complexes, bearing different overall charges, will have different properties which could be advantageous in a range of applications. For example, cationic di-iridium(III) complexes may be more water soluble and more applicable to bioimaging and water oxidation catalysis (WOCs).

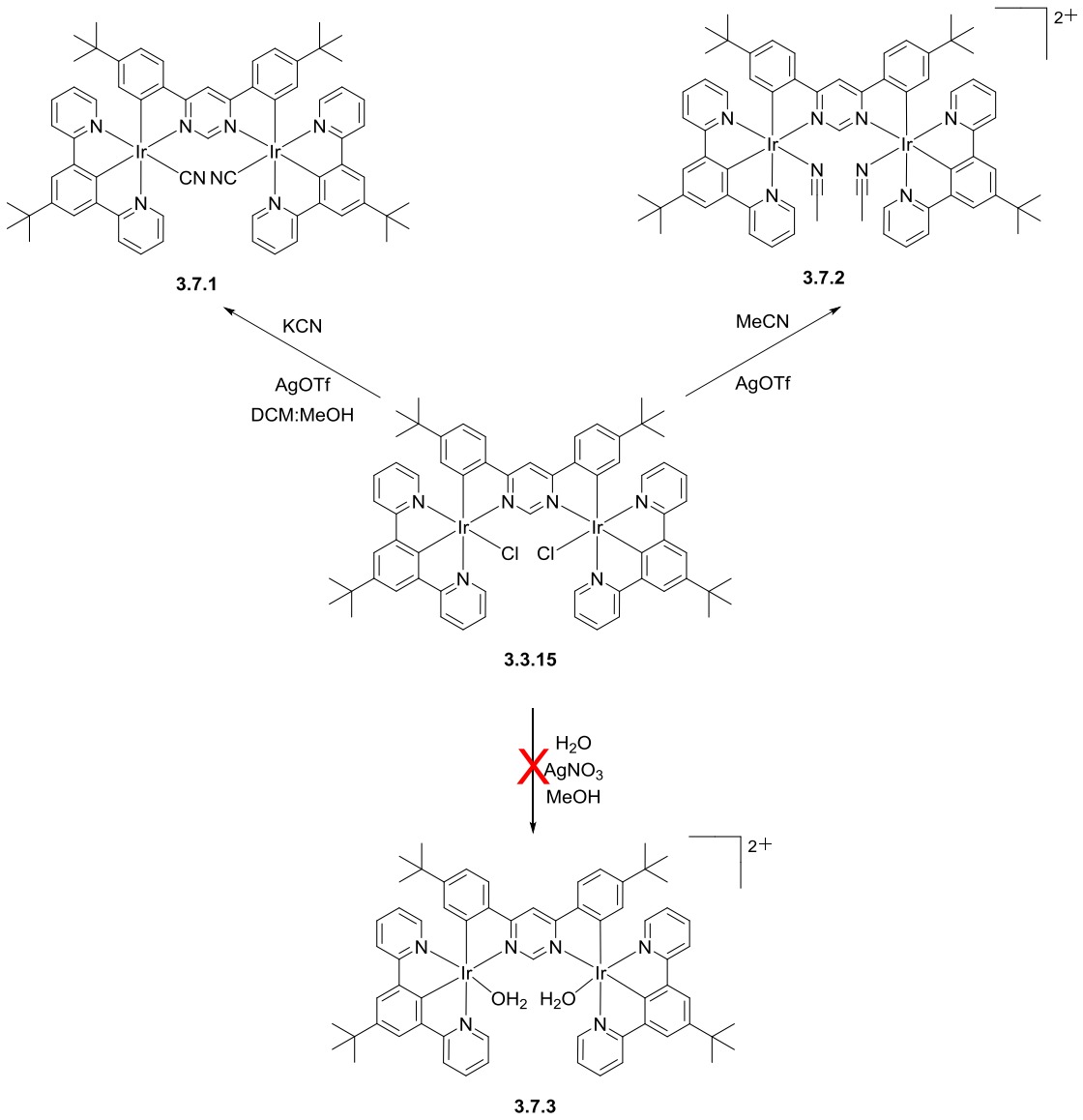

Figure 145: A reaction scheme to show the methathesis reactions carried out, starting with **3.3.15**, to replace the monodentate chloride ligands with alternative monodentate ligands such as CN, MeCN or H_2O.

The first metathesis reaction carried out on **3.3.15** was the equivalent reaction to that carried out on **3.3.7**, as previously discussed, in order to replace the chloride ligands with cyanide ligands. The product, **3.7.1**, was isolated as a yellow solid following treatment with methanol. The di-iridium(III) complex was characterised by ^{1}H and ^{13}C NMR spectroscopy and mass spectrometry. The aromatic region of the ^{1}H NMR spectrum of **3.7.1** is shown in Figure 146. The NMR spectrum is consistent with the product obtained being **3.7.1**.

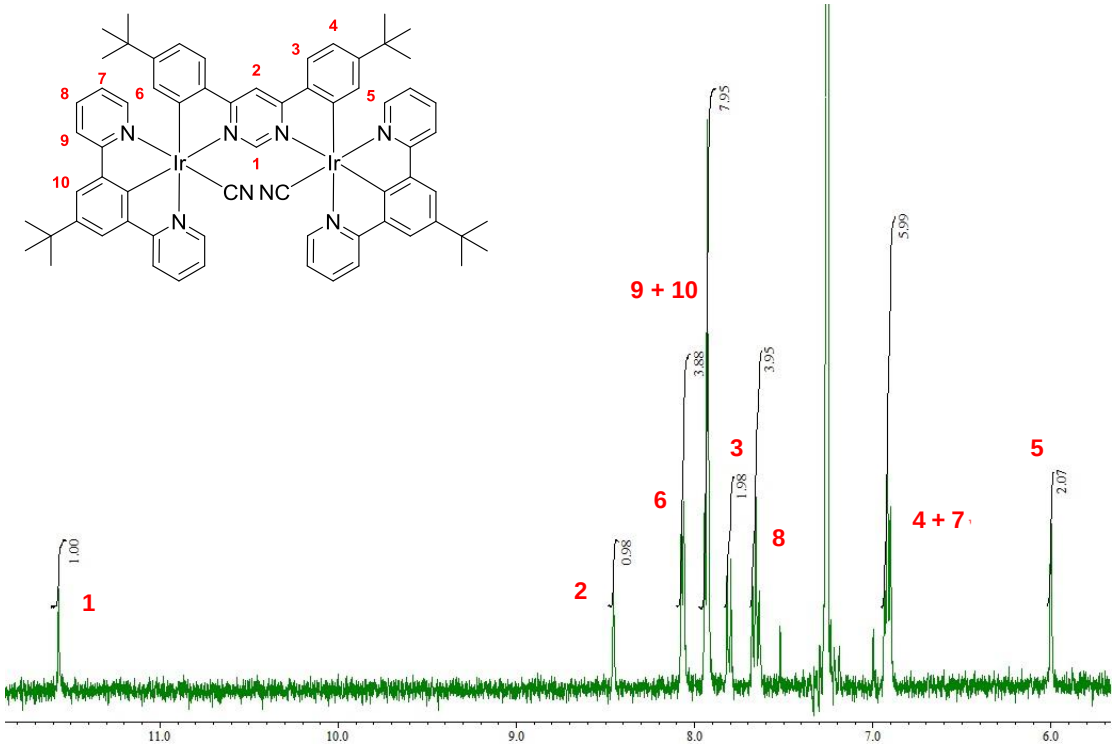

Figure 146: Aromatic region of the ^{1}H NMR spectrum of **3.7.1**. The spectrum shows the characteristic signals for a pyrimidine-linked di-iridium(III) complex; the singlet at δ 11.6 ppm corresponding to the proton at the 2-position of the pyrimidine ring and the peak at δ 6.00 ppm corresponding to the two protons *ortho* to the metallated carbons of the bridging ligand.

Following on from this success, the second metathesis reaction attempted was that to replace the Cl ligands with neutral MeCN ligands. The dinuclear complex **3.3.15** was stirred in acetonitrile at room temperature in the dark and in the presence of silver triflate as a chloride scavenger. An acetonitrile solution of the crude product was treated with a saturated KPF_6(aq) solution in order to exchange the chloride counterion for PF_6^-. The desired product, **3.7.2**, was isolated in high yield and was characterised by ^{1}H NMR spectroscopy. The aromatic region of the ^{1}H NMR spectrum of **3.7.2**, bearing monodentate acetonitrile ligands is shown in Figure 147. The NMR spectrum

shows 8 aromatic peaks corresponding to 10 aromatic proton environments. Within the aromatic region of the proton spectrum, at δ 10.6 ppm and δ 5.90 ppm, the characteristic peaks expected for a pyrimidine-linked dinuclear iridium(III) complex can be observed. In addition, the spectrum shows 3 aliphatic peaks accounting for the 3 aliphatic proton environments. The peak corresponding to the methyl groups of the acetonitrile ligands can be observed at δ 2.12 ppm. This ^{1}H NMR spectrum is therefore consistent with the isolation of **3.7.2**.

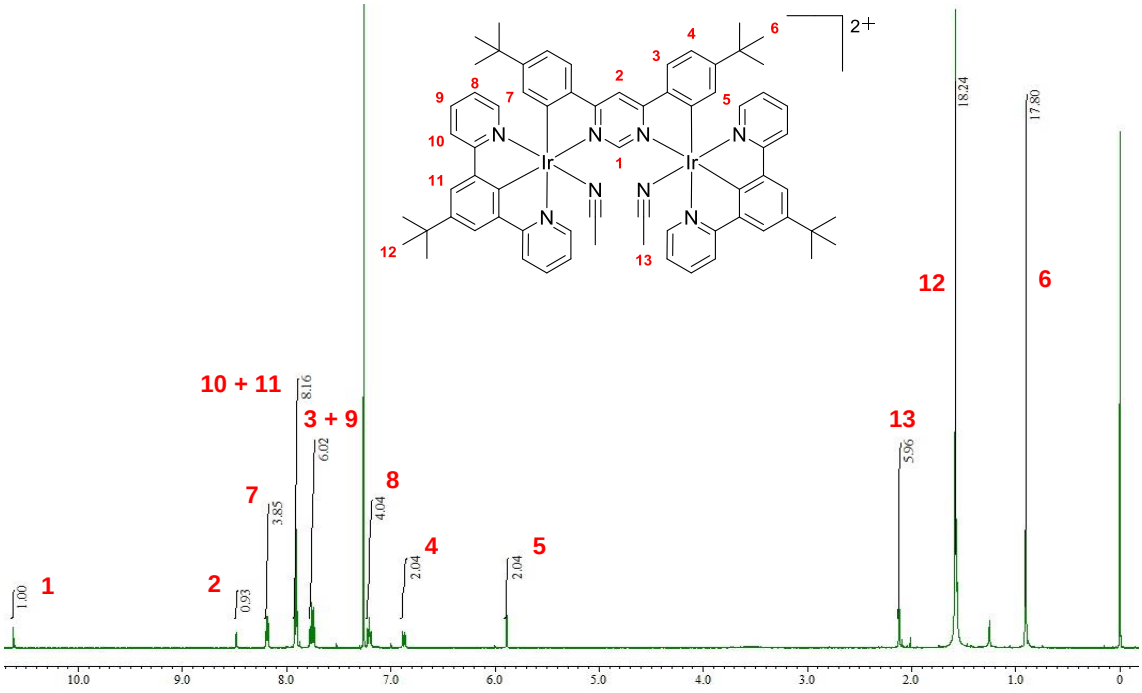

Figure 147: ^{1}H NMR spectrum of the dinuclear iridium(III) complex, **3.7.2**, in which the Cl ligands have been replaced with monodentate, neutral acetonitrile ligands.

The final metathesis reaction attempted was that to substitute the monodentate chloride ligands for water molecules. Water acts as a neutral monodentate ligand and therefore, would result in the formation of a dicationic bimetallic iridium(III) complex. The synthetic route utilised for the metathesis reaction is shown in Figure 145. Unfortunately, this reaction was unsuccessful and the product **3.7.3** could not be isolated. The crude mixture, isolated after counterion exchange with a saturated solution of KPF_6(aq), was analysed by thin layer chromatography (TLC) and ^{1}H NMR spectroscopy. The TLC plate showed an inseparable mixture in which the majority of material was insoluble and remained on the baseline. The proton NMR spectra also showed a mixture of

species in the crude material isolated. Therefore, it is possible that the reaction did not go to completion or there is the formation of undesired byproducts in the course of the reaction.

In this section of the work we have demonstrated facile methods for replacement of the monodentate chloride ligands in our pyrimidine-linked dinuclear iridium(III) complexes. Through metathesis reactions with the anionic cyanide and neutral acetonitrile ligands, neutral and cationic dinuclear iridium(III) complexes respectively have been produced. Unfortunately, the metathesis reaction carried out in an attempt to replace the chloride ligands with a neutral OH_2 ligand was unsuccessful. It was shown that incorporation of the anionic cyanide ligand resulted in a highly luminescent dinuclear complex with emission blue-shifted relative to the corresponding chloro complex. Investigation of the properties of the di-iridium(III) acetonitrile complex is now required in order to assess the effects of this monodentate ligand on both the photophysical properties and solubility. This is important for the evaluation of such a complex for use in applications such as bioimaging.

3.8 Experimental Section

3.8.1 Terdentate NCN Ligands

Compound 3.1.1 – 1,3-di(4-tertbutylpyridine-2-yl)-5-tert-butylbenzene[70, 173]

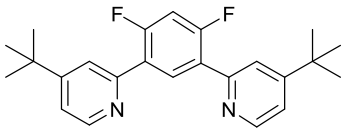

1,3-difluoro-4,6-di(4,4,5,5-tetramethyl-1,3,2-dioxaborolan-2-yl)benzene (1.56 g, 4.26 mmol), 2-chloro-4-(*tert*-butyl)pyridine (1.87 g, 11.1 mmol) and 2M potassium carbonate solution (10 mL) were added to a round-bottomed flask with a 9:1 toluene:ethanol solvent mixture (30 mL). The reaction mixture was degassed under a vigorous flow of argon for 10 min. Tetrakis(triphenylphosphine)palladium was added (0.296 g, 0.256 mmol) was added and the reaction mixture degassed for a further 10 min. The reaction mixture was then heated to reflux (100 °C) for 48 h. The reaction was cooled to room temperature and the solvent removed under reduced pressure. Petroleum ether was added and the solid collected by filtration *in vacuo* and washed with petroleum ether. The filtrate was dried with $MgSO_4$ and the solvent removed under reduced pressure. The crude product was purified by column chromatography (silica gel, hexane:ethyl acetate 4:1) to give the product as a pale yellow oil.

Yield: 0.221 g, 0.581 mmol, 14%

^{1}H NMR (400 MHz, $CDCl_3$): δ 8.62 (d, 2H, *J* = 5.6), 8.47 (t, 1H, *J* = 8.8), 7.73 (br s, 2H), 7.26 (dd, 2H, *J* = 5.6, 1.6), 7.04 (t, 1H, *J* = 10.5), 1.36 (s, 18H).

Compound 3.1.2 – 4-tert-butyl-2-[5-(4-tert-butylpyridin-2-yl)-2,4-difluoro-3-(hexyloxy)phenyl]pyridine[173]

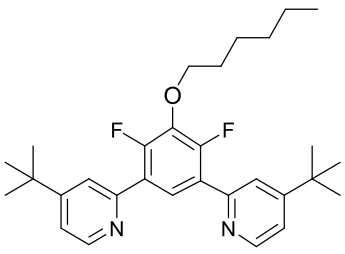

A solution of 4-*tert*-butyl-2-bromopyridine (0.772 g, 3.61 mmol) in 1,4-dioxane was degassed for 15 min. 5-(4-*tert*-butylpyridine-2-yl)-2,4-difluoro-3-*n*-hexyloxyphenyl boronic acid MIDA ester (1.81 g, 3.61 mmol) was added and the solution degassed for a further 5 min. 2-Dicyclohexylphosphino-2′,6′-dimethoxybiphenyl (0.112 g, 0.361 mmol) and palladium acetate (0.0470 g, 0.180 mmol) were added and the reaction mixture degassed for 5 min. A degassed aqueous 3M solution of potassium phosphate (3.82 g, 18.0 mmol, 6 mL) was added and the reaction mixture degassed for a further 10 min. The mixture was stirred at 95 °C for 17 h. The reaction mixture was cooled to room temperature and the solvent evaporated under reduced pressure. Brine (30 mL) was added and the mixture extracted with ethyl acetate (3 x 50 mL). The organic layer was dried with $MgSO_4$ and the solvent evaporated to dryness. The crude product was purified by column chromatography (silica gel, petroleum ether:ethyl acetate 3:1) to give the final product.

Yield: 0.272 g, 0.567 mmol, 16%

^{1}H NMR (400 MHz, $CDCl_3$): δ 8.60 (d, 2H, *J* = 5.4), 8.09 (t, 1H, *J* = 8.5), 7.69 (br s, 2H), 7.20 (dd, 2H, *J* = 5.4, 2.1), 4.21 (t, 2H, *J* = 7.0), 1.57 (q, 2H, *J* = 7.2), 1.34 (m, 6H), 0.90 (t, 3H, *J* = 7.2).

^{19}F NMR (400 MHz, $CDCl_3$): δ -131.30 (d, *J* = 21.5).

^{13}C NMR (100 MHz, $CDCl_3$) δ 160.53, 154.25 (dd, *J* = 249.3, 5.6), 152.88, 149.72, 136.35 (t, *J* = 15.8), 125.76 (br s), 125.35 (dd, *J* = 9.7, 5.7), 121.54 (t, *J* = 3.8), 75.39, 34.91, 31.65, 30.66, 30.14, 25.47, 22.68, 14.13.

Compound 3.1.4 - 1,3-di(2-pyridyl)-4,6-difluorobenzene[30]

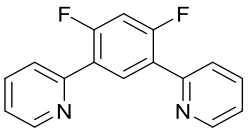

A mixture of 1,5-dibromo-2,4-difluorobenzene (2.65 g, 9.75 mmol), 2-(tributylstannyl)pyridine (8.76 g, 24.0 mmol) and tetrakis(triphenylphosphine)palladium (0.310 g, 0.268 mmol) were added to toluene (90 mL) and the reaction mixture degassed for 15 min under argon. The reaction

mixture was heated to reflux (140 °C) for 24 h. The solvent was removed under reduced pressure. Petroleum ether (8 mL) was added and the solid filtered off and washed with petroleum ether. The grey solid obtained was dissolved in dichloromethane and filtered through Celite. The filtrate was collected and the solvent removed under reduced pressure. The desired product was obtained as an off-white solid.

Yield: 1.58 g, 5.89 mmol, 60%

^{1}H NMR (400 MHz, $CDCl_3$): δ 8.73 (d, 2H, *J* = 5.0), 8.61 (t, 1H, *J* = 8.8, 9.2), 7.77-7.74 (m, 4H), 7.29-7.25 (m, 2H), 7.04 (t, 1H, *J* = 10.8).

^{19}F NMR (400 MHz, $CDCl_3$): δ

^{13}C DEPT135 NMR (100 MHz, $CDCl_3$): δ 161.83 (d, *J* = 12.4, C), 159.28 (d, *J* = 12.4, C), 152.59, 149.92 (CH), 136.53 (CH), 133.73 (CH), 124.29 (CH), 122.60 (CH), 105.07 (t, *J* = 27.2, CH).

Compound 3.1.5 – 1,3-di(2-pyridyl)-5-tert-butylbenzene[70]

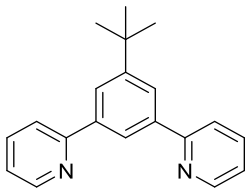

A mixture of 1,3-dibromo-5-(*tert*-butyl)benzene (3.01 g, 10.3 mmol), 2-(tributylstannyl)pyridine (9.54 g, 25.7 mmol) and tetrakis(triphenylphosphine)palladium (0.358 g, 0.309 mmol) were added to toluene (100 mL) and the reaction mixture degassed for 15 min under argon. The reaction mixture was heated to reflux (140 °C) for 20 h. The reaction mixture was purified by column chromatography (silica gel, petroleum ether:ethyl acetate 100:0 to 4:1 to 6:1 to 3:1) and a white solid was obtained.

Yield: 2.11 g, 7.31 mmol, 71%

^{1}H NMR (400 MHz, $CDCl_3$): δ 8.72 (d, 2H, *J* = 1.6), 8.34 (d, 1H, *J* = 1.4), 8.12 (d, 2H, *J* = 1.4), 7.82 (d, 2H, *J* = 7.8), 7.76 (t, 2H, *J* = 7.8), 7.23 (t, 2H, *J* = 6.0), 1.45 (s, 9H).

^{13}C NMR (100 MHz, $CDCl_3$): δ 157.83 (C), 152.23 (C), 149.66 (CH), 139.71 (C), 136.67 (CH), 124.75 (CH), 123.02 (CH), 122.08 (CH), 120.93 (CH), 35.12 (C), 31.48 (CH_3).

Compound 3.1.11 – 2-[3-tert-butyl-5-(1-phenyl-1H-1,3-benzodiazol-2-yl)phenyl]-1-phenyl-1H-1,3-benzodiazole[186]

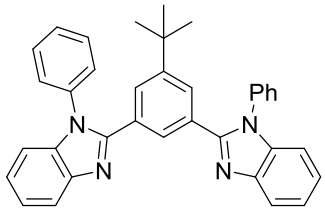

N-phenyl-o-phenylenediamine (2.28 g, 12.3 mmol) was placed in a round-bottomed flask with 1-methyl-2-pyrrolidinone (31 mL). To this mixture 5-*tert*-butylbenzene-1,3-dicarbonyl dichloride (1.60 g, 6.17 mmol) was added and the reaction mixture was stirred at room temperature for 2 h. The temperature was then increased to 50 °C for a further 2 h. The reaction was cooled to room temperature and then poured into cool water (100 mL). The precipitate formed was filtered off, washed with distilled water and dried *in vacuo* to give the crude diamide (5.51 g, 9.93 mmol). Cyclodehydration of the diamide intermediate (2.30 g, 4.15 mmol) at 290 °C under vacuum was then carried out in a Kugelrohr. The black solid was then dissolved in dichloromethane and purified by column chromatography (silica gel, DCM:ethyl acetate 3:1 to 3:2 to 1:1) to give the final product as a white solid.

Yield: 0.938 g, 1.81 mmol, 70%

^{1}H NMR (400 MHz, $CDCl_3$): δ 7.99 (t, 1H, *J* = 1.6, 1.2), 7.87 (d, 2H, *J* = 7.6), 7.49-7.39 (m, 8H), 7.36-7.30 (m, 4H), 7.26-7.25 (m, 6H), 0.94 (s, 9H).

^{13}C DEPT135 (100 MHz, $CDCl_3$): δ 152.15 (C), 150.70 (C), 143.04 (C), 137.02 (C), 136.88 (C), 129.99 (C), 129.79 (CH), 128.50 (CH), 128.09 (CH), 127.79 (CH), 127.44 (CH), 123.30 (CH), 122.91 (CH), 119.98 (CH), 110.40 (CH), 34.44 (C), 30.66 (CH_3).

Compound 3.1.12 - 2-[3-tert-butyl-5-(1-methyl-1H-1,3-benzodiazol-2-yl)phenyl]-1-methyl-1H-1,3-benzodiazole

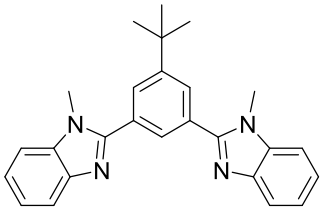

Polyphosphoric acid (18.7 mL) was added to a round-bottomed flask. To this 5-*tert*-butylisophthalic acid (1.01 g, 0.454 mmol) and N-methyl-1,2-phenylenediamine (1.39 g, 11.4 mmol) were added. The reaction mixture was heated to 190 °C for 17 h. The reaction mixture was removed from the heat and poured into vigorously stirred water (60 mL). The mixture was neutralised with NaOH (5 mL) solution. The blue precipitate was filtered *in vacuo* and washed with water and dried. The crude solid was purified by column chromatography (silica gel, DCM:acetone 4:1) to give the final product as a white solid.

Yield: 1.37 g, 3.48 mmol, 77%

^{1}H NMR (400 MHz, $CDCl_3$): δ 7.96 (s, 2H), 7.87-7.85 (m, 3H), 7.44-7.42 (m, 2H), 7.38-7.32 (m, 4H), 3.90 (s, 6H), 1.46 (s, 9H).

^{13}C DEPT135 NMR (100 MHz, $CDCl_3$): δ 153.51 (C), 153.72 (C), 142.95 (C), 136.56 (C), 130.47 (C), 128.23 (CH), 127.21 (CH), 122.98 (CH), 122.57 (CH), 119.92 (CH), 109.71 (CH), 35.19 (C), 31.79 (CH), 31.29 (CH).

Compound 3.1.17 – 1-[3-tert-butyl-5-(1H-pyrazol-1-yl)phenyl]-1H-pyrazole

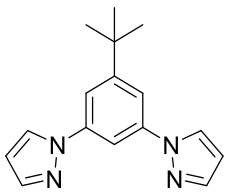

To a dry flask, 1,3-dibromo-5-(*tert*-butyl)benzene (1.00 g, 3.42 mmol), pyrazole (0.583 g, 8.56 mmol), syn-pyridine-2-aldoxime (0.0836 g, 0.685 mmol), copper(I) oxide (0.0490 g, 0.342 mmol)

and cesium carbonate (5.58 g, 17.1 mmol) were added. Anhydrous acetonitrile (60 mL) was added. The reaction mixture was degassed under a flow of argon for 20 min and heated to reflux for 3 d. The reaction mixture was cooled to room temperature. DCM (20 mL) was added and the mixture was filtered through Celite. The Celite was washed with further DCM. The filtrate was evaporated to dryness under reduced pressure. The crude residue was purified by column chromatography (silica gel, gradient elution, DCM:ethyl acetate 100:0, 9:1, 4:2) to give the product as an off-white solid.

Yield: 0.640 g, 2.18 mmol, 70%

^{1}H NMR (400 MHz, $CDCl_3$): δ 8.01 (d, 2H, *J* = 2.0), 7.83-7.82 (m, 1H), 7.76 (s, 2H), 7.68 (d, 2H, *J* = 1.6), 6.51-6.49 (m, 2H), 1.42 (s, 9H).

^{13}C DEPT135 NMR (100 MHz, $CDCl_3$): δ 154.55 (C), 141.24 (CH), 140.84 (C), 127.07 (CH), 114.45 (CH), 107.82 (CH), 107.58 (CH), 35.33 (C), 31.22 (CH_3).

3.8.2 Dichloro-Bridged Iridium(III) Dimers

Compound 3.2.1

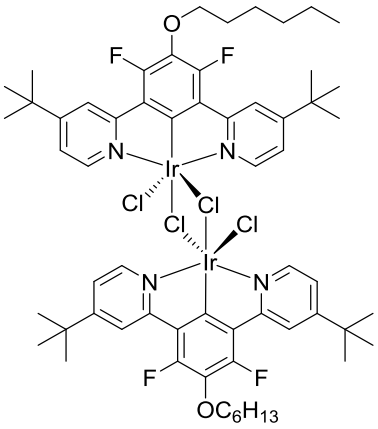

4-tert-butyl-2-[5-(4-*tert*-butylpyridin-2-yl)-2,4-difluoro-3-(hexyloxy)phenyl]pyridine (0.272 g, 0.567 mmol) and iridium chloride (0.206 g, 0.567 mmol) were placed in a round-bottomed flask with a 3:1 mixture of 2-ethoxyethanol and water (11 mL). The reaction mixture was heated to reflux for 14 h. The reaction mixture was cooled to room temperature and filtered to give an orange solid that was washed with ethanol and dried.

Yield: 0.345 g, 0.467 mmol, 82%

^{1}H NMR (400 MHz, $CDCl_3$): δ 8.42 (d, 2H, *J* = 6.4), 8.25 (s, 2H), 6.96 (dd, 2H, *J* = 6.0, 2.4), 4.18 (t, 2H, *J* = 6.8), 1.89 (quin, 2H, *J* = 14.4, 7.6), 1.59-1.56 (m, 2H), 1.49 (s, 18H), 1.43-1.40 (m, 4H), 0.96 (t, 3H, *J* = 7.2).

Compound 3.2.2

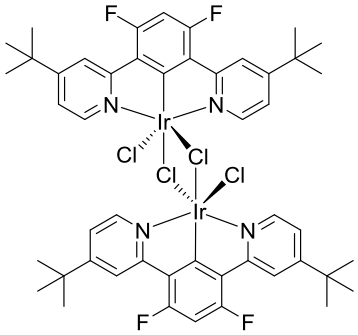

To a mixture of 2,6-difluoro-3,5-di(*tert*-butylpyridin-2-yl)pyridine (0.221 g, 0.581 mmol) and iridium chloride hydrate (0.211 g, 0.581 mmol), a 3:1 mixture of 2-ethoxyethanol and water (25 mL) was added. The reaction mixture was heated to reflux (130 °C) for 24 h under argon. The solvent was removed *in vacuo* and the resulting orange solid was filtered and washed with ethanol and water to give the desired product.

Yield: 0.308 g, 0.486 mmol, 84%

^{1}H NMR (400 MHz, d^6-DMSO): δ 8.93 (d, 2H, *J* = 6.4), 8.07 (d, 2H, *J* = 14.4), 7.73 (dd, 2H, *J* = 4.0, 1.8, 7.27 (t, 1H, *J* = 11.8), 1.40 (d, 18H, *J* = 3.2).

^{19}F NMR (400 MHz, d^6-DMSO): δ -107.38 (d, *J* = 12.8).

^{13}C NMR DEPT135 (100 MHz, d^6-DMSO): δ 169.27, 163.72 (d, *J* = 183.2), 160.66 (d, *J* = 49.6), 158.02 (d, *J* = 46.0), 152.03 (CH), 124.51 (t, *J* = 23.0), 121.80 (CH), 119.86 (t, *J* = 25.3, CH), 99.53 (t, *J* = 111.2, CH), 35.03 (C-*t*Bu), 29.92 (*t*Bu).

Compound 3.2.3

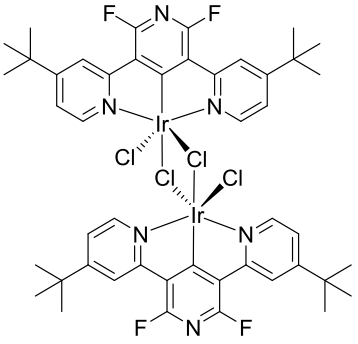

A mixture of 2.6-difluoro-3,5-di(*tert*-butylpyridin-2-yl)pyridine (0.151 g, 0.396 mmol) and iridium chloride hydrate (0.14 g, 0.396 mmol) were added to a 3:1 mixture of 2-ethoxyethanol and water (60 mL). The reaction mixture was heated to reflux (130 °C) for 24 h under argon. The solvent was removed *in vacuo* and the resulting orange solid was filtered and washed with ethanol and water to give the desired product.

Yield: 0.162 g, 0.267 mmol, 67%

^{1}H NMR (400 MHz, d^{6}-DMSO): δ 8.93 (d, 2H, *J* = 6.4), 8.04 (d, 2H, *J* = 1.8), 7.81 (dd, 2H, *J* = 6.0, 2.3).

Compound 3.2.4

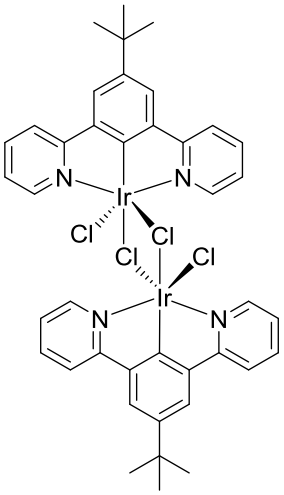

A mixture of 1,3-di(2-pyridyl)-5-(*tert*-butyl)benzene (0.724 g, 2.51 mmol) and iridium chloride hydrate (1.09 g, 3.01 mmol) were added to a 3:1 mixture of 2-ethoxyethanol and water (100 mL).

The reaction mixture was heated to reflux (130 °C) for 24 h under argon. The resulting orange solid was filtered *in vacuo* and washed with ethanol and water to give the desired product.

Yield: 1.25 g, 2.28 mmol, 91%

^{1}H NMR (d^{6}-DMSO, 400 MHz): δ 9.01 (d, 2H, *J* = 5.0), 8.40 (d, 2H, *J* = 8.2), 8.09 (t, 2H, *J* = 7.6), 8.05 (s, 2H), 7.55 (t, 2H, *J* = 6.4), 1.46 (s, 9H).

Compound 3.2.5

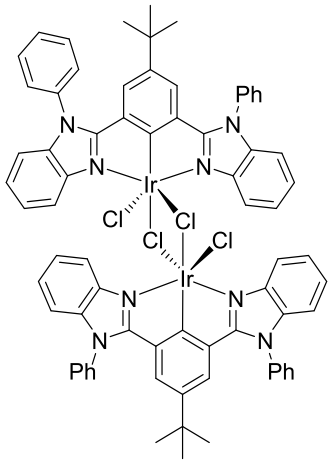

2-[3-*tert*-butyl-5-(1-phenyl-1H-1,3-benzodiazol-2-yl)phenyl]-1-phenyl-1H-1,3-benzodiazole (0.449 g, 0.866 mmol) and iridium chloride (0.316 g, 0.866 mmol) were placed in a round-bottomed flask with a 3:1 mixture of 2-ethoxyethanol and water (50 mL). The reaction mixture was heated to reflux for 18 h. The reaction mixture was cooled to room temperature and filtered to give an orange solid that was washed with ethanol and water and dried.

Yield: 0.602 g, 0.771 mmol, 89%

^{1}H NMR (400 MHz, $CDCl_3$): δ 7.96 (d, 2H, *J* = 7.6), 7.90-7.86 (m, 4H), 7.77-7.68 (m, 4H), 7.57 (d, 2H, *J* = 7.6), 6.90-6.82 (m, 4H), 6.75 (s, 2H), 6.53 (m, 2H), 0.98 (s, 9H).

^{13}C NMR DEPT135 (100 MHz, $CDCl_3$): δ 160.22 (C), 144.10 (C), 141.34 (C), 135.31 (C), 135.14 (C), 132.74 (C), 130.18 (CH), 130.12 (CH), 128.56 (CH), 128.31 (CH), 123.44 (CH), 122.90 (CH), 122.21 (CH), 117.44 (CH), 109.71 (CH), 34.42 (C), 31.31 (CH).

Compound 3.2.6

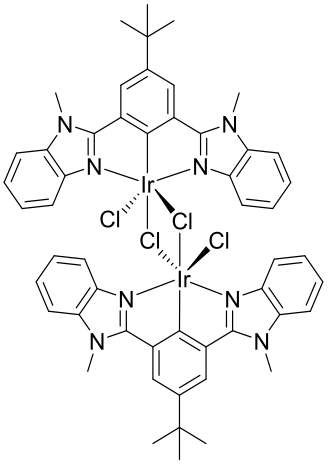

1-[3-*tert*-butyl-5-(1H-pyrazol-1-yl)phenyl]-1H-pyrazole (0.640 g, 2.40 mmol) and iridium chloride (0.872 g, 2.40 mmol) were placed in a round-bottomed flask. A 3:1 mixture of 2-ethoxyethanol and water (60 mL) was added and the mixture was heated to reflux for 18 h. The reaction mixture was cooled to room temperature and the precipitate collected by filtration *in vacuo*. The product was washed with ethanol and diethyl ether.

Yield: 0.969 g, 1.83 mmol, 76%

^{1}H NMR (400 MHz, $CDCl_3$): δ 8.58 (br s, 1H), 8.03-7.76 (m, 4H), 7.41-7.35 (m, 4H), 4.40-4.37 (m, 6H), 1.42 (s, 9H).

Compound 3.2.7

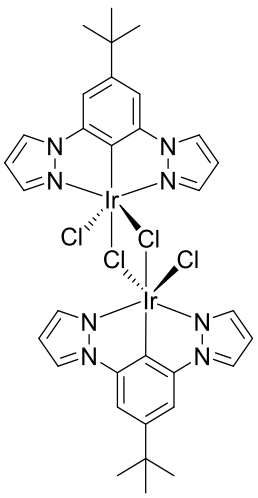

2-[3-tert-butyl-5-(1-methyl-1H-1,3-benzodiazol-2-yl)phenyl]-1-methyl-1H-1,3-benzodiazole (0.502 g, 1.27 mmol) and iridium chloride (0.462 g, 1.27 mmol) were placed in a round-bottomed flask. A 3:1 mixture of 2-ethoxyethanol and water (40 mL) was added and the mixture was heated to reflux for 18 h. The reaction mixture was cooled to room temperature and the precipitate collected by filtration *in vacuo*. The product was washed with ethanol and diethyl ether.

Yield: 0.772 g, 1.10 mmol, 87%

^{1}H NMR (400 MHz, $CDCl_3$,): δ 9.01 (d, 2H, *J* = 2.8), 7.89 (d, 2H, *J* = 2.3), 7.73 (s, 2H), 6.81 (t, 2H, *J* = 2.8), 1.39 (s, 9H).

3.8.3 Pyrimidine-Linked Dinuclear Iridium(III) Complexes

Compound 3.3.5 - 4,6-bis(4-methoxyphenyl)pyrimidine[173]

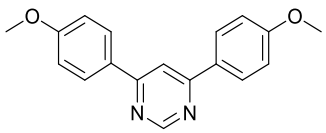

(4-methoxyphenyl)boronic acid (1.59 g, 10.5 mmol), 4,6-dichloropyrimidine (0.601 g, 4.03 mmol) and a 2M aqueous potassium carbonate solution (3.34 g, 24.2 mmol, 12.1 mL) were added to a round-bottomed flask. 1,4-Dioxane (35 mL) was added and the reaction mixture was degassed under argon for 15 min. Tetrakis(triphenylphosphine)palladium (0.280 g, 0.242 mmol) was added and the reaction mixture degassed for a further 10 m8inutes. The reaction mixture was heated to reflux for 48 h under an argon atmosphere. The reaction mixture was cooled to room temperature and toluene (20 mL) was added. The organic phase was separated and washed with water (3 x 10 mL). The organic phase was dried with MgSO4 and the solvent evaporated to dryness. The crude residue was recrystallised from ethyl acetate to give the product.

Yield: 0.377 g, 1.29 mmol, 32%

^{1}H NMR (400 MHz, $CDCl_3$): δ 9.21 (d, 1H, *J* = 1.4), 8.14-8.10 (m, 4H), 9.78 (d, 1H, *J* = 1.4), 7.06-7.02 (m, 4H), 3.90 (s, 6H).

^{13}C NMR (100 MHz, $CDCl_3$): δ 163.97 (C), 162.01 (C), 159.10 (CH), 129.61 (CH), 128.75 (CH), 114.42 (CH), 111.14 (CH), 55.55 (CH_3).

Compound 3.3.6 – 4,6-bis(4-tert-butylphenyl)pyrimidine[84]

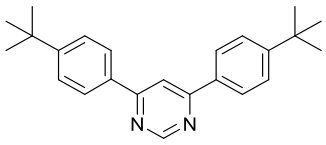

(4-tert-butylphenyl)boronic acid (2.01 g, 11.2 mmol), 4,6-dichloropyimidine (0.645 g, 4.30 mmol), potassium carbonate (3.59 g, 26.0 mmol) and 1,4-dioxane (30 mL) were placed in a round bottomed flask and the reaction mixture degassed with argon for 10 min. Tetrakis(triphenylphosphine)palladium (0.151 g, 0.129 mmol) was added and the reaction mixture degassed for a further 10 minutes. The reaction mixture was then heated to reflux for 48 h under an argon atmosphere. The reaction mixture was cooled to room temperature. Toluene (20 mL) was added and the solution washed with water. The organic layer was dried over $MgSO_4$ and the solvent evaporated under reduced pressure. The residue was recrystallised from ethyl acetate to give the product as a colourless solid.

Yield: 1.10 g, 3.20 mmol, 74%

^{1}H NMR (400 MHz, $CDCl_3$): δ 9.28 (s, 1H), 8.08 (d, 5H, *J* = 8.8), 7.56 (d, 4H, *J* = 8.4), 1.38 (s, 18H).

^{13}C DEPT135 NMR (100 MHz, $CDCl_3$): δ 164.45 (C), 159.15 (CH), 154.37 (C), 134.29 (C), 126.92 (CH), 126.00 (CH), 112.26 (CH), 34.92 (C), 31.23 (CH_3).

Compound 3.3.7

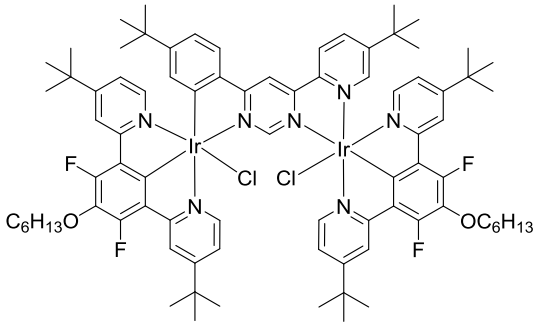

Compound **3.5.1** (0.161 g, 0.215 mmol), and 4,6-di-(4-tert-butylphenyl)pyrimidine (0.0373 g, 0.108 mmol) were placed in a round-bottomed flask with toluene (26 mL). Silver triflate (0.0840 g, 0.323 mmol) was added and the reaction mixture heated to reflux for 8 h. The heat was then removed and to a still warm reaction mixture a 3M HCl solution (5 mL) was added and the mixture stirred for 5 min. The organic phase was separated and the solvent removed under reduced pressure. Methanol (20 mL) was added to the red-orange residue and the solid filtered *in vacuo* and the solid washed with methanol. The resulting orange solid was dissolved in dichloromethane (10 mL) and filtered by gravity. Methanol (20 mL) was added to the filtrate and the volume of solvent reduced under reduced pressure to 10 mL. The orange solid was collected by filtration *in vacuo* and was shown to be the desired product.

Yield: 0.0735 g, 0.0419 mmol, 39%

^{1}H NMR (400 MHz, $CDCl_3$) δ 11.77 (s, 1H), 8.40 (s, 1H), 8.12 (s, 4H), 7.81 (d, 2H, *J* = 8.0 Hz), 7.79 (d, 4H, *J* = 5.9), 6.95 (dd, 2H, *J* = 8.0, 1.6), 6.92 (dd, 4H, *J* = 5.9, 1.6), 6.28 (d, 2H, *J* = 1.6), 4.20 (t, 4H, *J* = 6.5), 1.92 (m, 4H), 1.62 (m, 4H), 1.44 (m, 8H), 1.32 (s, 36H), 1.01 (s, 18H), 0.97 (t, 6H, *J* = 6.9).

^{19}F NMR (400 MHz, $CDCl_3$): δ -126.9.

^{13}C NMR DEPT135 (100 MHz, $CDCl_3$): δ 161.57 (CH), 150.69 (CH), 133.20 (CH), 125.87 (CH), 120.33 (CH), 120.07 (CH), 119.32 (CH), 105.93 (CH), 75.77 (CH_2), 31.7 (CH_2), 30.9 (CH_3), 30.5 (CH_3), 30.2 (CH_2), 25.6 (CH_2), 22.7 (CH_2), 14.1 (CH_3).

HRMS (FTMS^{+}): for $[M\text{-}Cl]^{+}$ calc'd 1721.6791, found 1721.6795; for $[M+Na]^{+}$ calc'd 1779.6362, found 1779.6771; for $[M+NH_4]$+ calc'd 1770.6761, found 1770.6771.

Compound 3.3.8

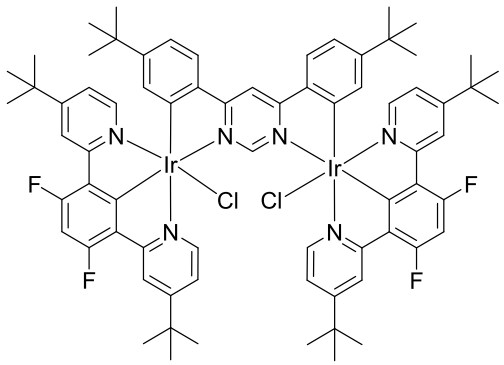

Compound **3.2.2** (0.150 g, 0.230 mmol) in xylene (30 mL), silver trifluoromethanesulfonate (0.0901 g, 0.351 mmol) was added. 4,6-di(4-tert-butylphenyl)pyrimidine (0.0403 mg, 0.117 mmol) was then added and the reaction mixture heated to reflux for 8 h. To the cooled reaction mixture, dichloromethane (10 mL) was added and the mixture filtered in vacuo. The filtered solid was washed with dichloromethane. Concentrated hydrochloric acid (3 mL) was added to the filtrate and the resulting mixture stirred for 5 min. The resulting mixture was filtered through Celite and the Celite washed with further dichloromethane. The filtrate was evaporated to dryness under reduced pressure and the residue treated with methanol (20 mL). The orange solid was filtered off and washed with methanol.

Yield: 0.125 g, 0.08 mmol, 69%

^{1}H NMR (400 MHz, $CDCl_3$): δ 11.75 (s, 1H), 8.41 (s, 1H), 8.11 (s, 4H), 7.81 (d, 6H, *J* = 6.8), 6.94 (d, 6H, *J* = 6.4), 6.82 (t, 2H, *J* = 11.8), 6.27 (s, 2H), 1.32 (s, 36H), 1.02 (s, 18H).

^{19}F NMR (400 MHz, $CDCl_3$): δ -109.49 (d, 4F, *J* = 12).

^{13}C DEPT135 (100 MHz, $CDCl_3$): δ 170.90, 165.28, 161.58, 160.30 (CH), 155.17, 152.23, 150.66 (CH), 138.42, 133.07 (CH), 125.80 (CH), 124.18, 120.29 (CH), 119.93 (CH), 119.30 (CH), 105.87 (CH), 96.77 (CH), 34.98 (C-*t*Bu), 34.52 (C-*t*Bu), 30.86 (CH_3), 30.50 (CH_3).

HRMS (FTMS^{+}): for $[M\text{-}Cl]^{+}$ calc'd 1521.5015, found 1521.5026; for $[M\text{-}(Ir(NCN)Cl)\text{-}Cl]^{+}$ calc'd 915.3789, found 915.3784; for $[M\text{-}2Cl]^{2+}$ calc'd 743.2663, found 743.2655.

Compound 3.3.9

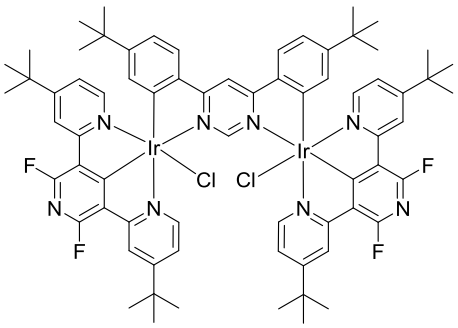

Compound **3.2.3** (0.150 g, 0.247 mmol) in xylene (30 mL), silver trifluoromethanesulfonate (0.101 g, 0.370 mmol) was added. 4,6-di(4-tert-butylphenyl)pyrimidine (0.0425 g, 0.123 mmol) was then added and the reaction mixture heated to reflux for 8h. To the cooled reaction mixture, dichloromethane (15 mL) and concentrated hydrochloric acid (3 mL) were added the mixture stirred for 5 min. The resulting mixture was filtered through Celite and the Celite washed with further dichloromethane. The filtrate was evaporated to dryness under reduced pressure and the residue treated with methanol (20 mL). The orange-yellow solid was filtered off and washed with methanol.

Yield: 0.114 g, 0.07 mmol, 59%

^{1}H NMR (400 MHz, $CDCl_3$): δ 11.76 (s, 1H), 8.46 (s, 1H), 8.12 (d, 4H, *J* = 2.0), 7.85 (d, 2H, *J* = 8.4), 7.82 (d, 4H, *J* = 6.0), 7.02 (dd, 4H, *J* = 6.4, 2.4), 6.99 (dd, 2H, *J* = 8.4, 1.6), 6.24 (s, 2H), 1.35 (s, 36H), 1.02 (s, 18H).

^{19}F NMR (400 MHz, $CDCl_3$): δ -69.43 (s, 4F).

^{13}C DEPT135 (100 MHz, $CDCl_3$): δ 170.79, 162.53, 155.90, 151.08 (CH), 137.98, 132.64 (CH), 126.20 (CH), 120.68 (CH), 119.96 (CH), 106.00 (CH), 50.92 (), 35.15 (C-*t*Bu), 34.74 (C-*t*Bu), 30.86 (CH_3), 30.47 (CH_3).

HRMS (FTMS^{+}) for $[M\text{-}Cl]^{+}$ calc'd 1523.7135, found 1523.4917.

Compound 3.3.10

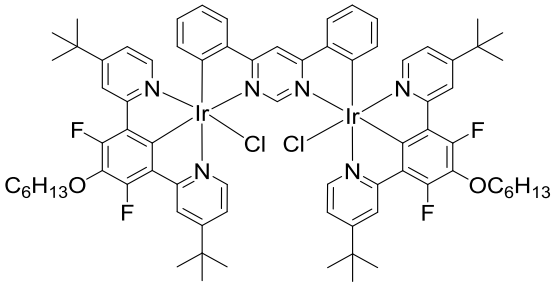

To a stirred solution of compound **3.5.1** (0.148 g, 0.200 mmol) and 4,6-diphenylpyrimidine (0.024 g, 0.100 mmol) in toluene (30 mL), silver triflate (0.077 g, 0.300 mmol) was added and the mixture was heated under reflux for 15 h. The heating was removed. To a still warm solution, 5 mL of 2M HCl was added and the mixture was stirred for 15 min (during this time orange luminescence developed). The volume of the mixture was reduced to approximately 3 mL. This caused formation of solid residue and transparent aqueous layer. The aqueous layer was decanted. The residue was triturated with methanol (25 mL), filtered and the solid on filter was washed with methanol. The solid was dissolved in dichloromethane and filtered through Celite. To the filtrate, methanol (5 mL) was added and the mixture was reduced to a volume of 2 mL, causing formation of solid. The solid was filtered off and washed with methanol to give the desired product as an orange solid.

Yield: 0.143 g, 0.0869 mmol, 87%.

^{1}H NMR (400 MHz, $CDCl_3$): δ 11.86 (s, 1H), 8.53 (s, 1H), 8.12 (br s, 4H), 7.91 (br d, 2H, *J* = 7.8), 7.74 (d, 4H, *J* = 6.0), 6.92 (m, 6H), 6.78 (br t, 2H, *J* = 7.8), 5.78 (d, 2H, *J* = 7.7), 4.21 (t, 4H, *J* = 6.4), 1.91 (m, 4H), 1.61 (m, 4H), 1.43 (m, 8H), 1.32 (s, 36H), 0.97 (t, 6H, *J* = 6.9).

^{19}F NMR (400 MHz, $CDCl_3$): δ -126.4 (s).

^{13}C NMR DEPT135 (100 MHz, $CDCl_3$): δ 171.51 (), 161.65 (), 150.49(CH), 141.09 (CH), 136.78 (CH), 132.04 (CH), 126.40 (CH), 121.79 (CH), 120.59 (CH), 120.00 (CH), 75.6(CH_2), 35.08 (C-tBu), 31.78 (CH_2), 30.60 (CH_3), 30.26 (CH_2), 25.65 (CH_2), 22.77 (CH_2), 14.20(CH_3).

HRMS (FTMS^{+}): for $[M\text{-}Cl]^{+}$ calc'd 1609.5539, found 1609.5524; for $[M+Na]^{+}$ calc'd 1667.5108, found 1667.5055.

Compound 3.3.11

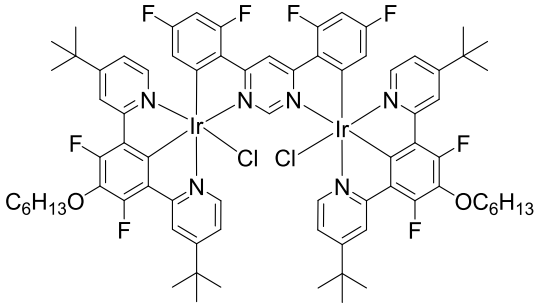

To a mixture of compound **3.5.1** (0.148 g, 0.200 mmol) and 4,6-bis(2,4-difluorophenyl)pyrimidine (0.030 g, 0.100 mmol) and toluene (30 mL), silver triflate (0.077 g, 0.300 mmol) was added and the mixture was heated under reflux for 15 h. The heating was removed. To a still warm solution, 5 mL of 2M HCl was added and the mixture was stirred for 15 min (during this time orange luminescence developed). The volume of the mixture was reduced to approximately 5 mL. The residue was triturated with methanol (40 mL), filtered and the solid on filter was washed with methanol. The solid was dissolved in dichloromethane and filtered through Celite. To the filtrate, methanol (5 ml) was added and the mixture evaporated to a volume of 2 mL causing formation of solid. The solid was filtered off, washed on filter with methanol to give the desired product as an orange solid.

Yield: 0.116 g, 0.0676 mmol, 68%.

^{1}H NMR (400 MHz, $CDCl_3$): δ 11.93 (s, 1H), 9.30 (br t, 1H, *J* = 3.7), 8.15 (d, 4H, *J* = 1.8), 7.79 (d, 4H, *J* = 6.0), 6.97 (dd, 4H, *J* = 6.0, 1.8), 6.38 (ddd, 2H, *J* = 11.2, 8.8, 2.4), 5.78 (dd, 2H, *J* = 8.8, 2.4), 4.21 (t, 4H, *J* = 6.4), 1.92 (m, 4H), 1.61 (m, 4H), 1.43 (m, 8H), 1.34 (s, 36H), 0.97 (t, 6H, *J* = 6.9).

^{19}F NMR (400 MHz): δ -103.3 (m), -105.6 (m), -126.9.

^{13}C NMR DEPT135 (100 MHz, $CDCl_3$): δ 160.3(CH), 150.1(CH), 120.7(CH), 120.1(CH), 118.4(d, *J* = 16.0, CH), 114.1(t, *J* = 20.7, CH), 98.1(t, *J* = 28.0, CH), 75.6(CH_2), 31.7(CH_2), 30.5(CH_3), 30.2(CH_2), 25.5(CH_2), 22.7(CH_2), 14.1(CH_3).

HRMS (FTMS^{+}): for $[M+Na]^{+}$ calc'd 1739.4731, found 1739.4670.

Compound 3.3.12

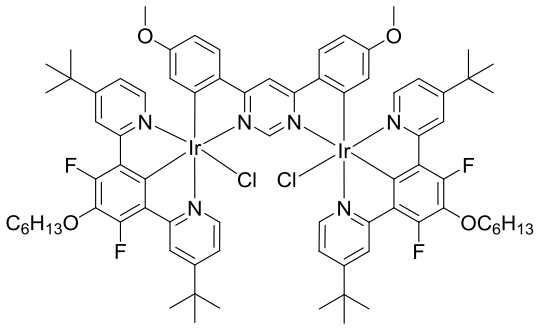

To a mixture of compound **3.5.1** (0.150 g, 0.200 mmol) and 4,6-bis(4-methoxyphenyl)pyrimidine (0.066 g, 0.220 mmol) in toluene (6 mL), silver triflate (0.067 g, 0.260 mmol) in toluene (1mL) was added. The reaction was heated to reflux for 8 h before the solution was allowed to cool to room temperature and the toluene removed under reduced pressure. The crude mixture was purified by column chromatography (silica gel, gradient elution, DCM:EtOAc 100:0→80:20). The product obtained after evaporation of the eluent was treated with methanol and filtered. The solid was recrystallized from DMSO, washed with methanol and dried under vacuum at 140°C for 24 h.

Yield: 0.057 g, 0.0334 mmol, 17%.

^{1}H NMR (400 MHz, $CDCl_3$): δ 11.65 (s, 1H), 8.23 (s,1H), 8.12 (s, 4H), 7.81 (d, 2H, *J* = 8.7), 7.78 (d, 4H, *J* = 6.0), 6.93 (dd, 2H, *J* = 6.0, 1.8), 5.75 (d, *J* = 2.8), 4.19 (t, 4H, *J* = 6.4), 3.55 (s, 6H) 1.91 (m, 4H), 1.61 (m, 9H), 1.49 (s, 2H), 1.42 (m, 8H), 1.33 (s, 36H), 1.25 (s, 6H), 0.96 (t, *J* = 6.9, 6H).

^{19}F NMR (400 MHz, $CDCl_3$): δ -126.49.

^{13}C DEPT135 (100 MHz, $CDCl_3$): δ 160.2, 150.4, 127.7, 120.5, 120.5, 119.9, 108.4, 104.8, 77.2, 75.6 (CH_2), 54.8, 31.7 (CH_2), 30.51, 30.2 (CH_2), 29.7 (CH_2), 25.6 (CH_2), 22.7 (CH_2), 14.1 (CH_3).

Compound 3.3.13

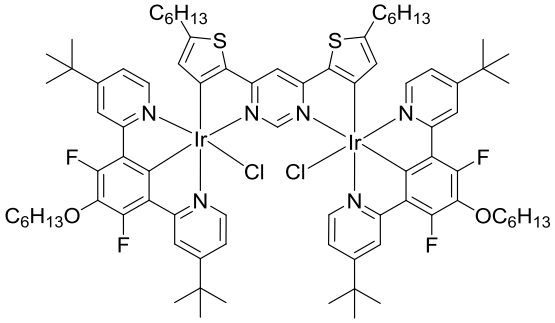

To a stirred solution of compound **3.2.1** (0.148 g, 0.200 mmol) and 4,6-di(5-hexylthiophenyl)pyrimidine (0.041 g, 0.100 mmol) in toluene (30 mL), silver triflate (0.077 g, 0.300 mmol) was added and the mixture was heated under reflux for 15 hours. The heating was removed. To a still warm solution 5 mL of 2M HCl was added and the mixture was stirred for 15 minutes (during this time orange luminescence developed). The mixture was evaporated to a volume of around 3 mL. This caused formation of solid residue and transparent aqueous layer. The aqueous layer was decanted. The residue was triturated with methanol (25 mL), filtered and the solid on filter was washed with methanol. The solid was then dissolved in DCM and filtered through Celite. To the filtrate, methanol (5 ml) was added and the mixture was evaporated to a volume of 2 ml causing formation of solid. The solid was filtered off, washed on filter with methanol to give the desired product as an orange solid.

Yield: 0.139 g, 0.0762 mmol, 76%.

^{1}H NMR (400 MHz, $CDCl_3$): δ 11.15 (s, 1H), 8.10 (s, 4H), 7.88 (d, 4H, *J* = 6.4), 7.39 (s, 1H), 7.00 (dd, 4H, *J* = 6.0, 1.6), 5.60 (s, 2H), 4.19 (t, 4H, *J* = 6.8), 2.62 (t, 4H, *J* = 7.8), 1.95-1.88 (m, 4H), 1.65-1.57 (m, 4H), 1.51-1.41 (m, 12H), 1.35 (s, 36H), 1.20-1.16 (m, 12H), 0.97 (t, *J* = 7.2, 6H), 0.81 (t, 6H, *J* = 6.8).

^{19}F NMR (400 MHz, $CDCl_3$): δ -126.76.

^{13}C DEPT135 (100 MHz, $CDCl_3$): δ 165.75, 164.97, 161.42, 160.53 (CH), 155.39, 151.12 (CH), 131.74, 131.41 (CH), 124.36, 119.96 (CH), 102.18 (CH), 100.11, 75.61 (CH_2), 35.00, 31.69 (CH_2), 31.32 (CH_2), 31.09 (CH_2), 30.63 (CH_2), 30.54 (CH_3), 30.18 (CH_2), 28.62 (CH_2), 25.57 (CH_2), 22.67 (CH_2), 22.50 (CH_2), 14.11 (CH_3), 13.99 (CH_3).

HRMS (FTMS$^+$): for $[M\text{-}Cl]^+$ calc'd 1789.6545, found 1789.6530; for $[M+Na]^+$ calc'd 1847.6114, found 1847.6053; for $[M+NH_4]$+ calc'd 1838.6525, found 1838.6506.

Compound 3.3.15

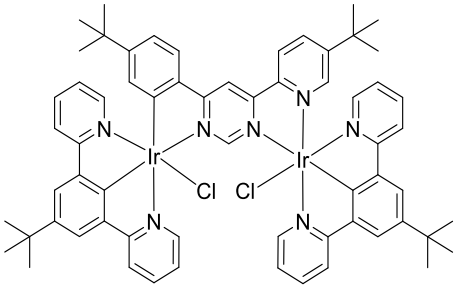

Compound **3.2.4** (0.162 g, 0.294 mmol) and 4,6-di-(4-tert-butylphenyl)pyrimidine (0.0515 g, 0.147 mmol) were placed in a round-bottomed flask with toluene (26 mL). Silver triflate (0.113 g, 0.441 mmol) was added and the reaction mixture heated to reflux for 8 h. The heat was then removed and to a still warm reaction mixture a 3M HCl solution (5 mL) was added and the mixture stirred for 5 min. The organic phase was separated and the solvent removed under reduced pressure. DCM (10 mL) was added and the solution filtered through Celite. Methanol (10 mL) was added in an attempt to crash out the product. The solvent was removed under reduced pressure. Diethyl ether (20 mL was added and the solid filtered in vacuo and the solid washed with diethyl ether. The NMR shows that the solid collected was the iridium dichloro-bridged dimer showing that the reaction had not gone to completion. The solvent was removed from the filtrate under reduced pressure and the residue was purified by column chromatography (silica gel, gradient elution, DCM:EtOAc 100:0→20:1→10:1 to DCM:MeOH 10:1). The product collected was further purified by column chromatography (silica gel, gradient elution, DCM:EtOAc 5:1 to DCM:MeOH 20:1 to 10:1) to give the desired bimetallic iridium complex.

Yield: 0.0305 g, 0.0221 mmol, 15%

^{1}H NMR (400 MHz, $CDCl_3$): δ 11.76 (s, 1H), 8.41 (s, 1H), 8.04 (d, 4H, *J* = 5.5), 7.91-7.89 (m, 8H), 7.75 (d, 2H, *J* = 8.2), 7.62 (t, 4H, *J* = 7.8), 6.93 (t, 4H, *J* = 6.6), 6.84 (dd, 2H, *J* = 8.2, 1.8), 6.00 (d, 2H, *J* = 1.8), 1.54 (s, 18H), 0.92 (s, 18H).

HRMS (FTMS$^+$): for $[M\text{-}2Cl]^{2+}$ calc'd 651.2225, found 651.2217.

Compound 3.3.16

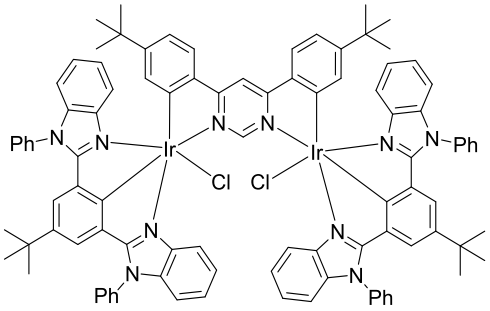

To the compound **3.2.5** (0.150 g, 0.192 mmol) in xylene (30 mL), silver trifluoromethanesulfonate (0.0777 g, 0.289 mmol) was added. 4,6-di(4-tert-butylphenyl)pyrimidine (0.0339 g, 0.0962 mmol) was then added and the reaction mixture heated to reflux for 8 h. To the cooled reaction mixture, dichloromethane (10 mL) was added and the mixture filtered in vacuo. The filtered solid was washed with dichloromethane. Concentrated hydrochloric acid (3 mL) was added to the filtrate and the resulting mixture stirred for 5 min. The resulting mixture was filtered through silica and the silica washed with excess dichloromethane. The filtrate was evaporated to dryness under reduced pressure and the residue treated with methanol (20 mL). The red solid was filtered off and washed with methanol.

Yield: 0.161 g, 0.0879 mmol, 91%

^{1}H NMR (400 MHz, $CDCl_3$): δ 8.51 (s, 1H), 7.75-7.68 (m, 20H), 7.46-7.44 (m, 3H), 7.39 (d, 4H, *J* = 8.2), 7.26-7.25 (m, 2H), 7.08-7.02 (m, 8H), 6.83-6.77 (m, 10H), 0.98 (s, 18H), 0.96 (s, 18H).

^{13}C DEPT135 (100 MHz, $CDCl_3$): δ 178.45 (C), 172.66 (C), 161.87 (C), 153.91 (C), 142.78 (C), 141.12 (C), 139.93 (C), 135.69 (C), 135.32 (C), 132.71 (CH), 131.66 (C), 130.31 (CH), 129.99 (CH), 129.90 (CH), 128.90 (CH), 128.71 (CH), 127.93 (CH), 125.35 (CH), 124.85 (CH), 122.78 (CH), 122.22 (CH), 118.04 (CH), 116.01 (CH), 110.33 (CH), 34.53 (C), 34.40 (C), 31.20 (*t*Bu), 30.85 (*t*Bu).

HRMS (FTMS$^+$): for $[M\text{-}Cl]^+$ calc'd 1797.5826, found 1797.5836; for $[M+2Na]^{2+}$ calc'd 881.3072, found 881.3067.

Compound 3.3.17

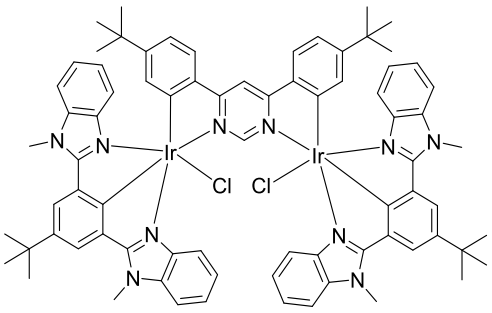

To compound **3.2.6** (0.150 g, 0.230 mmol) in toluene (30 mL), silver trifluoromethanesulfonate (0.0886 g, 0.345 mmol) was added. 4,6-di(4-tert-butylphenyl)pyrimidine (0.0396 g, 0.115 mmol) was then added and the reaction mixture heated to reflux for 18 h. The reaction mixture was removed from the heat. To the still warm reaction mixture, dichloromethane (10 mL) and 3M HCl (8 mL) were added. The resulting mixture stirred for 15 min before being filtered through Celite. The Celite was washed with excess DCM. The filtrate was evaporated to dryness under reduced pressure and the residue was purified by column chromatography (silica gel, gradient elution, DCM:EtOAc 10:1→5:1 to DCM:MeOH 10:1) to give the desired bimetallic iridium complex.

Yield: 0.060 g, 0.0380 mmol, 60%

^{1}H NMR (400 MHz, d^{6}-DMSO): δ 12.37 (s, 1H), 8.97 (s, 1H), 8.18 (br s, 4H), 8.02 (d, 2H, *J* = 7.3), 7.67 (d, 4H, *J* = 8.2), 7.19-7.16 (m, 4H), 7.02-7.00 (m, 4H), 6.75-6.72 (m, 2H), 6.59-6.56 (m, 4H), 5.84 (m, 2H), 4.47 (br s, 12H), 1.65 (s, 18H), 0.90 (s, 18H).

HRMS (FTMS^{+}): for $[M\text{-}2Cl]^{2+}$ calc'd 757.2757, found 757.2752.

Compound 3.3.18

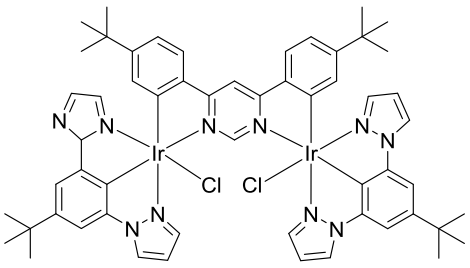

To compound **3.2.7** (0.150 g, 0.284 mmol) in toluene (40 mL), silver trifluoromethanesulfonate (0.109 g, 0.426 mmol) was added. 4,6-di(4-tert-butylphenyl)pyrimidine (0.0489 g, 0.142 mmol) was then added and the reaction mixture heated to reflux for 18 h. The reaction mixture was removed from the heat. To the still warm reaction mixture, 3M HCl (8 mL) was added and the reaction mixture stirred for 10 min. The resulting mixture was filtered through Celite and the Celite washed with excess dichloromethane. The bright orange filtrate was evaporated to dryness under reduced pressure. The orange residue was purified by column chromatography (silica gel, gradient elution, DCM:EtOAc 10:1→5:1→1:1 to DCM:MeOH 10:1) leading to isolation of the desired dinuclear complex.

Yield: 0.110 g, 0.0828 mmol, 58%

^{1}H NMR (400 MHz, $CDCl_3$): δ 11.47 (s, 1H), 8084 (s, 1H), 8.78 (d, 4H, *J* = 2.8), 8.08 (d, 2H, *J* = 8.2), 7.76 (s, 4H), 7.51 (d, 4H, *J* = 1.2), 6.80 (d, 2H, *J* = 8.2), 6.48 (t, 4H, *J* = 2.3), 5.87 (br s, 2H), 1.60 (s, 18H), 0.90 (s, 18H).

HRMS (FTMS$^+$): for $[M\text{-}2Cl]^{2+}$ calc'd 629.2150, found 629.2108.

3.8.4 2,5-Pyrazine- vs. Thiazole-Linked Dinuclear Iridium(III) Complexes

Compound 3.4.1 – 2,5-Bis(4-tert-butylphenyl)pyrazine[262]

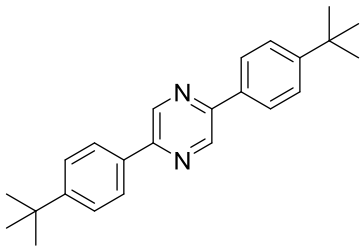

3,6-Bis(4-tert-butylphenyl)pyrazine (0.306 g, 1.29 mmol), (4-tert-butylphenyl)boronic acid (0.596 g, 3.35 mmol) and a 2M aqueous potassium carbonate solution (1.07 g, 7.72 mmol, 3.86 mL) were added to a round-bottomed flask. 1,4-Dioxane (10 mL) was added. The mixture was degassed under argon for 15 min. Tetrakis(triphenylphosphine)palladium (0.0892 g, 0.0772 mmol) was added and the reaction mixture degassed for a further 10 minutes. The reaction was heated to 95 °C for 65 h. The reaction was cooled to room temperature. Toluene (20 mL) was

added. The organic layer was separated and washed with water (2 x 10 mL). The organic phase was dried and evaporated to dryness. To the pale green residue, a small amount of methanol was added and a precipitate formed. The solid was filtered *in vacuo* and washed with further methanol. The product was obtained as a white solid.

Yield: 0.378 g, 1.10 mmol, 85%

^{1}H NMR (400 MHz, $CDCl_3$): δ 9.05 (s, 2H, *J* = 3.6), 8.00 (d, 4H, *J* = 8.8), 7.55 (d, 4H, *J* = 8.8), 1.38 (s, 18H).

^{13}C DEPT135 NMR (100 MHz, $CDCl_3$): δ 153.00 (C), 150.33 (C), 141.05 (C-H), 133.54 (C), 126.44 (CH), 126.05 (CH), 34.81 (C), 31.25 (CH_3).

HRMS (FTMS^{+}): for $[M+H]^{+}$ calc'd 345.2325, found 345.2326.

Compound 3.4.5 - 2,5-bis(4-tert-butylphenyl)-3aH,6aH-[1,3]thiazolo[5,4-d][1,3]thiazole

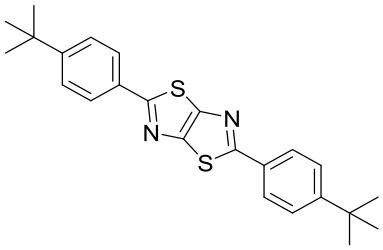

4-*tert*-butylbenzaldehyde (1.01 g, 6.22 mmol) and dithiooxamide (0.374 g, 3.11 mmol) were added to a round-bottomed flask. DMF (30 mL) was added and the reaction mixture was heated to reflux for 24 h. The reaction mixture was cooled to room temperature and further cooled in an ice bath. The mixture was filtered *in vacuo* and the product was isolated as a green solid.

Yield: 0.459 g, 1.13 mmol, 36 %

^{1}H NMR (400 MHz, $CDCl_3$): δ 7.93 (d, 4H, *J* = 8.7), 7.51 (d, 4H, *J* = 8.2), 1.37 (s, 18H).

^{13}C DEPT135 NMR (100 MHz, $CDCl_3$): δ 169.03 (C), 154.17 (C), 150.60 (C), 131.34 (C), 126.17 (CH), 126.09 (C-H), 34.97 (C), 31.18 (CH_3).

HRMS (FTMS^{+}): for $[M+H]^{+}$ calc'd 407.1610, found 407.1606.

Compound 3.4.4

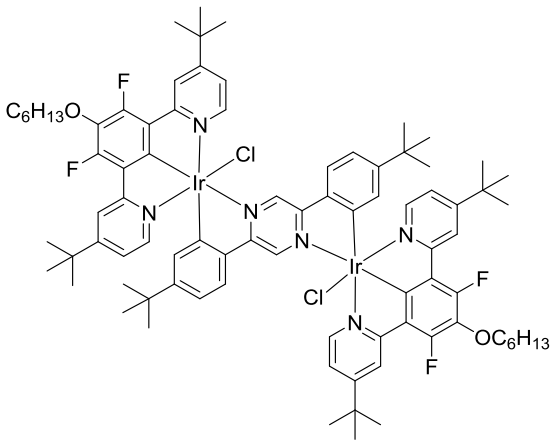

Compound **3.2.1** (0.148 g, 0.200 mmol), 2,5-bis(4-tert-butylphenyl)pyrazine (0.0340 g, 0.100 mmol) and toluene (25 mL) were added to a round-bottomed flask. Silver triflate (0.0770 g, 0.300 mmol) was added and the reaction mixture was heated under reflux for 17 hours. The heating was removed and, to a still warm mixture, 2M HCl (5 mL) was added. Toluene was evaporated leaving a suspension of the product in aqueous medial. The solid was separated, triturated with methanol and filtered. The solid was then dissolved in DCM (20 mL) and filtered through Celite. To the filtrate, methanol (40 mL) was added the volume of the mixture was reduced to approximately 10 mL using rotary evaporator. The red solid was filtered off, washed with little amount of methanol. The product was isolated as a red solid.

Yield: 0.112 g, 0.0637 mmol, 64%

^{1}H NMR (400 MHz, $CDCl_3$): δ 10.77 (s, 2H), 8.40 (s,1H), 8.15 (s, 4H), 7.89 (d, *J* = 8.0 Hz, 2H), 7.63 (d, *J* = 5.9 Hz, 4H), 6.90 (m,6H), 6.18 (d, *J* = 1.6 Hz, 2H), 4.23 (t, *J* = 6.5 Hz, 4H), 1.94 (m, 4H), 1.62 (m, 4H), 1.44 (m, 8H), 1.33 (s, 36H), 1.00 (s, 18H), 0.97 (t, *J* = 6.9 Hz, 6H).

^{19}F NMR (400 MHz): δ -126.5.

(MALDI MS): for $[M]^+$ calc'd 1756.6, found 1756.6.

Compound 3.4.8

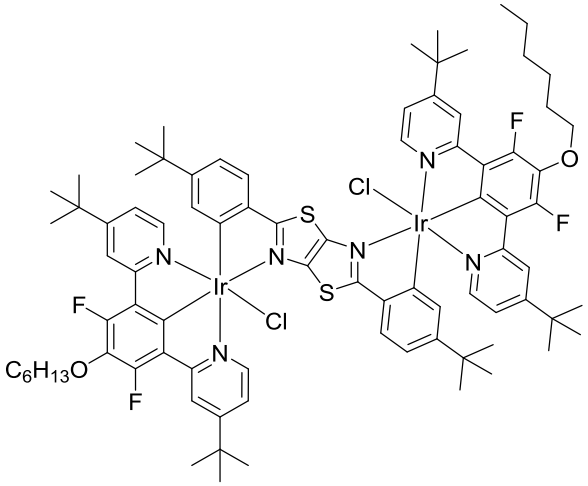

Compound **3.2.1** (0.149 g, 0.201 mmol) was added to a round-bottomed flask. Toluene (30 mL) was added and the mixture was stirred. Silver triflate (0.0774 g, 0.301 mmol) was added. Bis(4-*tert*-butylphenyl)-[1,3]thiazole[5,4-d][1,3]thiazole (0.0408 g, 0.100 mmol) was added and the reaction mixture heated to reflux for 17 h. The reaction mixture was removed from the heat and 3M hydrochloric acid solution (7 mL) was added. The mixture was stirred for a 10 min. The organic layer was separated and the solvent evaporated to dryness. The crude product was purified by column chromatography (silica gel, gradient elution, DCM:EtOAc) giving the product as a yellow solid.

Yield: 0.100 g, 0.0550 mmol, 55%

^{1}H NMR (400 MHz, $CDCl_3$): δ 8.14 (s, 4H), 7.82-7.80 (m, 4H), 7.52-7.50 (m, 2H), 6.98 (dd, 4H, *J* = 6.2, 1.8), 6.79 (dd, 2H, *J* = 8.2, 1.8), 6.08 (d, 2H, *J* = 0.4), 4.23 (t, 4H, *J* = 6.8), 1.97-1.90 (m, 4H), 1.66-1.59 (m, 4H), 1.48-1.42 (m, 8H), 1.34 (s, 36H), 0.97-0.96 (m, 24H).

^{19}F NMR (400 MHz): δ -126.67.

^{13}C NMR DEPT135 (100 MHz, $CDCl_3$): δ 180.11 (C), 171.60 (C), 167.34 (C), 165.60 (C), 161.78 (C), 156.50 (C), 153.86 (C), 153.57 (C), 151.36 (CH), 149.45 (C), 147.05 (C), 145.30 (C), 138.22 (C), 132.49 (CH), 124.46 (CH), 124.14 (C), 120.42 (CH), 119.54 (CH), 35.14 (C), 34.62 (C), 31.81 (CH_2), 31.01 (tBu), 30.61 (tBu), 30.26 (CH_2), 29.81 (CH_2), 25.67 (CH_2), 22.78 (CH_2) 14.28 (CH_3).

(MALDI MS): for $[M]^+$ calc'd 1818.6, found 1818.6.

3.8.5 2,3-Pyrazine-Linked Dinuclear Iridium(III) Complexes

Compound 3.5.1 - 1,2-Bis(4-tert-butylphenyl)-2-hydroxyethan-1-one[263]

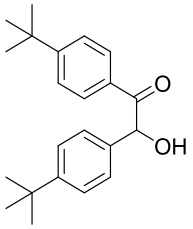

To a mixture of 4-(tert-butyl)benzaldehyde (5.00 g, 30.8 mmol) in ethanol:water (14:8.75 mL), was added potassium cyanide (0.435 g, 6.68 mmol) was added. The reaction mixture was refluxed under argon for 6 h. The reaction mixture was cooled to room temperature. The reaction mixture was filtered and the grey solid obtained washed with water. This crude product was recrystallised from methanol (≈65 mL). The product was isolated as an off-white solid.

Yield: 2.13 g, 6.56 mmol, 98%

^{1}H NMR (400 MHz, $CDCl_3$): δ 7.89 (d, 2H, J = 8.0), 7.42 (d, 2H, J = 8.8), 7.35 (d, 2H, J = 8.4), 7.27 (d, 2H, J = 8.4), 5.91 (d, 1H, *J* = 6.4), 4.52 (d, 1H, *J* = 6.0), 1.29 (s, 9H), 1.27 (s. 9H).

Compound 3.5.2 - Bis(4-tert-butylphenyl)ethane-1,2-dione[263]

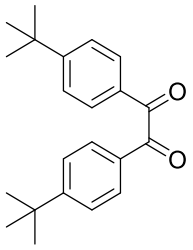

1,2-Bis(4-tert-butylphenyl)-2-hydroxyethan-1-one (1.01 g, 3.08 mmol), copper(II) acetate monohydrate (1.23 g, 6.16 mmol) and ammonium nitrate (0.111 g, 1.39 mmol) were added to a round-bottomed flask. Acetic acid (80%, 15 mL) was added. The reaction mixture was refluxed for 3 h. The reaction was cooled to room temperature and filtered *in vacuo*. The solid was washed

with water, methanol and ethyl acetate. The filtrate was separated and the organic layer was dried with sodium sulphate. The solvent was evaporated to dryness. To the residue, methanol was added and the flask placed in an ice bath. The resulting solid was filtered *in vacuo* and washed with cold methanol. The product was obtained as an off-white solid.

Yield: 0.672 g, 2.08 mmol, 68%

^{1}H NMR (400 MHz, $CDCl_3$): δ 7.91 (d, 4H, *J* = 8.7), 7.52 (d, 4H, *J* = 8.7), 1.34 (s, 18H).

^{13}C NMR (100 MHz, $CDCl_3$): δ 194.68 (C), 159.00 (C), 130.63 (C), 130.00 (CH), 126.11 (CH), 35.49 (C), 31.08 (CH_3).

Compound 3.5.3 – 5,6-bis(4-tert-butylphenyl)-2,3-dihydropyrazine

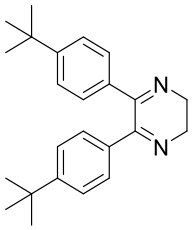

Ethylene diamine (0.0676 g, 1.13 mmol) was added slowly to a solution of bis(4-tert-butylphenyl)ethane-1,2-dione (0.302 g, 0.938 mmol) in ethanol at room temperature. The reaction mixture was refluxed for 3 h. The reaction was cooled to room temperature and the solvent was evaporated to dryness. The crude product was obtained as an off-white solid and was used in the next step without further purification.

Yield: 0.310 g, 0.894 mmol, 95%

^{1}H NMR (400 MHz, $CDCl_3$): δ 7.39-7.36 (m, 4H), 7.30-7.26 (m, 4H), 3.65 (s, 4H), 1.28 (s, 18H).

Compound 3.5.4 – 2,3-bis(4-tert-butylphenyl)pyrazine

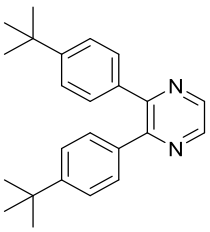

To 5,6-bis(4-tert-butylphenyl)-2,3-dihydropyrazine (0.310 g, 0.889 mmol), sulphur powder (0.0570 g, 1.78 mmol) was added and the mixture heated to 140 °C for 30 min. The reaction mixture was cooled to room temperature. The crude reaction mixture was purified by column chromatography (silica gel, hexane:ethyl acetate 10:1) to give the product as an off-white solid.

Yield: 0.106 g, 0.309 mmol, 35%

^{1}H NMR (400 MHz, $CDCl_3$): δ 8.55 (s, 2H), 7.42 (d, 4H, *J* = 8.2), 7.32 (d, 4H, *J* = 8.2), 1.31 (s, 18H).

^{13}C DEPT135 NMR (100 MHz, $CDCl_3$): δ 152.63 (C), 151.74 (C), 141.69 (CH), 135.82 (C), 129.19 (CH), 125.21 (CH), 34.65 (C), 31.25 (CH_3).

Compound 3.5.6 - 1,4-diazatriphenylene

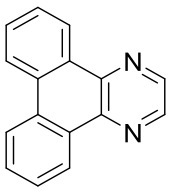

Ethylenediamine (0.341 g, 5.67 mmol) was added to a solution of 9,10-phenanthrenequinone (0.984 g, 4.73 mmol) in ethanol (50 mL) at room temperature with stirring. The reaction mixture was heated to reflux for 48 h. The reaction mixture was cooled to room temperature. The yellow precipitate formed was filtered and washed with excess ethanol until the washing became colourless. The product was isolated as an off-white solid.

Yield: 0.389 g, 1.69 mmol, 36%

^{1}H NMR (400 MHz, $CDCl_3$): δ 9.16 (dd, 2H, *J* = 8.0, 1.6), 9.08 (s, 2H), 8.88 (d, 2H, *J* = 8.2), 7.93-7.88 (m, 2H), 7.52-7.81 (m, 2H).

^{13}C DEPT135 NMR (100 MHz, $CDCl_3$): δ 143.61 (CH), 141.55 (C), 131.51 (C), 129.97 (C), 129.69 (CH), 127.80 (CH), 125.47 (CH), 122.85 (CH).

Compound 3.5.5

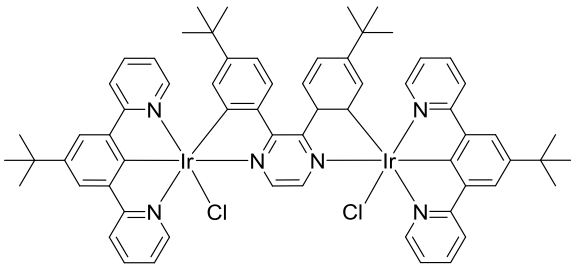

Compound **3.2.4** (0.163 g, 0.295 mmol) and toluene (40 mL) were placed in a round-bottomed flask and silver triflate (0.114 g, 0.443 mmol) was added. The reaction mixture was stirred. 2,3-Bis(4-tert-butylphenyl)pyrazine (0.0508 g, 0.148 mmol) was added and the reaction mixture was heated to reflux for 8 h. The heat was then removed from the reaction mixture and 2M HCl (7 mL) was added. The reaction mixture was then stirred for a further 10 min. The organic layer was separated and the solvent evaporated to dryness. The orange-red residue was treated with methanol (10 mL) and filtered. The resulting solid was filtered *in vacuo* and the solid washed with a small amount of methanol. The solid collected was dissolved in dichloromethane and the solution gravity filtered. The filtrate was evaporated to dryness and the red-orange precipitate treated with a small amount of methanol and the solid filtered *in vacuo*. The crude product was purified by column chromatography (silica gel, gradient elution, DCM:EtOAc 10:1→10:3). The desired product was isolated as a red solid.

Yield: 0.0233 g, 0.0170 mmol, 11%

^{1}H NMR (400 MHz, $CDCl_3$): δ 9.92 (s, 1H), 8.39 (d, 2H, *J* = 8.7), 8.32-8.27 (m, 4H), 8.24 (s, 2H), 8.12 (s, 2H), 7.93-7.82 (m, 6H), 7.71 (d, 2H, *J* = 8.2), 7.14 (q, 4H, *J* = 6.3), 6.46 (dd, 2H, *J* = 8.7, 1.8), 5.86 (d, 2H, *J* = 1.8), 1.56 (s, 18H), 0.76 (s, 18H).

HRMS (FTMS^{+}): for $[M-2H]^{2+}$ calc'd 685.1823, found 685.1815.

Compound 3.5.10

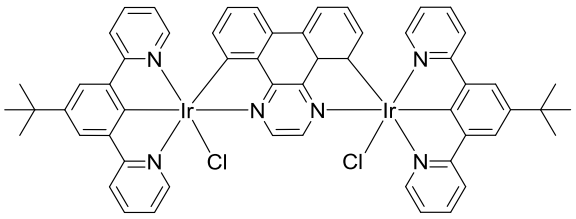

Compound **3.2.4** (0.152 g, 0.275 mmol) and toluene (40 mL) were placed in a round-bottomed flask and silver triflate (0.106 g, 0.413 mmol) was added. The reaction mixture was stirred. 1,4-diazatriphenylene (0.0317 g, 0.138 mmol) was added and the reaction mixture was heated to reflux for 17 h. The heat was then removed from the reaction mixture and 3M HCl (8 mL) was added. The reaction mixture was then stirred for a further 10 min. The organic layer was separated and the solvent evaporated to dryness. The crude product was purified by column chromatography (silica gel, DCM 100:0). The desired product was isolated as a dark red solid.

Yield: 0.0300 g, 0.0238 mmol, 17%

^{1}H NMR (400 MHz, $CDCl_3$): δ 10.49 (s, 2H), 7.98 (s, 4H), 7.93 (d, 4H, *J* = 7.8), 7.75 (d, 2H, *J* = 7.8), 7.70 (d, 4H, *J* = 5.5), 7.58 (t, 4H, *J* = 7.8), 6.99 (t, 2H, *J* = 7.6), 6.79 (t, 4H, *J* = 6.6), 6.25 (d, 2H, *J* = 7.3), 1.58 (s, 18H).

HRMS (FTMS$^+$): for $[M+H]^+$ calc'd 1257.2415, found 1257.2318.

3.8.6 3,6-Pyridazine-Linked Dinuclear Iridium(III) Complexes

Compound 3.6.5 – 3,6-Bis(4-tert-butylphenyl)pyridazine[257]

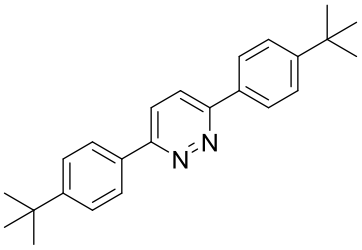

3,6-Dichloropyridazine (0.497 g, 3.33 mmol), (4-tert-butylphenyl)boronic acid (1.54 g, 8.67 mmol) and a 2M aqueous potassium carbonate solution (2.76 g, 20.0 mmol, 10.0 mL) were added

to a round-bottomed flask. 1,4-Dioxane (25 mL) was added. The mixture was degassed under argon for 20 min. Tetrakis(triphenylphosphine)palladium (0.231 g, 0.200 mmol) was added and the reaction mixture degassed for a further 10 minutes. The reaction was heated to 95 °C for 42 h. The reaction was cooled to room temperature. A precipitate formed and this precipitate was filtered *in vacuo*. The solid was then recrystallised from dimethlformamide to give the product as a lustrous white solid.

Yield: 0.659 g, 1.91 mmol, 57%

^{1}H NMR (400 MHz, $CDCl_3$): δ 8.11 (d, 4H, *J* = 8.2), 7.90 (s, 2H), 7.57 (d, 4H, *J* = 8.2), 1.39 (s, 18H).

^{13}C DEPT135 NMR (100 MHz, $CDCl_3$): δ 157.24 (C), 153.28 (C), 133.33 (C), 126.58 (CH), 126.02 (CH), 123.86 (CH), 34.83 (C-*t*Bu), 31.26 (*t*Bu).

Compound 3.6.8

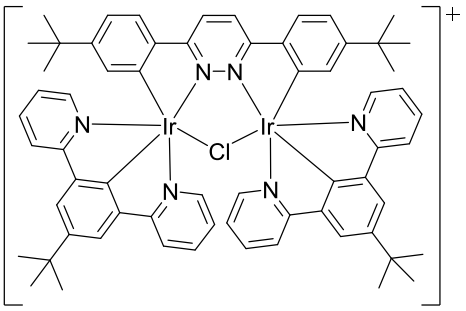

Compound **3.2.4** (0.170 g, 0.308 mmol) was added to a round-bottomed flask. Toluene (30 mL) was added and the mixture stirred. Silver triflate (0.122 g, 0.463 mmol) was added. 3,6-Bis(4-tert-butylphenyl)pyridazine (0.0531 g, 0.154 mmol) was added and the reaction mixture was heated to reflux for 15 h. The reaction mixture was removed from the heat and 3M hydrochloric acid solution (7 mL) was added. The mixture was stirred for a 5 min. The solvent was evaporated to dryness. A solution of 1:1 acetonitrile:water (4 mL) was added to the residue. To the solution formed, excess saturated aqueous ammonium hexafluorophosphate solution was added. An orange solid precipitated and was filtered *in vacuo* to give the crude product (0.233 g, 0.174

mmol). The crude solid was purified by column chromatography (silica gel, DCM:EtOAc 10:1). The product was isolated as a bright yellow solid.

Yield: 0.0781 g, 0.0584 mmol, 38%

^{1}H NMR (400 MHz, $CDCl_3$): δ 8.72 (s, 2H), 8.00 (d, 4H, *J* = 5.0), 7.71 (dd, 6H, *J* = 8.2, 3.2), 7.69 (s, 4H), 7.50 (td, 4H, *J* = 7.3, 1.8), 6.94-6.92 (m, 6H), 6.00 (d, 2H, *J* = 1.8), 1.37 (s, 18H), 0.87 (s, 18H).

^{19}F NMR (400 MHz, $CDCl_3$): δ -71.8

HRMS (FTMS^{+}) for $[M]^{+}$ calc'd 1337.4129, found 1337.4144; for $[M\text{-}(Ir(NCN))\text{-}Cl]^{+}$ calc'd 823.0780, found 823.3359.

3.8.7 Variation of Monodentate Ligand

Compound 3.3.14

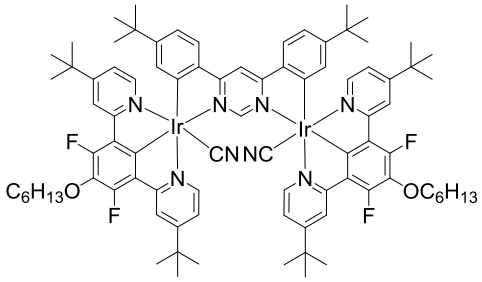

To a solution of compound **3.3.7** (0.088 g, 0.0500 mmol) in dichloromethane (15 mL), a solution of KCN (0.065 g, 1.00 mmol) in methanol (15 mL) was added and the mixture was stirred at RT for 4 h. The mixture was then reduced to a volume of 2-3 mL. Methanol (10 mL) was then added. The yellow solid was filtered off, washed with methanol and dried.

Yield: 0.065 g, 0.0374 mmol, 75%.

^{1}H NMR (400 MHz, $CDCl_3$): δ 11.47 (s, 1H), 8.47 (s,1H), 8.15 (br s, 4H), 7.87 (d, 2H, *J* = 8.0), 7.83 (d, 4H, *J* = 5.9), 7.00 (dd, 2H, *J* = 8.0, 1.6), 6.93 (dd, 4H, *J* = 5.9, 1.6), 6.30 (d, 2H, *J* = 1.6), 4.22 (t, 4H, *J* = 6.5), 1.94 (m, 4H), 1.64 (m, 4H), 1.44 (m, 8H), 1.34 (s, 36H), 1.02 (s, 18H), 0.97 (t, 6H, *J* = 6.9).

^{19}F NMR (400 MHz, $CDCl_3$): δ -126.5.

^{13}C NMR DEPT135 (100 MHz, $CDCl_3$): δ 164.5(CH), 150.4(CH), 132.5(CH), 125.9(CH), 120.5(CH), 120.1(CH), 120.0(CH), 107.4(CH), 75.8(CH_2), 31.7(CH_2), 30.9 (CH_3), 30.5(CH_3), 30.1(CH_2), 25.6(CH_2), 22.7(CH_2), 14.1(CH_3).

HRMS (FTMS$^+$) for $[M+H]^+$ calc'd 1739.7252, found 1739.7240.

Compound 3.7.1

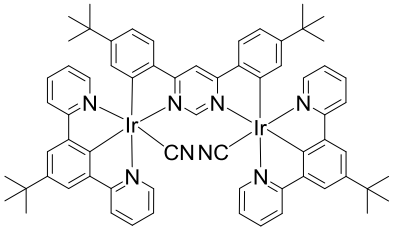

To compound **3.3.15** (0.0200 g, 0.0145 mmol) in dichloromethane (3 mL), potassium cyanide (0.0224 g, 0.291 mmol) in methanol (3 mL) was added. The reaction mixture was stirred at room temperature for 4 h. The solvent was evaporated to dryness and the residue treated with a small amount of methanol. The resulting solid was filtered to give the desired product.

Yield: 0.0156 g, 0.0115 mmol, 79%

^{1}H NMR (400 MHz, $CDCl_3$): δ 11.57 (s, 1H), 8.46 (s, 1H), 8.07 (d, 4H, *J* = 5.0), 7.94-7.93 (m, 8H), 7.81 (d, 2H, *J* = 8.2), 7.66 (t, 4H, *J* = 7.8), 6.92 (t, 6H, *J* = 6.6), 6.00 (m, 2H), 1.55 (s, 18H), 0.90 (s, 18H).

Compound 3.7.2

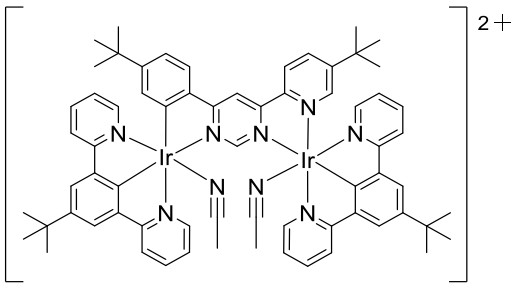

To compound **3.3.15** (0.118 g, 0.0861 mmol), silver triflate (0.0663 g, 0.258 mmol) was added. To this acetonitrile (2 mL) was added. The reaction mixture was stirred at room temperature under

argon for 15 h. To the reaction mixture, a small amount of acetonitrile was added and the mixture filtered through Celite. The filtrate was evaporated to dryness. To the residue, a small amount of acetonitrile was added. To the solution, excess saturated aqueous ammonium hexafluorophosphate solution was added. A solid precipitated and was filtered *in vacuo* and washed with water. The product was obtained as an orange-yellow solid.

Yield: 0.115 g, 0.0830 mmol, 96%

^{1}H NMR (400 MHz, $CDCl_3$): δ 10.63 (s, 1H), 8.49 (s, 1H), 8.19 (d, 4H, *J* = 5.0), 7.91 (t, 8H, *J* = 3.9), 7.76 (td, 6H, *J* = 7.7, 1.4), 7.21 (ddd, 4H, *J* = 6.0, 1.8, 1.4), 6.88 (dd, 2H, *J* = 8.2, 1.8), 5.89 (d, 2H, *J* = 1.8), 2.12 (s, 6H), 1.58 (s, 18H), 0.90 (s, 18H).

^{19}F NMR (400 MHz, $CDCl_3$): δ -70.69, -72.59

HRMS (FTMS^{+}) for $[M+H]^{+}$ calc'd 1739.7252, found 1739.7240.

Chapter 4

Conclusions and Further Work

4.0 Conclusions and Further Work

The aim of this project was to synthesise and investigate novel bimetallic emitters in which the metal centres are rigidly-linked by cyclometallating bridging ligands and to assess the suitability of such complexes for application in OLEDs and bioimaging.

The first section of this work was concerned with shifting the absorption and emission of dinuclear complexes to the red. Two strategies were used to achieve this, including the introduction of a second metal centre and extension of the conjugation length of the ligand. The di-platinum(II) complexes shown in Figure 148 were successfully prepared and shown to emit in the red and near-infrared regions of the spectrum. Work to evaluate these complexes as emitters in OLED devices is in progress and the results will be published in due course.

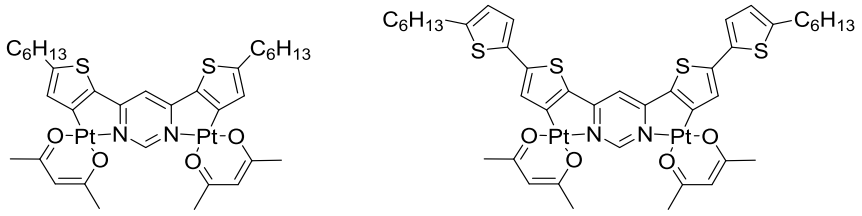

2.1.1
λ_{max} **610 nm**
Φ **0.85**

2.1.2
λ_{max} **730 nm**
Φ **0.15**

Figure 148: A figure to show the structures of orange- and red-emitting dinuclear platinum(II) complexes, **2.1.1** and **2.1.2**, prepared using bis-bidentate ligands incorporating electron-rich thiophene moieties and extended conjugation lengths.

Additionally, an unprecedented di-platinum(II) complex, in which the two Pt(II) centres were linked via a rigid, highly-conjugated bis-tetradentate ligand was synthesised. The identity of this complex, as shown in Figure 149, was confirmed. It is expected that the presence of two heavy metal centres, coupled with both the rigidity and highly-conjugated nature of the bis-tetradentate ligand, will give this dinuclear complex excellent photophysical properties being ideal for application as an emitter in OLEDs. Work is now ongoing to investigate the photophysical properties of this novel di-platinum(II) complex and its suitability for application in an OLED device.

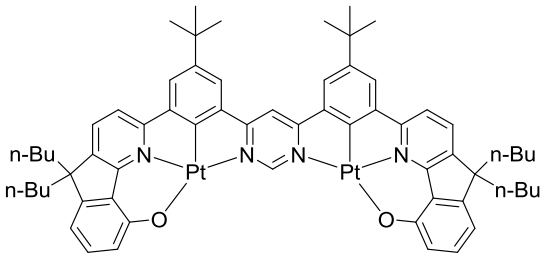

2.2.24

Figure 149: The structure of the novel dinuclear platinum(II) complex **2.2.24**, prepared in which the two metal centres are linked via a rigid bis-tetradentate ligand.

The second part of this work was concerned with the synthesis and photophysical investigation of dinuclear iridium(III) complexes. More specifically, those in which the metal centres were rigidly-linked via cyclometallating bis-bidentate bridging ligands. Firstly, dinuclear complexes linked by pyrimidine-based bridging ligands, of the general structure shown in Figure 150, were studied. The design of these systems leads to the formation of only one dinuclear product, with the laborious separation of diastereoisomers previously reported for similar dinuclear iridium(III) complexes avoided. These complexes were found to have excellent photophysical properties, with quantum yields in the range ϕ = 0.88–1.0 and luminescence lifetimes between 0.4 and 0.6 μs. These properties are ideal for application in OLED devices. The facile colour tunability of the emission wavelengths for these dinuclear iridium(III) complexes was successfully demonstrated through variation of the terdentate N^C^N auxiliary ligand, the pyrimidine-based bis-bidentate bridging ligand and the monodentate ligand.

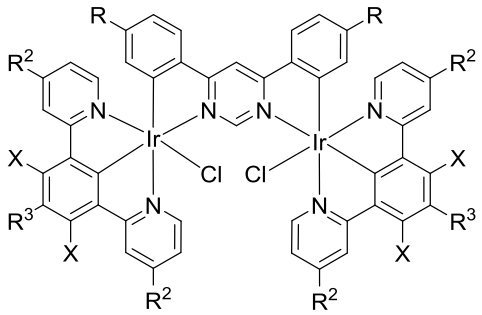

Figure 150: The general structure of our pyrimidine-linked dinuclear iridium(III) complexes.

Through the variation of the central heterocycle of the bis-bidentate bridging ligand, from 4,6-substituted pyrimidine to pyrazine and pyridazine, the effect of the bridging ligand structure on the properties of the resulting dinuclear iridium(III) complexes was evaluated. The alternative bridging ligands incorporated are shown in Figure 151 and were observed to have a significant effect on the properties of the dinuclear iridium(III) complexes obtained. The structural and photophysical properties of the resulting bimetallic Ir(III) complexes were studied, with the 3,6-pyridazine-linked complex being successfully applied in bioimaging applications. These dinuclear iridium(III) complexes show enormous potential for application in OLED devices and in bioimaging. Further work is required to obtain a deeper insight into the effect of the bis-bidentate bridging ligand structure on the photophysical properties of such complexes and also to thoroughly investigate the stability of these complexes in applications.

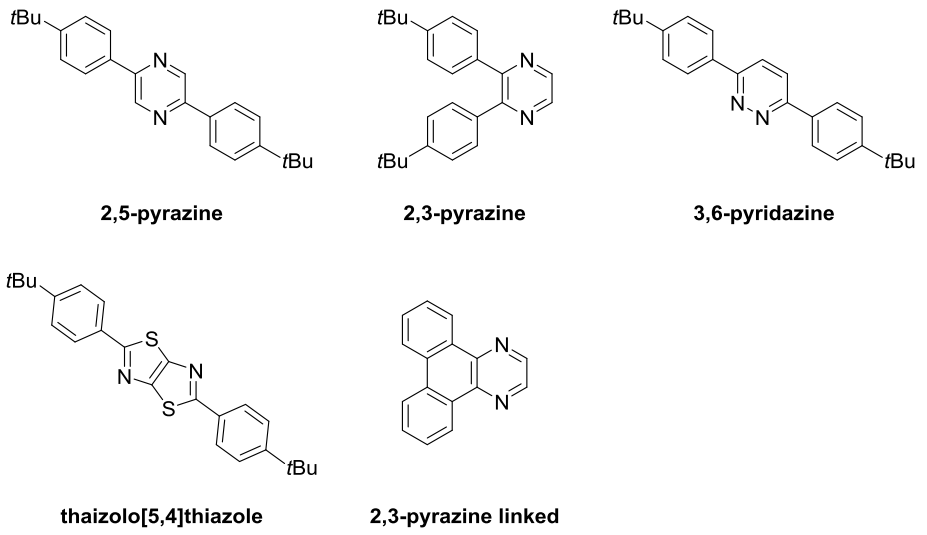

Figure 151: A figure to show the alternative bis-bidentate bridging ligands investigated in our dinuclear iridium(III) complexes.

The research completed in this project has highlighted the versatility and huge potential of dinuclear Pt(II) and Ir(III) complexes, rigidly-linked by cyclometallating bridging ligands, for utilisation in applications such as OLEDs and bioimaging.

Further study of these families of multimetallic complexes, including advanced optimisation of both their chemical and photophysical properties, is required in order to increase their suitability for use in the applications described above.

Of particular interest with regards to the dinuclear iridium(III) complexes discussed in chapter 3.0, is further work with variation of the monodentate ligands. The monodentate chloride ligands present in our dinuclear iridum(III) complexes are labile and therefore, the Ir-Cl bonds present a potential source of instability for these dinuclear iridium(III) complexes. Such instability is an issue with respect to application of such complexes in OLEDs as it may lead to device degradation and a reduction in device performance. Replacement of the chloride ligands with alternative monodentate ligands removes this source of instability and also offers additional opportunities for fine-tuning of the photophysiscal properties of our dinuclear iridium(III) complexes.

Although initial exploration of alternative monodentate ligands was discussed in section 3.7, further work in this area is required. In particular, investigation into the incorporation of monodentate acetylide ligands would be of interest, as this class of ligands have been shown to have a strong influence on the properties of luminescent metal complexes. Consequently, through variation of the R groups on the acetylide ligand, we may be able to further control and fine tune the photophysical properties of our dinuclear iridium complexes.[91, 258]

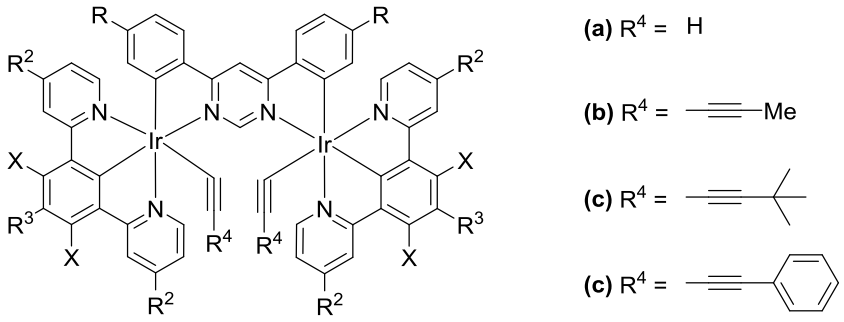

Figure 152: A figure to show the structure of acetylides that have the potential for use as monodentate ligands in our dinuclear iridium(III) complexes.[91, 258]

Figure 152 shows a selection of monodentate acetylide ligands that could be incorporated into our dinuclear iridium(III) complexes. The R groups present have a large effect on the size of the monodentate acetylide ligands and therefore will strongly influence whether incorporation of such ligands will be successful. In the presence of larger R groups, there may be unfavourable steric hinderance between the acetylide ligands. Conversely, the presence of an R group such as phenyl may allow favourable π-π stacking interactions between the acetylide ligands.

Further work is requied in order to assess the viability of incorpating such monodentate acetylide ligands into this class of dinuclear iridium(III) complexes and to investigate their effects on the photophysical properties.

Alternatively, rather than replacing the monodentate chloride with other monodentate ligands, it would be extremely interesting to investigate whether the addition of a bidentate ligand, capbable of linking the metal centres, would be possible. In addition, a study of the effects this has on both the structural and photophysical properties should be carried out.

R = H

R = Me

R = Ph

Figure 153: The structure of potential bidentate ligands that may be used in the replacement of the two monodentate chloride ligands to further bridge the two metal centres in our dinuclear iridium(III) complexes.

Figure 153 shows the structure of one class of bidentate ligand that may be used in attempts to replace the two monodentate chloride ligands and bridge the iridium centres.

Future work in this area should include the identification a wider range of potential bidentate ligands and also the further exploration of this concept in terms of viability, as well as the effects on the structural and photophysical properties of our dinuclear iridium(III) complexes.

Chapter 5

Appendices

5.0 Appendices

5.1 Appendix 1 - Equipment and Chemicals

Reagents were purchased from Sigma Aldrich, Alfa Aesar, Fluorochem and Apollo Scientific and were used without any further purification.

Solvents were purchased from Fisher Scientific, Sigma Aldrich and Alfa Aesar at reagent, HPLC or spectroscopic grade. When required, solvents were dried over activated 4 Å molecular sieves.

Column chromatography was performed using Fisher Scientific silica gel 60 Å (35-70 μL).

NMR spectroscopy was performed on JEOL ELS400 Delta spectrometer at frequencies of 400 MHz for ^{1}H and ^{19}F NMR and 101 MHz for ^{13}C NMR. Chemical shifts (δ) are in ppm, using tetramethylsilane (TMS) as an internal standard and coupling constants are in Hertz. Deuterated chloroform ($CDCl_3$) and deuterated dimethyl sulfoxide (d^6-DMSO) were used as solvents. Chemical shifts were observed with splitting, integrals and *J* values. The splitting of the signals were recorded as singlet (s), doublet (d), triplet (t), quartet (q), quintet (quin), sextet (sext) and multiplet (m). Additionally, further splitting of signals were recorded as e.g. doublet of doublets (dd) and triplet of doublets (td).

Mass spectra were obtained at the EPSRC National Mass Spectrometry Service Centre at Swansea University using spectrometers including a Thermo Scientific LTQ Orbitrap XL Mass spectrometer, a Waters Xevo G2-S ToF spectrometer, a Bruker ultrafleXtreme spectrometer and a Finnigan MAT 9S XP spectrometer. Ionisation techniques used included low resolution electrospray (ESI), high-resolution nano-electrospray (NSI) ionisation, atmospheric solids analysis probe (ASAP) and matrix-assisted laser desorption ionisation (MALDI).

Absorption spectra recorded at Durham University were measured on a Biotek Instruments XA spectrometer, using quartz cuvettes of 1 cm path length.

Absorption spectra recorded at Northumbria University were measured on a Varian Cary 50 UV-vis spectrophotometer, using quartz cuvetters of 1 cm path length.

Luminescence Spectra recorded at Durham University were measured using a Jobin Yvon Fluoromax®-2 spectrofluorimeter fitted with a red-sensitive Hamamatsu R928 photomultiplier tube; the spectra show in section 3.3 are corrected for the wavelength dependence of the detector,

and the quoted emission maxima refer to the values after correction. Samples for emission measurements were contained within quartz cuvettes of 1 cm path length modified with appropriate glassware to allow connection to a high-vacuum line. Degassing was achieved *via* a minimum of three freeze-pump-thaw cycles whilst connected to the vacuum manifold; final vapour pressure at 77 K was $<5 \times 10^{-2}$ mbar, as monitored using a Pirani gauge. Luminescence quantum yields were determined using *fac*-Ir(ppy)$_3$ in degassed 2-methyltetrahydrofuran solution as the reference ($\phi_{lum} = 0.97$[217]); estimated uncertainty in relative values of ϕlum is ±10% or better. The luminescence lifetimes of the complexes were measured by time-correlated single-photon counting, following excitation at 405 nm with a EPL-405 pulsed-diode laser. The emitted light was detected at 90° using a Peltier-cooled R928 PMT after passage through a monochromator. The lifetime of **3.3.13** at 77 K was measured using the same detector operating in multi-channel scaling mode, following excitation with a microsecond pulsed xenon flash-lamp. The estimated uncertainty in the quoted lifetimes is ±10% or better. Bimolecular rate constants for quenching by molecular oxygen, k_Q, were determined from the lifetimes in degassed and air-equilibrated solution, taking the concentration of oxygen in CH_2Cl_2 at 0.21 atm O_2 to be 2.2. mmol dm^{-3}.

Luminescence spectra recorded at Northumbria University were measured using a Horiba Jobin Yvon FluoroMax®-4 spectrofluorimeter. Samples for emission measurements were contained within quartz cuvettes of 1 cm path length. Deoxygenation was performed by bubbling of argon through the solution.

Density functional theory calculations were carried out using Gaussian 09W. The B3LYP hybrid functional was used, together with the LanL2DZ basis set for iridium, and 6-31+G(d) for all other atom types. Geometries were fully optimised *in vacuo*. UV-visible absorption spectra were obtained by single point TD-DFT calculations at the optimised geometries, using the same functional and basis sets, either *in vacuo* or with a PCM solvent correction for dichloromethane. The molecular orbitals and spectra were visualised using GaussView 5.0 with Gaussian line shapes and an arbitrary half-width at half-height of 1000 cm^{-1} for the latter.

Photophysical analysis carried out at the University of Sheffield involved UV-vis spectra recorded on a Varian Cary 5000 UV-Vis-NIR spectrophotometer in 1 cm quartz cuvettes.

Luminescence spectra were recorded on a Horiba Jobin Yvon FluoroMax®-4 spectrofluorimeter. Emission lifetimes were performed on the mini-τ spectrofluorometer (Edinburgh Instruments), with a 405 nm pulsed diode laser as an excitation source. The emission decays were detected in the spectral range 475-525 nm selected by a bandpass filter.

Singlet oxygen yield of **3.6.8** measured at the University of Sheffield was measured by direct detection of the singlet oxygen emission (λem = 355 nm) in aerated acetonitrile according to the method previously described.

Cell cultures carried out at the University of Sheffield used the cell lines HeLa (human cervical cancer) and U2OS (bone osteosarcoma), both purchased from American Type Culture Collection – LGC Partnership (Teddington, UK). The cells were cultured in Dulbecco's modified Eagles Medium (DMEM) (Lonza, Cambridge, UK) with 10% fetal calf serum (FCS) (Lonza, Cambridge, UK) and incubated at 37 °C (5% CO_2). Cells were routinely checked for mycoplasma contamination.

Cell imaging was carried out at the University of Sheffield. Cells were platied at 150000 cells/well onto sterile coverslips (22 x 22 mm) and left to incubate overnight. Staining solution at 10 or 20 μM was diluted from compound stock (1 mM in DMSO) and added to the well. Control wells were incubated with equivalent DMSO concentration and the plates were incubated for 5 hours. Following incubation, the cells were washed (3 x PBS) and fixed (4% paraformaldehyde in PBS, 20 mins) before being washed (3 x PBS) and mounted to microscope slides (immumount, 20 mins). For mitotracker red staining (MitoTracker™ Red CMXRos, Molecular Probes® by Life Technologies Ltd, Paisley, UK) a final staining concentration of 100 nM was added to the cells in 30 mins before washing, fixing and mounting. For lysotracker red staining (LysoTracker™ Red DND-99, Molecular Probes® by Life Technologies Ltd, Paisley, UK) a final staining concentration of 75 nM was added for 1 hour before washing, fixing and mounting. For multiphoton imaging (Coherent Chameleon femto-second pulsed laser, Inverted Zeiss LSM 510 NLO microscope) multiphoton light (800 nm) was used to excite **3.6.8**; emission was registered in the region 565 – 615 nm. For the co-localisation imaging, a confocal microscope was used (Nikon A1) using a 60× lens (CFI Plan Apochromat VC 60× oil, NA 1.4). An argon laser (405

nm) was used to excite **3.6.8** and a sapphire laser (561 nm) was used to excite the costains. Pearson's correlation coefficients were calculated using the open source imaging software Fiji (based on ImageJ) and the coloc 2 co-localisation tool. The threshold regression chosen was Bisection.

Proliferation assay – MTT was also carried out at the University of Sheffield. 96-well plates were seeded with cells (HeLa or U2OS at 8000 cells/well) in culture medium (DMEM with 10% FCS) and incubated (37 °C, 5% CO_2, overnight). Treatment solutions were made up in media (DMEM with 10% FCS) with the compound diluted from a DMSO stock (1 mM) to the desired staining concentrations (0, 5, 10 and 20 μM) with the final concentration of DMSO equal in all samples (2%).

Toxicity assay – clonogenic survival was carried out at the University of Sheffield. 6-well plates were seeded at low density (HeLa, 200 and 400 cells/well) in culture medium (DMEM with 10% FCS) and incubated (37 °C, 5% CO_2, overnight). Treatment solutions were prepared as above and added (1 mL/well, 5 hours). Following incubation, the treatment solution was removed and cells washed (1 X PBS) and fresh media was added (2 mL/well). The plates were left until visible cell colonies had formed. Media was replaced with staining solution (4% methylene blue, 70% methanol, minimum 30 mins). The staining solution was washed off and colonies counted with each colony representing a surviving cell.

Transmission electron microscopy was also carried out at the University of Sheffield. Cells were cultured in T-25 flasks as above until ~90% confluency is achieved. Media was then removed, and the cells washed with sterile PBS (5 mL) before incubation with 20 μM complex-1 for 4 h. **3.6.8** was the removed and the cells washed with sterile PBS (2 x 5 mL). Cells were detached using Trypsin EDTA, washed in media and glutaraldehyde (2.5% in cacodylate buffer) was added to fix the cells overnight at ~4 °C. Cells were then dehydrated, embedded in Araldite and sectioned in to 85 nm sections and mounted on copper grids before imaging under TEM, having either been unstained or stained with standard contrast agent (OsO4 2%, 1 h, UAc2 3%, 25 mins, Reynold's Lead Citrate, 5 mins). All TEM images were recorded using a FEI tecnai

120Kv G2 Biotwin TEM with an Orius SC100 bottom mounted camera using Gatan Digital Micrograph software. Image analysis was performed using ImageJ.

5.2 Appendix 2 - Pyrimidine-Linked Dinuclear Iridium(III) Complexes - TD-DFT HOMO-LUMO

Selected calculated excitation energies (ΔE), oscillator strengths (f), and main orbital components for complex **3.3.7**.[a]

vacuum			**dichloromethane**		
ΔE, nm	**f**	**transition (coefficient)**	**ΔE, nm**	**f**	**transition (coefficient)**
526	(triplet)	HOMO-1 → LUMO (0.59) HOMO → LUMO (0.32)	499	(triplet)	HOMO-1 → LUMO (0.50) HOMO → LUMO (-0.43)
516	(triplet)	HOMO-3 → LUMO (0.55) HOMO-2 → LUMO (0.37)	484	(triplet)	HOMO-5 → LUMO (0.16) HOMO-3 → LUMO (0.60)
499	(triplet)	HOMO-1 → LUMO (-0.32) HOMO → LUMO (0.60)	462	(triplet)	HOMO-2 → LUMO+1 (0.31) HOMO-1 → LUMO+2 (-0.32)
494	0.033	HOMO → LUMO (0.70)	461	(triplet)	HOMO-2 → LUMO+2 (-0.28) HOMO-1 → LUMO+1 (0.35)
490	0.118	HOMO-1 → LUMO (0.70)	459	(triplet)	HOMO-3 → LUMO+1 (0.26) HOMO → LUMO+2 (0.36)
441	0.060	HOMO-2 → LUMO+1 (0.42) HOMO → LUMO+2 (0.39)	459	(triplet)	HOMO-2 → LUMO+2 (-0.30) HOMO → LUMO+1 (0.41)
433	0.018	HOMO-3 → LUMO+1 (0.42) HOMO-1 → LUMO+2 (-0.38)	456	0.308	HOMO-1 → LUMO (-0.47) HOMO → LUMO (0.52)
418	0.115	HOMO-3 → LUMO+4 (-0.33) HOMO-1 → LUMO+3 (0.38)	408	0.157	HOMO-2 → LUMO+1 (0.44) HOMO → LUMO+2 (-0.37)
412	0.053	HOMO-2 → LUMO+4 (0.40) HOMO → LUMO+3 (0.40)	398	0.020	HOMO-3 → LUMO+1 (0.42) HOMO-1 → LUMO+2 (-0.37)
379	0.371	HOMO-5 → LUMO (-0.17) HOMO-4 → LUMO (0.60)	387	0.219	HOMO-3 → LUMO+5 (-0.34) HOMO-1 → LUMO+3 (0.37)
369	0.040	HOMO-6 → LUMO (0.49) HOMO → LUMO+4 (-0.28)	381	0.114	HOMO-2 → LUMO+5 (0.36) HOMO → LUMO+3 (-0.36)
369	0.030	HOMO-6 → LUMO (0.43) HOMO-2 → LUMO+3 (-0.35)	380	0.030	HOMO-2 → LUMO+3 (0.41) HOMO-1 → LUMO+5 (-0.31)
			374	0.092	HOMO-4 → LUMO (0.48) HOMO-3 → LUMO+4 (-0.36)
			373	0.018	HOMO → LUMO+4 (0.41) HOMO → LUMO+5 (0.40)
			364	0.160	HOMO-3 → LUMO+1 (0.39) HOMO-1 → LUMO+2 (0.36)
			362	0.054	HOMO-5 → LUMO (0.54) HOMO-3 → LUMO+2 (0.33)
			362	0.024	HOMO-5 → LUMO (-0.32) HOMO-3 → LUMO+2 (0.38)
			359	0.109	HOMO-2 → LUMO+1 (0.32) HOMO-2 → LUMO+4 (0.28
			359	0.075	HOMO-3 → LUMO+4 (0.32) HOMO → LUMO+2 (-0.30)

[a]For brevity, only transitions with f > 0.01 and/or ΔE > 350 nm are included, and only the two largest components of each transition are listed.

Frontier orbitals and their energies in Hartree (eV) for complex **3.3.7**

LUMO+1
-0.06970
(-1.897 eV)

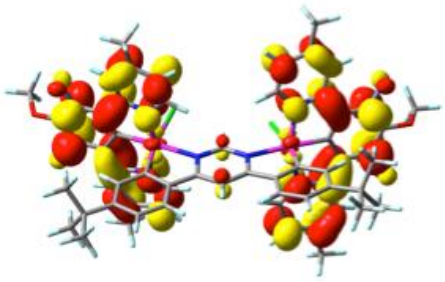

LUMO
-0.08221
(-2.237 eV)

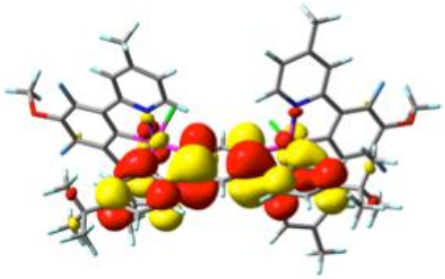

HOMO
-0.19687
(-5.357 eV)

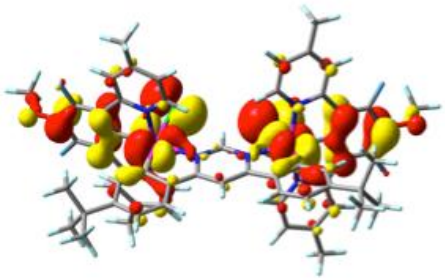

HOMO-1
-0.19803
(-5.389 eV)

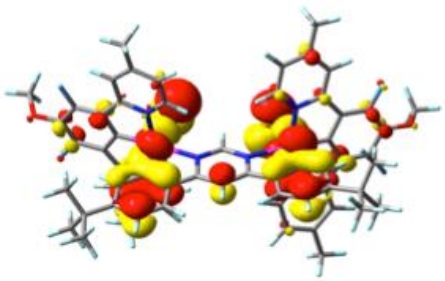

Selected calculated excitation energies (ΔE), oscillator strengths (f), and main orbital components for complex **3.3.8**.[a]

vacuum			**dichloromethane**		
ΔE, nm	**f**	**transition (coefficient)**	**ΔE, nm**	**f**	**transition (coefficient)**
527	(triplet)	HOMO-1 → LUMO (-0.20) HOMO → LUMO (0.64)	498	(triplet)	HOMO-4 → LUMO (0.18) HOMO → LUMO (0.66)
516	(triplet)	HOMO-3 → LUMO (-0.16) HOMO-2 → LUMO (0.65)	483	(triplet)	HOMO-3 → LUMO (-0.19) HOMO-2 → LUMO (0.59)
492	0.130	HOMO → LUMO (0.70)	453	0.305	HOMO → LUMO (0.70)
486	0.012	HOMO-1 → LUMO (0.70)	399	0.107	HOMO-3 → LUMO+1 (-0.35) HOMO-1 → LUMO+2 (0.44)
433	0.026	HOMO-2 → LUMO+1 (0.32) HOMO-1 → LUMO+2 (0.44)	393	0.011	HOMO-2 → LUMO+2 (0.36) HOMO → LUMO+1 (0.52)
428	0.026	HOMO-2 → LUMO+1 (-0.34) HOMO → LUMO+2 (0.49)	393	0.029	HOMO-2 → LUMO+1 (0.37) HOMO → LUMO+2 (0.50)
415	0.127	HOMO-2 → LUMO+5 (-0.34) HOMO → LUMO+3 (0.43)	383	0.268	HOMO-2 → LUMO+4 (-0.32) HOMO → LUMO+3 (0.45)
406	0.048	HOMO-2 → LUMO+4 (-0.37) HOMO-1 → LUMO+3 (0.42)	374	0.240	HOMO-4 → LUMO (0.37) HOMO-1 → LUMO+3 (0.41)
398	0.019	HOMO-2 → LUMO+4 (0.43) HOMO-2 → LUMO+5 (0.28)	373	0.034	HOMO-3 → LUMO+3 (0.32) HOMO-1 → LUMO+4 (0.33)
380	0.015	HOMO-3 → LUMO+1 (0.44) HOMO-1 → LUMO+2 (-0.39)	371	0.048	HOMO-4 → LUMO (0.43) HOMO-2 → LUMO+5 (0.42)
379	0.341	HOMO-4 → LUMO (0.61) HOMO-2 → LUMO+4 (-0.19)	369	0.045	HOMO-5 → LUMO (-0.36) HOMO → LUMO+5 (0.49)
369	0.067	HOMO-5 → LUMO (0.68)	360	0.128	HOMO-2 → LUMO+1 (-0.33) HOMO → LUMO+2 (0.43)
			360	0.046	HOMO-5 → LUMO (0.54) HOMO-1 → LUMO+4 (-0.25)
			356	0.111	HOMO-3 → LUMO+5 (-0.30) HOMO-2 → LUMO+5 (0.34)

[a]For brevity, only transitions with f > 0.01 and/or ΔE > 350 nm are included, and only the two largest components of each transition are listed.

Frontier orbitals and their energies in Hartree (eV) for complex **3.3.8**

LUMO+1
-0.06936
(-1.887 eV)

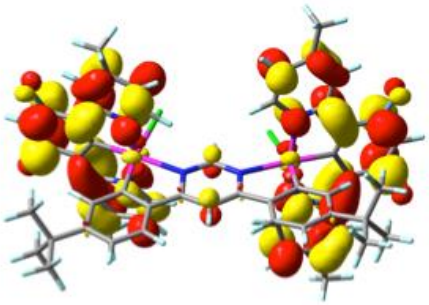

LUMO
-0.08302
(-2.259 eV)

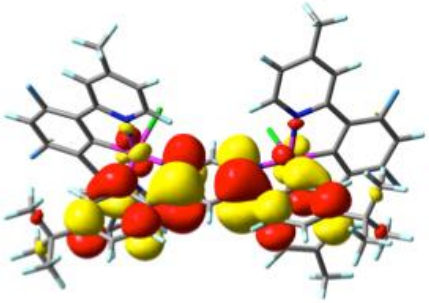

HOMO
-0.19835
(-5.397 eV)

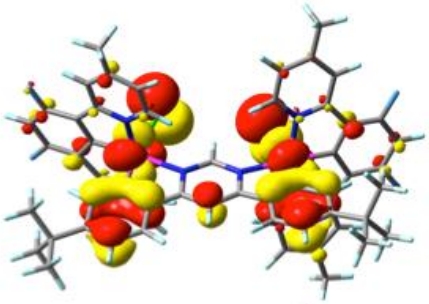

HOMO-1
-0.19963
(-5.432 eV)

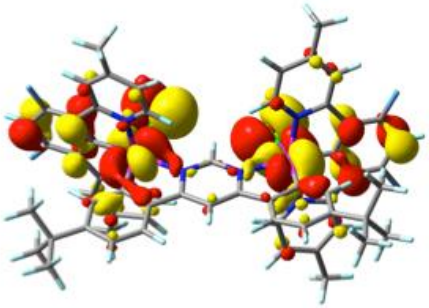

Selected calculated excitation energies (ΔE), oscillator strengths (f), and main orbital components for complex **3.3.9**.[a]

vacuum			**dichloromethane**		
ΔE, nm	**f**	**transition (coefficient)**	**ΔE, nm**	**f**	**transition (coefficient)**
520	(triplet)	HOMO-4 → LUMO (-0.17) HOMO → LUMO (0.67)	492	(triplet)	HOMO-4 → LUMO (0.19) HOMO → LUMO (0.65)
509	(triplet)	HOMO-7 → LUMO (-0.13) HOMO-1 → LUMO (0.66)	476	(triplet)	HOMO-1 → LUMO (0.61) HOMO → LUMO+5 (-0.18)
484	0.144	HOMO → LUMO (0.70)	449	(triplet)	HOMO-1 → LUMO+1 (-0.36) HOMO → LUMO+2 (0.38)
409	0.127	HOMO-3 → LUMO+1 (-0.35) HOMO-2 → LUMO+2 (0.42)	449	(triplet)	HOMO-1 → LUMO+2 (-0.36) HOMO → LUMO+1 (0.38)
396	0.014	HOMO-1 → LUMO+4 (-0.30) HOMO-1 → LUMO+5 (0.47)	448	0.324	HOMO → LUMO (0.70)
390	0.071	HOMO-3 → LUMO+4 (-0.31) HOMO-2 → LUMO+3 (0.44)	397	0.013	HOMO-1 → LUMO+2 (-0.43) HOMO → LUMO+1 (0.54)
376	0.142	HOMO-4 → LUMO (0.40) HOMO-3 → LUMO+5 (0.37)	397	0.016	HOMO-1 → LUMO+1 (-0.44) HOMO → LUMO+2 (0.52)
375	0.204	HOMO-4 → LUMO (0.45) HOMO-3 → LUMO+5 (-0.37)	374	0.277	HOMO-3 → LUMO+1 (-0.42) HOMO-2 → LUMO+2 (0.47)
365	0.070	HOMO-5 → LUMO (0.68)	368	0.093	HOMO-4 → LUMO (0.46) HOMO-1 → LUMO+5 (0.42)
			363	0.189	HOMO-1 → LUMO+1 (0.43) HOMO → LUMO+2 (0.38)
			360	0.246	HOMO-2 → LUMO+3 (-0.29) HOMO-1 → LUMO+5 (0.46)
			360	0.120	HOMO-5 → LUMO (0.63) HOMO-2 → LUMO+4 (0.20)

[a]For brevity, only transitions with f > 0.01 and/or ΔE > 350 nm are included, and only the two largest components of each transition are listed.

Frontier orbitals and their energies in Hartree (eV) for complex **3.3.9**

LUMO+1
-0.07691
(-2.093 eV)

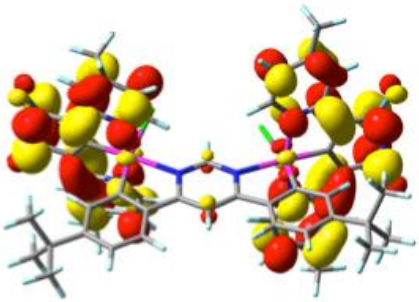

LUMO
-0.08950
(-2.435 eV)

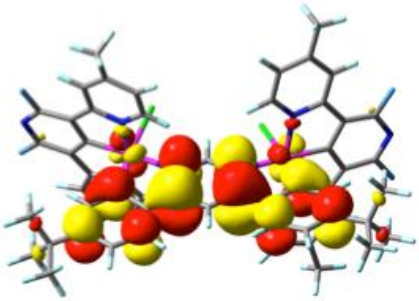

HOMO
-0.20637
(-5.616 eV)

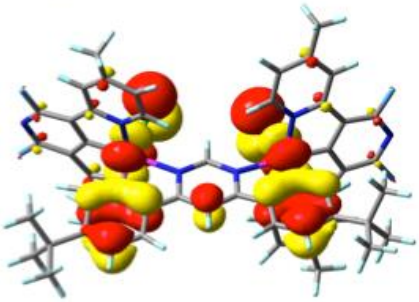

HOMO-1
-0.20781
(-5.655 eV)

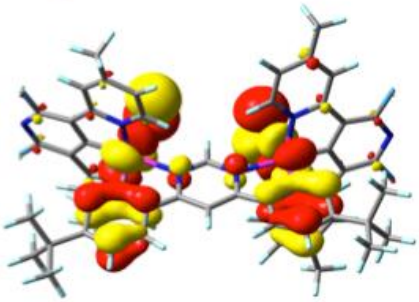

Selected calculated excitation energies (ΔE), oscillator strengths (f), and main orbital components for complex **3.3.10**.[a]

vacuum			**dichloromethane**		
ΔE, nm	**f**	**transition (coefficient)**	**ΔE, nm**	**f**	**transition (coefficient)**
535	(triplet)	HOMO-1 → LUMO (0.64) HOMO → LUMO (-0.21)	504	(triplet)	HOMO-1 → LUMO (0.64) HOMO → LUMO (-0.21)
525	(triplet)	HOMO-3 → LUMO (0.62) HOMO-2 → LUMO (-0.26)	490	(triplet)	HOMO-3 → LUMO (0.64) HOMO-1 → LUMO+3 (-0.14)
510	(triplet)	HOMO-1 → LUMO (0.22) HOMO → LUMO (0.66)	466	(triplet)	HOMO-1 → LUMO (0.20) HOMO → LUMO (0.62)
497	0.123	HOMO-1 → LUMO (0.70)	461	0.202	HOMO-1 → LUMO (-0.48) HOMO → LUMO (0.51)
438	0.070	HOMO-2 → LUMO+1 (-0.42) HOMO → LUMO+2 (0.45)	459	0.059	HOMO-1 → LUMO (0.51) HOMO → LUMO (0.48)
430	0.017	HOMO-3 → LUMO+1 (0.45) HOMO-1 → LUMO+2 (0.43)	405	0.177	HOMO-2 → LUMO+1 (-0.45) HOMO → LUMO+2 (0.46)
415	0.116	HOMO-3 → LUMO+5 (0.42) HOMO-1 → LUMO+4 (-0.42)	394	0.011	HOMO-3 → LUMO+2 (-0.40) HOMO-1 → LUMO+1 (0.48)
412	0.057	HOMO-2 → LUMO+5 (0.35) HOMO → LUMO+4 (0.41)	394	0.024	HOMO-3 → LUMO+1 (-0.42) HOMO-1 → LUMO+2 (0.45)
382	0.171	HOMO-5 → LUMO (-0.29) HOMO-4 → LUMO (0.58)	384	0.215	HOMO-3 → LUMO+5 (0.42) HOMO-1 → LUMO+4 (0.46)
380	0.110	HOMO-5 → LUMO (0.56) HOMO-4 → LUMO (0.36)	380	0.143	HOMO-2 → LUMO+5 (0.37) HOMO → LUMO+4 (0.41)
370	0.021	HOMO-7 → LUMO (0.33) HOMO-6 → LUMO (0.61)	379	0.018	HOMO-2 → LUMO+4 (0.36) HOMO → LUMO+5 (0.34)
368	0.013	HOMO-2→ LUMO+4 (0.38) HOMO → LUMO+5 (-0.37)	376	0.058	HOMO-4 → LUMO (0.48) HOMO-3 → LUMO+3 (-0.45)
368	0.025	HOMO-7 → LUMO (0.48) HOMO-2 → LUMO+4 (0.31)	373	0.023	HOMO-5 → LUMO (0.27) HOMO-1 → LUMO+3 (0.56)
			362	0.180	HOMO-4 → LUMO (0.39) HOMO-1 → LUMO+2 (0.33)
			362	0.061	HOMO-5 → LUMO (0.61) HOMO-1 → LUMO+3 (-0.19)
			358	0.026	HOMO-3 → LUMO+1 (0.38) HOMO-3 → LUMO+3 (-0.36)

[a]For brevity, only transitions with f > 0.01 and/or ΔE > 350 nm are included, and only the two largest components of each transition are listed.

Frontier orbitals and their energies in Hartree (eV) for complex **3.3.10**

LUMO+1
-0.07077
(-1.926 eV)

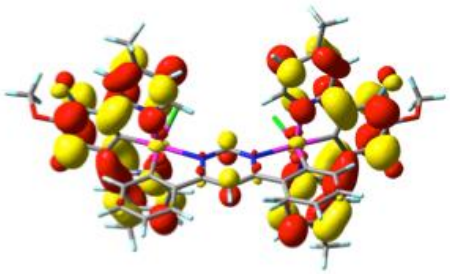

LUMO
-0.08548
(-2.326 eV)

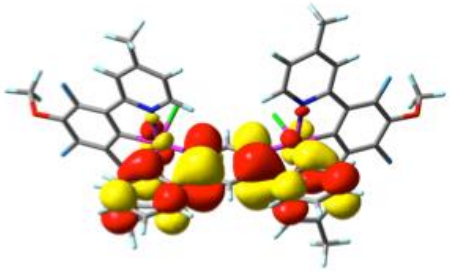

HOMO
-0.19841
(-5.399 eV)

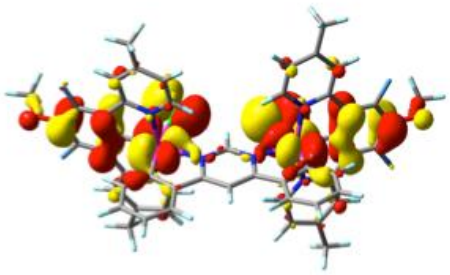

HOMO-1
-0.19992
(-5.440 eV)

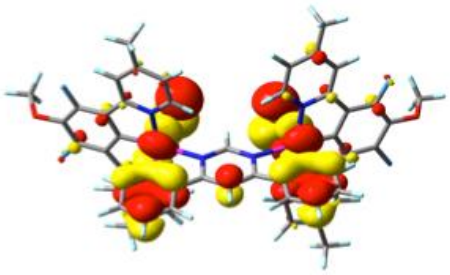

Selected calculated excitation energies (ΔE), oscillator strengths (f), and main orbital components for complex **3.3.11**.[a]

vacuum			**dichloromethane**		
ΔE, nm	**f**	**transition (coefficient)**	**ΔE, nm**	**f**	**transition (coefficient)**
518	(triplet)	HOMO-2 → LUMO (0.59) HOMO → LUMO (0.33)	492	(triplet)	HOMO-2 → LUMO (0.63) HOMO → LUMO (0.21)
509	(triplet)	HOMO-3 → LUMO (0.57) HOMO-1 → LUMO (-0.37)	481	(triplet)	HOMO-3 → LUMO (0.58) HOMO-1 → LUMO (-0.28)
506	(triplet)	HOMO-2 → LUMO (-0.33) HOMO → LUMO (0.61)	473	(triplet)	HOMO-2 → LUMO (-0.21) HOMO → LUMO (0.66)
501	(triplet)	HOMO → LUMO (0.70)	470	(triplet)	HOMO-3 → LUMO+2 (0.31) HOMO → LUMO+4 (-0.40)
487	0.092	HOMO-2 → LUMO (0.70)	468	0.016	HOMO → LUMO (0.70)
426	0.082	HOMO-1 → LUMO+1 (0.45) HOMO → LUMO+2 (0.46)	456	0.195	HOMO-2 → LUMO (0.70)
413	0.029	HOMO-3 → LUMO+1 (0.42) HOMO-2 → LUMO+2 (0.41)	397	0.016	HOMO-1 → LUMO+2 (-0.46) HOMO → LUMO+1 (0.50)
402	0.072	HOMO-3 → LUMO+4 (0.39) HOMO → LUMO+3 (-0.36)	396	0.214	HOMO-1 → LUMO+1 (-0.46) HOMO → LUMO+2 (0.49)
399	0.119	HOMO-2 → LUMO+3 (0.31) HOMO-1 → LUMO+4 (0.38)	379	0.011	HOMO-1 → LUMO+4 (-0.34) HOMO → LUMO+3 (0.37)
397	0.021	HOMO-1 → LUMO+3 (0.41) HOMO → LUMO+4 (-0.38)	378	0.402	HOMO-5 → LUMO (0.59) HOMO-2 → LUMO+2 (-0.23)
385	0.121	HOMO-5 → LUMO (-0.30) HOMO-4 → LUMO (0.48)	373	0.095	HOMO-4 → LUMO (0.55) HOMO → LUMO+4 (-0.24)
380	0.022	HOMO-1 → LUMO+1 (0.40) HOMO → LUMO+2 (-0.35)	371	0.036	HOMO-3 → LUMO+3 (-0.44) HOMO-2 → LUMO+4 (0.47)
374	0.015	HOMO-1 → LUMO+1 (0.27) HOMO-1 → LUMO+5 (0.56)	371	0.145	HOMO-3 → LUMO+4 (-0.45) HOMO-2 → LUMO+3 (0.48)
373	0.044	HOMO-3 → LUMO+1 (-0.43) HOMO-2 → LUMO+2 (0.46)			
373	0.018	HOMO-6 → LUMO (0.47) HOMO-3 → LUMO+2 (-0.34)			
368	0.084	HOMO-5 → LUMO (-0.22) HOMO-3 → LUMO+5 (0.60)			
368	0.043	HOMO-7 → LUMO (0.55) HOMO-2 → LUMO+5 (0.35)			

[a]For brevity, only transitions with f > 0.01 and/or ΔE > 350 nm are included, and only the two largest components of each transition are listed.

Frontier orbitals and their energies in Hartree (eV) for complex **3.3.11**

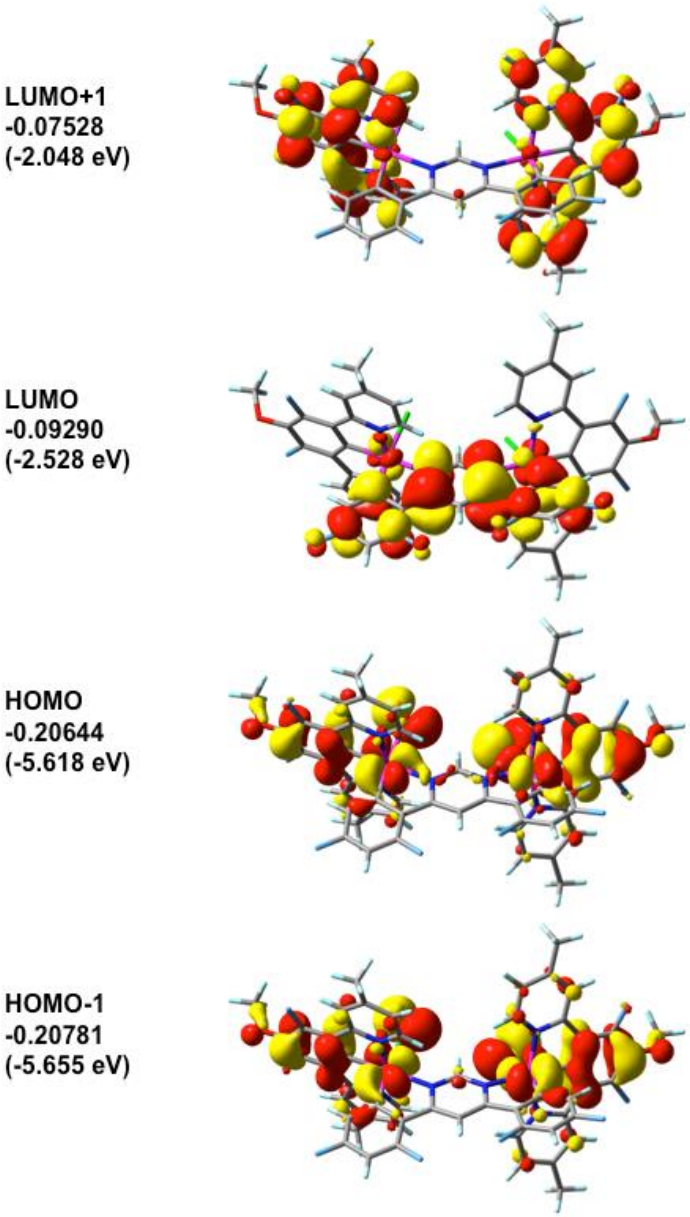

Selected calculated excitation energies (ΔE), oscillator strengths (f), and main orbital components for complex **3.3.12**.[a]

vacuum			**dichloromethane**		
ΔE, nm	**f**	**transition (coefficient)**	**ΔE, nm**	**f**	**transition (coefficient)**
510	(triplet)	HOMO-4 → LUMO (0.21) HOMO → LUMO (0.60)	497	(triplet)	HOMO-4 → LUMO (0.17) HOMO → LUMO (0.65)
490	(triplet)	HOMO-3 → LUMO (-0.39) HOMO-2 → LUMO (0.43)	475	(triplet)	HOMO-5 → LUMO (-0.26) HOMO-3 → LUMO (0.52)
485	(triplet)	HOMO-2 → LUMO+1 (0.37) HOMO-1 → LUMO+2 (0.41)	459	(triplet)	HOMO-3 → LUMO+1 (-0.22) HOMO → LUMO+2 (0.24)
485	(triplet)	HOMO-2 → LUMO+2 (0.34) HOMO-1 → LUMO+1 (0.46)	459	(triplet)	HOMO-3 → LUMO+2 (-0.23) HOMO → LUMO+1 (0.24)
476	(triplet)	HOMO-3 → LUMO+1 (0.31) HOMO → LUMO+2 (0.39)	456	(triplet)	HOMO-2 → LUMO+1 (0.40) HOMO-1 → LUMO+2 (0.41)
476	(triplet)	HOMO-3 → LUMO+2 (0.31) HOMO → LUMO+1 (0.40)	456	(triplet)	HOMO-2 → LUMO+2 (0.38) HOMO-1 → LUMO+1 (0.44)
461	0.238	HOMO → LUMO (0.69)	438	0.529	HOMO → LUMO (0.69)
457	0.024	HOMO-2 → LUMO+1 (0.10) HOMO-1 → LUMO (0.69)	406	0.148	HOMO-2 → LUMO+1 (0.43) HOMO-1 → LUMO+2 (0.47)
441	0.054	HOMO-2 → LUMO+1 (0.36) HOMO-1 → LUMO+2 (0.47)	387	0.224	HOMO-3 → LUMO+4 (-0.37) HOMO → LUMO+3 (0.50)
419	0.121	HOMO-3 → LUMO+4 (0.32) HOMO → LUMO+3 (0.46)	379	0.030	HOMO-2 → LUMO+4 (0.40) HOMO-1 → LUMO+3 (0.47)
410	0.021	HOMO-2 → LUMO+4 (0.33) HOMO-1 → LUMO+3 (0.48)	378	0.016	HOMO-2 → LUMO+3 (0.43) HOMO-1 → LUMO+4 (0.44)
384	0.062	HOMO-4 → LUMO (0.41) HOMO-2 → LUMO+5 (0.42)	367	0.232	HOMO-4 → LUMO (0.51) HOMO-3 → LUMO+1 (0.28)
370	0.366	HOMO-4 → LUMO (0.48) HOMO-3 → LUMO+5 (0.28)	352	0.091	HOMO-4 → LUMO (0.15) HOMO-2 → LUMO+5 (0.65)
368	0.073	HOMO-3 → LUMO+4 (0.36) HOMO-2 → LUMO+4 (0.37)	352	0.137	HOMO-7 → LUMO (-0.13) HOMO-5 → LUMO (0.67)
358	0.056	HOMO-8 → LUMO+1 (0.17) HOMO-4 → LUMO+2 (0.63)	350	0.292	HOMO-4 → LUMO (0.27) HOMO-3 → LUMO+5 (0.61)
354	0.103	HOMO-8 → LUMO (-0.16) HOMO-5 → LUMO (0.64)			
353	0.023	HOMO-7 → LUMO+1 (-0.14) HOMO-6 → LUMO (0.68)			

[a]For brevity, only transitions with f > 0.01 and/or ΔE > 350 nm are included, and only the two largest components of each transition are listed.

Frontier orbitals and their energies in Hartree (eV) for complex **3.3.12**

LUMO+1
-0.07036
(-1.915 eV)

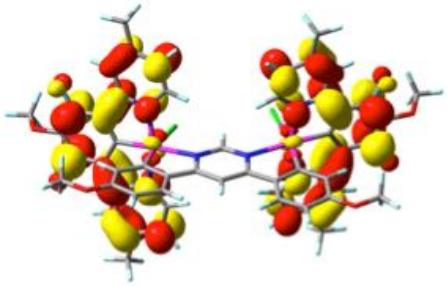

LUMO
-0.07564
(-2.058 eV)

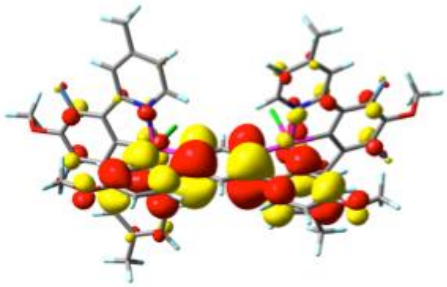

HOMO
-0.19668
(-5.352 eV)

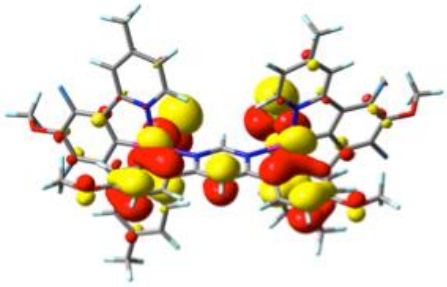

HOMO-1
-0.19791
(-5.385 eV)

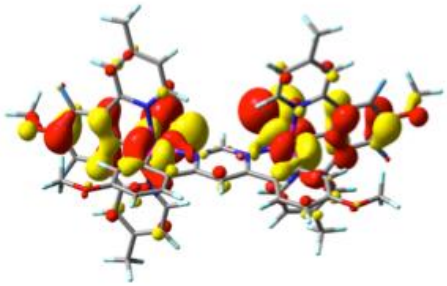

Selected calculated excitation energies (ΔE), oscillator strengths (f), and main orbital components for complex **3.3.13**.[a]

vacuum			**dichloromethane**		
ΔE, nm	**f**	**transition (coefficient)**	**ΔE, nm**	**f**	**transition (coefficient)**
581	(triplet)	HOMO-4 → LUMO (-0.18) HOMO → LUMO (0.63)	572	(triplet)	HOMO-2 → LUMO+5 (-0.13) HOMO → LUMO (0.65)
546	(triplet)	HOMO-2 → LUMO (0.51) HOMO → LUMO+5 (-0.30)	536	(triplet)	HOMO-2 → LUMO (0.51) HOMO → LUMO+5 (-0.35)
485	(triplet)	HOMO-3 → LUMO+1 (0.43) HOMO-1 → LUMO+2 (0.38)	461	(triplet)	HOMO-2 → LUMO+2 (0.28) HOMO → LUMO+1 (0.34)
484	(triplet)	HOMO-3 → LUMO+2 (0.39) HOMO-1 → LUMO+1 (0.48)	461	(triplet)	HOMO-2 → LUMO+1 (0.28) HOMO → LUMO+2 (0.33)
479	(triplet)	HOMO-2 → LUMO+2 (0.35) HOMO → LUMO+1 (0.45)	461	0.620	HOMO → LUMO (0.69)
478	(triplet)	HOMO-2 → LUMO+1 (0.36) HOMO → LUMO+2 (0.43)	408	0.049	HOMO-1 → LUMO+2 (0.37) HOMO → LUMO+3 (0.41)
477	0.362	HOMO-2 → LUMO+1 (0.10) HOMO → LUMO (0.69)	394	0.322	HOMO-1 → LUMO+2 (-0.35) HOMO → LUMO+3 (0.45)
455	0.012	HOMO-2 → LUMO (0.64) HOMO → LUMO+1 (0.21)	378	0.019	HOMO-2 → LUMO+1 (0.52) HOMO-1 → LUMO+3 (-0.22)
440	0.034	HOMO-3 → LUMO+1 (0.37) HOMO-1 → LUMO+2 (0.43)	373	0.013	HOMO-2 → LUMO+2 (0.54) HOMO-1 → LUMO+4 (-0.24)
422	0.157	HOMO-2 → LUMO+4 (-0.31) HOMO → LUMO+3 (0.47)	368	0.106	HOMO-4 → LUMO (0.56) HOMO-2 → LUMO+5 (-0.29
385	0.098	HOMO-4 → LUMO (0.55) HOMO-2 → LUMO+5 (0.38)	362	0.012	HOMO-2 → LUMO+4 (0.55) HOMO → LUMO+3 (-0.33)
368	0.088	HOMO-3 → LUMO+4 (0.43) HOMO-1 → LUMO+3 (-0.41)			
366	0.203	HOMO-3 → LUMO+4 (-0.34) HOMO-2 → LUMO+5 (0.45)			
355	0.066	HOMO-4 → LUMO+2 (0.61) HOMO-2 → LUMO+5 (-0.19)			
354	0.017	HOMO-7 → LUMO+1 (0.12) HOMO-5 → LUMO (0.68)			
350	0.148	HOMO-8 → LUMO (-0.26) HOMO-6 → LUMO (0.61)			

[a]For brevity, only transitions with f > 0.01 and/or ΔE > 350 nm are included, and only the two largest components of each transition are listed.

Frontier orbitals and their energies in Hartree (eV) for complex **3.3.13**

LUMO+1
-0.07026
(-1.912 eV)

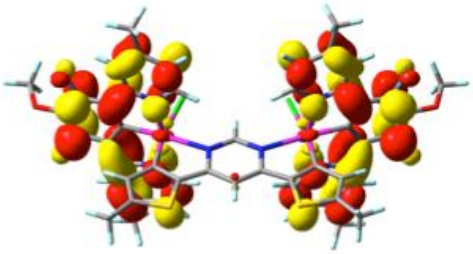

LUMO
-0.07730
(-2.103 eV)

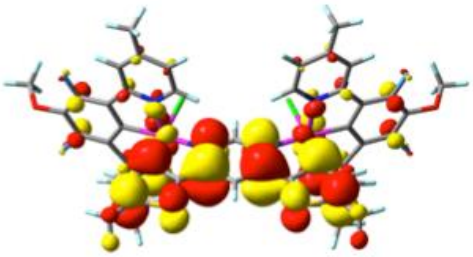

HOMO
-0.19339
(-5.262 eV)

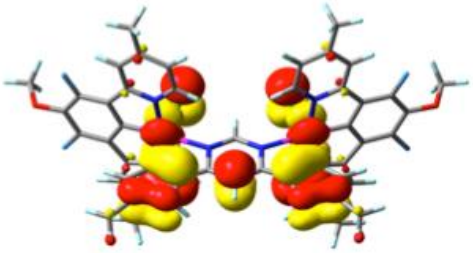

HOMO-1
-0.19777
(-5.382 eV)

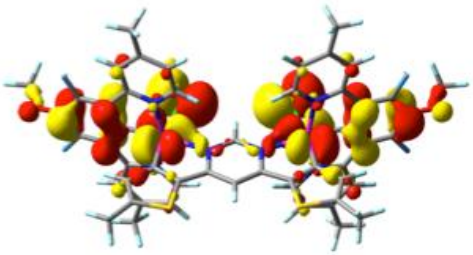

Selected calculated excitation energies (ΔE), oscillator strengths (f), and main orbital components for complex **3.3.14**.[a]

vacuum			**dichloromethane**		
ΔE, nm	**f**	**transition (coefficient)**	**ΔE, nm**	**f**	**transition (coefficient)**
496	(triplet)	HOMO-5 → LUMO (0.21) HOMO-2 → LUMO (0.65)	482	(triplet)	HOMO-5 → LUMO (0.24) HOMO-2 → LUMO (0.63)
483	(triplet)	HOMO-3 → LUMO (0.47) HOMO-1 → LUMO (0.36)	466	(triplet)	HOMO-4 → LUMO (0.36) HOMO-3 → LUMO (0.42)
472	(triplet)	HOMO-1 → LUMO+1 (-0.34) HOMO → LUMO (0.50)	451	(triplet)	HOMO-1 → LUMO+1 (0.37) HOMO → LUMO+2 (0.33)
470	(triplet)	HOMO-1 → LUMO+2 (0.40) HOMO → LUMO+1 (0.42)	451	(triplet)	HOMO-1 → LUMO+2 (0.37) HOMO → LUMO+1 (0.36)
463	(triplet)	HOMO → LUMO (0.47) HOMO → LUMO+2 (0.37)	445	(triplet)	HOMO-1 → LUMO+1 (0.26) HOMO → LUMO+2 (0.31)
450	0.237	HOMO-2 → LUMO (0.69)	445	(triplet)	HOMO-3 → LUMO+2 (0.26) HOMO → LUMO+1 (-0.30)
413	0.023	HOMO-1 → LUMO+2 (0.48) HOMO → LUMO+1 (0.48)	438	(triplet)	HOMO → LUMO (0.64) HOMO → LUMO+2 (0.18)
412	0.151	HOMO-1 → LUMO+1 (0.48) HOMO → LUMO+2 (0.48)	431	0.418	HOMO-2 → LUMO (0.69)
390	0.046	HOMO-3 → LUMO+1 (-0.40) HOMO-2 → LUMO+2 (0.50)	393	0.041	HOMO-1 → LUMO+2 (0.48) HOMO → LUMO+1 (0.49
379	0.010	HOMO-1 → LUMO+1 (-0.20) HOMO-1 → LUMO+3 (0.60)	392	0.286	HOMO-1 → LUMO+1 (0.48) HOMO → LUMO+2 (0.49)
375	0.177	HOMO-5 → LUMO (0.43) HOMO → LUMO+4 (-0.35)	371	0.017	HOMO-3 → LUMO+2 (0.36) HOMO-2 → LUMO+1 (0.54)
374	0.048	HOMO-1 → LUMO+4 (0.36) HOMO → LUMO+5 (0.40)	371	0.041	HOMO-3 → LUMO+1 (0.37) HOMO-2 → LUMO+2 (0.54)
370	0.032	HOMO-5 → LUMO (0.33) HOMO-3 → LUMO+3 (0.38)	364	0.133	HOMO-4 → LUMO (0.61) HOMO-1 → LUMO+4 (0.21)
368	0.109	HOMO-3 → LUMO+5 (-0.40) HOMO-2 → LUMO+4 (0.51)	363	0.351	HOMO-8 → LUMO (-0.17) HOMO-5 → LUMO (0.62)
367	0.057	HOMO-3 → LUMO+4 (-0.38) HOMO-2 → LUMO+5 (0.47)	358	0.035	HOMO-1 → LUMO+3 (0.51) HOMO → LUMO+4 (-0.29)
360	0.123	HOMO-3 → LUMO+1 (0.37) HOMO-2 → LUMO+2 (0.37)	354	0.014	HOMO-1 → LUMO+3 (0.33) HOMO-1 → LUMO+5 (-0.32
356	0.050	HOMO-3 → LUMO+1 (0.33) HOMO-3 → LUMO+3 (0.47)	351	0.096	HOMO-3 → LUMO+5 (-0.40) HOMO-2 → LUMO+4 (0.53)
			351	0.015	HOMO-2 → LUMO+3 (0.29) HOMO-2 → LUMO+5 (0.31)
			351	0.011	HOMO-2 → LUMO+3 (-0.32) HOMO-2 → LUMO+5 (0.41)

[a]For brevity, only transitions with f > 0.01 and/or ΔE > 350 nm are included, and only the two largest components of each transition are listed.

Frontier orbitals and their energies in Hartree (eV) for complex **3.3.14**

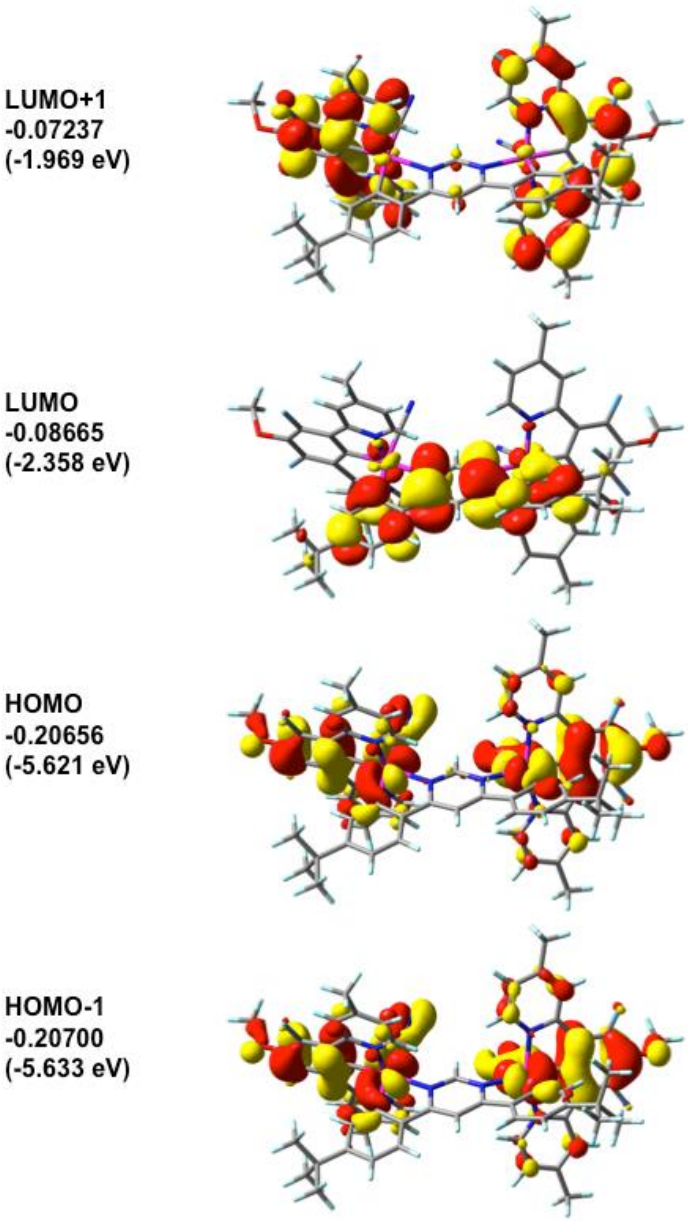

Chapter 6

References

6.0 References

1. S. W. Thomas, K. Venkatesan, P. Müller and T. M. Swager, *Journal of the American Chemical Society*, 2006, **128**, 16641-16648.
2. F. Neve, M. L. Deda, F. Puntoriero and S. Campagna, *Inorganica Chimica Acta*, 2006, **359**, 1666-1672.
3. B. Minaev, G. Baryshnikov and H. Agren, *Physical Chemistry Chemical Physics*, 2014, **16**, 1719-1758.
4. H. Yersin, *Transition Metal and Rare Earth Compounds*, 2004, 1-26.
5. J. A. G. Williams, A. J. Wilkinson and V. L. Whittle, *Dalton Transactions*, 2008, DOI: 10.1039/B716743A, 2081-2099.
6. J. Van Houten and R. J. Watts, *Journal of the American Chemical Society*, 1976, **98**, 4853-4858.
7. R. J. Watts, *Journal of Chemical Education*, 1983, **60**, 834-842.
8. A. Juris, V. Balzani, F. Barigelletti, S. Campagna, P. l. Belser and A. Von Zelewsky, *Coordination Chemistry Reviews*, 1988, **84**, 85-277.
9. Q. Sun, S. Mosquera-Vazquez, Y. Suffren, J. Hankache, N. Amstutz, L. M. L. Daku, E. Vauthey and A. Hauser, *Coordination Chemistry Reviews*, 2015, **282**, 87-99.
10. C. Kreitner and K. Heinze, *Dalton Transactions*, 2016, **45**, 5640-5658.
11. R. C. Evans, P. Douglas and C. J. Winscom, *Coordination Chemistry Reviews*, 2006, **250**, 2093-2126.
12. V. W.-W. Yam, K. H.-Y. Chan, K. M.-C. Wong and B. W.-K. Chu, *Angewandte Chemie International Edition*, 2006, **45**, 6169-6173.
13. B. Yin, F. Niemeyer, J. A. G. Williams, J. Jiang, A. Boucekkine, L. Toupet, H. Le Bozec and V. Guerchais, *Inorganic chemistry*, 2006, **45**, 8584-8596.
14. I. M. Dixon, J.-P. Collin, J.-P. Sauvage, L. Flamigni, S. Encinas and F. Barigelletti, *Chemical Society Reviews*, 2000, **29**, 385-391.
15. W. Leslie, A. S. Batsanov, J. A. K. Howard and J. A. Gareth Williams, *Dalton Transactions*, 2004, 623-631.
16. D. N. Chirdon, W. J. Transue, H. N. Kagalwala, A. Kaur, A. B. Maurer, T. Pintauer and S. Bernhard, *Inorganic chemistry*, 2014, **53**, 1487-1499.
17. J. A. G. Williams, *Chemical Society Reviews*, 2009, **38**, 1783-1801.
18. J. A. G. Williams, A. Beeby, E. S. Davies, J. A. Weinstein and C. Wilson, *Inorganic chemistry*, 2003, **42**, 8609-8611.
19. J. A. Gareth Williams, S. Develay, D. L. Rochester and L. Murphy, *Coordination Chemistry Reviews*, 2008, **252**, 2596-2611.
20. A. F. Rausch, L. Murphy, J. A. G. Williams and H. Yersin, *Inorganic chemistry*, 2009, **48**, 11407-11414.
21. Z. Wang, E. Turner, V. Mahoney, S. Madakuni, T. Groy and J. Li, *Inorganic chemistry*, 2010, **49**, 11276-11286.
22. E. Rossi, L. Murphy, P. L. Brothwood, A. Colombo, C. Dragonetti, D. Roberto, R. Ugo, M. Cocchi and J. A. G. Williams, *Journal of Materials Chemistry*, 2011, **21**, 15501-15510.
23. K. A. King, P. J. Spellane and R. J. Watts, *Journal of the American Chemical Society*, 1985, **107**, 1431-1432.
24. A. B. Tamayo, B. D. Alleyne, P. I. Djurovich, S. Lamansky, I. Tsyba, N. N. Ho, R. Bau and M. E. Thompson, *Journal of the American Chemical Society*, 2003, **125**, 7377-7387.
25. A. J. Wilkinson, A. E. Goeta, C. E. Foster and J. G. Williams, *Inorganic chemistry*, 2004, **43**, 6513-6515.
26. J. Li, P. I. Djurovich, B. D. Alleyne, M. Yousufuddin, N. N. Ho, J. C. Thomas, J. C. Peters, R. Bau and M. E. Thompson, *Inorganic chemistry*, 2005, **44**, 1713-1727.
27. A. J. Wilkinson, H. Puschmann, J. A. K. Howard, C. E. Foster and J. A. G. Williams, *Inorganic chemistry*, 2006, **45**, 8685-8699.
28. S. Obara, M. Itabashi, F. Okuda, S. Tamaki, Y. Tanabe, Y. Ishii, K. Nozaki and M.-a. Haga, *Inorganic chemistry*, 2006, **45**, 8907-8921.
29. M. S. Lowry and S. Bernhard, *Chemistry-A European Journal*, 2006, **12**, 7970-7977.
30. P. Brulatti, R. J. Gildea, J. A. K. Howard, V. Fattori, M. Cocchi and J. A. G. Williams, *Inorganic chemistry*, 2012, **51**, 3813-3826.
31. Y. Chi and P.-T. Chou, *Chemical Society Reviews*, 2010, **39**, 638-655.
32. D. M. Jenkins and S. Bernhard, *Inorganic chemistry*, 2010, **49**, 11297-11308.

33. J. A. Bailey, M. G. Hill, R. E. Marsh, V. M. Miskowski, W. P. Schaefer and H. B. Gray, *Inorganic chemistry*, 1995, **34**, 4591-4599.
34. S. Sprouse, K. King, P. Spellane and R. J. Watts, *Journal of the American Chemical Society*, 1984, **106**, 6647-6653.
35. J. Mamtora, S. H. Crosby, C. P. Newman, G. J. Clarkson and J. P. Rourke, *Organometallics*, 2008, **27**, 5559-5565.
36. K. P. Balashev, M. V. Puzyk, V. S. Kotlyar and M. V. Kulikova, *Coordination Chemistry Reviews*, 1997, **159**, 109-120.
37. L. Chassot, E. Mueller and A. Von Zelewsky, *Inorganic chemistry*, 1984, **23**, 4249-4253.
38. L. Chassot and A. Von Zelewsky, *Inorganic chemistry*, 1987, **26**, 2814-2818.
39. M. Maestri, D. Sandrini, V. Balzani, L. Chassot, P. Jolliet and A. Von Zelewsky, *Chemical physics letters*, 1985, **122**, 375-379.
40. M. Maestri, D. Sandrini, A. Von Zelewsky and C. Deuschel-Cornioley, *Inorganic chemistry*, 1991, **30**, 2476-2478.
41. J.-Y. Cho, K. Y. Suponitsky, J. Li, T. V. Timofeeva, S. Barlow and S. R. Marder, *Journal of organometallic chemistry*, 2005, **690**, 4090-4093.
42. C. Craig, F. Garces, R. Watts, R. Palmans and A. Frank, *Coordination chemistry reviews*, 1990, **97**, 193-208.
43. J. Brooks, Y. Babayan, S. Lamansky, P. I. Djurovich, I. Tsyba, R. Bau and M. E. Thompson, *Inorganic chemistry*, 2002, **41**, 3055-3066.
44. P.-I. Kvam, M. Puzyk, K. P. Balashev and J. Songstad, *Acta chemica scandinavica*, 1995, **49**, 335-343.
45. X. Mou, Y. Wu, S. Liu, M. Shi, X. Liu, C. Wang, S. Sun, Q. Zhao, X. Zhou and W. Huang, *Journal of Materials Chemistry*, 2011, **21**, 13951-13962.
46. K. Dedeian, P. Djurovich, F. Garces, G. Carlson and R. Watts, *Inorganic chemistry*, 1991, **30**, 1685-1687.
47. A. Tsuboyama, H. Iwawaki, M. Furugori, T. Mukaide, J. Kamatani, S. Igawa, T. Moriyama, S. Miura, T. Takiguchi and S. Okada, *Journal of the American Chemical Society*, 2003, **125**, 12971-12979.
48. S.-Y. Kim, J.-H. Kim, Y. Ha, S.-H. Lee, J.-H. Seo and Y.-K. Kim, *Current Applied Physics*, 2007, **7**, 380-383.
49. C. Adachi, M. A. Baldo, S. R. Forrest and M. E. Thompson, *Applied Physics Letters*, 2000, **77**, 904.
50. S. Lamansky, P. Djurovich, D. Murphy, F. Abdel-Razzaq, R. Kwong, I. Tsyba, M. Bortz, B. Mui, R. Bau and M. E. Thompson, *Inorg. Chem*, 2001, **40**, 1704-1711.
51. P. J. Hay, *The Journal of Physical Chemistry A*, 2002, **106**, 1634-1641.
52. T. Liu, B.-H. Xia, X. Zhou, H.-X. Zhang, Q.-J. Pan and J.-S. Gao, *Organometallics*, 2007, **26**, 143-149.
53. S. Lamansky, P. Djurovich, D. Murphy, F. Abdel-Razzaq, H.-E. Lee, C. Adachi, P. E. Burrows, S. R. Forrest and M. E. Thompson, *J. Am. Chem. Soc*, 2001, **123**, 4304-4312.
54. A. F. Rausch, M. E. Thompson and H. Yersin, *The Journal of Physical Chemistry A*, 2009, **113**, 5927-5932.
55. K. H. Kim, C. K. Moon, J. H. Lee, S. Y. Kim and J. J. Kim, *Advanced Materials*, 2014, **26**, 3844-3847.
56. G. Sarada, J. Yoon, W. Cho, M. Cho, D. W. Cho, S. O. Kang, Y. Nam, J. Y. Lee and S.-H. Jin, *Journal of Materials Chemistry C*, 2016, **4**, 113-120.
57. V. G. Sree, W. Cho, S. Shin, T. Lee, Y.-S. Gal, M. Song and S.-H. Jin, *Dyes and Pigments*, 2017, **139**, 779-787.
58. Q. Zhao, S. Liu, M. Shi, C. Wang, M. Yu, L. Li, F. Li, T. Yi and C. Huang, *Inorganic chemistry*, 2006, **45**, 6152-6160.
59. K. P. S. Zanoni, B. K. Kariyazaki, A. Ito, M. K. Brennaman, T. J. Meyer and N. Y. Murakami Iha, *Inorganic chemistry*, 2014, **53**, 4089-4099.
60. K. Hasan, A. K. Bansal, I. D. W. Samuel, C. Roldán-Carmona, H. J. Bolink and E. Zysman-Colman, *Scientific Reports*, 2015, **5**, 12325.
61. B. X. Yang, C. Yao and G. Zhou, *Platinum Metals Review*, 2013, **57**, 2-16.
62. S.-W. Lai, M. C.-W. Chan, T.-C. Cheung, S.-M. Peng and C.-M. Che, *Inorganic chemistry*, 1999, **38**, 4046-4055.
63. S.-W. Lai, H.-W. Lam, W. Lu, K.-K. Cheung and C.-M. Che, *Organometallics*, 2002, **21**, 226-234.
64. W. Lu, B.-X. Mi, M. C. Chan, Z. Hui, C.-M. Che, N. Zhu and S.-T. Lee, *Journal of the American Chemical Society*, 2004, **126**, 4958-4971.

65. D. J. Cárdenas, A. M. Echavarren and M. C. Ramírez de Arellano, *Organometallics*, 1999, **18**, 3337-3341.
66. S. J. Farley, D. L. Rochester, A. L. Thompson, J. A. K. Howard and J. A. G. Williams, *Inorganic chemistry*, 2005, **44**, 9690-9703.
67. S. W. Botchway, M. Charnley, J. W. Haycock, A. W. Parker, D. L. Rochester, J. A. Weinstein and J. G. Williams, *Proceedings of the National Academy of Sciences*, 2008, **105**, 16071-16076.
68. L. Murphy, P. Brulatti, V. Fattori, M. Cocchi and J. A. G. Williams, *Chemical communications*, 2012, **48**, 5817-5819.
69. T. Yutaka, S. Obara, S. Ogawa, K. Nozaki, N. Ikeda, T. Ohno, Y. Ishii, K. Sakai and M.-a. Haga, *Inorganic chemistry*, 2005, **44**, 4737-4746.
70. B. Tong, H.-Y. Ku, I. J. Chen, Y. Chi, H.-C. Kao, C.-C. Yeh, C.-H. Chang, S.-H. Liu, G.-H. Lee and P.-T. Chou, *Journal of Materials Chemistry C*, 2015, **3**, 3460-3471.
71. F. Neve, A. Crispini, S. Serroni, F. Loiseau and S. Campagna, *Inorganic chemistry*, 2001, **40**, 1093-1101.
72. R. Munoz-Rodriguez, E. Bunuel, N. Fuentes, J. A. G. Williams and D. J. Cardenas, *Dalton Transactions*, 2015, **44**, 8394-8405.
73. M. Fujita, M. Tominaga, A. Hori and B. Therrien, *Accounts of chemical research*, 2005, **38**, 369-378.
74. S. R. Seidel and P. J. Stang, *Accounts of chemical research*, 2002, **35**, 972-983.
75. B. Chen, S. Xiang and G. Qian, *Accounts of Chemical Research*, 2010, **43**, 1115-1124.
76. P. Coppo, M. Duati, V. N. Kozhevnikov, J. W. Hofstraat and L. De Cola, *Angewandte Chemie*, 2005, **117**, 1840-1844.
77. M. Cavazzini, P. Pastorelli, S. Quici, F. Loiseau and S. Campagna, *Chemical communications*, 2005, 5266-5268.
78. S. Welter, F. Lafolet, E. Cecchetto, F. Vergeer and L. De Cola, *ChemPhysChem*, 2005, **6**, 2417-2427.
79. A. Hagfeldt, G. Boschloo, L. Sun, L. Kloo and H. Pettersson, *Chemical reviews*, 2010, **110**, 6595-6663.
80. N. Kaveevivitchai, R. Chitta, R. Zong, M. El Ojaimi and R. P. Thummel, *Journal of the American Chemical Society*, 2012, **134**, 10721-10724.
81. Z. Deng, H.-W. Tseng, R. Zong, D. Wang and R. Thummel, *Inorganic chemistry*, 2008, **47**, 1835-1848.
82. V. Balzani, S. Campagna, G. Denti, A. Juris, S. Serroni and M. Venturi, *Accounts of Chemical Research*, 1998, **31**, 26-34.
83. P. H. Lanoe, C. M. Tong, R. W. Harrington, M. R. Probert, W. Clegg, J. A. Williams and V. N. Kozhevnikov, *Chemical communications*, 2014, **50**, 6831-6834.
84. V. N. Kozhevnikov, M. C. Durrant and J. A. G. Williams, *Inorganic chemistry*, 2011, **50**, 6304-6313.
85. S. Culham, P.-H. Lanoë, V. L. Whittle, M. C. Durrant, J. A. G. Williams and V. N. Kozhevnikov, *Inorganic chemistry*, 2013, **52**, 10992-11003.
86. B. Ma, J. Li, P. I. Djurovich, M. Yousufuddin, R. Bau and M. E. Thompson, *Journal of the American Chemical Society*, 2005, **127**, 28-29.
87. E. Baranoff, E. Orselli, L. Allouche, D. Di Censo, R. Scopelliti, M. Grätzel and M. K. Nazeeruddin, *Chemical communications*, 2011, **47**, 2799-2801.
88. J. Fernández-Cestau, N. Giménez, E. Lalinde, P. Montaño, M. T. Moreno and S. Sánchez, *Organometallics*, 2015, **34**, 1766-1778.
89. S. Gonell, M. Poyatos and E. Peris, *Dalton Transactions*, 2016, **45**, 5549-5556.
90. D. Kim and J.-L. Brédas, *Journal of the American Chemical Society*, 2009, **131**, 11371-11380.
91. F. N. Castellano, I. E. Pomestchenko, E. Shikhova, F. Hua, M. L. Muro and N. Rajapakse, *Coordination Chemistry Reviews*, 2006, **250**, 1819-1828.
92. J. G. Williams, in *Photochemistry and Photophysics of Coordination Compounds II*, Springer, 2007, pp. 205-268.
93. I. Eryazici, C. N. Moorefield and G. R. Newkome, *Chem. Rev*, 2008, **108**, 1834-1895.
94. K. M.-C. Wong and V. W.-W. Yam, *Accounts of chemical research*, 2011, **44**, 424-434.
95. V. W.-W. Yam, C.-K. Hui, S.-Y. Yu and N. Zhu, *Inorganic chemistry*, 2004, **43**, 812-821.
96. V. K.-M. Au, K. M.-C. Wong, D. P.-K. Tsang, M.-Y. Chan, N. Zhu and V. W.-W. Yam, *Journal of the American Chemical Society*, 2010, **132**, 14273-14278.
97. W. P. To, K. T. Chan, G. S. M. Tong, C. Ma, W. M. Kwok, X. Guan, K. H. Low and C. M. Che, *Angewandte Chemie International Edition*, 2013, **52**, 6648-6652.

98. V. K.-M. Au, D. P.-K. Tsang, K. M.-C. Wong, M.-Y. Chan, N. Zhu and V. W.-W. Yam, *Inorganic chemistry*, 2013, **52**, 12713-12725.
99. K. J. Arm and J. A. G. Williams, *Dalton Transactions*, 2006, 2172-2174.
100. C. Sabatini, A. Barbieri, F. Barigelletti, K. J. Arm and J. G. Williams, *Photochemical & Photobiological Sciences*, 2007, **6**, 397-405.
101. R. D. Costa, G. Fernández, L. Sánchez, N. Martín, E. Ortí and H. J. Bolink, *Chemistry-A European Journal*, 2010, **16**, 9855-9863.
102. V. Chandrasekhar, T. Hajra, J. K. Bera, S. M. W. Rahaman, N. Satumtira, O. Elbjeirami and M. A. Omary, *Inorganic chemistry*, 2012, **51**, 1319-1329.
103. T. Hajra, J. K. Bera and V. Chandrasekhar, *Inorganica Chimica Acta*, 2011, **372**, 53-61.
104. J.-G. Cai, Z.-T. Yu, Y.-J. Yuan, F. Li and Z.-G. Zou, *ACS Catalysis*, 2014, **4**, 1953-1963.
105. S.-Y. Yao, Y.-L. Ou and B.-H. Ye, *Inorganic chemistry*, 2016, **55**, 6018-6026.
106. L. Donato, C. E. McCusker, F. N. Castellano and E. Zysman-Colman, *Inorganic chemistry*, 2013, **52**, 8495-8504.
107. A. Auffrant, A. Barbieri, F. Barigelletti, J. Lacour, P. Mobian, J.-P. Collin, J.-P. Sauvage and B. Ventura, *Inorganic chemistry*, 2007, **46**, 6911-6919.
108. A. Wragg, M. R. Gill, D. Turton, H. Adams, T. M. Roseveare, C. Smythe, X. Su and J. A. Thomas, *Chemistry-A European Journal*, 2014, **20**, 14004-14011.
109. T. F. Anjong, G. Kim, H. Y. Jang, J. Yoon and J. Kim, *New Journal of Chemistry*, 2016, **41**, 377-386.
110. K. J. Arm and J. A. G. Williams, *Chemical communications*, 2005, 230-232.
111. T. F. Anjong, G. Kim, H. Y. Jang, J. Yoon and J. Kim, *New Journal of Chemistry*, 2017, **41**, 377-386.
112. A. Tsuboyama, T. Takiguchi, S. Okada, M. Osawa, M. Hoshino and K. Ueno, *Dalton Transactions*, 2004, 1115-1116.
113. X. Yang, Z. Feng, J. Zhao, J.-S. Dang, B. Liu, K. Zhang and G. Zhou, *ACS Applied Materials & Interfaces*, 2016, **8**, 33874-33887.
114. X. Yang, X. Xu, J.-s. Dang, G. Zhou, C.-L. Ho and W.-Y. Wong, *Inorganic chemistry*, 2016, **55**, 1720-1727.
115. G. Turnbull, J. A. G. Williams and V. N. Kozhevnikov, *Chemical communications*, 2017, **53**, 2729-2732.
116. D.-H. Suh, J.-S. Choi, J.-S. Lim, S.-H. Kim and D.-B. Kim, *U.S. Patent 20080269484A1*, 2007, 4.
117. E. S. Andreiadis, D. Imbert, J. Pécaut, A. Calborean, I. Ciofini, C. Adamo, R. Demadrille and M. Mazzanti, *Inorganic chemistry*, 2011, **50**, 8197-8206.
118. Y. Zheng, A. S. Batsanov, M. A. Fox, H. A. Al-Attar, K. Abdullah, V. Jankus, M. R. Bryce and A. P. Monkman, *Angewandte Chemie International Edition*, 2014, **53**, 11616-11619.
119. K. He, X. Wang, J. Yu, H. Jiang, G. Xie, H. Tan, Y. Liu, D. Ma, Y. Wang and W. Zhu, *Organic Electronics*, 2014, **15**, 2942-2949.
120. C. H. Shin, J. O. Huh, S. J. Baek, S. K. Kim, M. H. Lee and Y. Do, *European Journal of Inorganic Chemistry*, 2010, **2010**, 3642-3651.
121. B. Ma, P. I. Djurovich, M. Yousufuddin, R. Bau and M. E. Thompson, *The Journal of Physical Chemistry C*, 2008, **112**, 8022-8031.
122. A. Auffrant, A. Barbieri, F. Barigelletti, J.-P. Collin, L. Flamigni, C. Sabatini and J.-P. Sauvage, *Inorganic chemistry*, 2006, **45**, 10990-10997.
123. V. L. Whittle and J. A. G. Williams, *Inorganic chemistry*, 2008, **47**, 6596-6607.
124. S.-H. Wu, S. E. Burkhardt, J. Yao, Y.-W. Zhong and H. D. Abruña, *Inorganic chemistry*, 2011, **50**, 3959-3969.
125. S. Develay and J. A. G. Williams, *Dalton Transactions*, 2008, 4562-4564.
126. S. Develay, O. Blackburn, A. L. Thompson and J. A. G. Williams, *Inorganic chemistry*, 2008, **47**, 11129-11142.
127. H. Houjou, Y. Hoga, Y.-L. Ma, H. Achira, I. Yoshikawa, T. Mutai and K. Matsumura, *Inorganica Chimica Acta*, 2017, **461**, 27-34.
128. P.-T. Chou and Y. Chi, *Chemistry – A European Journal*, 2007, **13**, 380-395.
129. M. Cocchi, D. Virgili, V. Fattori, D. L. Rochester and J. A. G. Williams, *Advanced Functional Materials*, 2007, **17**, 285-289.
130. B. Mi, C. Zhong, J. Sang, Z. Liao, H. Wang and Z. Gao, *Journal of Luminescence*, 2016, **180**, 51-57.
131. C. Adachi, M. A. Baldo, M. E. Thompson and S. R. Forrest, *Journal of Applied Physics*, 2001, **90**, 5048-5051.

132. M. A. Baldo, S. Lamansky, P. E. Burrows, M. E. Thompson and S. R. Forrest, *Applied Physics Letters*, 1999, **75**, 4-6.
133. C. Ulbricht, B. Beyer, C. Friebe, A. Winter and U. S. Schubert, *Advanced Materials*, 2009, **21**, 4418-4441.
134. C.-L. Ho, H. Li and W.-Y. Wong, *Journal of Organometallic Chemistry*, 2014, **751**, 261-285.
135. C.-H. Yang, Y.-M. Cheng, Y. Chi, C.-J. Hsu, F.-C. Fang, K.-T. Wong, P.-T. Chou, C.-H. Chang, M.-H. Tsai and C.-C. Wu, *Angewandte Chemie International Edition*, 2007, **46**, 2418-2421.
136. E. Baranoff and B. F. Curchod, *Dalton Transactions*, 2015, **44**, 8318-8329.
137. K. T. Kamtekar, A. P. Monkman and M. R. Bryce, *Advanced Materials*, 2010, **22**, 572-582.
138. Y. Sun and S. R. Forrest, *Applied Physics Letters*, 2007, **91**, 263503.
139. X.-M. Yu, H.-S. Kwok, W.-Y. Wong and G.-J. Zhou, *Chemistry of materials*, 2006, **18**, 5097-5103.
140. Y. Sun, N. C. Giebink, H. Kanno, B. Ma, M. E. Thompson and S. R. Forrest, *Nature*, 2006, **440**, 908.
141. K. J. Suhr, L. D. Bastatas, Y. Shen, L. A. Mitchell, G. A. Frazier, D. W. Taylor, J. D. Slinker and B. J. Holliday, *Dalton Transactions*, 2016, **45**, 17807-17823.
142. M. S. Lowry, J. I. Goldsmith, J. D. Slinker, R. Rohl, R. A. Pascal, G. G. Malliaras and S. Bernhard, *Chemistry of materials*, 2005, **17**, 5712-5719.
143. J. D. Slinker, J. Rivnay, J. S. Moskowitz, J. B. Parker, S. Bernhard, H. D. Abruna and G. G. Malliaras, *Journal of Materials Chemistry*, 2007, **17**, 2976-2988.
144. A. B. Tamayo, S. Garon, T. Sajoto, P. I. Djurovich, I. M. Tsyba, R. Bau and M. E. Thompson, *Inorganic chemistry*, 2005, **44**, 8723-8732.
145. E. Baggaley, J. A. Weinstein and J. A. G. Williams, *Coordination Chemistry Reviews*, 2012, **256**, 1762-1785.
146. Y. Chen, L. Qiao, L. Ji and H. Chao, *Biomaterials*, 2014, **35**, 2-13.
147. Y. You, *Current opinion in chemical biology*, 2013, **17**, 699-707.
148. Q. Zhao, C. Huang and F. Li, *Chemical Society Reviews*, 2011, **40**, 2508-2524.
149. P. Wu, E. L. M. Wong, D. L. Ma, G. S. M. Tong, K. M. Ng and C. M. Che, *Chemistry-A European Journal*, 2009, **15**, 3652-3656.
150. C.-K. Koo, K.-L. Wong, C. W.-Y. Man, Y.-W. Lam, L. K.-Y. So, H.-L. Tam, S.-W. Tsao, K.-W. Cheah, K.-C. Lau, Y.-Y. Yang, J.-C. Chen and M. H.-W. Lam, *Inorganic chemistry*, 2009, **48**, 872-878.
151. K. Y. Zhang, S. P.-Y. Li, N. Zhu, I. W.-S. Or, M. S.-H. Cheung, Y.-W. Lam and K. K.-W. Lo, *Inorganic chemistry*, 2010, **49**, 2530-2540.
152. K. K.-W. Lo, S.-K. Leung and C.-Y. Pan, *Inorganica Chimica Acta*, 2012, **380**, 343-349.
153. S. P. Y. Li, T. S. M. Tang, K. S. M. Yiu and K. K. W. Lo, *Chemistry-A European Journal*, 2012, **18**, 13342-13354.
154. S. Moromizato, Y. Hisamatsu, T. Suzuki, Y. Matsuo, R. Abe and S. Aoki, *Inorganic chemistry*, 2012, **51**, 12697-12706.
155. L. Murphy, A. Congreve, L.-O. Palsson and J. A. G. Williams, *Chemical communications*, 2010, **46**, 8743-8745.
156. M. Yu, Q. Zhao, L. Shi, F. Li, Z. Zhou, H. Yang, T. Yi and C. Huang, *Chemical communications*, 2008, 2115-2117.
157. Q. Zhao, F. Li and C. Huang, *Chemical Society Reviews*, 2010, **39**, 3007-3030.
158. Z. Liu, W. He and Z. Guo, *Chemical Society Reviews*, 2013, **42**, 1568-1600.
159. V. Guerchais and J.-L. Fillaut, *Coordination Chemistry Reviews*, 2011, **255**, 2448-2457.
160. Q. Zhao, T. Cao, F. Li, X. Li, H. Jing, T. Yi and C. Huang, *Organometallics*, 2007, **26**, 2077-2081.
161. Q. Zhao, S. Liu, M. Shi, F. Li, H. Jing, T. Yi and C. Huang, *Organometallics*, 2007, **26**, 5922-5930.
162. A. Dorazco-Gonzalez, *Organometallics*, 2014, **33**, 868-875.
163. D. N. Kozhevnikov, V. N. Kozhevnikov, M. Z. Shafikov, A. M. Prokhorov, D. W. Bruce and J. A. Gareth Williams, *Inorganic chemistry*, 2011, **50**, 3804-3815.
164. S. C. F. Kui, P. K. Chow, G. S. M. Tong, S.-L. Lai, G. Cheng, C.-C. Kwok, K.-H. Low, M. Y. Ko and C.-M. Che, *Chemistry – A European Journal*, 2013, **19**, 69-73.
165. G. Cheng, P.-K. Chow, S. C. F. Kui, C.-C. Kwok and C.-M. Che, *Advanced Materials*, 2013, **25**, 6765-6770.

166. P. K. Chow, C. Ma, W.-P. To, G. S. M. Tong, S.-L. Lai, S. C. F. Kui, W.-M. Kwok and C.-M. Che, *Angewandte Chemie International Edition*, 2013, **52**, 11775-11779.
167. S. C. F. Kui, P. K. Chow, G. Cheng, C.-C. Kwok, C. L. Kwong, K.-H. Low and C.-M. Che, *Chemical communications*, 2013, **49**, 1497-1499.
168. D. N. Kozhevnikov, V. N. Kozhevnikov, M. M. Ustinova, A. Santoro, D. W. Bruce, B. Koenig, R. Czerwieniec, T. Fischer, M. Zabel and H. Yersin, *Inorganic chemistry*, 2009, **48**, 4179-4189.
169. H.-F. Xiang, S.-C. Chan, K. K.-Y. Wu, C.-M. Che and P. T. Lai, *Chemical communications*, 2005, DOI: 10.1039/B415711G, 1408-1410.
170. C.-M. Che, C.-C. Kwok, S.-W. Lai, A. F. Rausch, W. J. Finkenzeller, N. Zhu and H. Yersin, *Chemistry – A European Journal*, 2010, **16**, 233-247.
171. K. Li, X. Guan, C.-W. Ma, W. Lu, Y. Chen and C.-M. Che, *Chemical communications*, 2011, **47**, 9075-9077.
172. K. Li, G. Cheng, C. Ma, X. Guan, W.-M. Kwok, Y. Chen, W. Lu and C.-M. Che, *Chemical Science*, 2013, **4**, 2630-2644.
173. R. E. Daniels, S. Culham, M. Hunter, M. C. Durrant, M. R. Probert, W. Clegg, J. A. G. Williams and V. N. Kozhevnikov, *Dalton Transactions*, 2016, **45**, 6949-6962.
174. C. Che, C. Kui and C. C. Kwok, *U.S. Patent 9306178 B2*, 2016.
175. V. L. Whittle and J. A. G. Williams, *Dalton Transactions*, 2009, 3929-3940.
176. J. W. Slater, D. P. Lydon, N. W. Alcock and J. P. Rourke, *Organometallics*, 2001, **20**, 4418-4423.
177. J. W. Slater and J. P. Rourke, *Journal of Organometallic Chemistry*, 2003, **688**, 112-120.
178. P. J. Steel and G. B. Caygill, *Journal of Organometallic Chemistry*, 1990, **395**, 359-373.
179. L. F. Gildea, A. S. Batsanov and J. A. G. Williams, *Dalton Transactions*, 2013, **42**, 10388-10393.
180. A. Steudel and V. Kozhevnikov, *U.S. Patent 20150171351A1*, 2014, 2-5.
181. Z. Wang, Z. Sun, X.-Q. Hao, J.-L. Niu, D. Wei, T. Tu, J.-F. Gong and M.-P. Song, *Organometallics*, 2014, **33**, 1563-1573.
182. W.-W. Yang, Y.-W. Zhong, S. Yoshikawa, J.-Y. Shao, S. Masaoka, K. Sakai, J. Yao and M.-a. Haga, *Inorganic chemistry*, 2012, **51**, 890-899.
183. J.-Y. Shao, N. Fu, W.-W. Yang, C.-Y. Zhang, Y.-W. Zhong, Y. Lin and J. Yao, *RSC Advances*, 2015, **5**, 90001-90009.
184. A. Herbst, C. Bronner, P. Dechambenoit and O. S. Wenger, *Organometallics*, 2013, **32**, 1807-1814.
185. A. Y.-Y. Tam, D. P.-K. Tsang, M.-Y. Chan, N. Zhu and V. W.-W. Yam, *Chemical communications*, 2011, **47**, 3383-3385.
186. J. Shi, E. W. Forsythe and D. C. Morton, *U.S. Patent US 20130172570A1*, 2013.
187. S. A. Willison, H. Jude, R. M. Antonelli, J. M. Rennekamp, N. A. Eckert, J. A. Krause Bauer and W. B. Connick, *Inorganic chemistry*, 2004, **43**, 2548-2555.
188. S. A. Willison, J. A. Krause and W. B. Connick, *Inorganic chemistry*, 2008, **47**, 1258-1260.
189. L. Yang, F. Okuda, K. Kobayashi, K. Nozaki, Y. Tanabe, Y. Ishii and M.-a. Haga, *Inorganic chemistry*, 2008, **47**, 7154-7165.
190. J. Kuwabara, T. Namekawa, M.-a. Haga and T. Kanbara, *Dalton Transactions*, 2012, **41**, 44-46.
191. S. Serroni, A. Juris, S. Campagna, M. Venturi, G. Denti and V. Balzani, *Journal of the American Chemical Society*, 1994, **116**, 9086-9091.
192. S. Campagna, S. Serroni, A. Juris, M. Venturi and V. Balzani, *New journal of chemistry*, 1996, **20**, 773-780.
193. G. Di Marco, M. Lanza, A. Mamo, I. Stefio, C. Di Pietro, G. Romeo and S. Campagna, *Analytical Chemistry*, 1998, **70**, 5019-5023.
194. E. Baranoff, E. Orselli, L. Allouche, D. Di Censo, R. Scopelliti, M. Gratzel and M. K. Nazeeruddin, *Chemical communications*, 2011, **47**, 2799-2801.
195. N. Yoshikawa, S. Yamabe, N. Kanehisa, Y. Kai, H. Takashima and K. Tsukahara, *Inorganica Chimica Acta*, 2009, **362**, 361-371.
196. A. F. Rausch, H. H. H. Homeier, P. I. Djurovich, M. E. Thompson and H. Yersin, 2007.
197. H. Yersin, A. F. Rausch, R. Czerwieniec, T. Hofbeck and T. Fischer, *Coordination Chemistry Reviews*, 2011, **255**, 2622-2652.
198. B. J. Powell, *Coordination Chemistry Reviews*, 2015, **295**, 46-79.
199. M. A. Baldo, D. O'brien, Y. You and A. Shoustikov, *Nature*, 1998, **395**, 151.
200. H. Yersin, *Highly efficient OLEDs with phosphorescent materials*, John Wiley & Sons, 2008.

201. A. Buckley, *Organic light-emitting diodes (OLEDs): Materials, devices and applications*, Elsevier, 2013.
202. I. M. Dixon, J.-P. Collin, J.-P. Sauvage, L. Flamigni, S. Encinas and F. Barigelletti, *Chemical Society Reviews*, 2000, **29**, 385-391.
203. E. Baranoff, J.-P. Collin, L. Flamigni and J.-P. Sauvage, *Chemical Society Reviews*, 2004, **33**, 147-155.
204. L. Flamigni, A. Barbieri, C. Sabatini, B. Ventura and F. Barigelletti, *Photochemistry and Photophysics of Coordination Compounds II*, 2007, 143-203.
205. E. Kim and S. B. Park, *Chemistry – An Asian Journal*, 2009, **4**, 1646-1658.
206. G. Zhou, W.-Y. Wong and X. Yang, *Chemistry – An Asian Journal*, 2011, **6**, 1706-1727.
207. K. K.-W. Lo, S. P.-Y. Li and K. Y. Zhang, *New Journal of Chemistry*, 2011, **35**, 265-287.
208. G. R. Freeman and J. A. G. Williams, *Top. Organomet. Chem.*, 2013, **40**, 89.
209. C. E. Welby, L. Gilmartin, R. R. Marriott, A. Zahid, C. R. Rice, E. A. Gibson and P. I. Elliott, *Dalton Transactions*, 2013, **42**, 13527-13536.
210. S. Ladouceur and E. Zysman-Colman, *European Journal of Inorganic Chemistry*, 2013, **2013**, 2985-3007.
211. J. Frey, B. F. E. Curchod, R. Scopelliti, I. Tavernelli, U. Rothlisberger, M. K. Nazeeruddin and E. Baranoff, *Dalton Transactions*, 2014, **43**, 5667-5679.
212. C. Xu, A. l. Guenet, N. Kyritsakas, J.-M. Planeix and M. W. Hosseini, *Inorganic chemistry*, 2015, **54**, 10429-10439.
213. K. Beydoun, M. Zaarour, J. G. Williams, T. Roisnel, V. Dorcet, A. l. Planchat, A. Boucekkine, D. Jacquemin, H. Doucet and V. r. Guerchais, *Inorganic chemistry*, 2013, **52**, 12416-12428.
214. G. J. Hedley, A. Ruseckas and I. D. W. Samuel, *The Journal of Physical Chemistry A*, 2009, **113**, 2-4.
215. G. J. Hedley, A. Ruseckas and I. D. W. Samuel, *The Journal of Physical Chemistry A*, 2010, **114**, 8961-8968.
216. F. Messina, E. Pomarico, M. Silatani, E. Baranoff and M. Chergui, *The Journal of Physical Chemistry Letters*, 2015, **6**, 4475-4480.
217. T. Sajoto, P. I. Djurovich, A. B. Tamayo, J. Oxgaard, W. A. Goddard and M. E. Thompson, *Journal of the American Chemical Society*, 2009, **131**, 9813-9822.
218. G. Denti, S. Campagna, L. Sabatino, S. Serroni, M. Ciano and V. Balzani, *Inorganic chemistry*, 1990, **29**, 4750-4758.
219. A. Dessi, M. Calamante, A. Mordini, L. Zani, M. Taddei and G. Reginato, *RSC Advances*, 2014, **4**, 1322-1328.
220. J. Ephraim, *Berichte der deutschen chemischen Gesellschaft*, 1891, **24**, 1026-1031.
221. J. R. Johnson and R. Ketcham, *Journal of the American Chemical Society*, 1960, **82**, 2719-2724.
222. G. Seybold and H. Eilingsfeld, *Liebigs Ann. Chem.*, 1979, 1271.
223. E. H. L. Falcão, Naraso, R. K. Feller, G. Wu, F. Wudl and A. K. Cheetham, *Inorganic chemistry*, 2008, **47**, 8336-8342.
224. J. A. Zampese, F. R. Keene and P. J. Steel, *Dalton Transactions*, 2004, 4124-4129.
225. D. M. D'Alessandro, P. H. Dinolfo, M. S. Davies, J. T. Hupp and F. R. Keene, *Inorganic chemistry*, 2006, **45**, 3261-3274.
226. M. Milkevitch, E. Brauns and K. J. Brewer, *Inorganic chemistry*, 1996, **35**, 1737-1739.
227. M. Marcaccio, F. Paolucci, C. Paradisi, S. Roffia, C. Fontanesi, L. J. Yellowlees, S. Serroni, S. Campagna, G. Denti and V. Balzani, *Journal of the American Chemical Society*, 1999, **121**, 10081-10091.
228. J. D. Scott and R. J. Puddephatt, *Organometallics*, 1986, **5**, 2522-2529.
229. S. Ghumaan, B. Sarkar, S. Patra, K. Parimal, J. van Slageren, J. Fiedler, W. Kaim and G. K. Lahiri, *Dalton Transactions*, 2005, 706-712.
230. Y. Fang, Y. Li, S. Wang, Y. Meng, J. Peng and B. Wang, *Synthetic Metals*, 2010, **160**, 2231-2238.
231. S. J. Lee, J. Sung Lee, K.-J. Hwang, Y. K. Kim, Y. S. Kim, N. G. Park, E. J. Shin and S. H. Lee, *Current Applied Physics*, 2005, **5**, 43-46.
232. E. Baggaley, S. W. Botchway, J. W. Haycock, H. Morris, I. V. Sazanovich, J. G. Williams and J. A. Weinstein, *Chemical Science*, 2014, **5**, 879-886.
233. A. Martin, A. Byrne, C. S. Burke, R. J. Forster and T. E. Keyes, *Journal of the American Chemical Society*, 2014, **136**, 15300-15309.
234. A. Parpaleix, Y. G. Houssen and S. Charpak, *Nature medicine*, 2013, **19**, 241-246.

235. K. Qiu, H. Huang, B. Liu, Y. Liu, Z. Huang, Y. Chen, L. Ji and H. Chao, *ACS applied materials & interfaces*, 2016, **8**, 12702-12710.
236. S. Liu, H. Liang, K. Y. Zhang, Q. Zhao, X. Zhou, W. Xu and W. Huang, *Chemical communications*, 2015, **51**, 7943-7946.
237. C.-L. Ho, K.-L. Wong, H.-K. Kong, Y.-M. Ho, C.-L. Chan, W.-M. Kwok, K.-Y. Leung, H.-L. Tam, M.-W. Lam and X.-F. Ren, *Chemical communications*, 2012, **48**, 2525-2527.
238. A. Frei, R. Rubbiani, S. Tubafard, O. Blacque, P. Anstaett, A. Felgenträger, T. Maisch, L. Spiccia and G. Gasser, *Journal of medicinal chemistry*, 2014, **57**, 7280-7292.
239. H. Huang, B. Yu, P. Zhang, J. Huang, Y. Chen, G. Gasser, L. Ji and H. Chao, *Angewandte Chemie*, 2015, **127**, 14255-14258.
240. J. Hess, H. Huang, A. Kaiser, V. Pierroz, O. Blacque, H. Chao and G. Gasser, *Chemistry-A European Journal*, 2017, 9888–9896.
241. C. Mari and G. Gasser, *CHIMIA International Journal for Chemistry*, 2015, **69**, 176-181.
242. M. G. Walker, P. J. Jarman, M. R. Gill, X. Tian, H. Ahmad, P. A. Reddy, L. McKenzie, J. A. Weinstein, A. J. Meijer and G. Battaglia, *Chemistry-A European Journal*, 2016, **22**, 5996-6000.
243. J. Fong, K. Kasimova, Y. Arenas, P. Kaspler, S. Lazic, A. Mandel and L. Lilge, *Photochemical & Photobiological Sciences*, 2015, **14**, 2014-2023.
244. S. Lazic, P. Kaspler, G. Shi, S. Monro, T. Sainuddin, S. Forward, K. Kasimova, R. Hennigar, A. Mandel and S. McFarland, *Photochemistry and Photobiology*, 2017.
245. Y. Li, C.-P. Tan, W. Zhang, L. He, L.-N. Ji and Z.-W. Mao, *Biomaterials*, 2015, **39**, 95-104.
246. C. Mari, H. Huang, R. Rubbiani, M. Schulze, F. Würthner, H. Chao and G. Gasser, *European Journal of Inorganic Chemistry*, 2017, **2017**, 1745-1752.
247. S. P.-Y. Li, C. T.-S. Lau, M.-W. Louie, Y.-W. Lam, S. H. Cheng and K. K.-W. Lo, *Biomaterials*, 2013, **34**, 7519-7532.
248. L. He, Y. Li, C.-P. Tan, R.-R. Ye, M.-H. Chen, J.-J. Cao, L.-N. Ji and Z.-W. Mao, *Chemical Science*, 2015, **6**, 5409-5418.
249. R.-R. Ye, C.-P. Tan, L. He, M.-H. Chen, L.-N. Ji and Z.-W. Mao, *Chemical communications*, 2014, **50**, 10945-10948.
250. F. Xue, Y. Lu, Z. Zhou, M. Shi, Y. Yan, H. Yang and S. Yang, *Organometallics*, 2014, **34**, 73-77.
251. D. Maggioni, M. Galli, L. D'Alfonso, D. Inverso, M. V. Dozzi, L. Sironi, M. Iannacone, M. Collini, P. Ferruti and E. Ranucci, *Inorganic chemistry*, 2015, **54**, 544-553.
252. L. K. McKenzie, I. V. Sazanovich, E. Baggaley, M. Bonneau, V. Guerchais, J. A. G. Williams, J. A. Weinstein and H. E. Bryant, *Chemistry – A European Journal*, 2017, **23**, 234-238.
253. X. Tian, Y. Zhu, M. Zhang, L. Luo, J. Wu, H. Zhou, L. Guan, G. Battaglia and Y. Tian, *Chemical communications*, 2017, **53**, 3303-3306.
254. J. Liu, C. Jin, B. Yuan, X. Liu, Y. Chen, L. Ji and H. Chao, *Chemical communications*, 2017, **53**, 2052-2055.
255. J. S. Nam, M.-G. Kang, J. Kang, S.-Y. Park, S. J. C. Lee, H.-T. Kim, J. K. Seo, O.-H. Kwon, M. H. Lim and H.-W. Rhee, *Journal of the American Chemical Society*, 2016, **138**, 10968-10977.
256. E. M. Boreham, L. Jones, A. N. Swinburne, M. Blanchard-Desce, V. Hugues, C. Terryn, F. Miomandre, G. Lemercier and L. S. Natrajan, *Dalton Transactions*, 2015, **44**, 16127-16135.
257. W. Wang, W. Meng and H. Du, *Dalton Transactions*, 2016, **45**, 5945-5948.
258. Y. Chen, K. Li, W. Lu, S. S.-Y. Chui, C.-W. Ma and C.-M. Che, *Angewandte Chemie International Edition*, 2009, **48**, 9909-9913.
259. E. Rossi, A. Colombo, C. Dragonetti, S. Righetto, D. Roberto, R. Ugo, A. Valore, J. A. G. Williams, M. G. Lobello, F. De Angelis, S. Fantacci, I. Ledoux-Rak, A. Singh and J. Zyss, *Chemistry – A European Journal*, 2013, **19**, 9875-9883.
260. E. C. Constable, R. P. Henney, T. A. Leese and D. A. Tocher, *Journal of the Chemical Society, Dalton Transactions*, 1990, 443-449.
261. B. Soro, S. Stoccoro, G. Minghetti, A. Zucca, M. A. Cinellu, S. Gladiali, M. Manassero and M. Sansoni, *Organometallics*, 2005, **24**, 53-61.
262. Z. Chen, D. Ye, G. Xu, M. Ye and L. Liu, *Organic & Biomolecular Chemistry*, 2013, **11**, 6699-6702.
263. C. J. Song, C. K. Jang, W. Yao and J. Y. Jaung, *Journal of Chemical Research*, 2013, **37**, 268-272.